THE EFFECT OF AGING AND DEGRADATION ON THE RE-USE OF POLYAMIDE 12 WITHIN POWDER BED FUSION PROCESSES

by

BENJAMIN LUKE SANDERS

UNIVERSITY OF BIRMINGHAM

A thesis submitted to the University of Birmingham for the degree of

DOCTOR OF PHILOSOPHY

School of Metallurgy & Materials

College of Engineering & Physical Sciences

University of Birmingham

June 2024

Abstract

Powder bed fusion (PBF) of thermoplastic materials, such as polyamide-12 (PA-12), can provide complex, individualised components with a high strength-to-weight ratio. However, during every build, 80-90% of powder remains un-sintered. The remaining powder is recoverable and can be re-used, but it has been exposed to physical aging and degradation processes that hinder the recyclability of the material. As a result, PBF processes are capable of generating significant amounts of waste. This work aims to improve the sustainability of PBF, by determining optimal strategies for quantifying the effect of aging on the properties of recycled PA-12 powder, and how to maximise its re-use across future builds, without detriment to the quality of final components.

To understand its complex aging behaviour, PA-12 powder was conditioned at 170 °C, within an oxygenated environment, for up to 336 hours. This time-temperature profile aims to replicate the harsh thermal conditions that PA-12 powder could be exposed to if repeatedly re-used across multiple PBF builds. Differential scanning calorimetry revealed an initial increase in melting temperature and crystallinity, representative of secondary crystallisation. However, for extended storage times beyond 100 hours, all measured variables indicate that thermo-oxidative degradation becomes the dominant aging mechanism. In an attempt to counteract the effect of aging, used material is typically blended with virgin powder before re-use; a 50:50 refresh ratio is most common. This study quantified the effectiveness of employing a more resource efficient 70:30 refresh rate. Successive powder re-use affected various material properties, such as reduced material coalescence and melt

flowability, deteriorated particle morphology, and a 4.5 °C increase in melting temperature. Nonetheless, a 20% reduction in particle flowability had the most significant effect on the quality of final parts. Despite identifying a direct correlation between specific powder and part properties, an 11% reduction in strength across 7 build cycles is relatively modest. Therefore, a 70:30 refresh ratio offers a good compromise between maintaining part performance, particularly for non-critical applications, without having to add an unnecessary amount of virgin powder.

The functionality of PBF parts is also dependent on the crystallisation process. With increased powder re-use, polycondensation and cross-linking cause structural changes that reduce the rate and extent of primary crystallisation. As a result, the common Avrami model is unsuitable for describing the crystallisation kinetics of aged PA-12 powder. Alternatively, the Hay theory accounts for both primary and secondary crystallisation, so can model the full phase transformation of re-used PA-12 powder more accurately. Despite limited reports in the literature, secondary crystallisation is a crucial aging process in the context of PBF. Flash scanning calorimetry (FSC) verified that secondary crystallisation, via lamellar thickening, can occur when PA-12 is exposed to elevated temperatures. FSC quantified that the mechanism and rate of lamellar thickening is dependent on temperature, time, and the polymorphic nature of PA-12. This insight into the crystallisation behaviour of PA-12 could be utilised to improve the consistency of PBF parts.

Acknowledgements

Most importantly, I would like to express my sincere thanks and gratitude to my supervisor Dr. Mike Jenkins for his invaluable guidance, advice, and constant encouragement throughout the duration of my PhD.

I am also grateful to my industry supervisor Dr. Edward Cant for regularly offering his expertise and assistance, despite his busy schedule. I appreciate the extra efforts he made to assist me alongside his regular responsibilities.

Further, I extend my gratitude to the Manufacturing Technology Centre for funding this work, and to Dr. Hoda Amel for her contributions to the project's conceptualisation. I also express my thanks to the Manufacturing Technology Centre for providing samples and consumables; as well as allowing me to use their outstanding facilities to conduct some of my experiments.

Finally, I would like to thank all my loved ones for their unwavering support throughout the duration of my PhD.

List of publications

This thesis is presented in an alternative format and incorporates the following publications:

1. Sanders B, Cant E, Amel H, Jenkins M. The Effect of Physical Aging and Degradation on the Re-Use of Polyamide 12 in Powder Bed Fusion. Polymers. 2022;14(13):2682.
2. Sanders B, Cant E, Jenkins M. Re-use of polyamide-12 in powder bed fusion and its effect on process-relevant powder characteristics and final part properties. Additive Manufacturing. 2024:103961.
3. Sanders B, Cant E, Kelly CA, Jenkins M. The Effect of Powder Re-Use on the Coalescence Behaviour and Isothermal Crystallisation Kinetics of Polyamide 12 within Powder Bed Fusion. Polymers. 2024;16(5):612.

Please note that all references are collated in one individual bibliography at the end of the thesis.

Table of Contents

List of Figures

Chapter 1

Chapter 2

Chapter 3

Chapter 4

Chapter 5

Chapter 6

Chapter 7

Chapter 8

List of Tables

CHAPTER 1 – INTRODUCTION TO ADDITIVE MANUFACTURING

1.1 The importance of additive manufacturing

In 2021, it was reported that, globally, the manufacturing industry contributes to 25% of energy demand, 20% of CO_2 emissions, and 40% of material consumption [1]. Given the increasing threat of climate change and global warming, the manufacturing industry now faces stringent government legislations advocating for a transition toward more sustainable processing methods [1].

Traditional subtractive manufacturing (SM), such as cutting, drilling, and milling, involves the extensive use of machinery to form parts into the desired shape and size, by removing unwanted raw material from a solid block [1-3]. SM is valuable for the mass production of simple, identical components whereby the unit cost of parts progressively decreases with increased production scale. In addition, computer numeric controlled (CNC) machining has delivered advancements within SM in terms of improved resource efficiency and part performance. However, SM has significant initial start-up costs due to the necessary installation of complex tooling, fixtures, and jigs. Similarly, there are problems associated with clamping, so production is limited to components with a simple geometry [1, 4, 5]. Furthermore, in the context of sustainability, the most significant limitation of SM is that excess, removed material is discarded, resulting in a considerable amount of waste [2, 6, 7].

Additive manufacturing (AM), more commonly known as “3D printing”, was first developed in 1981 with the intention of solving some of the issues associated with

SM [6, 7]. AM is an automated rapid prototyping technique, that allows physical components to be fabricated from virtual three-dimensional computer aided design (3D-CAD) models [3, 4, 8]. The material is usually printed layer by layer using a combination of two main sub-processes occurring simultaneously: the deposition of each layer onto the build platform, and the bonding with subsequent layers, in sequence, until a 3D part is formed [4]. According to the ISO/ASTM52900_15 standard of AM categorisation there are currently seven AM processes *(Table 1.1)*, including Powder Bed Fusion [7], which is of particular importance to this project.

AM allows design freedom and high precision of complex parts, including personal customisation. Furthermore, tooling and clamping are not required [2, 4, 7]. This helps deliver versatility and the ability to fabricate components with a unique geometry that would not be possible with conventional manufacturing methods [4, 5, 7]. Furthermore, product scaling can be achieved in CAD files, removing the data exchange problems found in SM; therefore, parts of different sizes and material types can be obtained from the same data set [4, 5]. More importantly, AM is a resource-efficient manufacturing technology that can reduce material waste and energy consumption, whilst continuing to provide high-quality parts with functional properties comparable to SM components [1, 6, 9]. Nevertheless, the use of expensive materials, issues associated with thermal stresses and dimensional inaccuracies within fabricated parts, and limits on the recyclability of feedstock material, has hindered the widespread adoption of AM technology [1, 10]. As a result, AM is generally restricted to the production of low-volume parts, so improvements are required to maximise material savings and increase the sustainability of the process.

Table 1.1 - Classification of the seven additive manufacturing techniques based on ASTM descriptions [11, 12].

AM Type	Techniques	General description	Pros	Cons	Common materials	Common Applications
Powder bed fusion (PBF)	Electron beam melting, direct metal laser sintering (metal) High speed sintering, , laser sintering, multi-jet fusion (polymer)	Thermal energy (laser/election beam), or infrared energy, selectively fuses regions of a powder bed to form a 3D object	- Highly complex geometries - Powder acts as support structure - Precision and accuracy - Low cost	- Post-processing requirements - Low powder utilisation rate - Relatively slow and long print time	Metals, polymers, ceramics, hybrids, and composites	Automotive (tyre moulds, brake calliper); medical (knee replacement); aerospace (GEPC engine)
Material jetting (MJT)	Inkjet printing, Object PolyJet and 3D systems ProJet	Droplets of photosensitive feedstock material are selectively deposited and then solidify when exposed to UV light	- Full colour parts possible - Multiple materials can be incorporated into a single part. - High levels of accuracy	- Poor mechanical properties so restricted to non-functional prototypes - Photosensitive material prone to degradation - Relatively expensive	Photopolymers, thermoplastics, ceramics, composites, waxes	Medical (visualisation models); engineering (prototypes);jewellery (casting patterns)
VAT photo-polymerisation (VPP)	Digital light processing, stereolithography and micro-SLA	Liquid photopolymer is selectively cured by light-activated polymerisation in a vat. An initially liquid material hardens when exposed to UV light	- High accuracy and complexity - Large build areas possible - Smooth surface finish	- Inadequate strength - Brittle parts - Lack of material choices	UV-curable photopolymer resins	Medical (hearing aids, facial prosthetics); dental; jewellery
Sheet lamination (SHL)	Layered object manufacturing and ultrasound additive manufacturing	Sheets of material bonded to form a 3D part	- Extra material recycled. - Full-colour parts possible - Ease of material handling	- Limited material options - Layer height cannot be changed without altering sheet thickness	Metal foils, plastic sheets, and paper	Not suitable for structural use – limited to aesthetic & visual models
Directed energy deposition (DED)	Laser Engineered Net Shaping	Thermal energy such as laser or plasma melts and fuses material as it is deposited	- High single-point deposition rates - No limits on direction or axis - High build rates - Dense and strong parts	- Low build resolution - Poor surface finish - High capital cost	Metal and metal-based hybrids with ceramics	Repair & maintenance of high value structural parts e.g., nickel alloy turbine blade
Material extrusion (MEX)	Fused filament fabrication, fused deposition modelling, 3D dispensing	Material selectively dispensed through nozzle and 3D parts are constructed layer by layer	- Good structural properties - Multi-colours possible - Inexpensive - User and office friendly	- Visible layer lines - Support structures required - Susceptible to warping	Thermoplastic filaments, rods, and pellets	Non-functional prototypes, concept models, production jigs
Binder jetting (BJT)	Voxeljet, Exone binder jetting	Liquid bonding agent selectively deposited to fuse powdered feedstock material, with the assistance of a chemical binder	- Large products possible - Wide range of materials - High productivity - Full-colour parts	- Use of binder makes BJT unsuitable for some structural parts - Significant post-processing often required	Metals, polymers, sands, ceramics	Full colour prototypes, cores & moulds, jewellery; tooling

1.2 Powder Bed Fusion

Powder Bed Fusion (PBF) is a subset of AM whereby a heat source, such as laser, infrared, or thermal print head, is applied to consolidate powdered material into a 3D object [13]. As shown in *Table 1.1,* this technique can operate with a variety of materials, however this project is solely focussed on polymer based PBF processes. PBF shares similarities to other AM methods because material is added gradually, layer-by-layer into a geometry fabricated directly from a 3D-CAD model [13-15]. Powder particles are stored within a bed chamber and, as each layer is completed, the build platform indexes down and new powder is spread over the build area, ready for the next layer to be selectively melted and consolidated into the desired geometry [13].

The PBF build process is usually comprised of three key stages [13, 16-18]. The warm-up phase involves the entire build chamber being gradually heated from room temperature to the required processing temperature, which is dependent upon the material used; this usually occurs within 1-2 hours. Secondly, the processing stage describes the layer-by-layer fusion of selected areas of powder into a 3D component. Once the parts are completed, the “part-cake”, which refers to the un-sintered powder and final parts within the powder bed chamber, slowly cools down until the parts can be removed [13]. This cool-down phase may extend for twice the duration of the processing stage because a slow cooling rate is required to prevent warpage and distortion of fabricated parts. Therefore, the complete build process often extends beyond 24 hours.

A significant advantage of PBF is that the removal of support structures is not required because sintered particles, unconnected islands, and overhangs are

contained within the surrounding un-sintered powder bed [13, 17, 19, 20]. As a result, the most complex geometries can be manufactured and multiple parts, of different sizes and shapes, can be stacked freely in the powder bed. This enhances part nesting, whilst increasing efficiency and productivity [13, 16-18, 20] *(Figure 1.1).*

On the other hand, as consolidated parts are contained within the un-fused powder bed, PBF has a low build conversion rate, and ~80-90% of powder from each build remains un-sintered. This un-sintered powder is recoverable and can be re-used in future build cycles [16-18, 21]. However, during part production the surrounding powder bed is exposed to high temperatures, approaching the material melting point, for long periods of time [21-26]. This can result in physical aging and chemical degradation processes that could cause deterioration of the polymers properties [18, 21, 27, 28]. As such, the extent of powder re-use is relatively unknown, and difficulties related to powder recycling has become a big challenge for the polymer PBF industry.

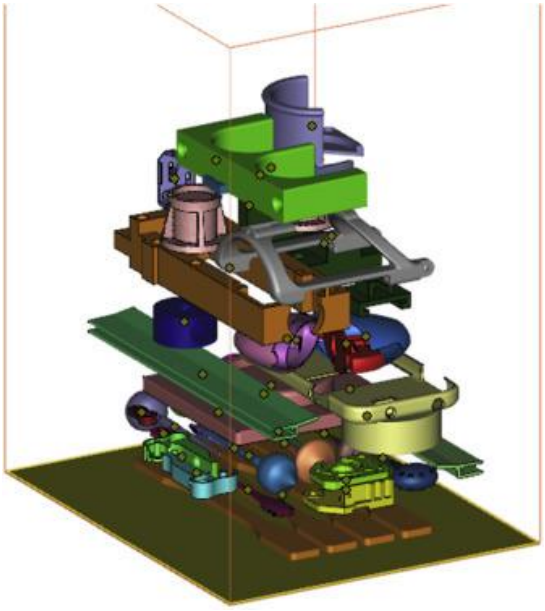

Figure 1.1 – Illustrates the uniqueness of a PBF build set up because multiple individual parts, all with different build geometries and sizes, can be arranged freely within the build volume [13].

1.2.1 Types of Powder Bed Fusion

Additive Manufacturing (AM) is a rapidly growing industry [29]. The current AM market is valued at $16.83 billion, with annual growth expected to continue at a rate of 21% until at least 2027 [30]. Therefore, there has been large investment into innovating new types of PBF technology, which each aim to offer benefits over previous processes. Current established PBF techniques include laser sintering (LS), high speed sintering (HSS), and multi-jet fusion (MJF) [31]; more recently Stratasys have introduced selective absorption fusion (SAF). In this project, there is a particular focus on the two most commonly used PBF techniques: LS and MJF.

Selective laser sintering, now referred to as laser sintering (LS) [12], was introduced in 1992 and became the first commercially available polymer PBF process [32]. During LS, to ensure homogeneous heating within the build chamber, the production zone and surrounding part-cake material are heated to the same temperature [33]. The build temperature is just below the onset of melting yet above the crystallisation temperature, which ensures powder consolidation does not occur before laser scanning [14, 33]. Additionally, in an attempt to create a controlled environment and restrict oxidative degradation, a LS build chamber is filled with nitrogen [28, 34-36], although most LS machines usually retain 2-5% residual oxygen [37, 38]. After a layer of powder is deposited onto the build platform, a high-power CO_2 laser melts selected regions of the powder layer, based on the 3D-CAD data provided for the designed part. The build platform is then lowered, and a fresh layer of powder is deposited before another scan causes polymer particles to fuse together, within the layer and with the underlying layer [16, 17]. This is repeated until all the necessary powder coalesces to form the 3D part [13, 14, 39, 40]. The common practice of an LS machine is depicted in *Figure 1.2.*

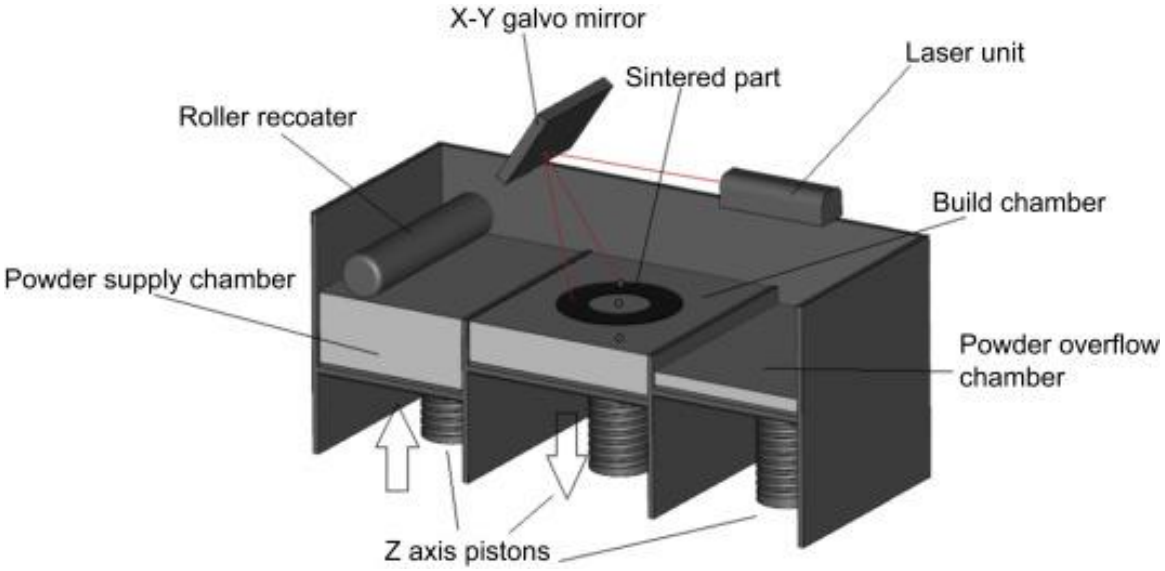

Figure 1.2 - Diagram showing the Laser Sintering (LS) process [13] .

Multi-Jet Fusion (MJF) is a relatively new PBF process, introduced by Hewlett-Packard (HP) in 2016 [7]. In MJF, following the deposition of each coating of powder onto the build platform, the entire powder layer is uniformly heated via infrared radiation before two separate printing inks, known as the fusing agent (FA) and detailing agent (DA), are added on selected areas of the powder surface [7, 15, 22, 24, 41, 42]. An automated 3D-CAD model provides the cross-section of the part which is then fused and printed using a combination of these two inks [24, 42] *(Figure 1.3).* The fusing agent assists heat transfer and helps the coalescence of particles into a consolidated layer; therefore, only the powder particles impregnated with FA melt when the infra-red lamp irradiates the powder surface [22, 42, 43]. During this printing phase the detailing agent inhibits heat diffusion outside the molten material, improving the dimensional accuracy of geometrically complex features [22, 24, 43, 44].

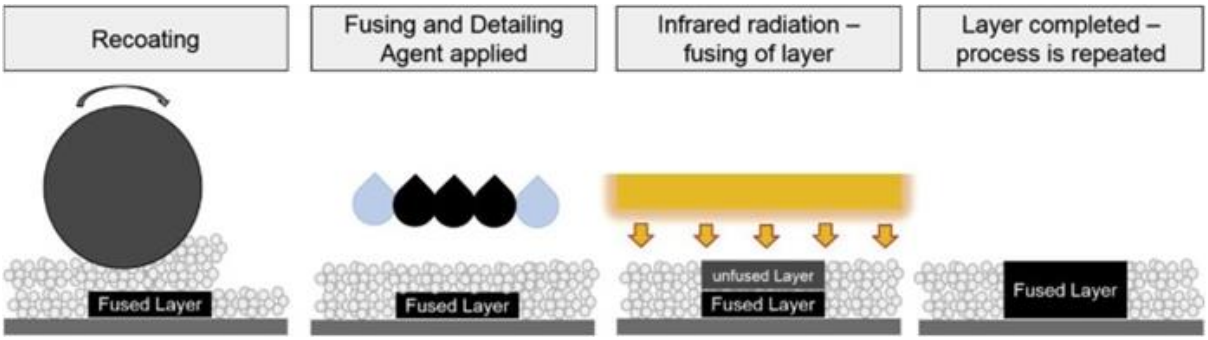

Figure 1.3 - Diagram showing the Multi-Jet Fusion (MJF) process [24].

1.2.2 Applications of Powder Bed Fusion

PBF is used across many different industries due to the advantageous ability to fabricate complex and personalised components, in a cost-effective manner [5-7]. Industrial sectors such as medical (e.g., individualised protheses and eyewear frames), domestic (e.g., household appliances), aerospace (e.g., cable routing covers), and sports (e.g., bicycle saddle padding) have benefitted immensely from the use of PBF technology [2, 45]. This is a result of the benefits the technology offers including customisation, high performance to weight ratio, and the potential to automate production, without expensive tooling [46-49]. Similarly, PBF can fulfil many unique requirements associated with these industries; providing flexibility in producing complex shapes which can suit the specific needs of each application *(Figure 1.4)* [2].

Furthermore, as binders are not necessary within LS, there is no risk of toxicity, which is particularly beneficial for biomedical applications where more conventional processing methods, such as injection moulding, cannot be used [21]. On the other hand, the FA and DA used within MJF are potentially toxic; emphasising how it is important to select the most appropriate type of PBF for specific applications. In

addition, as a result of increased regulations surrounding environmental sustainability, the importance of producing lightweight parts, with sufficient mechanical properties, has become increasingly crucial. Within the aerospace and automotive industry, lightweighting can be achieved by replacing complex metallic components, such as brake brackets and window guide rails, with polymeric parts fabricated using PBF [45]. Lightweight parts enhance the fuel efficiency of the aircraft or vehicle, considerably reducing the CO_2 emissions in each case.

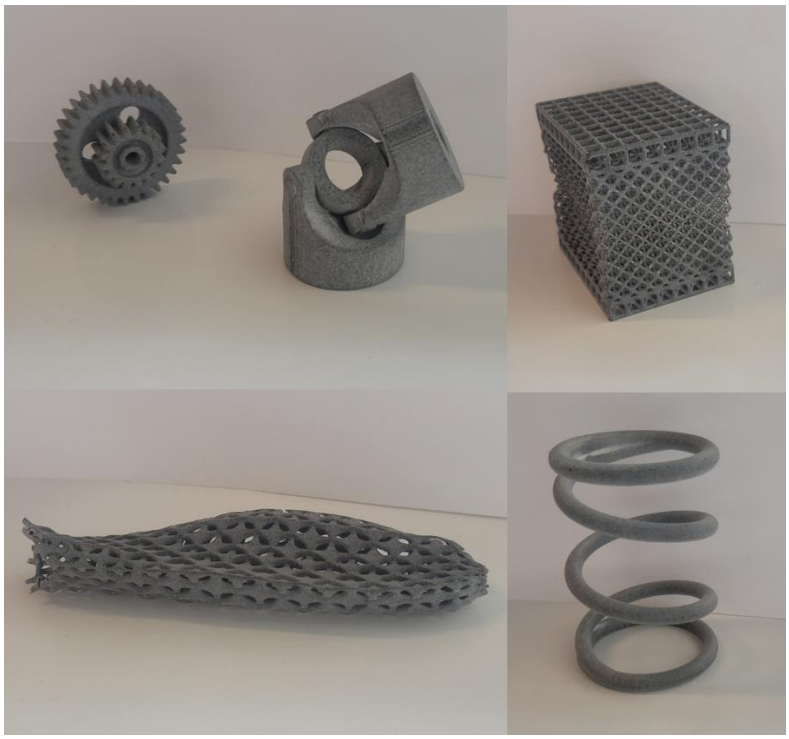

Figure 1.4 – A variety of protypes printed by polymer PBF highlight advantages of the technology such as the ability to fabricate extremely complex geometries, and intricate component features, with high precision.

1.2.3 Materials for PBF

Theoretically any polymer able to be produced in powdered form can be used for PBF. However, due to the complex thermal properties of polymers, only a few are known to be successful at producing multi-layered parts with sufficient properties

[13]. To be suitable for PBF a large processing window, whereby the melting temperature (T_m) is significantly higher than the crystallisation temperature (T_c), is required [38, 50]. This ensures that the crystallisation process is delayed during the build, which reduces residual stresses, distortions, and warpage of final parts [22, 38, 51]. Semi-crystalline thermoplastics *(section 2.1.2),* in particular nylons, are common to PBF and polyamide 12 (PA-12) is the most widely used [15, 21-23, 28, 38, 51-53]. PA-12 is considered the benchmark material as it can form strong, highly crystalline structures, is recyclable, and, relative to other polyamides, is more resistant to moisture [54-56]. Nonetheless, other materials such as polyamide-11 (PA-11), and polyetheretherketone (PEEK) have also been used previously [23, 57]. Standard PA-12 powders *(Figure 1.5)* have a peak melting temperature of 178-180°C [19, 57]. However, prior to use in PBF, powders are subjected to a unique thermal treatment which increases the materials melting temperature and, more importantly, enlarges the processing window [19]. Therefore, most PBF-modified PA-12 powders show a higher melting temperature of 182-187°C [34, 58].

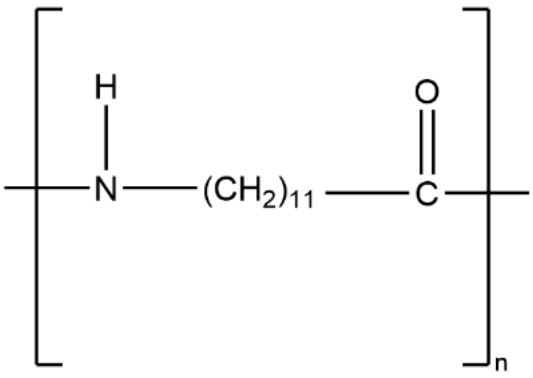

Figure 1.5 - Repeating unit of PA-12. The long, linear hydrocarbon chain and reactive amide group are key features which influence the physical and chemical properties of PA-12.

1.2.3.1 Polyamide 12

Polyamide 12 (PA-12) is the most commonly used material within PBF [15, 21-23, 28, 38, 51-53]. PA-12 is a semi-crystalline, aliphatic nylon which consists of amide groups separated by a methylene sequence. Within polyamides, hydrogen bonding represents the dominant intermolecular interaction, and these bonds can form between N-H and C=O groups across adjacent chain segments [54, 59]. Due to the presence of hydrogen bonds, PA-12 can develop relatively high levels of crystallinity *(Figure 1.6)* [54, 59, 60]. This is preferential for PBF because a high crystallinity relates to a greater enthalpy of fusion, which helps prevent unintentional melting of PA-12 powder in the vicinity of particles targeted by the heat source [50]. Also, the crystalline phase improves the mechanical properties of fabricated parts, as more hydrogen bonds can form between adjacent layers, increasing inter-layer bonding, whilst enhancing part strength and stiffness [54, 59]. As a result, PA-12 parts can be used for functional, end-use applications [61]. Another key characteristic of PA-12 powder, which makes it superior over many other thermoplastic materials, is a large processing window. This prevents premature crystallisation and limits distortion or warpage of parts, reducing the number of discarded components [21-23, 28, 38, 51, 62].

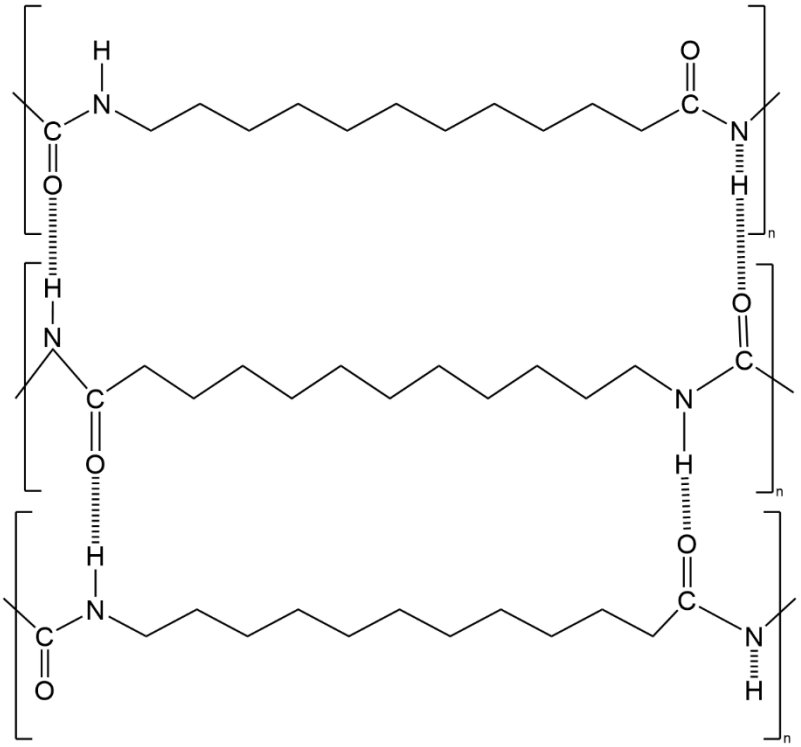

Figure 1.6 – Schematic diagram illustrating hydrogen bonding (linkages) between adjacent PA-12 chains; this allows close packing of chains so highly crystalline structures can develop.

1.2.4 Requirement for powder re-use within PBF

It was envisaged that the introduction of AM would provide a resource efficient alternative to more traditional manufacturing methods that often produce considerable amounts of waste material [63]. However, due to the large amount of support material used, and relatively sparse packing density of parts, PBF has a low powder utilisation rate and material waste remains a significant industry problem. PBF-grade PA-12 powder is expensive [16, 17, 21, 26], and can cost between $100-$150 per kg [25, 64], whilst equivalent polyamide feedstock for injection moulding (IM) costs $3 per kg [64]. Compared to IM, there is a limited number of materials that can be used to fabricate functional PBF components, so the high demand for PA-12 powder contributes to this significant difference in cost [64]. Similarly, production of

the powder itself is costly and energy intensive [27], so if batches of un-sintered powder were to be discarded and remain un-utilised, then the energy-efficiency of PBF would be critically compromised [27]. Furthermore, as PA-12 powder is such a high-value material, recycling used PA-12 powder for low cost everyday items such as plastic bottles and packaging would be uneconomical [27].

In order for PBF to be economically viable and environmentally sustainable, it is crucial that un-sintered powder remaining at the end of each build, is re-used in subsequent build cycles. Nonetheless, powder re-use is complex because during each build cycle PA-12 powder is exposed to high temperatures, for extended periods of time, which results in aging and degradation of the material. It has been established that various aging processes could be active during a build cycle; depending on the specific processing method, the most prevalent are polycondensation, secondary crystallisation, and thermo-oxidative degradation. These aging processes, which are discussed in detail in *section 3.2*, have the potential to alter the quality of un-sintered powder, and ultimately its suitability for re-use in future builds. Therefore, to be suitable for reuse, the un-sintered, yet used powder, is usually “refreshed” with new, virgin material in an attempt to restore the properties of the feedstock material [16-18, 21]. The volume of fresh powder added to the used powder is known as the refresh rate or the refresh ratio [23-25, 65, 66].

In LS, typically 30-50% of virgin material is blended with used powder before re-use in subsequent builds, although the exact refresh rate differs from supplier to supplier [16-18, 21, 23, 26]. Conversely, in MJF the use of fusing and detailing agents allows for a lower powder bed temperature, so the recyclability of PA-12 powder is greater, and the recommended refresh rate is only 20% [24]. However, these refresh ratios are arbitrary and rarely account for variation in the properties of used powder [16, 17,

25]. PBF operators are constantly working with powder mixtures of an unknown, inconsistent quality, so the property profile of a final component is difficult to predict [17, 18]. As such, a common issue within both LS and MJF is the fabrication of components with unreliable mechanical and physical properties. This has restricted the widespread adoption of these technologies for the production of functional end-use parts; so, the manufacture of low-value prototypes remains the most common industry use of PBF.

Operating with rigid refresh ratios is ineffective because aging of PA-12 powder during each build cycle is a multi-factorial, complex problem, with various processes occurring simultaneously and interacting with each other. Similarly, multiple process-specific factors can also influence the deterioration of powder properties. For example, material aging is more prominent in longer builds and systems with larger, more complex, build volumes [13, 16], whilst increased part density and packing density can also affect the extent of material aging. Used powder remaining from these builds would likely need a greater influx of virgin powder to maintain the necessary properties. Furthermore, temperature gradients within the build chamber may cause different regions of powder to be exposed to inconsistent temperature/time profiles, resulting in varying levels of powder deterioration [18]. These factors have great impact from an industrial standpoint because variations in the extent of powder aging causes the recommended refresh ratio to become inaccurate and un-fit for purpose. As a result, for time and cost-saving purposes, industry operators often use a higher proportion of new powder than necessary to avoid the risk of final components having inadequate properties [16, 17]. However, this is inefficient and unsustainable because using excessive amounts of new powder, when it is not necessarily required, is wasteful. Alternatively, when dealing

with more severely aged powder, an insufficient refresh rate could render the subsequent build unsuccessful, leading to unserviceable parts which have to be discarded [16, 17, 21, 25, 28, 67].

Therefore, a greater understanding of aging and degradation is required, in order to deliver more information about whether un-sintered powder is suitable for re-use within PBF. A holistic approach is essential, using a wide range of characterisation techniques to determine powder quality and formulate a structured recycling strategy, based off quantitative data. This would help ease current environmental and economic concerns regarding powder waste, which is necessary for growth and extensive use of this technology.

1.3 Scope of the work

This work aims to improve the sustainability of powder bed fusion, by determining optimal strategies for defining the effect of aging on recycled polyamide-12 powder, and how to maximise its re-use without detriment to the quality and performance of final parts. Utilising a wide range of characterisation techniques, the complex aging mechanisms occurring during a build cycle are untangled. Therefore, the influence of specific aging phenomenon, namely polycondensation, secondary crystallisation, and thermo-oxidative degradation, can be better understood. In addition, the relationship between the deterioration of powder quality and the reduced performance of final parts is quantified; indicating how aging processes may restrict the re-usability of PA-12 powder. Finally, it is hoped that the findings of this study will help inform more efficient classification of used powder and provide guidance to industry operators on how to incorporate recycled PA-12 powder into future build cycles. This could help enhance powder re-use, minimise waste, and lead to more

reliable final part properties; allowing PBF to be used more regularly for the fabrication of functional, end-use components.

The thesis includes an introduction to polymers (chapter 2), providing the information required to understand the complex aging and degradation mechanisms discussed in the literature review (chapter 3). Chapters 4 to 6 are comprised of three published articles, whereby the aims and their rationale are identified in each individual paper. This is followed by an additional chapter investigating secondary crystallisation of PA-12, providing useful information that was complimentary to the prior schemes of work. Finally, the most crucial findings and conclusions of these studies are brought together in a subsequent integrated discussion.

CHAPTER 2 – INTRODUCTION TO THERMOPLASTIC MATERIALS

2.1 Microstructure and morphology of thermoplastics

Polymers are comprised of molecules with long sequences of atoms, or groups of atoms, which are linked together by primary bonds, often in the form of covalent bonding [68]. These sequences are known as monomers. Macromolecular polymers form through polymerisation and this involves combining multiple monomers together through chemical reactions [68]. There are two main types of polymers: thermosets and thermoplastics. A thermosetting plastic is a polymer that irreversibly hardens after application of heat or pressure [69]. Thermoplastics, which are of particular interest to this project, are made up of polymer chains that become soft when heated but can harden when cooled [70]. Therefore, structural changes within thermoplastic materials are reversible. Depending on the degree of microstructural order, thermoplastics can be categorised as either amorphous or semi-crystalline materials.

2.1.1 Amorphous polymers

Amorphous polymers are completely disordered, exist in a liquid-like state, and do not exhibit any level of arrangement or structural regularity [68, 71]. These polymers are incapable of crystallisation and, as they have no ordered phase, cannot melt. Amorphous polymer chains are instead characterised by the glass-to-liquid transition temperature (T_g), which corresponds to a change in molecular motion, rather than a change in structure. At temperatures below T_g, amorphous polymers are in a solid-state and can be generically classified as ‘frozen polymer liquids’ [68]. The polymer

system remains disordered in a random orientation, but the chains are immobile and there is insufficient energy to overcome the rotational energy barriers within the chain [72]. Similarly, the material is considered to be in a state of non-equilibrium, whereby conformational change and long-range motion is restricted. At these low temperatures, the material is hard, glassy, and brittle [68]. As temperature rises above T_g, the thermal energy within the system increases, allowing amorphous chains to rotate. At this point, there is an abrupt transition to the rubbery (“soft”) state and chain mobility is greater, so molecules are able to move effortlessly throughout the free volume present within the system [68, 73]. With further increases in temperature into the “liquid” state, the thermal energy within the polymer is raised significantly. The viscosity of the polymer is low and chain mobility is high, so molecules can spontaneously rotate and there is unrestricted conformational change, which results in a significantly coiled and entangled microstructure [74]. Common amorphous polymers that are widely used across a wide range of industrial applications include polystyrene, polyvinyl chloride (PVC), and acrylonitrile butadiene styrene (ABS).

2.1.2 Semi-crystalline materials

In the “liquid” state, macromolecular polymer chains display long-range motion and molecules exist in a highly entangled and chaotic system, whereby there is thought to be a random coil conformation [75]. As such, thermoplastics struggle to crystallise on cooling back to the solid state, because this would require extensive un-coiling and organisation of the chains, therefore it is near impossible to attain a perfectly crystalline polymer [68]. Nonetheless, many thermoplastics are semi-crystalline and contain organised crystalline blocks which are separated by regions of disordered amorphous chains.

The crystalline phase contains folded polymer chains which align into ordered structures known as lamella [76]. Numerous models have been proposed for the morphology of crystalline lamellae; however, the structure of semi-crystalline polymers is best described by the 3-phase model [77, 78], which combines aspects of the more traditional regular re-entry and random switchboard models [74, 79-81]. The 3-phase model concludes that there are three main regions which define a semi-crystalline polymer: crystalline, interfacial, and amorphous [74]. This model allows for regular re-entry of aligned polymer chains into the lamellae; chains fold back and forth via hairpin-type turns, as shown by the tight, medium, and long loops in *Figure 2.1*. As a result, polymer crystals display a closely packed, uniform lamellae structure. In the 3-phase model, polymer chains can also integrate into the crystalline lamellae via random re-entry, whereby chain folding is more limited. In this case, chains meander through the inter-lamellar amorphous regions before aligning and re-entering the crystalline lamellae at random locations [72]. Additionally, the 3-phase model displays cilia which indicate chains with free ends present; whilst tie-chains are portions of disordered polymer sequences that form structural connections between adjacent crystalline lamellae. This phenomenon is also known as cross-linking [75, 82, 83]. The inter-lamellar amorphous region is divided into the mobile amorphous fraction (MAF) and the rigid amorphous fraction (RAF), which is also known as the interfacial structure [74]. The MAF behaves as a normal amorphous material with no ordered regions, whilst the RAF is sandwiched between the crystalline regions and the MAF, so some segments of the chain are held within the lamella by covalent bonding and have restricted mobility.

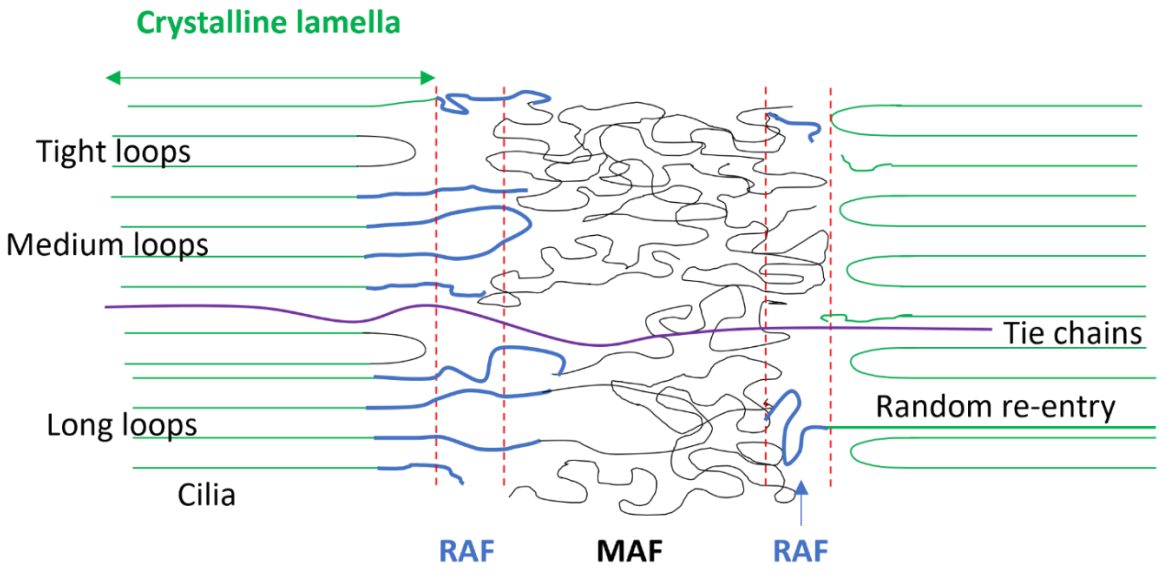

Figure 2.1 – Schematic of the 3-phase model, which describes the morphology of a semi-crystalline thermoplastic.

2.2 Glass transition and melting temperatures

As a semi-crystalline polymer comprises of both amorphous and crystalline regions, it goes through two thermal transitions on heating. Firstly, the glass-transition temperature (T_g) describes a change in mobility of amorphous chains [72]. Below T_g, the material behaves as a hard, brittle glass; long range motion of amorphous chains is hindered, so chain mobility is limited to local conformational change such as the partial rotation of individual C-C bonds from the cis to trans position, and vice versa [68, 81]. Upon heating through T_g, the increased thermal energy present within amorphous regions allows greater chain mobility and the polymer system transforms into a soft, rubbery state whereby the amorphous phase displays long range cooperative motion [68, 72]. The glass transition occurs over a wide temperature range, because T_g is influenced by many factors such as chain length, chain

entanglements/branching, chain flexibility, and cross-linking, amongst other intermolecular interactions [68, 72].

With further increases in temperature, highly ordered crystalline regions begin to melt when the increased energy provided by higher temperatures breaks the intermolecular bonding present within the crystalline phase of the polymer system. Following melting, the previously ordered crystalline regions have no internal structure, causing an increase in disorder and entropy, as well as significant changes in volume [75]. The melting of polymer crystals can be distinguished from other materials as it displays various unique characteristics. Firstly, unlike metals, melting is not an abrupt, sharp event but instead occurs over a broad temperature range due to variations in the thickness of different lamellae [62, 68]. This is displayed in *Figure 2.2,* which demonstrates that a single endothermic peak is actually compromised of multiple melting events, representative of different lamellae structures that melt over a range of temperatures. Thicker lamellae contain additional intermolecular bonding, and are more thermodynamically stable, so further thermal energy is required to disrupt the structure and their melting point increases. Furthermore, the thermal history of the sample, and the rate at which the material is heated, will have a significant effect on the melting behaviour [68, 75]. The melting temperature (T_m) can also be adjusted by the crystallisation temperature (T_c), which alters the crystal microstructure *(Section 2.4)*, and a secondary crystallisation process that causes continuous and progressive thickening of lamella *(Section 2.3.2).*

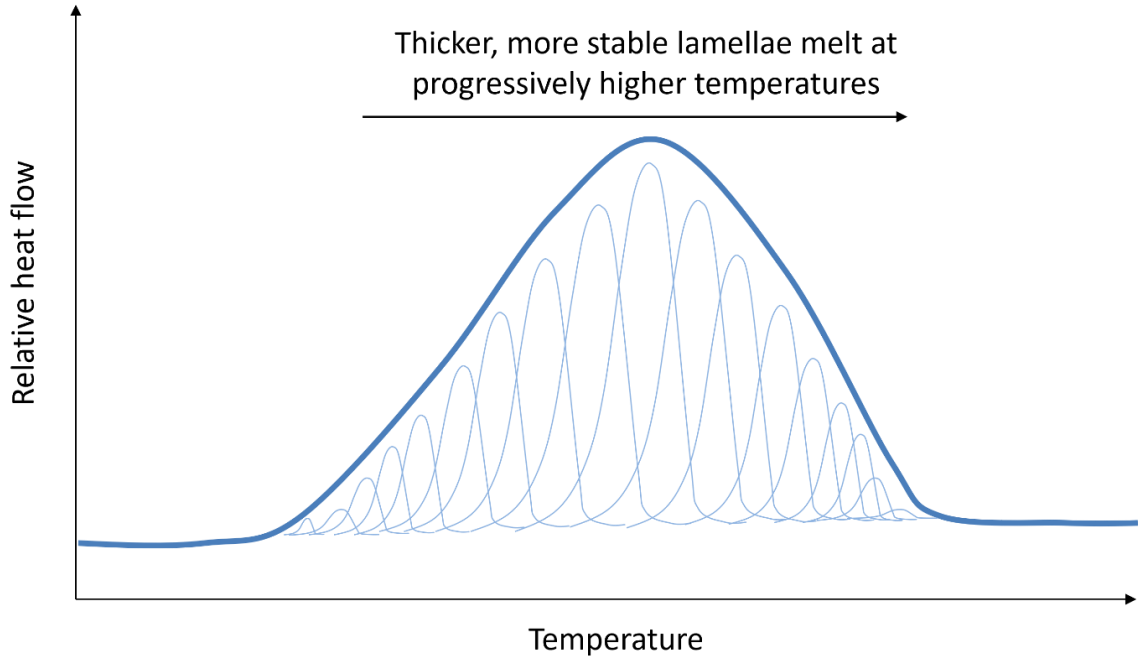

Figure 2.2 – Schematic illustration of an endothermic melting peak, indicating how melting occurs over a broad temperature range due to differences in lamellar thickness [62].

Due to the unique thermal behaviour of polymers, an equilibrium melting temperature (T_m^0) has been introduced to offer a more realistic estimation of the melting point. According to Hoffman and Weeks, T_m^0 describes the melting of an infinitely large crystal, whereby a polymer has been crystallised infinitely slowly and, as a result, melting and crystallisation theoretically occur at the same temperature [68, 84]. Crystal thickness increases with T_c so is inversely proportional to the extent of under-cooling. Therefore, there is a linear increase in T_m, as a function of T_c, and T_m^0 is defined by the point at which an extrapolation of this positive, linear trendline intersects with $T_c = T_m$. This relationship can be expressed in the equation:

$$T_m = {T_m}^0 \left(1 - \frac{1}{2}\beta\right) + \frac{T_c}{2\beta} \qquad \textit{(Equation 2.1)}$$

where β is the thickening factor, equal to 1 if recrystallisation does not occur during melting, and the slope of the line is expected to equal to ½ β. As shown in *Figure 2.2,* thicker lamellae melt at considerably higher temperatures than thinner, more unstable crystalline structures. Therefore, above the peak T_m it is conceivable that some thicker lamella may not be fully melted, and un-molten spherulite cores could be present within the polymer "melt". Through a process known as "self-seeding", these un-molten cores could act as self-nucleation sites, causing enhanced crystallisation temperatures, and a faster crystallisation rate on cooling [85, 86]. However, T_m^0 is useful because it estimates complete polymer melting. At temperatures > T_m^0, the material should be in a fully molten, amorphous state with no remnants of crystalline structures remaining, so self-seeding should not be possible.

Relative to other materials, the use of polymers within practical, structural applications is often restricted by their lower melting temperatures and poor thermal stability. However, multiple factors can be altered to control T_m and produce polymers with superior thermal properties. The melting point of different polymers is generally determined by its chemical structure; stiff chain backbones have a higher T_m because there is restricted rotation of chemical bonds along the chain. Similarly, the presence of bulky side groups can also hinder rotation of bonds around the chain backbone, which has the same effect of increasing T_m. The addition of polar groups, for example amide linkages (-CONH-), causes intermolecular hydrogen bonding to take place which also raises the melting temperature because each individual hydrogen bond will increase the overall enthalpy of fusion of the polymer. Therefore, greater hydrogen bond density, and a reduction in the number of $-CH_2-$ linkages between the amide bonds, causes an increase in T_m [68].

2.3 The Crystallisation Process

2.3.1 Nucleation and growth during primary crystallisation

Crystallisation is a kinetic process which describes the transformation of a disordered phase into an ordered structure with greater stability. Primary crystallisation is initiated when the pure polymer melt is cooled below T_m, via a process called nucleation. As temperature reduces, there is a tendency for disordered molecules to rotate and become aligned into small, ordered regions described as nuclei or embryos [60, 68, 87]. Such rotations occur around carbon-carbon bonds within the chain's backbone and these local, randomised variations in order provide sufficient energy to overcome the energy barrier for crystallisation [87]. This type of nucleation is defined as homogeneous and small nuclei are spontaneously formed in random locations throughout the polymer melt. However, the primary mechanism of nucleation is heterogeneous nucleation, whereby impurities (e.g., dust particles) present in the polymer system, act as artificial primary nuclei. This occurs more commonly because the presence of a foreign surface significantly reduces the energy barrier for crystallisation and the required nucleus size for crystal growth [68, 87].

Once a primary nucleus is formed, crystallisation theories envisage that crystal growth can occur as a secondary nucleation process, whereby molecules stick to the smooth growth surface of the pre-existing nucleus, via a chain folding mechanism. Growth can occur in 1-(rods), 2-(discs) or 3-(spheres) dimensions and growth morphology is dependent on the geometric shape of the crystals [68, 72]. The activation energy barrier for secondary nucleation is significantly lower than primary nucleation, so once a stable nucleus has been formed, crystal growth can occur

relatively quickly. Following nucleation, polymer chains are mobile and flexible, so free rotation of the polymer backbone allows chain folding and alignment of polymer molecules into a lamella structure. Crystalline lamellae contain fibrils, which grow out from the nucleation site and spread into the disordered polymer melt, expanding radially, and forming a multi-layered chain-folded structure, whereby amorphous chains are trapped in between the ordered, crystalline blocks [88-90]. This results in the formation of structures known as spherulites; given there is sufficient time and thermal energy within the system, the spherulites will continue to grow out radially until spherulite impingement occurs. At this stage, the previously growing spherulites display a polyhedral shape and are separated by linear boundaries (*Figure 2.4* in *section 2.4)*. Spherulite impingement represents termination of primary crystallisation, but crystal growth can continue via a secondary crystallisation process.

2.3.2 Secondary crystallisation

Secondary crystallisation refers to a process whereby a polymer continues to increase in crystallinity. Generally, the secondary process is differentiated from primary crystal growth because it occurs following spherulite impingement, which represents termination of the primary process [91-93]. As such, crystallisation continues within the amorphous phase, in the presence of existing crystals, rather than crystallisation from the melt [94]. However, it has also been suggested that primary and secondary crystallisation can occur simultaneously [91, 92, 95-97]. In this case, the secondary process can occur within spherulites and instigates as soon as lamellae are formed [95, 98].

Within the current literature, there are many theories for explaining the mechanisms underlying secondary crystallisation within polymeric materials. Some have reported

that secondary crystallisation occurs via lamellar thickening. Following primary crystallisation, crystalline stems are generally quite thin, and lamellae have a high surface to volume ratio so are thermodynamically metastable. To minimise the crystal to liquid interfacial free energy and achieve a greater thermodynamic stability, lamellae tend to thicken within the chain axis direction [99-103]. Although there is agreement that the thermodynamic driving force for lamellar thickening is a reduction in the surface free energy, debate remains regarding how thickening occurs. It has previously been suggested that thickening develops through solid-state chain diffusion, whereby folded chains reconfigure their arrangements via chain sliding [99, 101-106] or chain refolding [79, 105, 107, 108]. Alternatively, Hay's reptation-diffusion model [93, 95, 109] refers to the movement of amorphous chains across the crystal boundary. The key differential of this theory is that fractions of amorphous chains, within the polymer melt, are able to become incorporated into the pre-existing crystalline lamellae *(Figure 2.3a)*.

On the other hand, it has been reported that polymer crystallinity can increase through lamellar infill or lamellar insertion [105, 110-113] *(Figure 2.3b)*. Lamellar infill involves the growth of thin, small crystals in the interlamellar MAF, within regions not occupied by lamellae initially formed during primary crystallisation [113]. This process is thought to occur at temperatures lower than the primary crystallisation temperature. As a result, lamella structures that form via lamellar infill are unstable and weak, so they melt at significantly lower temperatures than the main bulk crystals [113, 114].

Secondary crystallisation may also occur upon heating the polymer, through a reversible process known as melt-recrystallisation [105, 110, 111, 115-117]. Depending on the crystallisation conditions, primary polymer crystals could be

comprised of thin, unstable lamellae. On heating, these “metastable” structures melt at lower temperatures, followed by rapid recrystallisation from the molten phase, resulting in the formation of thicker, more stable crystal structures which then re-melt at higher temperatures [103, 105, 117]. If there is sufficient time, melt-recrystallisation can result in double melting of the material [84, 116, 118].

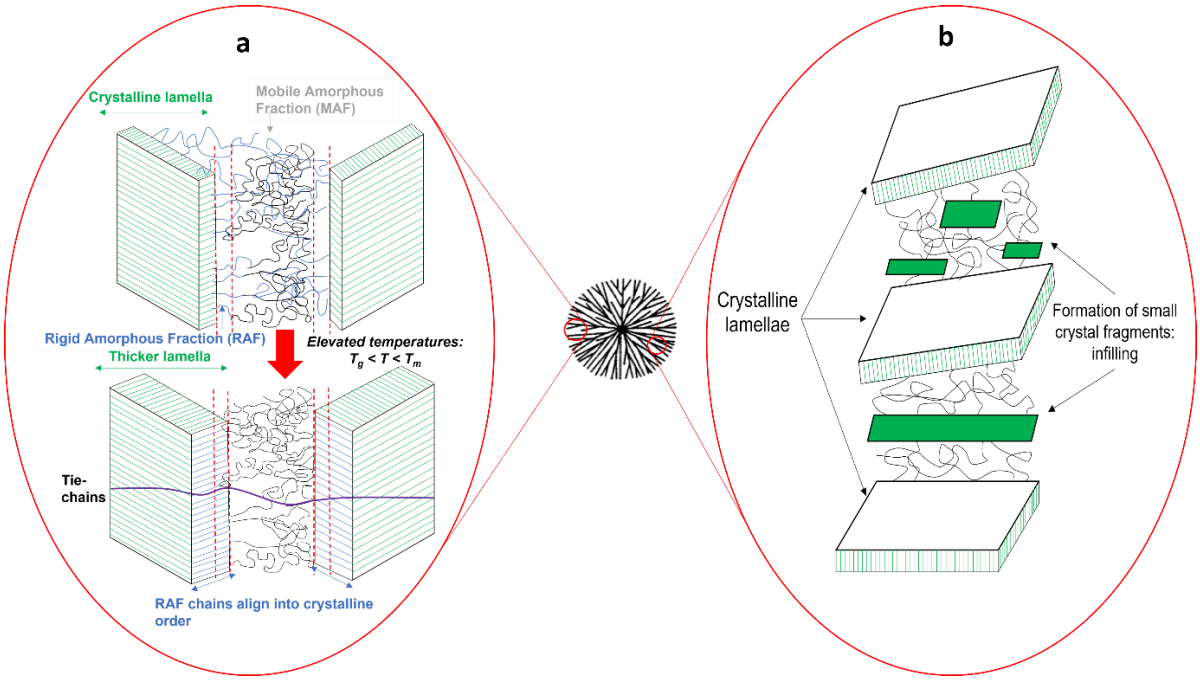

Figure 2.3 – Diagram portraying two different secondary crystallisation processes, based off the 3-phase model for semi-crystalline thermoplastics; a) lamella thickening and b) lamella infill (right) [119].

2.4 Isothermal crystallisation

Crystallisation can occur over a wide temperature range between T_g and T_m where there is appropriate chain motion. Below T_g, crystallisation cannot occur as chains become immobile, so there is insufficient thermal energy for chain motion and crystal growth. Conversely, above T_m, stable crystal nuclei cannot form because the

polymer system is highly disordered, and chains are constantly moving and rotating. The number of nuclei which form, and the extent of crystal growth, is heavily dependent on temperature and the degree of undercooling (ΔT). This is also known as supercooling and $\Delta T = T_m^0 - T_c$, whereby T_m^0 is the equilibrium melting temperature and T_c is the crystallisation temperature.

At high crystallisation temperatures (low supercooling), the crystallisation process is nucleation limited, and crystal growth is thermodynamically favoured. Increased thermal energy raises molecular mobility so the formation of stable nuclei is challenging, and nucleation is more sporadic. As such, the resulting morphology displays a relatively low number of larger spherulites. Similarly, at low supercooling, heterogeneous nucleation is thermodynamically favoured, and crystallisation is initiated almost exclusively via heterogeneous nucleation [120, 121]. At these temperatures, nucleation can effectively only occur on pre-existing surfaces where the free energy barrier to nucleation has reduced sufficiently. In contrast, at higher levels of supercooling, homogeneous nucleation is thermodynamically favoured, and a greater number of nuclei can form. At lower crystallisation temperatures, the mobility of polymer chains is limited, whilst available free volume is hindered by the high number of nuclei, so the rate of crystal growth is significantly reduced. As a result, the final morphology contains a high number of much smaller spherulites [68, 122]. It has also been suggested that at very high supercooling, near T_g, homogeneous nucleation density is so high that it causes non-spherulitic growth and the resulting morphology is instead described as a nodular mesophase [120, 123, 124].

Evidently, the isothermal crystallisation temperature has a significant effect on the type of nucleation and resulting crystalline morphology of a polymer *(Figure 2.4).*

From a polymer processing standpoint, understanding the temperature dependence of crystallisation is crucial because the mechanical properties of a polymer are influenced by the type of crystal morphology which forms. As such, altering T_c allows the crystal morphology and mechanical properties to be tailored to specific applications. A polymer crystallised at temperatures closer to T_m usually has a small number of larger spherulites. Due to increased intermolecular bonding, this increases the tensile strength and modulus of the material, but leads to embrittlement and reduced toughness [73]. Conversely, at crystallisation temperatures closer to T_g, the resulting crystalline structure generally displays ductile behaviour, with a higher elongation at break, but low strength and stiffness [73, 125, 126]. This is because there are a greater number of spherulites, with a reduced diameter, so the fracture energy can be dissipated across numerous spherulite boundaries, increasing the ductility of the material [126]. As shown in *Figure 2.4,* the maximum rate of crystallisation usually occurs halfway between T_g and T_m; this is due to the crystallisation rate being growth limited at temperatures tending to T_g, and nucleation limited near the T_m. Therefore, this optimum temperature represents a compromise between the conflicting temperature dependence of nucleation and growth.

To summarise, the crystalline morphology of thermoplastics, and subsequently the mechanical and physical properties of the material, are heavily influenced by T_c and crystallisation rate. This is relevant to PBF because the onset and rate of crystallisation of PA-12 significantly affects the processing window and printability of the powder. Also, the crystallisation process causes residual stresses which can result in shrinkage of consolidated parts within the build chamber. Consequently, the geometrical accuracy of final parts is often hindered by non-uniform crystallisation,

leading to inconsistent volume reductions, part curling, and part warpage [127]. Therefore, an extensive understanding of the crystallisation kinetics of thermoplastic polymers, is necessary to ensure homogeneous crystallisation during the PBF build process; this is crucial for the fabrication of functional end-use parts.

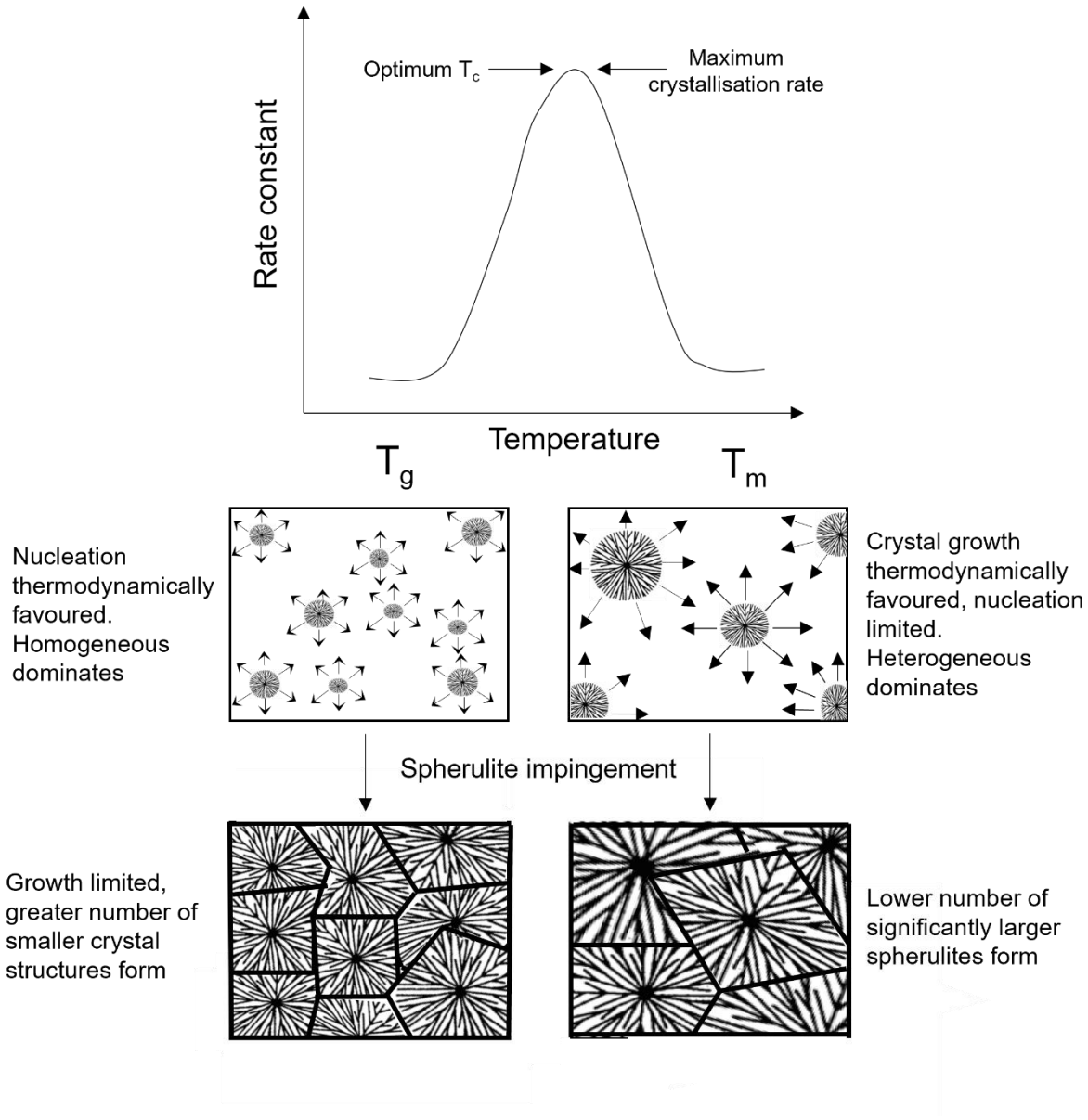

Figure 2.4 – Schematic illustration of the temperature dependence of crystallisation. The effect of temperature on the type of nucleation, extent of crystal growth, and resulting crystalline morphology is also depicted.

2.4.1 Modelling isothermal crystallisation kinetics

Using differential scanning calorimetry (DSC), the isothermal crystallisation kinetics of polymers can be analysed [112, 127-131]. The polymer is initially heated to temperatures above its equilibrium melting point and held in the molten phase. This provides sufficient time for the complete melting of any pre-existing crystals. Once a completely amorphous, liquid state has been established, the sample is cooled rapidly to the desired crystallisation temperature (T_c) and then remains at this temperature for a pre-determined amount of time (t_c). During this time period, variations in heat flow, as a function of time, are monitored by the DSC. Assuming the sample is stored for a sufficient period of time, an exothermic peak is observed which is characteristic of an isothermal crystallisation process. The exothermic energy released is directly proportional to the development of crystallinity. Therefore, integrating the DSC crystallisation exotherms can provide a measurement for relative crystallinity (X_c) as a function of time [112, 132]. However, this method is restricted to a specific temperature range. At low temperatures crystallisation occurs rapidly, and cannot be measured by the DSC, whereas at higher temperatures crystallisation is slow, so storage for extended periods could result in degradation. Similarly, at elevated T_c's, any alteration in heat flow is negligible and falls below the detection threshold of the DSC.

A variety of models have been proposed to reveal more information about the crystallisation behaviour of polymeric materials. These models, described in more detail within *Table 2.1*, aim to analyse and replicate crystallinity development across the full phase-transformation from an amorphous structure to a semi-crystalline material.

Table 2.1 – Summary of the main models used to describe the isothermal crystallisation kinetics of polymers.

Model	Equation(s)	Definitions	Key points
Avrami **[133-135]**	$\boldsymbol{X_t = \left(1 - e^{-k_a t^{n_a}}\right)}$	• X_t - fractional crystallinity at time, t. • t - crystallisation time • k_a - Avrami rate constant. • n_a - Avrami exponent	• k_a determines crystallisation rate. • n_a is the sum of the nucleation mechanism & geometry of growth. • In theory, n_a should be an integer between 1 and 4, whereby: 1 = one-dimensional rods, 2 = two-dimensional discs & 3 = three-dimensional spheres. • Parameters of the Avrami equation are calculated from the gradient (n_a) and anti-logarithm of the y-intercept (k_a) when $\log(-\ln(1 - X_t))$ is plotted against log time.
Simplified Hillier **[112, 136, 137]**	$\boldsymbol{X_t = X_{p,\infty}\left(1 - e^{-k_a t^{n_a}}\right)}$	• $X_{p,\infty}$ is the relative crystallinity upon completion of primary crystallisation.	• $X_{p,\infty}$ restricts the data to primary crystallisation alone. • In a fractional crystallinity vs time plot, $X_{p,\infty}$ is measured from the intersect of tangents drawn from the primary & secondary regions. • Using a plot of $\log\left(-\ln\left(1 - \frac{X_t}{X_{p,\infty}}\right)\right)$ versus log time, n_a and k_a are resolved from the gradient & anti-logarithm of the y-intercept, respectively.
Tobin **[138-140]**	$\boldsymbol{X_t = \frac{k_t t^{n_t}}{1 + (k_t t^{n_t})}}$	• k_t - Tobin rate constant. • n_t - Tobin exponent.	• Alteration of the Avrami equation which attempts to account for spherulite impingement. • k_t and n_t have similar meanings to the Avrami parameters, although n_t does not need to be an integer. • A plot of $\log\left(\frac{X_t}{(1 - X_t)}\right)$ versus log time, allows n_t and k_t to be measured from the gradient and antilogarithm of the y-intercept, respectively.

Malkin **[132, 141-143]**	$X_t = 1 - \frac{C_0 + 1}{C_0 + e^{C_1 t}}$ $C_0 = 4^{n_a} - 4$ $C_1 = ln(4^{n_a} - 2)\left(\frac{k_a}{\ln(2)}\right)^{\frac{1}{n_a}}$	• C_0 – Malkin exponent. • C_1 - Malkin rate constant	• Assumes that the overall rate of crystallisation is the combined sum of the rate of primary nuclei formation and the rate of secondary crystal growth. • C_0 is proportional to the ratio of primary crystal growth to primary nucleation rate; C_1 can be derived from the addition of numerous fractions related to these two parameters. • C_0 and C_1 cannot be derived from a double log plot and can only be derived via curve fitting. This is achieved using the two extra equations.
Hay **[92, 95, 144]**	$X_t = X_{p,\infty}\left(1 - e^{-k_p t^{n_a}}\right)\left(1 + k_s t^{1/2}\right)$	• k_p & k_s are the Avrami rate constants of primary & secondary crystallisation, respectively. • n_a becomes **fixed** (estimated for expected nucleation & growth mechanism) during modelling. In the other models, n_a is allowed to vary.	• Assumes primary & secondary crystallisation occur concurrently. • Secondary crystallisation appeared to be most significant at the centre of spherulites, indicating that the secondary process occurs almost immediately after the formation of a stable, growing nuclei. • Primary process continues to follow the standard Avrami equation. • Secondary crystallisation is determined by a square root dependence on fractional crystallinity. • Traditional models assume that full crystal phase transformation is complete on the ambiguous return of the DSC trace to baseline values of heat flow [128, 145, 146]. Hay shows that the crystallisation process can continue for extended periods of time, due to a significant involvement of secondary crystallisation. • Hay's approach calculates where the secondary process tends to zero so is able to estimate the latter stages of crystallisation more accurately.

CHAPTER 3 – LITERATURE REVIEW

3.1 The effect of build parameters on the processability of PA-12 within PBF

The physical, structural, and mechanical properties of PBF parts are essential to fulfilling the functional requirements for various applications. Aging and degradation of PA-12 during PBF has the potential to significantly alter the properties of feedstock powder, its suitability for re-use across future build cycles, and the performance of final components. However, the processability of PA-12 powder within PBF, as well as the mechanical behaviour and surface quality of fabricated parts, is also dependent on the close control of numerous build specific processing parameters. Similarly, limitations of different PBF techniques influence the relationship between the properties of feedstock powder and the consistency of fabricated parts. Therefore, before exploring the various aging and degradation processes that can occur within PA-12 *(section 3.2.)*, it is necessary to provide a more in-depth understanding of the intricacies of laser sintering and multi jet fusion.

3.1.1 Laser sintering (LS)

LS is particularly susceptible to various processing parameters [147-149], including:

- Scanning parameters, such as scan spacing, direction, and speed.
- Laser parameters, for instance laser power, quality, and spot size.
- Build parameters, for example build chamber temperature, build chamber atmosphere, build chamber humidity, part position, and scan length.

- Part specific quantities, including build orientation, part thickness, and part density.

This can be beneficial because varying any of these factors allows material properties to be controlled and tailored for specific applications. For example, increasing laser intensity maximises melting and consolidation of PA-12 particles, which reduces part porosity and improves the mechanical properties. However, heightened laser power also increases degradation of un-sintered powder in the heat-affected zones near to the print surface; a compromise is therefore required. So, where possible, operators are advised to keep laser power at a minimum and instead adjust other key process variables to achieve optimum part properties [148, 150, 151].

Various other parameters can also affect the LS build process. Firstly, following a LS build, cooling rates are restricted by conduction through the large powder bed, which is slow due to the poor thermal conductivity of PA-12 powder [61]. In addition, to prevent warpage and deformation, sintered parts can only be withdrawn once the chamber temperature is below the relatively low T_g (~45 °C) of PA-12 [16, 17]. As a result, the cool down phase can, depending on the build conditions, last for extended periods of time and in some cases as long as 80 hours [16, 17, 33]. During this time, un-sintered PA-12 powder continues to be exposed to high temperatures, so aging processes will remain active, and the un-sintered powder will continue to deteriorate. Furthermore, inconsistent powder deposition and incomplete particle melting, due to temperature gradients within the part bed, can cause non-homogeneous melting, which often leads to particle coring and, subsequently, increased part porosity [38, 50, 61]. In this case, particle coring refers to the presence of un-molten particle cores, whereby solid crystalline fragments remain due to incomplete melting. This

leads to an increased number of pores within fabricated parts because un-molten regions hinder complete consolidation of powder particles within each layer, and between subsequent layers, during the layer-by-layer build process. As such, the ductility of LS parts is generally lower than components fabricated by conventional methods, such as injection moulding [61].

In addition, build orientation is vital because LS parts display anisotropic behaviour, and this has a significant effect on part density and mechanical properties. LS parts fabricated vertically in the powder bed show the weakest tensile strength and are the most brittle [41, 152-157]. Vertical samples display reduced tensile properties because the tensile force is applied perpendicular to the print and pore layer direction, which act as crack propagation and failure initiation sites [41, 153]. Similarly, due to the fusion method used in LS, vertically orientated samples display reduced layer-layer bonding compared to equivalent parts printed in the horizontal orientation. Aforementioned, poor layer-layer bonding increases porosity and interlayer defects which contribute to the anisotropic behaviour observed within LS components [41].

3.1.2 Multi-jet fusion (MJF)

As MJF has been developed more recently, the technology was invented with the intention of solving some of the processing restrictions associated with LS. MJF is reportedly up to 10 times faster than LS, which increases productivity, thus providing economic benefits in terms of energy and material consumption [15, 42, 44]. One of the main differences between the two technologies is that MJF uses two inks during the printing process: the fusing agent (FA) and detailing agent (DA). These printing inks help improve the processability of the material. The DA inhibits heat transfer out the part, allowing the MJF process to print more geometrically complex features,

more accurately [22, 24, 44]. The FA contains carbon black, which increases the energy absorption of PA-12 powder, assisting the melting and consolidation process. This improves sintering quality and bonding strength, leading to less porous components. As a result, in contrast to LS parts, MJF components usually display isotropic mechanical behaviour [22, 24, 41, 150].

The printing inks (FA and DA) also help to improve the re-usability of the feedstock material [15, 44]. Due to the energy absorption capabilities of the DA, the surrounding un-sintered part-cake is exposed to less severe thermal conditions and powder deterioration is reduced [20]. In addition, as the FA assists particle melting and consolidation, the bed temperature and infrared radiation intensity during printing, can be minimised, which reduces aging of the feedstock powder. As a result, relative to LS, a greater amount of unfused powder can be recycled for future builds, and the manufacturer recommended refresh rate is only 20% virgin material. This limits waste and delivers a substantial productivity gain, unlocking heightened cost efficiencies for industrial applications [22, 24, 41, 42, 154]. Nonetheless, due to the large production scale of MJF powder, waste remains a significant industry-wide issue, so improving the material re-use strategy further could improve the economic and environmental sustainability of the process.

Although it offers benefits over LS, the MJF process has important limitations that have to be considered. Despite displaying isotropic mechanical behaviour, the benchmark mechanical properties of MJF parts in the XY horizontal orientation are generally lower than LS components [19, 154]. The IR lamp used within MJF allows the whole build layer to be fused in one pass, which yields higher productivity; but it can also result in large thermal gradients that may reduce the consistency of parts, depending on their location in the bed chamber [44]. As a result, aging of un-sintered

powder can vary significantly across the powder bed and powder quality is inconsistent. When using a fixed 20% refresh rate, which does not account for any variation in powder properties, unpredictable feedstock powder affects the performance of MJF parts. This emphasises the importance of understanding the various aging and degradation processes that can occur during a build cycle, in order to quantify powder quality and its potential for re-use in future build cycles.

3.2 Aging and degradation of PA-12 during PBF

Powder bed fusion (PBF) has numerous benefits over other AM processes. However, for PBF to be successful it must comply with stringent processing conditions *(section 3.1)*, and this requires extremely close control of various process-relevant material properties [62, 64]. Intrinsic powder characteristics are those which are inherent to the material, for example rheological, thermal, and optical properties; whilst extrinsic parameters, such as particle morphology and flowability, are also dependent upon external factors [62, 64]. In the context of PBF, the melting temperature of PA-12 is an intrinsic property because it is determined by changes in the chemical structure of PA-12. In contrast, as well as being affected by particle morphology and other powder properties, particle flowability is also dependent upon its interaction with the re-coater blade, so is an extrinsic parameter. The interaction between all the process relevant properties, that are imperative to fabricating high quality parts, is outlined in *Figure 3.1.* Aging and degradation processes occurring during PBF builds have a significant impact on many of these process-relevant powder properties, which limits the re-usability of un-sintered PA-12 powder. Subsequently, the properties of PBF components made from re-used powder are

also heavily dependent on aging and degradation. It is therefore important to have a holistic understanding of the aging phenomena that may take place during both LS and MJF, as well as the effect that each specific aging process has on PA-12 powder. Similarly, some insight into necessary characterisation techniques required to detect such changes in powder behaviour is equally important. During PBF, the powder bed temperature of 150 °C to 170 °C is just below the T_m of PA-12. Exposure of PA-12 to high temperatures during the build can result in multiple physical aging and chemical degradation processes which could all occur simultaneously during a build cycle [16-18, 21, 23, 38, 51, 53]. An extensive understanding of these processes is imperative to improving the re-usability of PA-12.

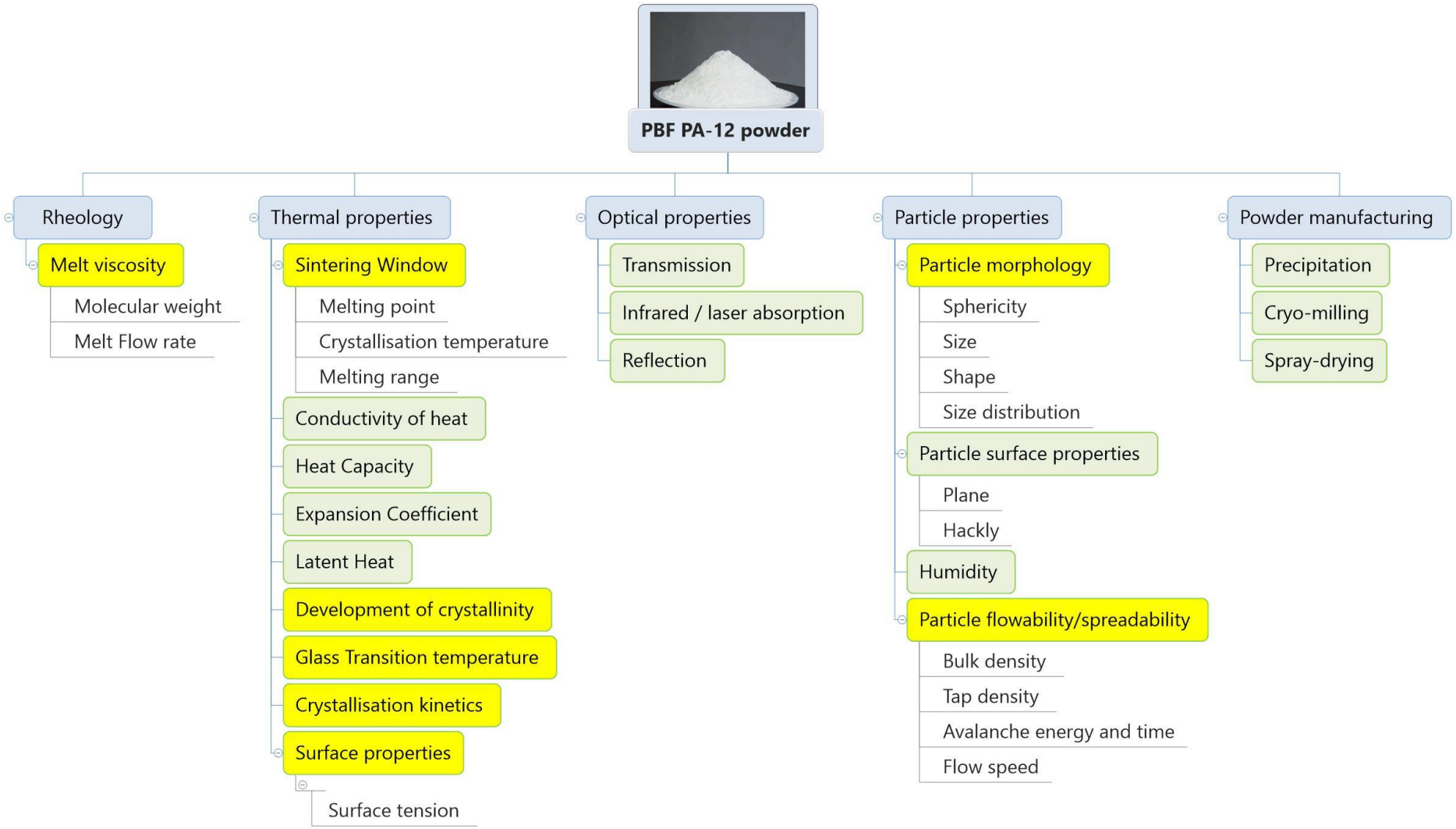

Figure 3.1 - The key polymer properties which have an impact on the fabrication of parts using PBF. Highlighted regions emphasise parameters which may be affected by aging and degradation processes. Adapted from [64].

3.2.1 Solid-state polycondensation

Solid-state polycondensation (post-condensation) is a step growth reaction which can occur between T_g and T_m [21, 26, 158], therefore may be active at the common PBF bed temperature of 150 °C to 170 °C. Polycondensation describes linear macromolecular chain growth through reactions of end groups, causing increased molecular weight (M_w) [15, 21, 26, 53, 65]. At elevated temperatures, increased molecular mobility of amorphous polymer chains allows reactive amide linkages and open chain ends of adjacent sequences to connect [16, 24, 26, 38]. More specifically, C=O and O-H end groups combine into a COOH functional group, which frees up NH_2 chain ends, under H_2O elimination *(Figure 3.2)* [21, 24-26, 38, 42, 51, 159, 160]. This process is thought to occur exclusively in the amorphous phase where polymeric chains have the freedom and mobility to connect; within crystalline regions chain mobility is restricted.

LS provides the ideal conditions for solid-state polycondensation due to the high bed temperature, long reaction times and inert, or low oxygen, atmosphere [21, 24, 38]. High temperatures increase the rate of polycondensation [21, 24, 28, 38], whilst end group concentration and degree of crystallinity also influence the extent and rate of the reaction [21, 26, 61, 158]. In addition, although polycondensation is usually a reversible process, an inert atmosphere shifts the equilibrium towards continuous water removal [15]. This effectively renders polycondensation non-reversible under LS conditions, resulting in high rates of chain lengthening.

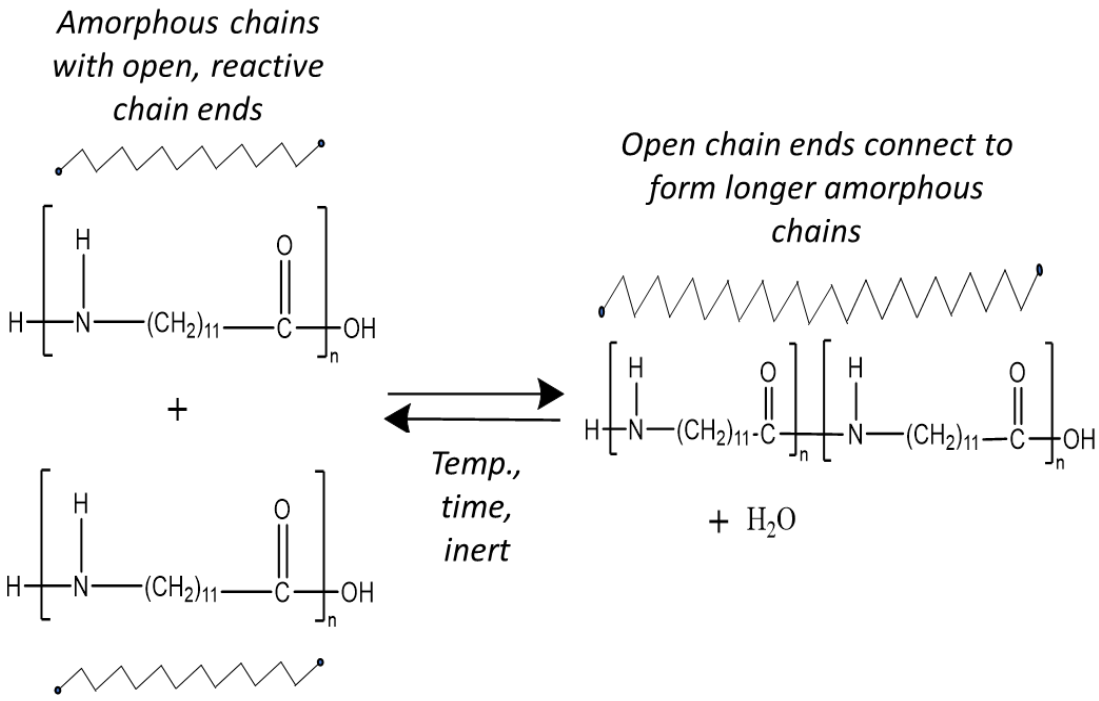

Figure 3.2 - Diagram showing the equilibrium equation for polycondensation, whereby two PA-12 chains combine with elimination of water.

Previous studies have attempted to explore the extent of polycondensation, during PBF, using a range of characterisation techniques. Increases in M_w can be quantified using size exclusion chromatography (SEC). Wudy and Drummer recycled EOS GmbH PA2200 PA-12 powder (EOS PA-12) across 5 build cycles in a Sinterstation 2000 LS machine, whereby the recovered un-sintered powder was re-used in the next build without refreshing with any virgin powder. Across a total cumulative build time of 26.6 hours, they observed an increase in the average M_w from 32,900 $gmol^{-1}$ to 61,100 $gmol^{-1}$. By utilising a linear Mark-Houwink plot, they showed that increases in M_w were a result of linear chain growth, whilst cross linking and chain branching were insignificant [26].

However, Sillani et al., observed a more significant increase in M_w following the re-use of PA-12 within a different LS system. The M_w of virgin 3D systems Duraform

PA-12 powder increased from 49,734 $gmol^{-1}$ to 134,120 $gmol^{-1}$ after only one build cycle in the DTM 2500+ LS machine, which represents a 170% increase in M_w [15]. Sillani et al., also analysed the behaviour of MJF HP 3D high reusability PA-12 (HP PA-12). There was only a relatively insignificant 17.5% increase in M_w over one MJF build cycle, which suggests that the extent of polycondensation during MJF is minimal [15]. This may be explained by the different processing conditions, such as an increased presence of oxygen, whilst it has also been reported that HP PA-12 polymer chains are “end-capped” to prevent degradation via polycondensation [15, 20]. Therefore, previous investigations into the change in M_w of PA-12, during a PBF build cycle, emphasise the complexity of the polycondensation process. It also indicates the variation between different PBF powder types, and machines, highlighting that material aging is multi-factorial and various processing parameters will also alter the extent of polycondensation.

Multiple studies have also characterised polycondensation by analysing the change in thermal properties of PA-12 using differential scanning calorimetry (DSC). Longer polymer chains may exhibit hindered mobility due to increased chain entanglements and knots, which postpones the crystallisation process because more energy is required for chain ordering [161]. As a result, polycondensation is thought to cause reductions in crystallisation kinetics and decreases in crystallisation temperature (T_c) [16, 17, 26, 28, 38, 51, 87]. It has also been reported that polycondensation increases T_m [15, 24-26, 38, 41, 61, 67, 159, 160]. For example, Pham et al., observed a 5 °C increase in T_m, and 3 °C decrease in T_c when EOS PA-12 powder was recycled across 3 build cycles with a total cumulative build time of ~120 - 150 hours [16]. Polycondensation increases M_w and causes a rise in the number of amide groups, resulting in additional hydrogen bonding within the polymer chains

[23, 24, 26]. As such, it is suggested that more energy is required to fully breakdown these longer chains, which causes an upwards shift in the melting point [24, 41, 159, 160]. However, these studies give no explanation as to how a process which occurs exclusively in the amorphous phase could significantly influence the size, stability, and melting temperature of crystalline spherulites. Furthermore, due to the relatively long hydrocarbon chain present between amide groups within PA-12, any increase in chain length and M_w, as a result of polycondensation, are unlikely to cause a substantial rise in the number of amide groups. Therefore, it is hard to envisage that changes to the amide group density would be significant enough to cause an increase in melting temperature. Consequently, the possibility of secondary crystallisation *(section 2.3.2)* occurring simultaneously within PA-12 during the PBF build process, requires more attention *(section 3.2.2).*

Within current PBF literature, plastic melt flow rate (MFR) is the most common method for reporting changes in the properties of PA-12 powder as a result of polycondensation. Multiple studies have found that with increased storage of PA-12 powder at elevated temperatures, there is a reduction in MFR which corresponds to increased polymer viscosity and reduced flowability of the melt [15, 16, 18, 21, 24, 26, 28, 41, 51, 53, 61, 159, 160]. These changes can be explained by increased chain length and M_w, as a result of polycondensation. Some studies used MFR to show that chain growth via polycondensation occurs primarily on thermally unstressed (virgin) powder, but such growth cannot maintain the same rate within used powder [18, 24]. Riedelbauch et al., re-used HP PA-12 across six MJF processing cycles; during the first build, MFR decreased from 84 $cm^3 10min^{-1}$ to 30 $cm^3 10min^{-1}$, but with continued powder re-use a plateau occurs and there is no further change across the next five cycles [24]. This suggests there is a point of

maximum chain growth, whereby there are no more active end groups available for polycondensation to occur [18, 21, 24, 53, 158].

MFR values have also been used previously to define the refresh ratio [49], and one study concluded that a powder MFR > 26 g10min^{-1} will produce a LS component with sufficient properties [17]. However, the use of MFR as a metric for powder quality is limited in that it only measures one material property: melt viscosity. This prevents complete understanding of the underlying aging processes. Similarly, MFR is energy intensive, and it takes a long time to obtain results that can be inconsistent, so it is not the most cost-effective measurement tool. A further limitation of MFR tests is that, within previous studies, critical experimental parameters such as the specific dies, weights, and plate geometries used, are not standardised across different studies. This is an important consideration because alterations to these parameters will affect the shear rate and, subsequently, the measured viscosity of the material. Additionally, it is unlikely that a MFR test replicates the conditions that PA-12 is exposed to during the PBF process, so any measurements of viscosity and flow may not be accurate in the context of a PBF build cycle. Therefore, a more extensive use of multiple characterisation techniques to measure the quality of PA-12 powder would provide a holistic understanding of the effect of aging during PBF. Similarly, focussing on more process relevant powder properties, such as particle morphology and flowability, will reveal more direct information about the effect of powder re-use on the properties of final parts.

3.2.2 Secondary crystallisation of PA-12

Storage of semi-crystalline polymers at elevated temperatures can cause further developments in crystallinity via secondary crystallisation. As discussed in *section 2.3.2,* there are various different theories that seek to explain how secondary crystallisation occurs, but the most prominent mechanisms are lamellar thickening and lamellar insertion.

During PBF, un-sintered PA-12 powder within the build chamber is exposed to elevated temperatures for long time periods. As a result, amorphous polymer chains exhibit enhanced chain mobility and the capacity to undergo secondary crystallisation via either lamellar thickening or lamellar insertion. Therefore, the PBF build process provides ideal conditions for secondary crystallisation to occur; this could have a significant effect on the resulting quality and performance of fabricated parts. During crystallisation, PA-12 displays a volume shrinkage which reduces the dimensional accuracy of printed parts [162, 163]. Further developments in crystallinity and alterations in crystalline morphology, as a result of secondary crystallisation, could heighten the effects of this shrinkage process. In addition, secondary processes may cause variations in the structure and morphological stability of the material, which ultimately affects the material properties. For example lamellar insertion forms unstable, thin lamella, leading to premature melting and a reduction in thermal stability [113]. In contrast, the tensile strength, stiffness, and thermal conductivity can all be enhanced by thicker lamella [99, 164]. Despite its importance to the processability of PA-12 powder within PBF, and the subsequent properties of fabricated parts, previous work investigating secondary crystallisation within PA-12 is limited.

Previous studies have begun to explore the crystallisation behaviour of PA-12 powder when storing the material under similar time-temperature profiles to those found in PBF [24, 38, 159, 165, 166]. However, these investigations are more related to the polymorphic nature of PA-12, and the transformation between different crystal phases that can occur upon heating. Gogolewski et al., reported that thermal annealing at temperatures greater than 160 °C triggered a gradual growth of the alpha-prime (α') crystal phase. Furthermore, Dadbakhsh et al., used wide angle x-ray scattering (WAXS) to show an α'-crystal structure is present within EOS PA-12 powder, whilst LS parts display the gamma (γ) form [38].

Increases in crystallinity as a result of secondary crystallisation can be detected using DSC by monitoring alterations in the shape, size, area, and position of the endothermic melting peak. This allows changes in peak T_m and enthalpy of fusion, which is directly related to percentage crystallinity (X_c), to be measured. Previous PBF studies have commonly reported increases in the T_m of PA-12 powder, as a result of thermal aging or powder re-use [24-26, 41, 51, 160, 167-169]. However, authors almost exclusively attribute increases in T_m to the polycondensation process, and reports of secondary crystallisation occurring during a build cycle are rare.

Similarly, there is contradiction and inconsistent trends within the few papers which do measure the change in crystallinity of PA-12 powder, as a function of powder re-use [24, 38, 168, 169]. For example, Dadbakhsh et al., presented an increase in the crystallinity of PA-12 powder, from 44% to 48%, across just one build cycle; however they attributed the increase in crystallinity to a rise in M_w, as a result of polycondensation [38]. This explanation indicates that there is confusion surrounding the effect of some aging processes on the morphology and microstructure of polymers. Polycondensation leads to greater chain lengths and, subsequently,

increased chain entanglements which create more disorder and knots within the polymer. Therefore, polycondensation is more likely to restrict chain mobility and prevent amorphous chains rearranging into a rigid crystalline structure via secondary crystallisation. This lack of understanding may be related to the complexity of secondary crystallisation, whereby there are numerous different theories and models, leading to inconsistencies and contradictions within the literature. Consequently, further work is required in order to understand the specific mechanism by which secondary crystallisation occurs when PA-12 is exposed to similar conditions to those found within a PBF build chamber. In the context of PBF this is significant because industry practitioners need to be aware of how secondary crystallisation can alter the properties of PA-12 powder, its ability to be reused in multiple build cycles, and the effect these changes have on the performance of final fabricated parts.

3.2.3 Degradation processes

The term “thermal degradation” refers explicitly to the effect of high temperatures, independent of the surrounding atmospheric conditions [66, 166, 170]. Levantovkay suggested that thermal degradation of polyamides only occurs at temperatures >250 °C [170]; however, the rate and extent of thermal degradation can be significantly increased by a heightened oxygen content and humidity. Within MJF, un-sintered PA-12 powder is prone to thermo-oxidative degradation due to a high bed temperature of 150 °C to 170 °C, combined with the presence of oxygen [171]. Similarly, despite LS machines operating with an inert atmosphere, processing of PA-12 into powder at elevated temperatures could cause the formation of free radicals [166], whilst laser radiation could also instigate oxidation [54, 168]. Both of these factors could lead to accelerated degradation during LS. In addition, a small

amount of unavoidable, residual oxygen (2-5%) is usually present within a LS build chamber, so thermo-oxidation becomes a distinct possibility [35, 38, 168]. Therefore, it is necessary to thoroughly investigate the various degradation processes that may occur when re-using PA-12 powder within both LS and MJF.

3.2.3.1 Thermo-oxidation

Thermo-oxidative degradation, also known as thermo-oxidation, is the integrated effect of heat and oxygen. Under extreme storage conditions, i.e., high temperatures for long periods, thermo-oxidative degradation can occur via an auto-oxidation mechanism [66, 168, 170, 172, 173]. As shown in *Figure 3.3,* the auto-oxidation cycle begins with the generation of polymer radicals via the separation of hydrogen. These radicals react with oxygen in the surrounding atmosphere to form peroxyl radicals. At this stage, oxidation can occur with a low activation energy and accelerate, without an induction period, due to the production of highly destabilised alpha amino hydroperoxides [173]. At the end of the auto-oxidation mechanism there are ultimately two different outcomes. Termination can occur via recombination of two or more radicals which results in the production of macroradicals. This is expected to occur through a chain reaction involving peroxide formation, resulting in cross-linking and the formation of tie-molecules [82, 83, 159]. Conversely, hydroperoxides can decompose to alkoxy radicals which abstract hydrogen atoms from the polymer backbone via chain scission, leading to the formation of various unstable oxidation products [172, 174-176]. The dominant outcome of the thermo-oxidation mechanism is dependent upon the type of polymer, environmental conditions, and time/temperature dependencies [23, 53, 66, 83].

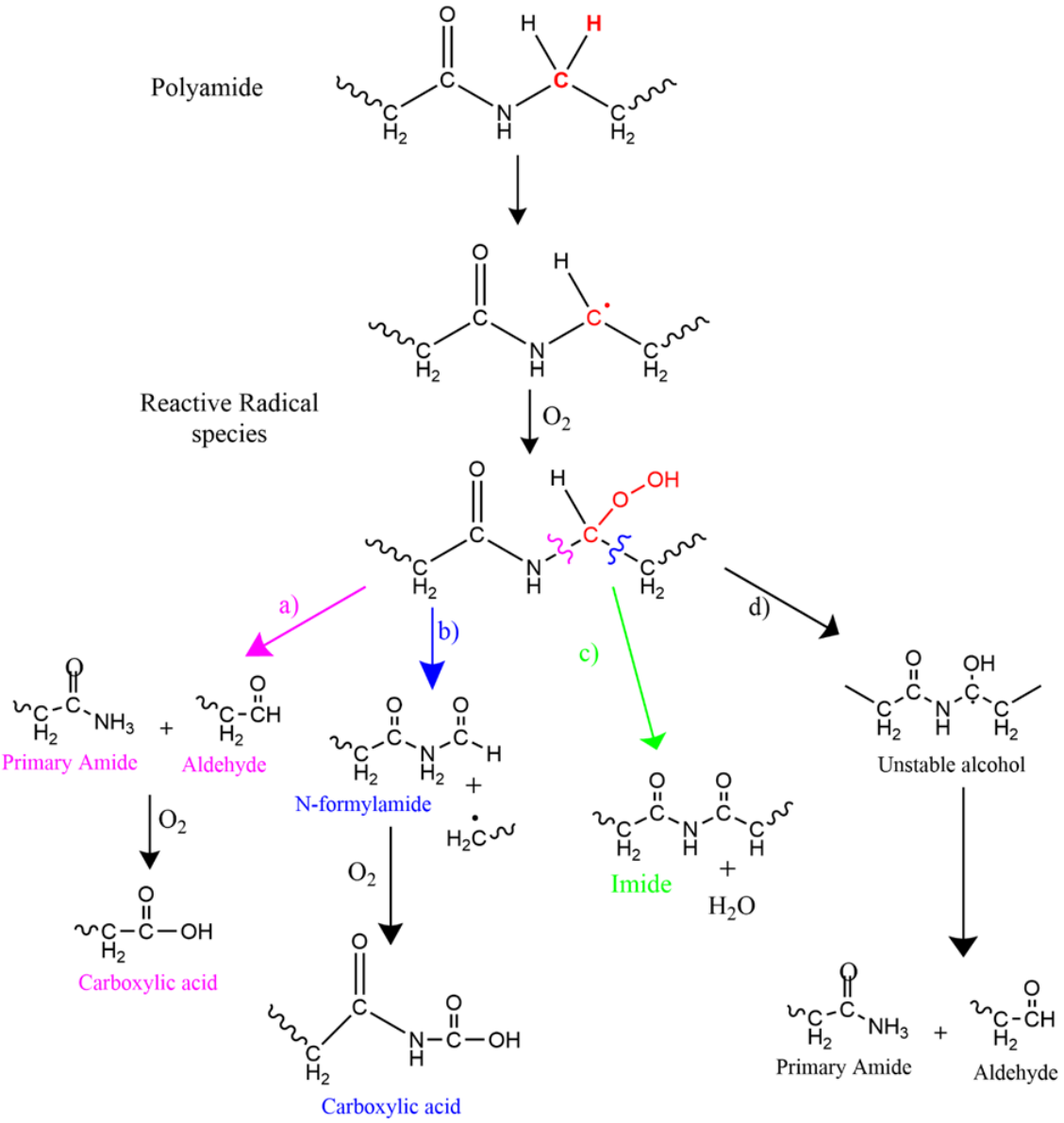

Figure 3.3 - Schematic displaying the expected thermo-oxidation mechanism of PA-12 based on literature reports for other polyamide structures [174, 175].

3.2.3.1.1 Cross-linking

Cross-linking involves the formation of covalent bonds between polymer chains, which leads to increased molecular weight [25, 38, 66, 82]. Such cross-links, also known as tie-chains, are molecular connections which form in interlamellar amorphous regions and effectively act as bridges holding crystallites together [75, 82, 83]. It has been suggested that in the presence of oxygen, polyamides undergo

cross-linking at temperatures >140 °C [159]. Elevated temperatures increase the thermal energy present within the polymer, so amorphous chains obtain the sufficient mobility required for the development of cross-links. However, depending on the M_w of the material, cross linking can also occur in an inert, or low oxygen, environment. This can be explained by a study from Seguela, which suggests that above a certain critical molar mass, amorphous chains become intertwined into a macro-molecular network. Due to the elevated molecular weight, there is an increased volume of entanglements which cannot contribute to crystallisation. Instead, intertwining chains belonging to two adjacent crystallites can form a bridge between the crystalline regions, resulting in the formation of tie-chains [82].

This would suggest that cross-linking can occur under the conditions present during both LS and MJF. In fact, some authors have suggested that, within oxygenated conditions, degradation of PA-12 occurs primarily via chain scission, whilst cross-linking becomes more predominant in an inert atmosphere [177, 178]. However, a limitation of primarily using conventional characterisation techniques such as MFR, is that it can be difficult to differentiate cross-linking from polycondensation because both processes cause increases in M_w and melt-viscosity. Some studies have attributed reductions in MFR to cross-linking [24, 66, 168], but generally cross-linking is often overshadowed by polycondensation within PBF studies, particularly those aiming to replicate the inert atmosphere found within a LS build chamber. This can become problematic because cross-linking will have different effects on the behaviour of PA-12 powder, its suitability for re-use, and the mechanical properties of final parts *(section 3.2.5)*.

3.2.3.1.2 Chain scission

Chain scission involves random cleavage of the polymer backbone, which results in a rapid decrease in M_w [24, 179]. In polyamides, scission occurs primarily at the α methylene group, whereby the C-H bonds are adjacent to the nitrogen in the amide unit; these are the weakest bonds because they contain the most mobile, and reactive hydrogen atoms (*Figure 3.4)* [54, 170, 172, 173, 175, 180, 181]. Some have hypothesised that diffusion of oxygen and water cannot happen in crystalline regions of the material [173, 175, 176]. However, others suggest oxidative degradation occurs via a two-step process. Firstly, preferential attack of the more easily accessible amorphous chains, before degradation of crystalline regions, which coincides with polymer mass loss [182, 183]. Regardless, chain scission due to thermo-oxidation (and hydrolysis, *section 3.2.3.3*) is thought to occur primarily in the amorphous phase.

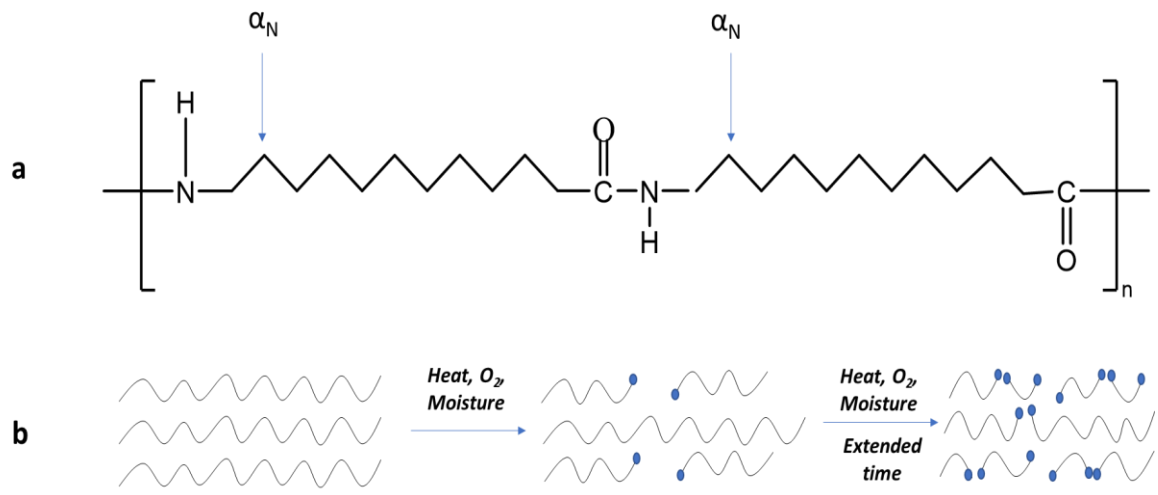

Figure 3.4 - a) Molecular structure of PA-12, methylene carbon adjacent to the amide nitrogen is donated by α_N and shown by an arrow. The α_N carbon is the weakest link in the polymer chain so most susceptible to oxidative chain scission. b) Random chain scission in a linear polymer chain.

Chain cleavage removes hydrogen atoms from the polymer backbone, resulting in multiple oxidation by-products, such as aldehydes and carboxylic acids [172, 174-176]. The generation of imide groups following oxidative chain scission has also been reported [166, 172-175, 180, 181]. These new functional groups, and other changes in polymer morphology, have previously been observed within various polyamide materials using Fourier transform infrared spectroscopy (FTIR) [166, 172, 175, 180, 181, 184]. Additionally, chain scission can result in substantial and rapid reductions in molecular weight which significantly effects the thermal and mechanical properties of polyamide materials [66, 166, 172, 180]. Another indicator of thermo-oxidation is sample discolouration (yellowing) [172, 174, 180, 181, 185], which is thought to occur due to the formation of different functional groups, e.g., reaction of amine end groups [172, 186]. Alternatively, the production of pyrrole derivatives increases the amount of chromophore, which may trigger yellowing [180, 181].

It has been suggested that, with a long enough exposure time, thermo-oxidation can occur at temperatures as low as 80 °C to 90 °C [170]. However, the higher temperatures present within the oxygenated MJF build chamber would accelerate the process [66, 181], so thermo-oxidative chain scission is likely to occur with extended powder re-use. However, due to the MJF process being a relatively new PBF process, previous work is often focussed on replicating LS build conditions; only a few studies have investigated long term storage of PA-12 powder under oxygenated conditions. Wudy et al., compared the change in MFR of PA-12 powder samples stored for up to 128 hours, at 175 °C, in air, vacuum, and nitrogen oven conditions. For all three storage types there was initially a large reduction in MFR, which is caused by cross-linking. But, with storage between 32 and 128 hours in air, there is a substantial increase in MFR, whilst no further change is observed in the

other two conditions. A higher MFR indicates improved melt flowability due to the shorter chain molecules present following thermo-oxidative chain scission [66]. Furthermore, Pandelidi et al., exposed polyamide-11 (PA-11) powder to thermo-oxidative aging at 180 °C, for up to 168 hours. Parallel plate rheology illustrated a reduction in complex viscosity, which suggests a decrease in chain length and a lower chain entanglement density, indicating that chain scission can occur after only 24 hours of oven conditioning [177].

3.2.3.2 Chemi-crystallisation

Due to the macromolecular nature of semi-crystalline polymers, a high number of entanglements is expected to be present in the melt. This entangled system restricts the crystallisation process because long polymer chains are unable to easily organise and align into an ordered structure [187]. However, thermo-oxidation can cause chain scission of amorphous chains resulting in a polymer system with a greater number of short chain molecules. This allows further crystallisation via rearrangement of the smaller, and subsequently more mobile, polymer chains [176, 187, 188]. This process is known as chemi-crystallisation and can enhance the degree of crystallinity as a result of degradative chain scission [166, 174, 176, 187, 188].

Chemi-crystallisation can increase the degree of crystallinity via aforementioned secondary crystallisation mechanisms. Molecular segments freed by chain scission can incorporate into pre-existing crystals through lamellar thickening, or new crystals can form in the bulk of the amorphous region via lamellar insertion [176, 187, 188]. Crystals formed by chemi-crystallisation can be identified from primary crystals because they grow from segments that become progressively more defective as exposure to degradation continues [187]. As such, chemi-crystallisation is thought to

create less stable crystalline regions, because they are formed from imperfect molecules, in less favourable conditions. This can result in a material with inconsistent thermal and mechanical properties since the new crystals will likely have lower melting temperatures and an increased defect content [176, 187].

3.2.3.3 Hydrolysis

Thermo-oxidative degradation accelerates in the presence of moisture, through a process known as hydrolysis [54, 166, 170, 180, 188]. PA-12 is hydrophilic and has a strong affinity for water due to the existence of amide groups and hydrogen bonding within the polymer system. As such, PA-12 is sensitive to chain scissions when exposed to an environment containing moisture, for example high humidity, or when water is present within the material [166, 188]. During hydrolysis, similarly to the oxidation mechanism, sorption of water occurs primarily in the amorphous phase and interactions between water molecules and hydrogen bonds results in an increased number of chain scissions [180, 188]. Ingress of water molecules into the polymer can also mobilise amorphous chains, enhancing the rate of diffusion of oxygen into the polymer, which subsequently increases the rate of thermo-oxidation [54, 170]. Within PBF, an advantage of PA-12 is a relatively long methylene sequence, which decreases the amide group concentration [54-56]. As a result, PA-12 has reduced polarity and a lower affinity for water compared to other, shorter-chain polyamides. Nonetheless, the issue of hydrolysis persists so controlling the moisture content of PA-12 during powder storage, handling, and re-use is vital.

3.2.4 Interaction between aging processes during PBF

During a PBF build, there is an interplay between the different aging and degradation processes which may occur within un-sintered PA-12 powder. At the powder bed

temperature, multiple aging phenomena can take place simultaneously and interact with each other [24, 28]. This creates a complex aging mechanism which is problematic for the PBF industry because there can be inconsistencies in the properties of different batches of powder. These aging processes are also influenced by temperature, time, and the specific processing conditions *(Figure 3.5),* thus the dominant aging process when re-using powder in multiple build cycles, is prone to change and difficult to predict.

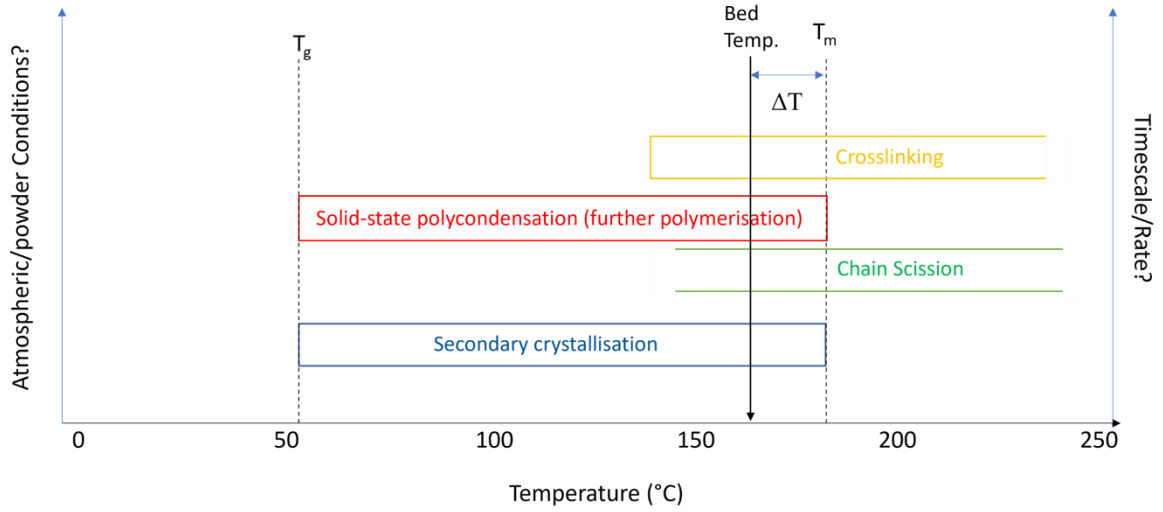

Figure 3.5 - Illustrates that at the bed temperature, there are 4 key aging processes that are likely occurring simultaneously. These processes will have an effect on each other, whilst also having collective and opposing effects on PA-12 powder properties.

For example, chain scission alters the morphology of PA-12, forming shorter polymer chains which are able to align more easily into an ordered crystalline structure. As such, chain scission can increase crystallinity through chemi-crystallisation [176, 187, 188] . Conversely, secondary crystallisation can be hindered by cross-linking and polycondensation because tie molecules and chain entanglements restrict motion of polymer chains, preventing reorganisation of amorphous regions into a

more aligned arrangement [16, 17, 23, 26, 28, 38, 51]. However, alterations in polymer structure, such as increased crystallinity, can restrict motion of reactive polymer chains which raises the activation energy for cross-linking [83]. Further examples of the interaction between the various aging processes that can occur during a PBF build are summarised in *Table 3.1.* Evidently, the chemical and physical aging of PA-12 during PBF is a multifaceted problem. Understanding the interaction between these processes, and how that relationship may change when PA-12 powder is stored for long periods of time, across multiple build cycles, is vital to improving the re-usability of PA-12.

Table 3.1 – Aging mechanisms of PA-12 powder within powder bed fusion processes.

	Solid-state Polycondensation	**Secondary crystallisation**	**Cross-linking**	**Chain scission**	**Hydrolysis**	**Chemi-crystallisation**
Type of aging	Chemical	Physical	Chemical	Chemical	Chemical	Chemical
Reversibility	Reversible (under the right conditions)	Reversible	Irreversible	Irreversible	Irreversible	Reversible
Cause	High temperatures whereby: T_g < temp. < T_m Accelerates in inert atmosphere. Long reaction times Laser radiation Microstructure – e.g., end-group concentration	High temperatures whereby: T_g < temp. < T_m	High temperatures Oxygen content Laser radiation Time dependent	High temperatures Oxygen content Laser radiation Longer time periods	High temperatures Presence of water/moisture	Rearrangement of short amorphous chains following chain scission High temperature
Effects on PA-12 powder properties	Increased M_w Increased T_m Reduced T_c Reduced crystallisation kinetics Reduced % crystallinity (X_c) Reduced MFR / MVR Increased melt viscosity	Increased X_c Increased T_m Transition between α' & γ crystal structures Increased lamellae thickness Growth of larger spherulites	Increased M_w Increased melt viscosity Reduced MFR Reduced crystallisation kinetics Reduced T_c	Decreased M_w Mass loss Oxidation by-products e.g., imide groups Discolouration Increased MFR	Increases the rate & extent of chain scission, so has the same effect on PA-12 powder.	May cause reduced T_m. Increased X_c Formation of imperfect, less stable crystalline regions
Interaction with other aging processes	*Secondary crystallisation* – rate of polycondensation is dependent upon degree of crystallinity, as the reaction occurs in amorphous regions. On the other hand, it reduces the rate of *secondary crystallisation* due to the entangled polymer chains following polycondensation	*Polycondensation* – increased M_w hinders secondary crystallisation. *Cross-linking* – formation of tie chains restricts chain mobility. Conversely, increased X_c may raise the activation energy for *cross-linking*	Hard to differentiate from *polycondensation* as both processes have similar effects on powder properties. Reduces likelihood of *secondary crystallisation* due to restricted chain mobility	Can lead to *chemi-crystallisation & secondary crystallisation* due to reduced chain length	Increases *chain scission*, so could also contribute to *chemi-crystallisation*	Caused by *chain scission. Polycondensation & cross-linking* would prevent chemi-crystallisation occurring.

3.2.5 Effect of powder re-use and aging on part properties

Assuming that the PA-12 powder used in the build contains recovered powder, aging and degradation processes have the potential to significantly affect the properties of final parts. This is particularly problematic when the refresh ratio is insufficient or if the used powder is severely degraded. When producing final components with recycled, used powder, the fabricated parts commonly experience a variation in their mechanical properties, higher shrinkage, and a rough surface finish known as "orange peel" *(Figure 3.6)* [16, 17, 23, 26, 38, 160]. Previous studies have measured the change in surface roughness of PBF parts using a profilometer. Crane et al., showed that a novel post-processing, chemical surface enhancement technique, known as PUSh™, can reduce the average surface roughness (R_a) of LS PA-12 parts from 21.8±6.8 µm to 6.1±1.6 µm [189]. The PUSh™ process utilises automated solvent vapour smoothing technology; as the solvent condenses onto the surface of a part, it forms a boundary layer which is able to flow, fill up pores, and smoothen the surface of the fabricated part [189, 190]. In addition, Petzold et al., found that the R_a of LS parts made from virgin PA-12 powder is 13.2 µm; this value rises by 8.8 µm when LS parts are fabricated from recycled PA-12 powder [191]. Virgin MJF parts also display similar R_a values [192]. However, to the best of the authors knowledge, no previous papers have quantified the effect of extended powder re-use, across multiple build cycles, on the surface quality of PBF parts.

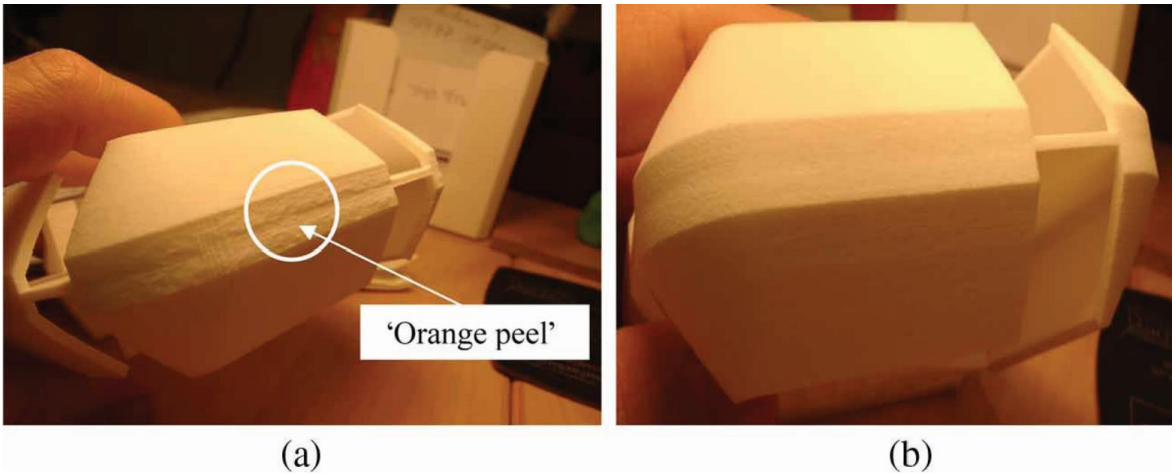

Figure 3.6 – LS components displaying (a) orange peel texture and b) an acceptable surface finish [16].

Changes in the physical properties of PBF parts, in particular porosity and density, are also caused by a deterioration of feedstock powder quality as a result of material aging. For example, polycondensation and cross-linking cause increases in M_w, reduced melt flowability, and hindered material coalescence [50, 53, 168, 169]. This leads to increases in part porosity [38, 53, 154, 169]. Furthermore, due to either secondary crystallisation or polycondensation, aged powder likely contains particles with a higher melting temperature. Assuming the processing parameters are kept constant for each build, these higher melting point, "nascent" particles may remain unmolten, which prevents a homogeneous melt and limits part density [23, 38, 53, 168]. Within industry, monitoring porosity is vital because an increase in the number and size of pores will likely result in a significant reduction in the mechanical performance of final components.

As such, the ultimate tensile strength (UTS), Young's modulus (E), and elongation at break (EAB) of fabricated parts, which are crucial for functional applications within PBF, can be affected by powder re-use and subsequent material aging [23, 24, 35,

38, 53, 168, 193]. The standard mechanical properties of parts produced from new, virgin powder are generally well understood; however, there are inconsistencies in the literature regarding the effects of PA-12 powder re-use on the properties of LS and MJF parts *(Table 3.2).* Several studies have claimed no significant change in UTS, E, and EAB within parts made using re-used, aged powders [24, 51, 53, 160], whilst others reported a reduction in strength and stiffness with increased build number [49, 66, 169, 194]. On the other hand, it has been suggested that aging processes are time dependent, so with increased cycle number, there could be two opposing trends in terms of the effect of re-use on the mechanical properties of PBF parts. Furthermore, the results of these studies often contradict each other [169, 193]. Alo et al., observed a 27.8 MPa reduction in strength for the first 6 build cycles, followed by a 21.5 MPa increase in UTS with further powder re-use across build 6 to build 8 [169]. Conversely, Yao et al., stated an initial 6.7 MPa increase in strength between builds 1 and 2, before a 9.5 MPa reduction in UTS across the next 7 build cycles [193].

Therefore, there is significant debate surrounding the effects of powder re-use on the quality and performance of PBF parts. Inconsistencies in the results of previous studies can be explained by many factors. Firstly, within the studies shown in *Table 3.2,* there are variations in PA-12 powder grade, PBF machine, processing parameters, and testing conditions; all of which may have an effect on the success of the print and the resulting mechanical properties of the part *(section 3.1).* Nonetheless, *Table 3.2* does not appear to show any clear trends in terms of the specific effects of any particular build parameter, and there were further inconsistencies between studies. Zarringhalam et al., showed that LS parts had a higher strength, modulus, and elongation at break when operating with a significantly

greater laser power [51]. It is expected that increasing laser power ensures complete fusion of particles, which increases layer-layer bonding and limits porosity development. In contrast, Wudy and Drummer used a substantially lower laser power of only 7.8 W and virgin parts displayed a higher UTS than parts made using a laser power of 45.7 W [53]. Therefore, multiple other build parameters such as build chamber temperature, scan speed, scan spacing, and layer thickness must also have a significant impact on the mechanical and structural properties of PBF parts [35]. Identifying the most appropriate build parameters for printing with either virgin or used PA-12 powder would help to improve the performance of PBF components. Nonetheless, that is beyond the scope of this project, which focusses specifically on the effects of powder re-use and material aging. With repeated powder re-use, multiple aging and degradation phenomenon can occur simultaneously, with an interplay between the conflicting and harmonious effects of each aging mechanism *(*as shown in *Table 3.1).* This creates a highly convoluted problem, whereby the effects of aging on mechanical properties of PBF parts are almost impossible to predict, therefore the resulting performance and serviceability of parts is uncertain.

The aforementioned reductions in UTS can be attributed to changes in powder properties, such as melt flowability, as a result of polycondensation *(section 3.2.1)* and cross-linking *(section 3.2.3.1.1)* [49, 66, 169, 194]. However, others have suggested that an increased cross-link density promotes intermolecular interactions, and creates more complex molecular chains, which ultimately enhances the strength and stiffness of LS parts [169, 193]. Similarly, increases in M_w and chain entanglements, due to polycondensation, can lead to a higher cross-link density with stronger Van der Waals forces, resulting in a higher tensile strength [35, 195]. This

emphasises how polycondensation and cross-linking are closely linked, yet there is uncertainty and disagreement surrounding their impact on the functionality of end-use PBF parts.

It is also important to try and isolate polycondensation from secondary crystallisation *(section 3.2.2)* because each of these processes will have an opposite effect on part crystallinity and, subsequently, mechanical behaviour. Increased crystallinity, due to secondary crystallisation, causes improved intermolecular bonding, which may increase the strength and stiffness of final parts [35, 51, 160, 193, 196]. However, highly crystalline parts are also expected to be more brittle [35, 43, 50]. Conversely, polycondensation causes increased chain length and entanglement which hinders crystallisation and reduces the crystallinity of final parts, so components are expected to be more ductile, but weaker [38, 51, 168]. More confusion arises when considering thermo-oxidation. Chain scission *(section 3.2.3.1.2)* is a degradation process which causes deterioration of a polymers macromolecular structure, reducing the number of covalent bonds and Van der Waals forces present within the chain. Therefore, thermo-oxidative chain scission is expected to lower the tensile strength [35, 180], as well as cause significant part embrittlement [166, 172]. Nonetheless, chain scission can ultimately lead to chemi-crystallisation *(section 3.2.3.2)*, which would have the opposite effect of increasing crystallinity, creating more interactions and bonding between chains, thus increasing part strength [166]. This represents another example where a single degradation process can influence the mechanical performance of PBF parts in two different directions.

Overall, due to the complexity of material aging as a function of powder re-use, printed parts are often of reduced quality, and this is a significant challenge which has hindered the advancement of polymer PBF processes.

Table 3.2 – Mechanical properties of PBF parts fabricated from PA-12 powder at different levels of aging/powder re-use.

Reference	Process Type	Number of re-use cycles	Reported printing parameters	Horizontal (XY) build orientation			Effect of build / powder re-use
				Ultimate tensile strength (MPa)	Young's modulus (MPa)	Elongation at break (%)	
[160]	Duraform PA-12 3D systems SLS2000	7 build cycles No refresh rate	N/A	Build 1 = 29.4 Build 4 = 27.6 Build 7 = 20.7	N/A	Build 1 = 3.5 Build 4 = 5.5 Build 7 = 7.8	No significant change in UTS until after build 5 EAB shows a small, gradual increase
[51]	EOS PA2200 PA-12 EOS P380 LS machine	Comparing parts made from virgin, once used, & once refreshed (70:30 RR) powder	0.15 mm layer thickness 45.7 W laser power 4000 mm/s scan speed 0.3 mm scan spacing	Virgin = 45.0 Refreshed =45.5	Virgin = 1750 Refreshed= 1750	Virgin = 14 Refreshed =18.5	In both systems there is an insignificant change in UTS & Young's modulus, as well as increased ductility
	Duraform PA-12 3D systems Vanguard LS machine		0.1 mm layer thickness 11 W laser power 5000 mm/s scan speed 0.15 mm scan spacing	Virgin = 37.5 Refreshed = 35 Used = 40	Virgin = 1600 Refreshed = 1400 Used = 1650	Virgin = 4 Refreshed = 7 Used = 12	
[66]	EOS PA2200 PA-12 3D systems Sinterstation 2000 LS machine	10 build cycles 50:50 RR	175°C pre-heating temperature 0.1 mm layer thickness 5 W laser power 1257 mm/s scan speed	Build 1 = 35 Build 5 = 5 Build 10 = 2	N/A	Build 1 = 5.3 Build 5 = 0.8 Build 10 = 0.2	Significant reductions in UTS and severe embrittlement
[194]	Sinterit PA-12 Sharebot SnowWhite LS printer	8 build cycles No refreshing	160°C plate temperature 0.1 mm layer thickness 14 W laser power	Build 1 = 31.7 Build 2 = 27.2 Build 5 = 21.9 Build 8 = 20.5	Build 1 = 1276 Build 2 = 1190 Build 5 = 985 Build 8 = 1035	Build 1 = 6.2 Build 2 = 5.5 Build 5 = 4.9 Build 8 = 4.6	Significant & gradual reductions in UTS Insignificant change in stiffness & EAB

[53]	EOS PA2200 PA-12 Research sintering station	5 build cycles Cumulative build time 42 hours No refreshing	172°C build temperature 100 µm layer thickness 7.8 W laser power 904 mm/s scan speed	Build 1 = 50 Build 3 = 48 Build 5 = 42	Build 1 = 1650 Build 3 = 1600 Build 5 = 1550	N/A	Insignificant change in UTS until build 4, then small reduction No change in stiffness
[23]	EOS PA2200 PA-12 DTM Sinterstation 2000 LS machine	5 build cycles 25 cumulative build time No refreshing	N/A	Build 1 = 49 Build 3 = 43 Build 5 = 38	Build 1 = 1800 Build 3 = 1550 Build 5 = 1500	Build 1 = 14 Build 3 = 14 Build 5 = 14	Significant reduction in UTS No change in stiffness or ductility
[38]	EOS PA2200 PA-12 DTM Sinterstation 2000 LS machine	Compares virgin, used, & refreshed powder Used powder exposed for '2-10 cycles'	170°C bed temperature 5W laser power 600 mm/s scan speed 150 µm scan spacing	Virgin = 32.7 Refreshed =32.2 Used = 25.2	N/A	Virgin = 18.5 Refreshed = 22.1 Used = 15.4	Reduction in strength, although refreshing does help restore part performance. Minimal change in ductility.
[193]	EOS PA2200 PA-12 EOS P110 LS machine	8 build cycles No refreshing	168°C build temperature 0.1 mm layer thickness 30 W laser power 1500 mm/s scan speed 0.15 mm scan spacing	Build 1 = 42.8 Build 2 = 49.5 Build 8 = 40.0	Build 1 = 1068 Build 2 = 1658 Build 8 = 824	Build 1 = 20 Build 5 = 26 Build 8 = 23	Strength and stiffness increase significantly after build 1 but then gradually reduces. EAB shows no significant change in XY orientation
[169]	EOS PA2200 PA-12 EOS Formiga P110 LS printer	8 build cycles Cumulative build time 77 hours no refreshing	169°C build temperature 30 W laser power 1500 mm/s scan speed 0.15 mm scan spacing	Build 1 = 40.6 Build 6 = 12.8 Build 8 = 34.3	Build 1 = 1450 Build 6 = 510 Build 8 = 1190	N/A	Significant reductions in strength & stiffness over the first 6 builds Significant increase in strength & stiffness between build 6 & build 8

Multi-Jet Fusion examples, including PA-11 & PA-12							
[24]	HP high reusability PA-12 HP MJF 3D 4200	5 build cycles RR varied: 0/100, 20/80, 40/60, 60/40, 80/20, 100/0	Balanced print mode	Build 1 = 46.9 Build 2 = 45.0 Build 5 = 44.5	Build 1 = 1446 Build 2 = 1467 Build 5 = 1437	Build 1 = 12.9 Build 2 = 14.5 Build 5 = 13.1	Insignificant change in all mechanical properties
[49]	HP 3D high reusability PA11 HP MJF 3D 4200	Compare parts made from virgin and used PA11 powder	Balanced print mode	Build 1 = 45 Build 2=39	Build 1 = 1421 Build 2 = 955	Build 1 = 21 Build 2 = 24	Significant reduction in strength and stiffness after just one-reuse cycle No embrittlement observed

3.3 Rationale of the work

There is a general lack of understanding regarding the convoluted aging mechanisms that occur within PA-12 during PBF. Similarly, the effect of aging on the behaviour of un-sintered PA-12 powder, and its suitability for re-use in future builds, is relatively unknown. Previous work has begun to investigate the aging and degradation of PA-12 in the context of PBF. However, many of these studies have attempted to quantify powder quality using specific material characterisation techniques, such as melt flow rate. Although MFR has some benefits, the aging behaviour of PA-12 during PBF is far too complex to be determined by a technique that effectively only measures one material property: melt viscosity. A more extensive classification of used PA-12 powders, utilising a wide range of characterisation techniques, is required in order to establish whether or not aged material is suitable for re-use in future builds.

Furthermore, the predominant utilisation of MFR has influenced PBF operators to focus primarily on the polycondensation process when considering the aging behaviour of PA-12 powder. Although polycondensation is a pivotal aging phenomenon, that absolutely affects the properties of PA-12 powder and its potential for re-use, the wider industry is largely naïve to various other aging processes that can occur simultaneously. Of utmost significance is secondary crystallisation, which has rarely been discussed in previous literature. Despite its importance to the processability of PA-12, the mechanism, rate, and extent of secondary crystallisation during a PBF build cycle is generally unknown. This is concerning because the secondary process not only has the potential to alter the properties of un-sintered PA-12 powder, but also the dimensional precision and mechanical performance of PBF parts. As a result, the current work involves an in-depth investigation into the

secondary crystallisation behaviour of PA-12 when it is exposed to conditions similar to those found in a PBF build chamber.

Finally, PBF components often display a wide range of physical and mechanical properties, which has hindered the widespread adoption of this technology for the production of functional, end-use parts. Subsequently, the most common application of PBF is currently limited to the development of prototypes. One of the main causes for inconsistent part properties is the complex, multifaceted aging behaviour of PA-12. With increased powder re-use, the quality of feedstock powder becomes progressively more unpredictable, particularly when operating with fixed refresh ratios that do not account for any variability in the properties of used material. Therefore, PBF part performance becomes very difficult to predict. As such, an enhanced understanding of the close relationship between aging, powder re-use, and subsequent part properties is necessary. This thesis determines the optimal characterisation techniques for quantifying powder quality, identifying a correlation between alterations in specific powder properties and the performance of fabricated parts. This insight could be utilised to improve the consistency of PBF parts, allowing the technology to be used more regularly for the production of functional, end-use components. Overall, the primary objective is to enhance the environmental sustainability and cost effectiveness of the PBF process, which faces ongoing challenges related to material waste due to inefficient powder re-use strategies.

CHAPTER 4 – THE EFFECT OF PHYSICAL AGING AND DEGRADATION ON THE RE-USE OF POLYAMIDE 12 IN POWDER BED FUSION

Published article.

Alterations to published article made within this thesis:

1. *Page 83 – Figure 4.3 – Caption altered to explain why there are variations in the starting values in Figure 4.3 b, c, and d.*

Polymers 2022, 14(13), 2682; https://doi.org/10.3390/polym14132682

Benjamin Sanders[1], Edward Cant[2], Hoda Amel[2], and Michael Jenkins[1]

1. School of Metallurgy and Materials, University of Birmingham, Elms Road, Birmingham B15 2SE, UK
2. The Manufacturing Technology Centre, Ansty Park, Coventry CV7 9JU, UK

Author contributions:

B.S. – conceptualisation, methodology, investigation, formal analysis, visualisation, writing original draft, draft review and editing; E.C. – conceptualisation, resources, draft review and editing, supervision; H.A. – conceptualisation, resources; M.J. – conceptualisation, methodology, draft review and editing, supervision.

4.1 Abstract

Powder Bed Fusion (PBF) is an Additive Manufacturing (AM) technique which offers efficient part-production, light-weighting, and the ability to create complex geometries. However, during a build cycle, multiple aging and degradation processes occur which may affect the reusability of the polyamide 12 (PA-12) powder. Limited understanding of these phenomena can result in discarding re-usable powder unnecessarily, or the production of parts with insufficient properties; both of which lead to significant amounts of waste. This paper examines the thermal, chemical, and mechanical characteristics of PA-12, via an oven storage experiment that simulates multi jet fusion (MJF) conditions. Changes in the properties of PA-12 powder during oven storage showed two separate, time-dependent trends. Initially, differential scanning calorimetry showed a 4.2 °C increase in melting temperature (T_m) and a rise in crystallinity (X_c). This suggests that secondary crystallisation is occurring instead of, or in addition to, the more commonly reported further polycondensation process. However, with extended storage time, there were substantial reductions in T_m and X_c, whilst an 11.6 °C decrease in crystallisation temperature was observed. Fourier transform infrared spectroscopy, a technique rarely used in PBF literature, shows an increased presence of imide bonds – a key marker of thermo-oxidative degradation. Discolouration of samples, an 81% reduction in strength and severe material embrittlement provided further evidence that thermo-oxidative degradation becomes the dominant process following extended storage times beyond 100 hours. An additional pre-drying experiment showed how moisture present within PA-12 can also accelerate degradation via hydrolysis.

4.2 Introduction

Polymer powder bed fusion (PBF) is a subset technique in additive manufacturing (AM) which has attracted attention because it offers great design freedom and high efficiency, as parts can be stacked freely in the powder bed [13, 14, 16-18]. Industrial sectors such as medical, aerospace and architecture have benefitted immensely from the use of additive manufacturing and more specifically PBF technology. This is a result of the advantages the technology offers including customization, light-weighting, and the ability to create complex geometries [46-49]. The most common PBF technique is laser sintering (LS) [13], but more recently HP introduced the multi-jet fusion (MJF) process [49]. Both processes involve storing thermoplastic powder at an elevated temperature, close to the melting point, before the localised application of heat to consolidate the material into a 3D part [13]. As per other AM methods, powder is added layer-by-layer into a geometry fabricated directly from a 3D-CAD model [13, 24].

Materials for PBF require a large processing window, in which the powder melting temperature (T_m) is significantly higher than the crystallisation temperature (T_c). Maintaining a high temperature in the build volume delays the crystallisation process during a PBF build, which reduces the residual stresses, prevents distortions, and provides a more homogeneous microstructure [22, 28, 38, 51, 197]. Due to its large processing window and the ability to form highly crystalline structures, polyamide 12 (PA-12) is the most widely used polymer in PBF [15, 21, 22, 38, 51]. Polyamides are also popular due to their high recyclability, which can be a major cost saving advantage [49, 198]. Nonetheless, PBF has a low powder utilisation rate whereby at least 80% of the powder deposited for each build cycle remains un-sintered [16, 23,

25, 26, 49]. For the process to be economically viable and environmentally sustainable, the un-sintered powder needs to be reused [16, 17, 21]. A key consideration regarding the re-usability of PA-12 powder is aging of the un-sintered powder during each build. This occurs because the bed chamber is heated to elevated temperatures for extended periods, which can lead to thermal aging processes such as secondary crystallisation [24, 26, 168] and, in the case of MJF, thermo-oxidative degradation [22, 24, 49] . The PBF process also includes a slow cool down phase which extends aging of the un-sintered powder [16, 17, 33]. As a result, the un-sintered, or “used” powder, is “refreshed” with virgin material and used in subsequent builds. The ratio of used to virgin powder is known as the refresh ratio and, although it differs for LS and MJF, typically about 20% to 50% of the used powder is discarded after every build cycle [15, 18, 21, 26, 66]. This incurs significant costs and environmental impacts [49].

Furthermore, assuming that the PA-12 powder used in the build contains recovered powder, these aging processes have the potential to affect the physical properties of final parts. Components made using aged powder are often more porous and brittle [28], whilst the “orange peel” effect is a common surface defect [16, 23, 26, 38]. To limit the number of parts which are discarded due to their insufficient properties, manufacturers often use a higher proportion of new powder than necessary [16, 17, 21, 25, 28]. Owing to the high cost of PA-12 [17, 21, 26], maximizing the re-use of un-sintered powder is economically desirable. Currently, powder recycling protocols do not fully account for any variation in the properties of “used” powder, and refresh ratios are arbitrary [16, 17, 25]. As such, the quality of refreshed powder mixtures is often inconsistent, or unknown, so the property profile of a final component is difficult

to predict [18]. Therefore, a greater understanding of aging and degradation processes is required to help ease current environmental and economic concerns regarding powder waste, which is necessary for proliferation and widespread use of this technology.

Under PBF conditions, at elevated powder bed temperatures, PA-12 may undergo complex aging mechanisms. Storing PA-12 at high temperatures can cause irreversible chemical changes, resulting in a change to the polymer molecular weight (M_w) [23, 25, 65]. Polycondensation (also referred to as postcondensation) describes linear macromolecular chain growth through reactions of end groups, resulting in increased M_w [15, 21, 26, 53, 65]. Also, thermo-oxidation often leads to cross-linking and chain scission which can result in opposing effects [18, 26, 38]. Cross-linking involves the formation of covalent bonds between polymer chains, leading to increased M_w [25, 38, 66], whilst chain scission in the polymer backbone results in a rapid decrease in M_w [24, 179]. Furthermore, when polyamides are heated to elevated temperatures, the chain mobility in the amorphous regions allows the degree of crystallinity in the polymer to increase. This is known as secondary crystallisation and it can occur via a slow, but continuous lamellar thickening mechanism [105, 117, 199]; depending on the temperature, new lamellae can form in the amorphous interlayer [105, 110, 111]. These processes can affect the behaviour of PA-12 powder, and, subsequently, the properties of final parts. Secondary crystallisation results in an increased T_m, which may cause incomplete melting, leading to un-molten, nascent particles remaining in the part [50]. Similarly, increases in melt viscosity, due to rising M_w or enhanced cross-link density, can cause insufficient powder coalescence [18, 23, 24, 26] and part consolidation [38, 42, 65,

67]. At the powder bed temperature, physical aging and degradation processes may occur simultaneously and interact with each other [24, 28]. For example, chain scission alters the morphology of PA-12, which can increase secondary crystallisation through chemi-crystallisation [176, 187, 188]. Conversely, cross linking may reduce secondary crystallisation by restricting motion and reorganisation of polymer chains [23]. Clearly, the chemical and physical aging of PA-12 during PBF is a complex problem and previous work has explored it from a range of perspectives.

Plastic melt flow rate (MFR) has been used previously to characterise the effect of degradation on the melt-flow properties of PA-12 powder [16, 17, 21, 24, 49, 160]. MFR values have been used to define the refresh ratio [49], and Dotchev and Yusoff concluded that a powder MFR > 26 g10min^{-1} will produce a component with sufficient properties [17]. However, the use of MFR as a metric for powder quality is limited in that it only focuses on one material property: melt flowability/viscosity. Differential scanning calorimetry (DSC) has been used in previous studies to explore the thermal aging of PA-12, within the context of PBF processes. Increased T_m, broadening of the melting region, and decreased crystallisation temperature are common observations [23, 25, 49]. However, there is contradiction within PBF literature regarding the cause of the changes in T_m. The majority of current studies use polycondensation, and rising M_w, as an explanation for increased T_m [15, 24-26, 38, 41, 61, 67, 159, 160]. A few papers state that secondary crystallisation may explain the shift in T_m [24, 26, 168] but, the possibility of this lamellar thickening process occurring simultaneously is generally overlooked and requires more attention. Previous studies that age powder in-situ in LS or MJF systems tend to be limited to relatively short aging time periods [21, 26, 53], or only compare the difference

between “virgin” and “aged” samples [42, 51, 168]. Other studies have attempted to replicate LS conditions over extended time periods by storing virgin PA-12 powder in a deoxygenated vacuum oven, set at 170 °C [16, 18, 28, 167]. As MJF is a more recently developed process, studies exploring aging and degradation of PA-12 in a high-temperature, oxygenated environment are far more limited.

Therefore, this study aims to develop current understanding of the aging and degradation processes which occur when PA-12 is stored at an elevated temperature, for a range of extended time periods, in an oxygenated environment. Since Fourier transform infrared spectroscopy (FTIR) has rarely been used as a characterisation technique in the PBF literature, FTIR will be used in conjunction with DSC and mechanical testing to elucidate the aging processes occurring under simulated MJF conditions.

4.3 Materials and Methods

4.3.1 Characterisation of virgin PA-12 powder

Commercial grade HP high reusability polyamide 12 (PA-12) was supplied by Hewlett-Packard as virgin powder. Sample variability was assessed by recording the melting point of six unconditioned powder samples, whilst the thermal stability of virgin PA-12 powder was also studied (see *section 4.3.2.1* for further information).

4.3.2 Oven conditioning of virgin PA-12 powder

The exact temperature of the MJF bed chamber is confidential, so the storage conditions used within this work were informed by the patent for MJF [171]. To

simulate the conditions found within MJF, the as-received, “virgin”, PA-12 powder was stored at a temperature of 170 °C, in an air circulating Carbolite-Gero PF 60 oven. Storage times were selected to reveal the extent to which the aging processes could occur and the interplay between them. Virgin powder was stored for up to 336 hours, with samples removed at the following time intervals (hours): 24, 48, 72, 96, 120, 144, 168, 192, 226, 264, 310, 336. A minimum of three samples were analysed per storage time to ensure reproducibility of measurements. Following oven conditioning, powder was stored at room temperature and sealed with parafilm to prevent any further degradation.

4.3.2.1 Thermal analysis using Differential Scanning Calorimetry (DSC)

A Mettler Toledo DSC-1, calibrated from the melting behaviour of zinc (T_m 419.5 °C, ΔH_f 107.5 Jg^{-1}) and indium (T_m 156.6 °C, ΔH_f 28.45 Jg^{-1}) and purged under nitrogen gas flow, was used for the thermal characterisation of PA-12. The different DSC procedures for each experimental section are shown in *Table 4.1.*

Table 4.1 - Experimental conditions adopted for thermal analysis.

Experiment	Sample mass (mg)	Heating/ cooling rate ($Kmin^{-1}$)	Heating range (°C)	No. of heat-cool runs
Sample variability	6±0.5	10	25 – 220	2
Thermal stability		40	25-205, 25-215, 25-225	25
Post-oven conditioning		10	25 – 220	2

Following oven conditioning, analysis of the thermal response was primarily carried out on the first heating and cooling cycle to study the effect of thermal annealing on PA-12. Aging and degradation processes often cause melting and crystallisation peaks to shift [24-26, 160, 167, 168]. The heat of fusion (ΔH_f) was determined from the melting peak and this was used to calculate percentage crystallinity (X_c) using *Equation 4.1*, whereby ΔH_f^0 = 209.3 Jg^{-1} (100% crystalline PA-12) [15].

$$\boldsymbol{X_c}\ (\%) = \frac{\Delta \boldsymbol{H_f}}{\Delta \boldsymbol{H_f^0}}\ \boldsymbol{X}\ \mathbf{100} \qquad \textit{(Equation 4.1)}$$

4.3.2.2 Attenuated Total Reflectance Fourier Transform Infrared Spectroscopy (ATR-FTIR)

Samples were recovered from the DSC pans and characterised using a Nicolet 8700 FTIR with an ATR accessory. Preliminary experiments revealed that exposing conditioned PA-12 powder to two heat-cool cycles in the DSC did not alter the observed IR spectra. Therefore, samples were recovered from the DSC pans for subsequent ATR-FTIR analysis. Spectra were recorded at 4 cm^{-1} resolution and 125 scans, with 4 levels zero filling and 0.482 cm^{-1} data spacing.

4.3.3 Fabrication and conditioning of PA-12 tensile specimens

To characterise the mechanical properties of conditioned PA-12, plaques were hot pressed from PA-12 powder using a Moore E1127 Hydraulic Press. 10 g of virgin PA-12 powder was placed in the centre of a polytetrafluoroethylene (PTFE) frame (18 cm x 18 cm x 0.022 cm) and sandwiched between two stainless steel plates. This was inserted between the pre-heated hot press platens, at 200 °C for 3 minutes, then

pressed with a 10-tonne load for 3 minutes, at the same temperature. A slow cooling method under atmospheric conditions (~12 °Cminute^{-1}), with no pressure applied, produced a plaque with thermal properties most similar to PA-12 powder.

Dog-bone tensile samples, with a gauge length of 28 mm, width 4 mm and thickness of ~0.23 mm were stamped from the PA-12 plaques using a cutting die. Thickness was measured using a micrometer screw gauge and taken from an average of 3 locations across the sample. Tensile samples were then stored under the same oven conditions as PA-12 powder (*section 4.3.2)*. Following removal from the oven, the specimens were tested on an Instron 5566 materials tester using a 1 kN load cell and 10 mm/s crosshead speed. Proprietary Instron Bluehill analysis software enabled measurements of Yield Strength (YS), Ultimate Tensile Strength (UTS), Fracture Strength (FS), Elongation at break (EAB) and Young's Modulus. For each parameter, an average was determined from six tensile samples per storage time to ensure reproducibility. Statistical analysis on the measured data was carried out using a simple T-test. We note that there are limitations to this aspect of the study. To create the plaques for mechanical testing, the powder material was exposed to one thermal cycle, but this is unavoidable.

4.3.4 Effect of drying PA-12 powder before oven conditioning

To determine the effect of water content on degradation, virgin PA-12 was dried in a desiccator for the following time periods (days): 4, 40, 100. Following this pre-treatment, "dried" PA-12 was annealed under identical oven storage conditions to virgin ("un-dried") PA-12 *(section 4.3.2)*. Comparisons between the behaviour of virgin and dried PA-12 were made.

4.4 Results and Discussion

4.4.1 Characterisation of Virgin PA−12 Powder

4.4.1.1 Sample Variability

Un-conditioned, “virgin” PA−12 powder displays consistent and reproducible thermal properties, as shown by the insignificant sample-to-sample variability and low standard deviation values (*Figure 4.1).*

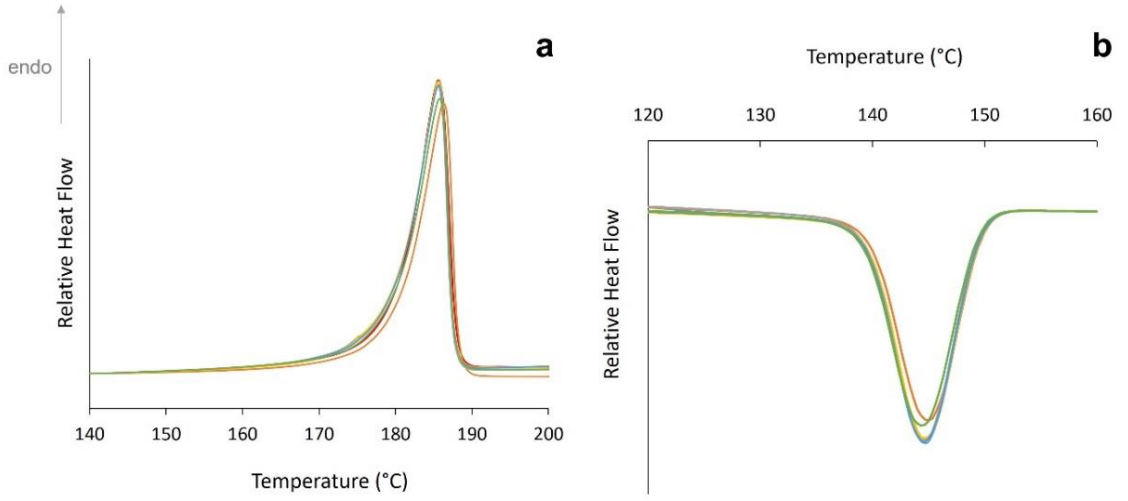

	T_m onset (°C)	Peak T_m (°C)	T_m endpoint (°C)	ΔH_f (Jg^{-1})	X_c (%)	Peak T_c (°C)	ΔH_c (Jg^{-1})
Mean	179.4	185.8	187.8	107	51	144.7	56
Standard deviation	0.27	0.27	0.27	3.21	1.53	0.21	2.33

*Figure 4.1 - Virgin PA−12 powder sample variability for (**a**) melting behaviour and (**b**) crystallisation behaviour.*

4.4.1.2 Initial assessment of thermal stability

An initial assessment of the stability of the polymer was investigated by exposing virgin PA-12 powder to repeated thermal cycling. A sample was subjected to 25 heat-

cool cycles, with a temperature range of 25 °C to 215 °C. With increased cycle number, both peak melting temperature (T_m) and heat of fusion (ΔH_f) reduced (*Figure 4.2a).* There is also a significant change in the crystallisation behaviour, as shown by reductions in peak crystallisation temperature (T_c) and heat of crystallisation (ΔH_c) (*Figure 4.2b)*. This indicates a progressive hindrance to the crystallisation process and results in the observed changes in the subsequent re-heat. Repeated heating of PA-12 to high temperatures makes polymer chains highly mobile and more reactive, which can result in linear chain growth via further polycondensation [16, 17, 26, 28, 38, 51]. It can be envisaged that these longer polymer chains then exhibit hindered mobility due to increased chain entanglement which restricts the formation of ordered crystalline regions [26]. Alternatively, some have suggested that cross-links can form within PA-12 [23, 24], creating physical links between amorphous chains that could be described as tie-molecules [75]; their effect being to hinder the crystallisation process. However, as the DSC is flushed with nitrogen, it is more likely that polycondensation causes the observed changes in melting and crystallisation behaviour.

Initially, a notable low temperature endotherm was apparent on the main melting peak (demonstrated by the small shoulder to the left of the main peak), but with increasing cycle number, the shoulder reduces in size and disappears (*Figure 4.2a)*. There are two theories that could explain this behaviour. Some suggest that it represents the melting of thinner, less “perfect” crystals [51, 158, 165]. However, one can also interpret that the shoulder peak is caused by the reorganisation of polymer chains during heating; as a result of melt-recrystallisation, which stems from the metastability of the system [105, 111, 166, 199]. With increased time spent above the

melting temperature, further polycondensation and cross-linking hinders chain mobility and limits polymer reorganisation on heating, so the shoulder on the main peak diminishes.

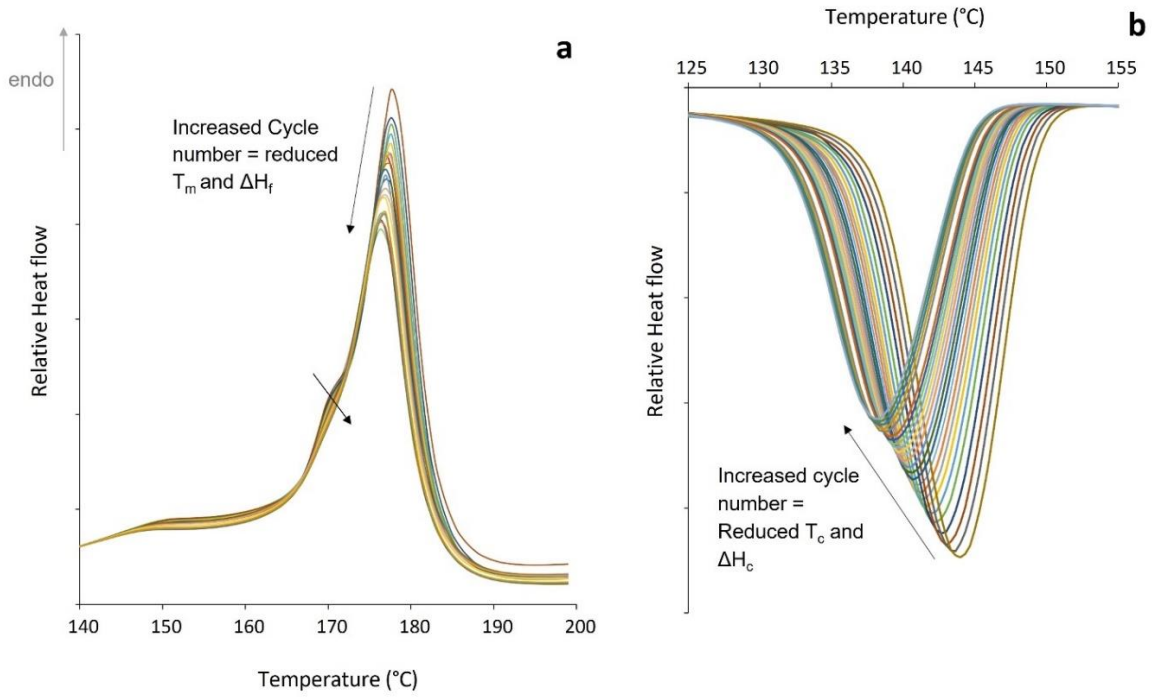

*Figure 4.2 - Change in (**a**) melting behaviour on heating and (**b**) crystallisation behaviour on cooling with repeated thermal cycling, to an upper temperature limit of 215 °C.*

This thermal cycling DSC experiment was repeated to investigate how the thermal stability of PA-12 may vary, when powder samples are repeatedly heated to different temperatures in the melt. On this occasion, two separate samples of virgin PA-12 were subjected to 25 heat-cool cycles, with a temperature range of 25 °C to 205 °C and 25 °C to 225 °C, respectively. *Figure 4.3* indicates that the behaviour of the polymer depends on the upper temperature limit. When repeatedly heated to 205 °C,

the melting and crystallisation behaviour of PA-12 shows what can conveniently be described as a parabolic response. This could be explained by a “self-seeding” process [91, 92]. Although 205 °C is greater than the observed melting point, some thicker lamellae may not fully melt which can result in residual lamellae. These small crystalline fragments persist into the melt and can act as nucleation sites which accelerate the re-crystallisation process on cooling [111, 199]. Thus, as indicated by the blue trends in *Figure 4.3*, there is an initial increase in T_c, ΔH_c, T_m, and ΔH_f. But, with continued thermal cycling the residual lamellae eventually fully melt, halting the “self-seeding” process, and a reduction in these parameters is then observed. As previously shown in *Figure 4.2*, with an upper limit of 215 °C, there is a progressive, albeit small, reduction in T_m, ΔH_f, T_c, and ΔH_c, which indicates some degradation in the form of polycondensation and cross-linking. When heating to 225 °C, the polymeric sample is repeatedly exposed to a higher temperature, so the level of degradation is greater. Polycondensation and cross-linking are time and temperature dependant processes, thus they occur to a greater extent in the sample heated to 225 °C. As such, more significant reductions in T_m, ΔH_f, T_c, and ΔH_c were observed, as indicated by the grey trend lines *(Figure 4.3).*

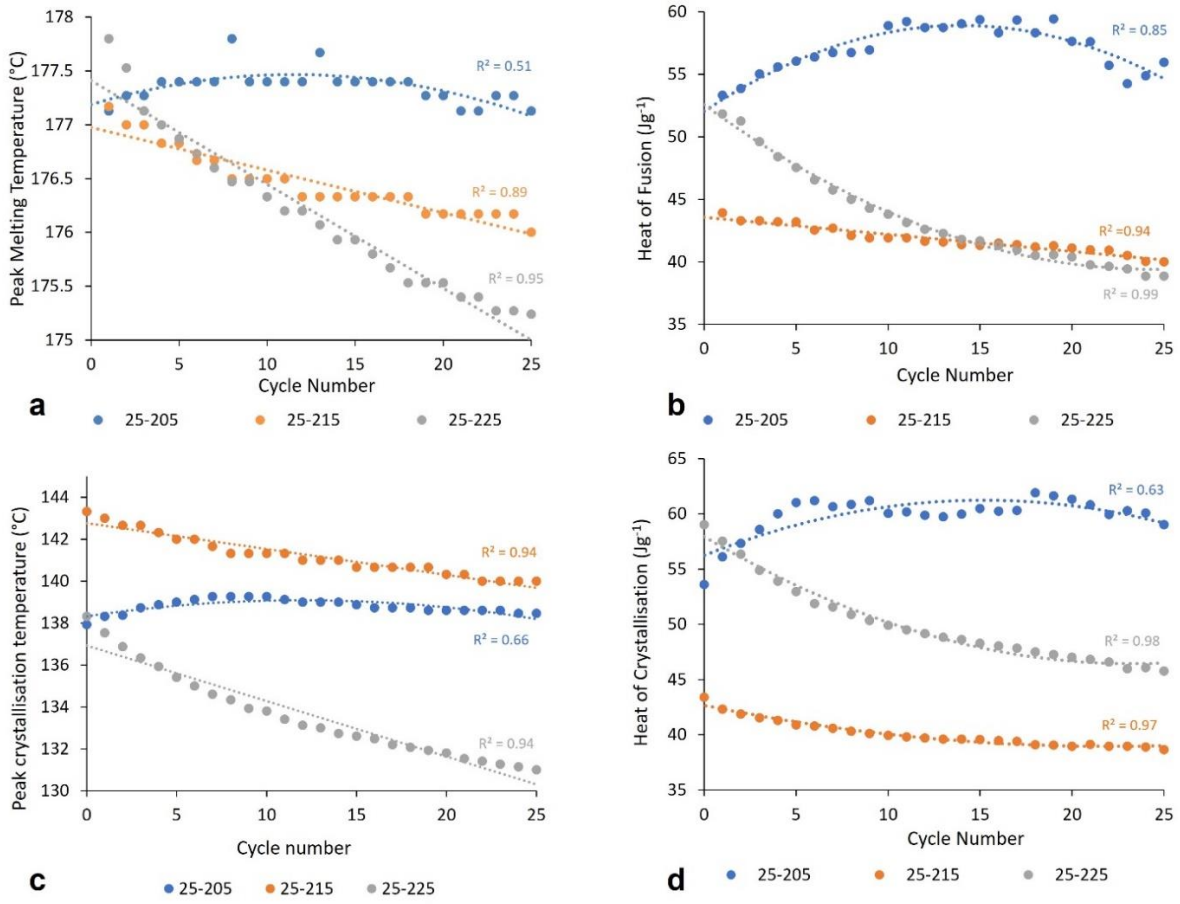

*Figure 4.3 - The change in (**a**) peak T_m, (**b**) heat of fusion, (**c**) peak T_c, and (**d**) heat of crystallisation with increased thermal cycling, with varied upper temperature limits. Note that the starting values (cycle number 0) for the 25-205 °C and 25-225 °C datasets are slightly different to 25-215 °C because these experiments were conducted on a new batch of virgin PA-12 powder. The new powder had a reduced T_c in order to enlarge the processing window of PA-12, ultimately, this altered the baseline values for the heat of fusion and heat of crystallisation as well. Nonetheless, the chemical structure of the powder remains the same, so the slight change in the baseline value does not alter the observed trends regarding the thermal stability of the material.*

4.4.2 Oven conditioning of virgin PA-12 powder

4.4.2.1 Differential Scanning Calorimetry (DSC)

Over 336 hours of oven storage there appeared to be a marked time-dependency to the aging and degradation processes that were dominant over this timescale

(Supplementary Information 1). The melting and crystallisation behaviour of PA-12 powder showed two separate trends dependent upon storage time, these are considered separately.

4.4.2.1.1 The first 100 hours of storage

After the first 100 hours of storage, T_m increased by 4.2 °C. There was also a progressive increase in ΔH_f and ΔH_c, while T_c displayed a slight reduction *(Figure 4.4)*. Increases in T_m have previously been explained by polycondensation [15, 24-26, 38, 41, 61, 67, 159, 160] and secondary crystallisation [23, 24, 26, 158, 159, 166].

Polycondensation increases molecular weight; some suggest a higher temperature is therefore required to overcome the additional hydrogen bonding present in the lamellae of long polymer chains [23, 24, 26]. However, this process occurs exclusively in the amorphous phase and causes an increased number of entanglements, which hinders the crystallisation process [16, 17, 26, 28, 38, 51]. As such, polycondensation alone would be expected to result in a larger reduction in T_c, whilst ΔH_f, a direct measure of crystallinity, would remain unchanged.

Secondary crystallisation and polycondensation could both occur simultaneously under the conditions of this study. Previous studies have shown that chain growth via polycondensation occurs primarily on thermally unstressed (virgin) PA-12 and, due to reduced availability of end-groups, is unable to continue at the same rate within aged powder [18, 21, 24, 53, 158]. As such, continued growth of T_m for 100 hours provides strong evidence that secondary crystallisation, via lamellar thickening [24, 159, 165, 166, 174, 176, 185], also contributed to the observed changes. This is further

supported by increased ΔH_f and a rise in ΔH_c which links to the previously explained "self-seeding" process and the formation of thicker lamellar structures [111].

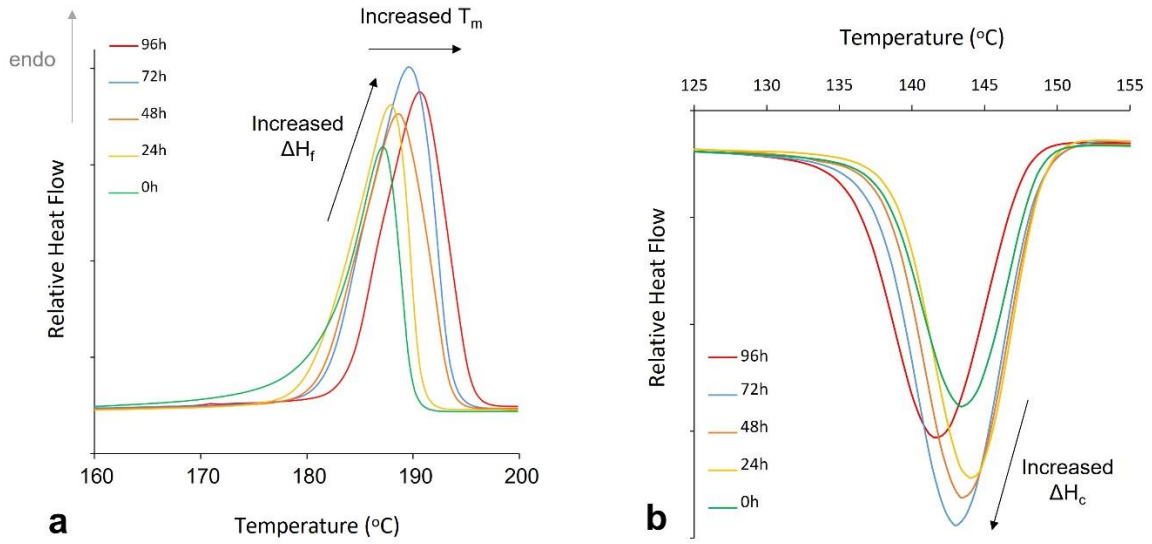

*Figure 4.4 - DSC first heat–cool showing the change in (**a**) melting behaviour and (**b**) crystallisation behaviour, for the first 100 h of oven storage.*

4.4.2.1.2 Storage times greater than 100 hours

For storage times greater than 100 hours the initial trends reverse. After extended storage times there is a significant decrease in T_m and ΔH_f *(Figure 4.5a),* as well as substantial reductions in T_c *(Figure 4.5b)*. These changes provide evidence of degradation and, as storage time increases, degradative processes become predominant over previous aging phenomena. Prolonged oven storage provides suitable conditions for thermo-oxidative degradation as PA-12 powder is exposed to high temperatures, in the presence of oxygen, for extended time periods [18, 21, 24, 66, 174, 176, 184]. This results in rapid chain scission and significant reductions in

molecular weight are expected [23, 166, 174, 184, 188]. As such, melting point depression occurs due to the acidic degradation products of thermo-oxidation [184].

Thermo-oxidative degradation may also cause the decrease in ΔH_f and the accelerated reduction in T_c, which both signify a delayed and diminished crystallisation process. Thermo-oxidation can result in oxidation products such as carboxylic acids, aldehydes, and imides [174]. These products have additional, bulky side chains which prevent polymer chains rearranging into an ordered structure and may explain the observed reduction in T_c. As such less crystalline regions form during cooling, and lamellar structures are generally thinner, so T_m and ΔH_f also reduce. There is a strong relationship between the melting and crystallisation behaviour (*Figure 4.6)*, emphasising that degradation is the underlying causation of the changes in thermal properties at extended storage times.

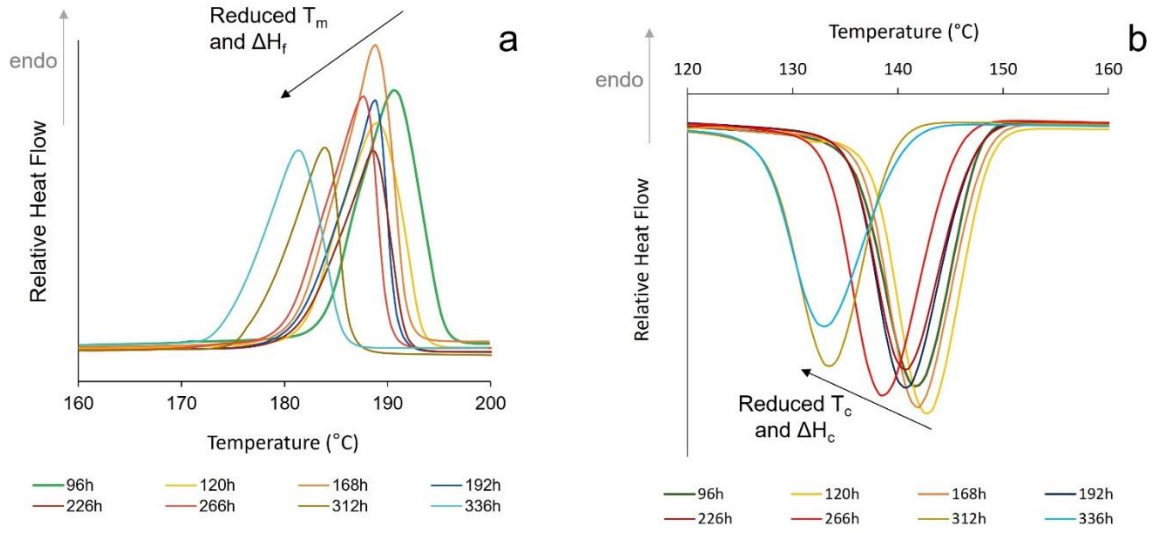

*Figure 4.5 - DSC first heat–cool showing the change in (**a**) melting behaviour and (**b**) crystallisation behaviour, for storage times greater than 100 h.*

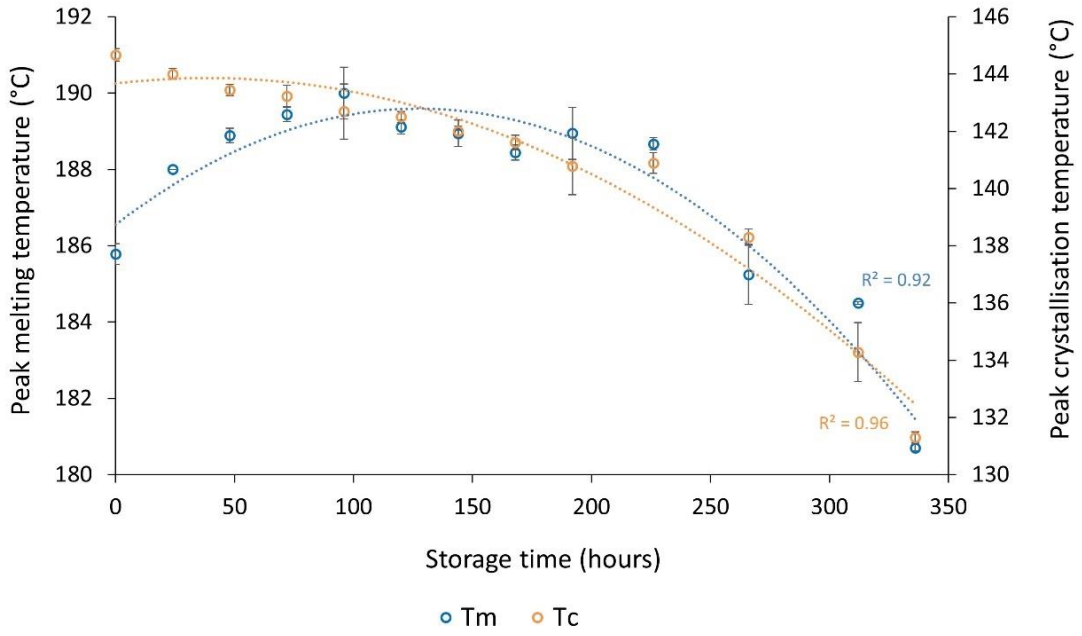

Figure 4.6 - The overall change in T_m and T_c after storage of PA−12 at 170 °C for up to 336 h.

4.4.2.2 Attenuated Total Reflection—Fourier Transform Infrared Spectroscopy (ATR-FTIR)

Infrared spectroscopy is a characterisation technique commonly used to investigate oxidative aging [166, 172, 174, 175, 180], but it has not been fully utilised in previous PBF studies. In the current study, following extended oven storage (>150 hours), a new absorbance band, containing various absorption maxima, began to form as a notable shoulder on the Amide I carbonyl peak *(Figure 4.7).* Similar behaviour has been seen previously within polyamides and is associated with thermo-oxidative degradation of PA-12 [166, 172, 174, 175, 180, 181]. As such, the growth of this shoulder peak can be used as an indicator for the onset of degradation.

With increased storage time, three distinct absorption peaks became apparent *(Figure 4.7).* An increase in absorbance at 1733 cm^{-1} is associated with the formation of imide bonds, often used as the main marker of thermo-oxidative degradation [166, 172-175, 180, 181]. Similar increases in absorbance occurred at 1715 cm^{-1} and 1705 cm^{-1}, which are caused by other products of the polyamide oxidation cycle, such as carboxylic acids [166, 174] and aldehydes [180, 181], respectively.

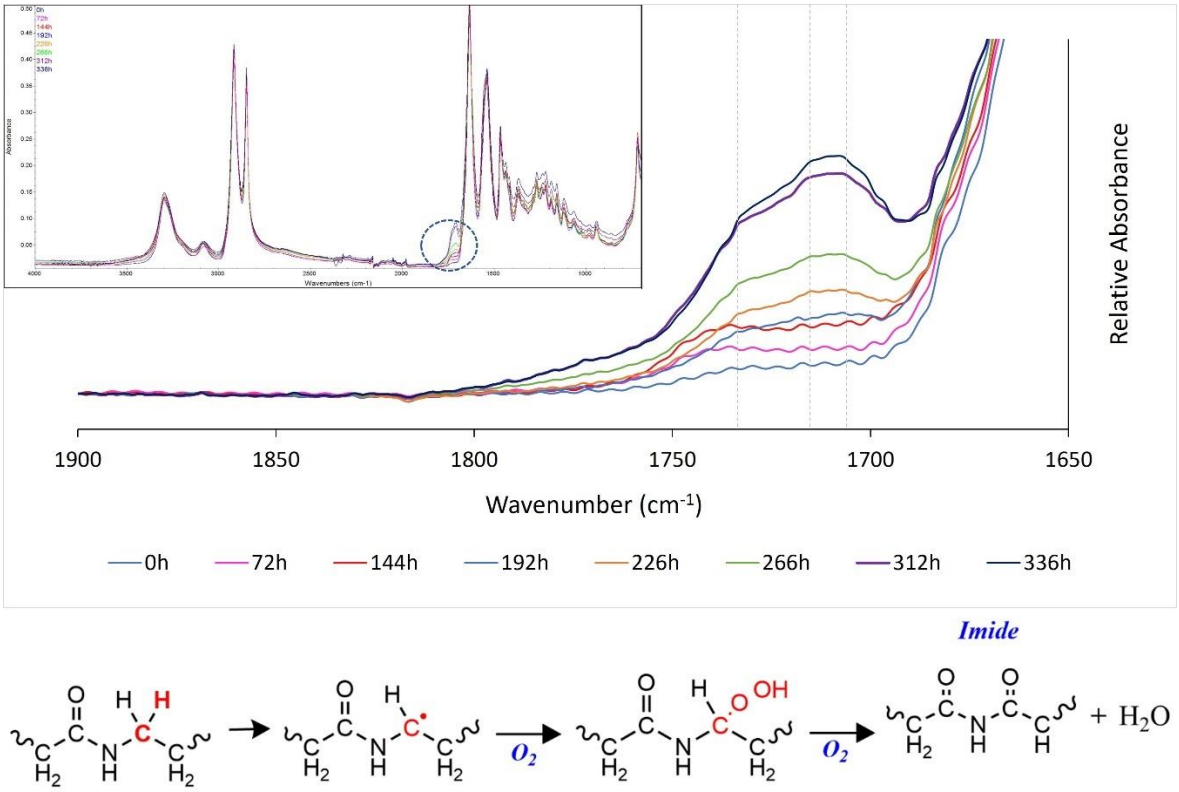

Figure 4.7 - A full ATR-FTIR spectra for PA−12, with the carbonyl region magnified to show the development of a new band at 1700 − 1760 cm^{-1}, with absorption maxima appearing at 1705 cm^{-1}, 1715 cm^{-1}, and 1733 cm^{-1}, as indicated by the dashed grey lines. The chemical reaction resulting in the formation of imide bonds is displayed.

The primary degradation pathway of polyamides involves oxidation of the methylene carbon adjacent to the amide nitrogen, resulting in the formation of an imide group from the amide *(Figure 4.7)* [66, 170, 172, 173, 175, 181]. Storage of PA-12 powder at high temperatures, close to the melting point, accelerates this process [66, 181]. The production of an imide group facilitates chain scission at the carbon-nitrogen bond [172, 175, 181] which creates a strongly destabilised polymer. Within polyamides this instability allows thermo-oxidative degradation to proceed without an induction period [173]. As such, once degradation becomes dominant it can accelerate with a low activation energy resulting in rapid reductions in molecular weight, as well as significant changes to the thermal (*section* 4.4.2.1) and mechanical properties *(section 4.4.2.4)* of the material.

4.4.2.3 Relationship between Aging and Degradation Processes

Characterisation of PA-12 powder using DSC and FTIR provides evidence of multiple aging and degradation processes occurring during storage at 170 °C in air. *Figure 4.8* indicates that there is an interplay between these aging phenomena and, across the full duration of storage time, the dominant aging process changes.

Initially, there is an increase in peak melting temperature (T_m) and crystallinity (X_c), which can be associated with lamellar thickening [23, 24, 26, 158, 159, 166], yet there is an insignificant change to imide peak height. However, with extended storage beyond 150 hours, there is a reduction in T_m and X_c. This is closely correlated with a significant increase in imide peak height, indicating thermo-oxidative degradation [166, 172, 174, 175, 180, 181]. The extent to which degradation occurs

is exposed by the discolouration of the samples, whereby they changed from translucent, to yellow and then dark brown (*Figure 4.8)*, as seen previously [172, 174, 180, 181, 185]. Lamellar thickening may still be occurring, but any effects on polymer morphology and thermal properties are masked by the ever-accelerating degradation process.

Furthermore, polymer morphology, particularly the crystallinity of PA-12, influences the extent of degradation processes. Some have hypothesized that diffusion of oxygen and water cannot happen in crystalline regions of the material [173, 175, 176]. However, others suggest degradation occurs via a two-step process. Firstly, preferential attack of the more easily accessible amorphous chains, before the degradation of crystalline regions, which coincides with polymer mass loss [182, 183]. Regardless, chain scission due to thermo-oxidation (and hydrolysis, see *section 4.4.3*) is thought to occur primarily in the amorphous phase. As such, with extended storage time, degradation of PA-12 is accelerated by the reduction in crystallinity, because there are less crystalline regions remaining to combat the intake of oxygen. This is exacerbated by an increased presence of acidic groups, which accelerate degradation through a process known as “autocatalysis” [200, 201].

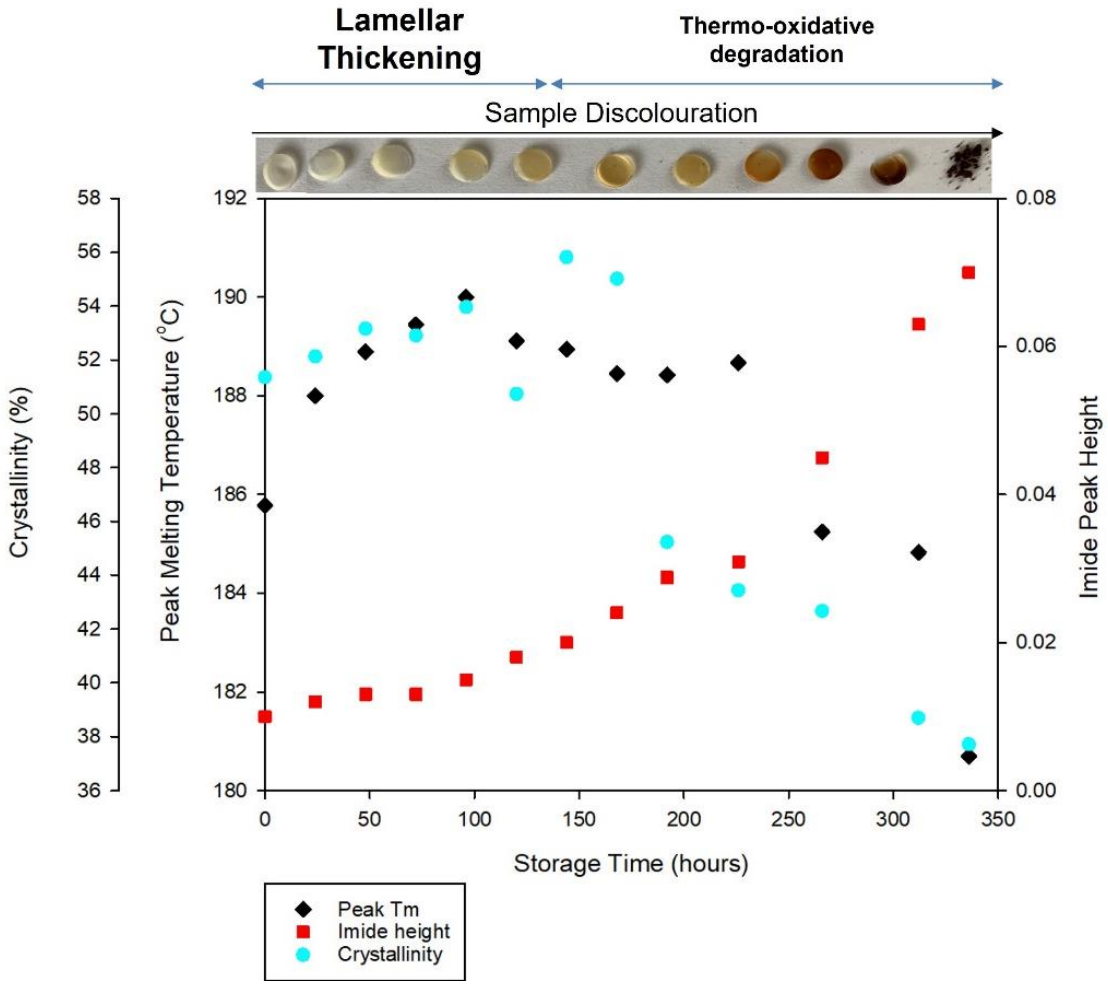

Figure 4.8 - Correlation between changes in PA12 Tm, crystallinity, imide peak height growth and sample discoloration, with storage time. Displays the relationship between polymer morphology and degradation.

4.4.2.4 Mechanical Properties of PA−12 Plaques

There was a significant change in the mechanical properties of PA-12 following storage at 170 °C for an extended period. Un-conditioned PA-12 displayed ductile behaviour, but with increased storage time there was progressive embrittlement of the material until almost immediate fracture *(Figure 4.9)*. All measures of strength exhibited similar behaviour; a gradual reduction observed for the first 72 hours of storage, followed by a more rapid decrease *(Table 4.2)*. There was an 81% reduction

in ultimate tensile strength (UTS) between un-conditioned PA-12 and tensile samples stored for 144 hours. Values of elongation at break (EAB) significantly reduce with increased storage time, with a corresponding rise in Young's modulus *(Figure 4.10).* Un-conditioned PA-12 samples presented an EAB of 436.7% with a standard deviation of 67.9 (436.7±67.9%). This value decreased to 213.7±21.8% after 48 hours of storage and 1.03±0.3% after 144 hours, demonstrating significant embrittlement of the material. This provides more evidence of severe degradation, so no further oven storage times were required.

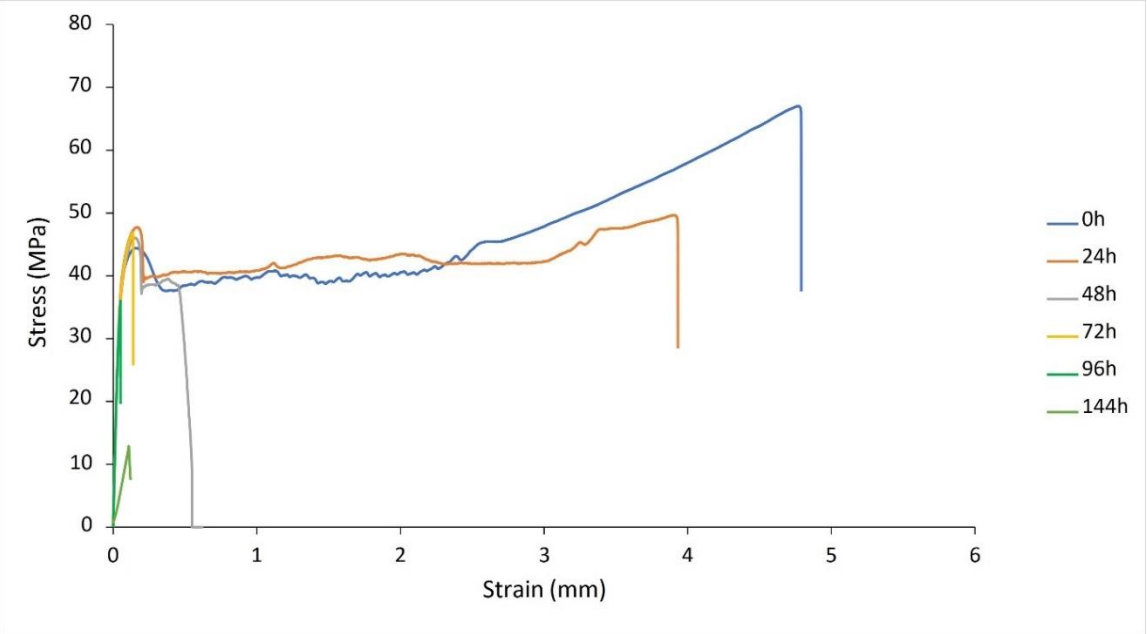

Figure 4.9 - Stress Strain curves for PA-12 tensile samples as a function of storage time at 170 °C.

Table 4.2 - The variation of mechanical properties with storage time.

Storage time (hours)	Yield Strength (MPa)	Ultimate Tensile Strength (MPa)	Fracture Strength (MPa)
0	28.1 ± 1.2	62.1 ± 8.2	59.8 ± 7.2
24	27.1 ± 0.9	49.2 ± 2.8	44.8 ± 4.0
48	25.4 ± 0.6	47.1 ± 3.9	46.1 ± 4.7
72	25.3 ± 1.4	44.8 ± 2.0	44.0 ± 2.3
96	25.2 ± 1.8	34.6 ± 1.1	34.6 ± 1.1
144	11.6 ± 2.4	11.6 ± 2.4	11.6 ± 2.4

As discussed in *section 4.4.2.1.2* and *section 4.4.2.2*, the conditions adopted in this study ultimately result in thermo-oxidative degradation and subsequently chain scission of PA-12 [23, 24, 66, 174, 176, 184]. The observed changes in mechanical properties provides more evidence of oxidative degradation because reduced tensile strength is a strong indicator of decreasing molecular weight [202-204]. Within PA-12, degradation involves an auto-oxidation mechanism whereby hydrogen atoms are abstracted from the polymer backbone, causing a loss of amide groups, and a reduction in hydrogen bonding between adjacent polymer chains [66, 168, 170, 172, 173]. This contributes to a significant decrease in molecular weight [18, 21, 166, 188], as well as substantial reductions in strength and EAB [66, 170, 172, 175, 176, 181, 205].

Degradation can cause a reduction in Young's modulus [39, 180], but in this case, within the first 24 hours of oven conditioning, Young's modulus increased by 109 MPa. Across the same period a 12% increase in the crystallinity of PA-12 tensile samples was observed *(Figure 4.10).* For the duration of oven storage, the changes in Young's modulus and crystallinity are linked and both remain elevated relative to un-conditioned PA-12 plaques. This suggests that secondary crystallisation may have occurred in the conditioned tensile samples, albeit alongside degradation processes.

During oven storage, morphological and structural changes to PA-12 could be attributed to two different phenomena; lamellar thickening via thermal annealing [105, 159, 166] or chemi-crystallisation, which is initiated by degradation [166, 174, 176, 187, 188]. Due to the macromolecular nature of semi-crystalline polymer chains, they usually contain a high number of entanglements, which can limit further crystallisation [187]. However, during chemi-crystallisation, chain scission allows previously entangled amorphous sections to be released which permits further crystallisation via rearrangement of the smaller, and subsequently more mobile polymer chains [176, 187, 188]. Both secondary processes enhance the degree of crystallinity, reducing the volume fraction of the amorphous phase, which explains the observed reduction in EAB [176, 188, 206] and increase in Young's modulus [166, 206].

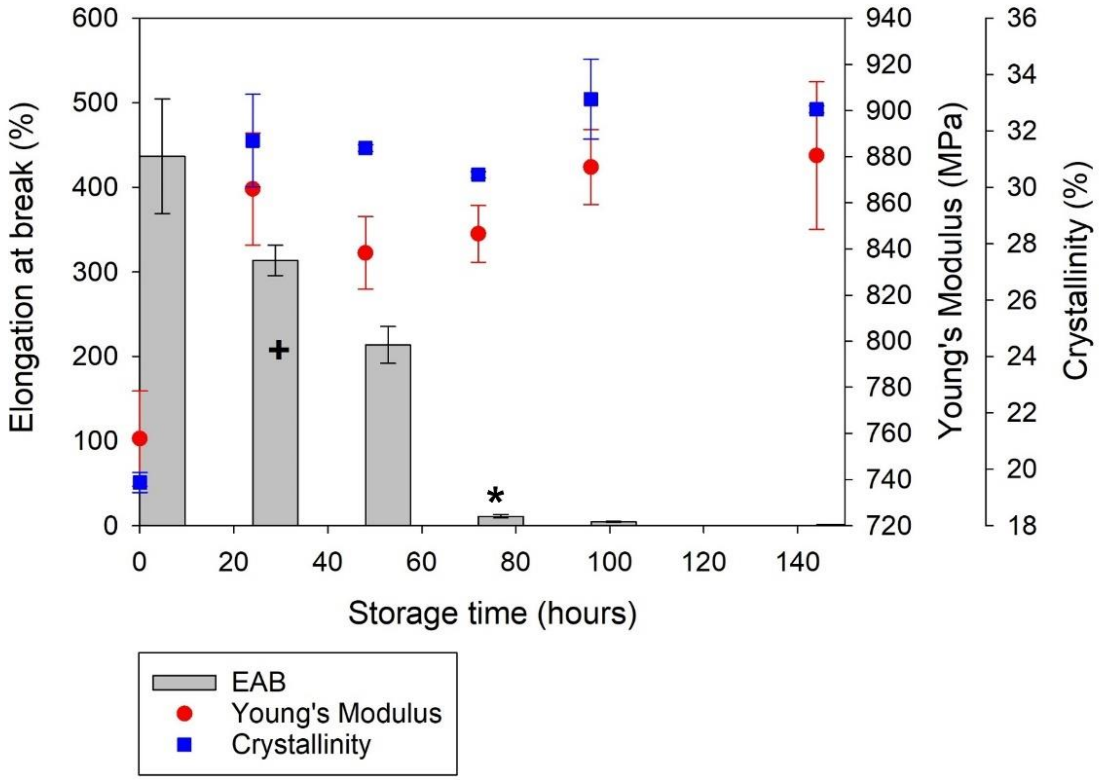

*Figure 4.10 - The change in elongation at break (EAB) Young's modulus, and crystallinity of PA−12 plaques with increased storage time. + Significant change in EAB when compared to the 0h sample ($p < 0.05$). * Very significant change in EAB when compared to the 0h sample ($p < 0.005$).*

Characterisation of the PA-12 plaques using DSC and FTIR allows the aging behaviour of the plaques to be compared to that of the powder. *Figure 4.11* displays the thermal, chemical, mechanical, and optical properties of PA-12 plaques and generally the observed behaviour is comparable to PA-12 powder (as shown in *Figure 4.8).* A similar initial increase in T_m occurs and with extended storage time, PA-12 plaques show decreased T_m, increased imide peak height and sample discolouration. These changes indicate thermo-oxidative degradation, which also explains embrittlement of PA-12 [166, 172, 176, 180]. Although the observed trends are similar, the key difference is that degradation occurs at an accelerated rate within

PA-12 plaques which are less stable, and melt at a lower temperature than the powder samples. This is due to the unavoidable degradation that occurs during hot-pressing. As such, after only ~150 hours of storage the samples were so heavily degraded that oven conditioning was discontinued. Similarly, reprocessing altered the changes in PA-12 crystallinity. Accelerated degradation, as well as storage conditions being closer to the T_m of the reprocessed material, allows chemi-crystallisation to occur within PA-12 plaques, resulting in increased crystallinity.

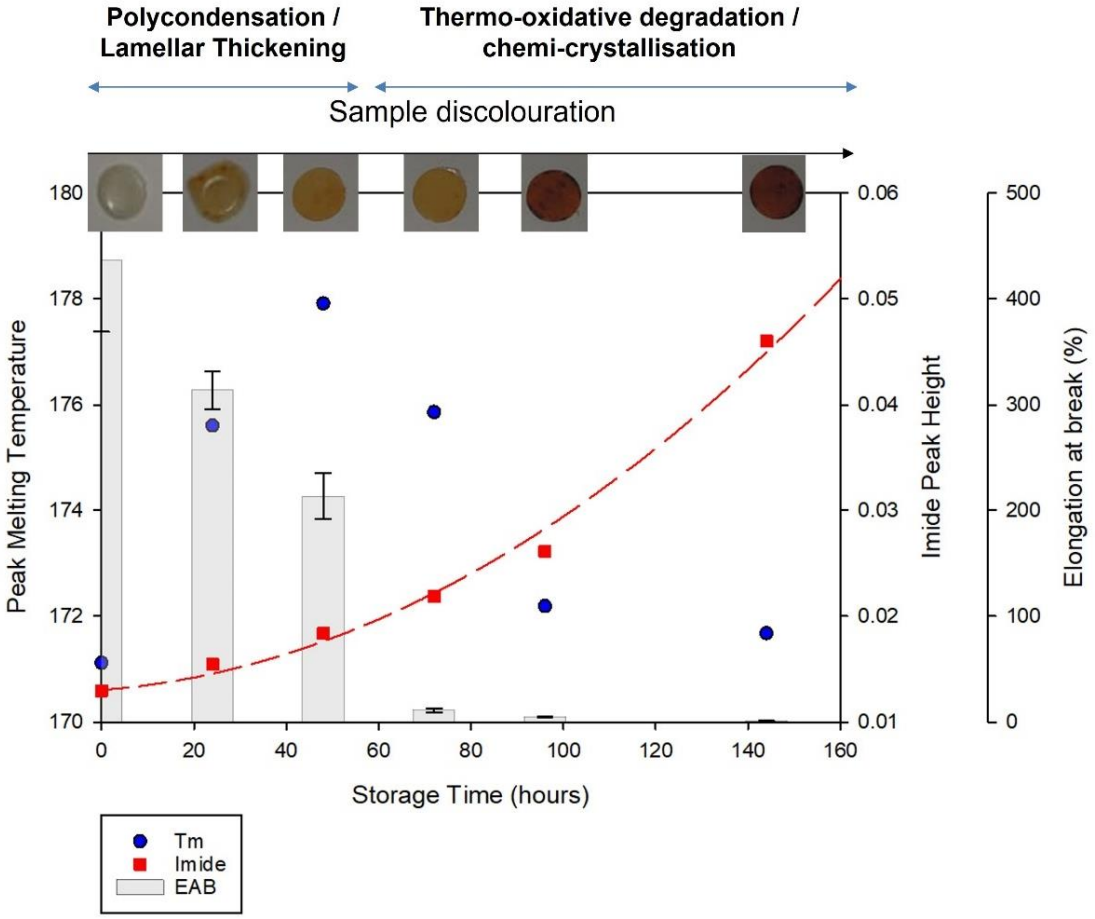

Figure 4.11 - Relationship between PA−12 plaques thermal, chemical, mechanical, and optical properties as a function of storage time.

4.4.3 Oven Conditioning of Pre-Dried PA−12 Powder

As shown in *section 4.4.2* degradation processes alter the thermal properties of PA-12, resulting in significant changes to the melting and crystallisation behaviours. However, the presence of amide groups and hydrogen bonding renders polyamides polar and highly hydrophilic, so PA-12 is also sensitive to chain scissions in the presence of water and moisture, through hydrolysis [166, 188]. Water molecules mobilise polymer chains which increases the rate of diffusion of oxygen into the polymer [54, 170, 175].

To limit the possibility of hydrolysis, unconditioned PA-12 powder was dried in a desiccator, without elevating the temperature. Dried samples were then conditioned in the oven (as explained in *section 4.3.2*) and compared to un-dried PA-12. With increased pre-drying time, melting point depression diminished *(Figure 4.12a)*, whilst the change in T_c was also lowered *(Figure 4.12b).* Similarly, the maximum T_m observed during oven conditioning is deferred to later storage times, which suggests the onset of degradation is delayed. After 100 days pre-drying, the reduction in T_m is only 6.3 °C, compared to a 9.3 °C decrease in un-dried PA-12 (*Figure 4.13).* This provides evidence that thermo-oxidative degradation is accelerated by moisture within PA-12, leading to more rapid chain scissions and subsequently more significant reductions in molecular weight [166, 170, 180, 188]. As a result, pre-drying PA-12 before exposure to heat and oxygen assists water removal, which reduces the extent of polymer degradation.

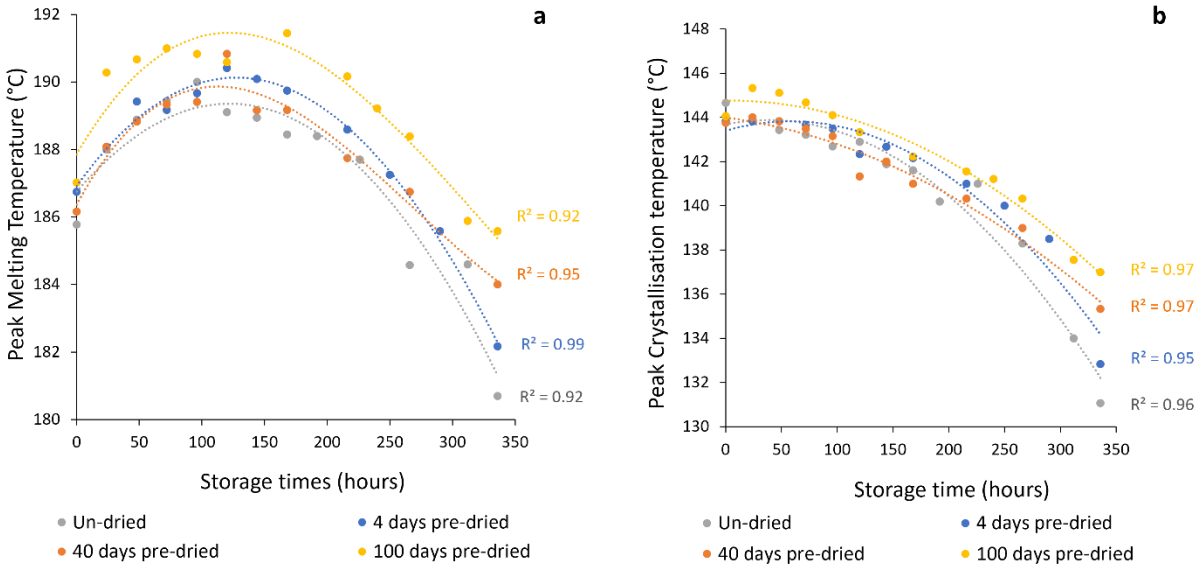

*Figure 4.12 - The change in (**a**) peak melting temperature and (**b**) peak crystallisation temperature with storage time, as a function of time spent drying in a desiccator prior to oven conditioning. Error bars were removed for clarity of the data trends, whilst all standard deviation values for these datasets was < 1.0 °C, so considered insignificant in relation to the observed trend.*

The effect of pre-drying PA-12 before oven conditioning is further supported by FTIR data. *Figure 4.14* displays the change in imide peak height as a function of storage and pre-drying time; the growth of the imide band is significantly greater in un-dried PA-12. With increased pre-drying time there was a consistent reduction in imide growth, emphasising decreased thermo-oxidative degradation. After 336 hours of oven storage un-dried PA-12 has an imide peak height of 0.07, with 100 days of pre-drying imide peak intensity is only 0.039. This highlights the effect of hydrolysis on the extent of PA-12 degradation.

Another indicator of thermo-oxidative degradation is sample discolouration [172, 174, 180, 181, 185] , which appears linked to imide growth *(Figure 4.14)*. With increased storage time, all samples change from translucent to yellow to dark brown. However,

as shown by the table in *Figure 4.14,* sample discolouration becomes less pronounced as pre-drying time is increased, with the most notable differences appearing in the samples stored for greater than 200 hours. This provides further evidence that pre-drying PA-12 can reduce degradation.

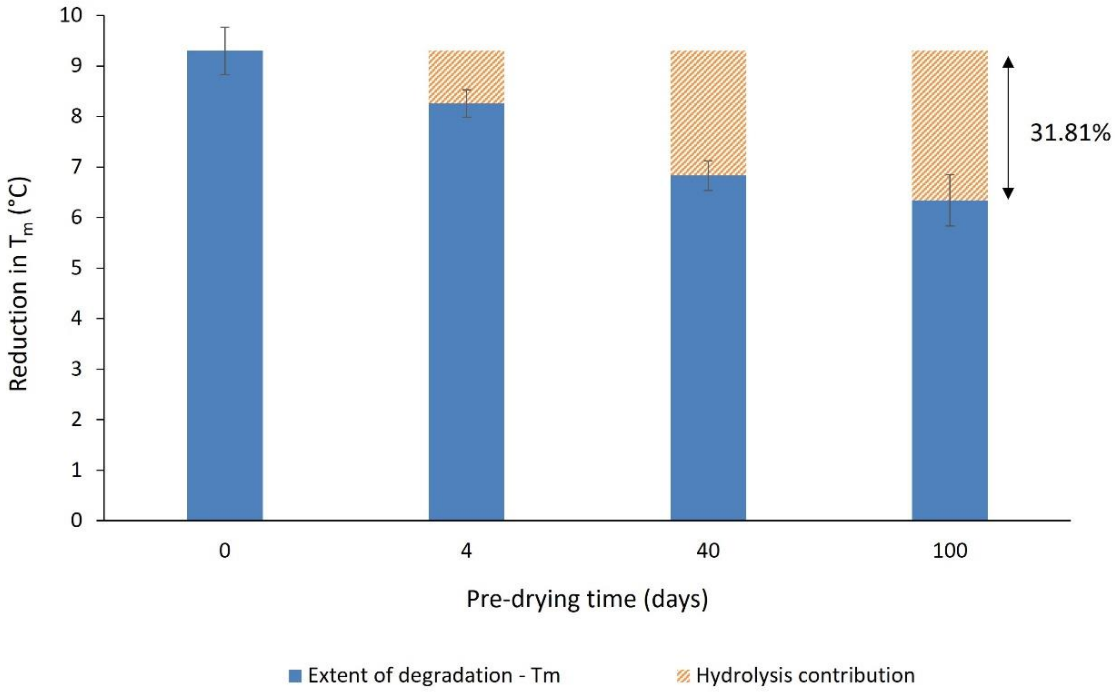

Figure 4.13 - The reduction in melting temperature of PA−12, as a function of pre-drying time. Changes in T_m were calculated from the highest value during oven storage to the final value observed after 336 h.

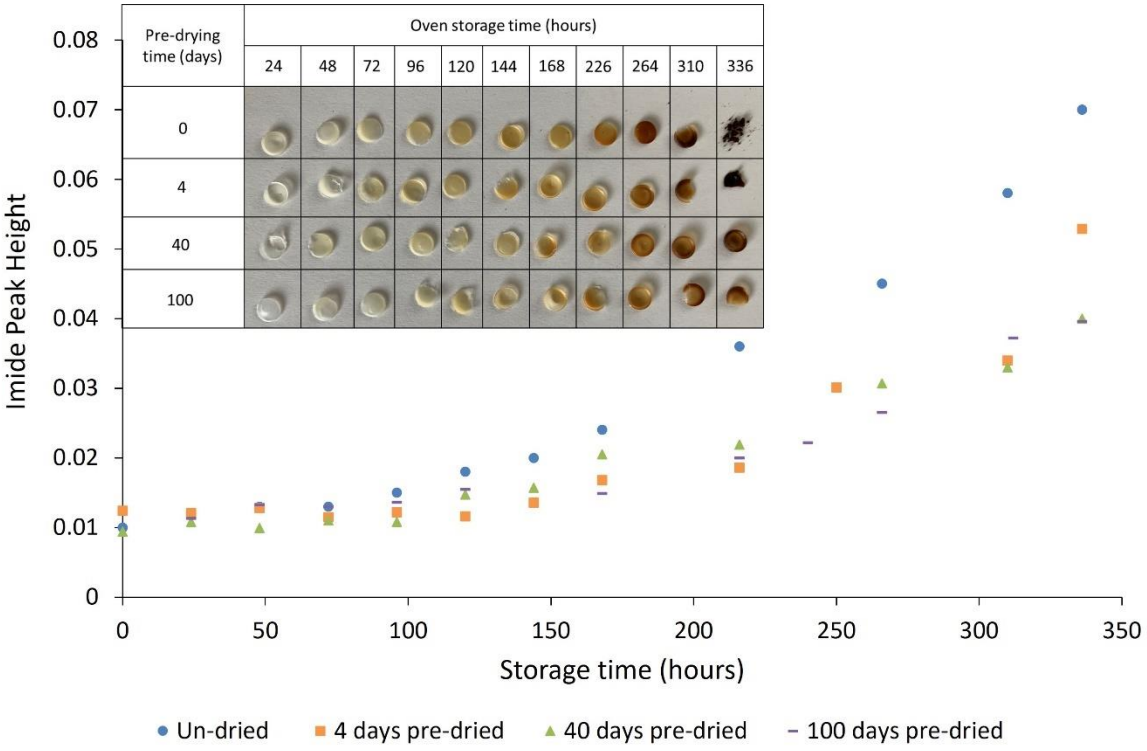

Figure 4.14 - The effect of drying PA−12 powders before oven conditioning on the growth of the imide peak and sample discolouration.

4.5 Conclusions

This investigation included a unique analysis of conditioned PA−12 samples using FTIR, a technique rarely utilized in PBF literature, in addition to DSC. Characterisation indicated that across 336 hours of oven conditioning, there were two separate, time-dependant trends, which suggested an interplay between the multiple aging processes occurring during PBF.

Initially, DSC showed a 4.2 °C increase in T_m, as well as progressive increases in ΔH_f and ΔH_c, but only a 1.8 °C reduction in T_c. Across the same period of storage, FTIR spectra displayed an insignificant change in imide peak height. As such, due to the increase in crystallinity over the first 100 hours, secondary crystallisation appears to

be the dominant aging process over this period. However, between 100 hours and 336 hours of storage, there was a 9.3 °C reduction in T_m and a 11.8 °C decrease in T_c. These changes are closely correlated with an accelerated increase in imide peak absorbance and significant sample discolouration. Hence, with extended storage times, thermo-oxidative degradation became dominant over other aging processes. The mechanical behaviour of PA−12 plaques supports the trends observed in PA−12 powder. Un-conditioned PA−12 displayed ductile behaviour, but with increased storage time, there was progressive embrittlement of the material and significant reductions in strength. The loss of mechanical properties is likely a consequence of chain scission and subsequent reductions in molecular weight as a result of thermo-oxidation. Samples of virgin PA−12 powder were pre-dried in a desiccator to examine the effect of hydrolysis on PA−12 degradation. With 100 days pre-drying, the reduction in T_m after 336 hours of storage was 3 °C less than un-dried PA−12. Similarly, pre-drying saw a decrease in the presence of imide bonds and reduced sample discolouration. These differences show that thermo-oxidative degradation is accelerated by moisture present within PA−12.

These results illustrate an interaction between the multiple aging and degradation processes which can occur when PA−12 is exposed to conditions found within MJF. Through a combination of characterisation techniques, the dominant aging process across different periods of storage was quantified. As well as adding to the research community, this improved understanding could be utilised by the AM industry. The current use of set, arbitrary refresh ratios could be addressed to help develop a more sustainable and cost-effective recycling strategy in the future.

4.6 Supplementary Information 1

Experimental data at all storage times for PA−12 powder, whereby the values shown are taken as an average from 3 repeats.

Storage Time (hours)	Peak T_m (°C)	T_m Endpoint (°C)	ΔH_f (Jg^{-1})	Crystallinity (%)	Peak T_c (°C)	ΔH_C (Jg^{-1})
0	185.8 (±0.27)	187.8 (±0.27)	107 (±3.2)	51 (±1.5)	144.7 (±0.21)	54 (±2.3)
24	188.0 (±0.00)	190.9 (±0.58)	109 (±4.2)	52 (±2.1)	144.0 (±0.13)	56 (±3.5)
48	188.9 (±0.11)	193.6 (±0.14)	111 (±2.9)	53 (±1.4)	143.4 (±0.11)	59 (±2.3)
72	189.4 (±0.11)	193.4 (±0.43)	111 (±3.1)	53 (±1.5)	143.2 (±0.22)	60 (±2.7)
96	190.0 (±0.28)	194.5 (±0.42)	113 (±2.8)	54 (±1.4)	142.7 (±0.39)	58 (±1.7)
120	189.1 (±0.11)	192.8 (±0.38)	106 (±0.8)	51 (±0.4)	142.9 (±0.11)	54 (±1.8)
144	188.9 (±0.20)	192.8 (±0.28)	117 (±7.0)	56 (±3.4)	141.9 (±0.11)	62 (±2.8)
168	188.4 (±0.08)	192.4 (±0.21)	115 (±0.9)	55 (±0.4)	141.6 (±0.10)	59 (±1.2)
192	188.4 (±0.39)	190.8 (±0.70)	95 (±7.3)	45 (±3.5)	140.2 (±0.67)	48 (±4.1)
226	188.7 (±0.09)	191.3 (±0.38)	91 (±6.2)	43 (±2.9)	141.0 (±0.17)	48 (±3.5)
266	184.8 (±0.45)	187.1 (±0.63)	107 (±4.7)	51 (±2.2)	138.3 (±0.17)	58 (±0.1)
312	184.6 (±0.02)	187.5 (±0.00)	81 (±0.7)	39 (±2.5)	134.0 (±0.49)	47 (±0.2)
336	180.7 (±0.04)	184.5 (±0.79)	79 (±7.2)	38 (±3.5)	131.1 (±1.24)	49 (±0.9)

CHAPTER 5 – RE-USE OF POLYAMIDE-12 IN POWDER BED FUSION AND ITS EFFECT ON PROCESS-RELEVANT POWDER CHARACTERISTICS AND FINAL PART PROPERTIES

Published article.

Additive Manufacturing; Volume 80; 25 January 2024, 103961;

https://doi.org/10.1016/j.addma.2024.103961

Benjamin Sanders[1], Edward Cant[2], Mike Jenkins[1*]

1. School of Metallurgy and Materials, University of Birmingham, Elms Road, Birmingham B15 2SE, UK
2. The Manufacturing Technology Centre, Ansty Park, Coventry CV7 9JU, UK

Author contributions:

Sanders, Benjamin: Writing – original draft, Writing – review & editing, Visualization, Validation, Methodology, Investigation, Formal analysis, Data curation, Conceptualization. Cant, Edward: Writing – review & editing, Resources, Methodology, Conceptualization. Jenkins, Michael: Writing – review & editing, Supervision, Methodology, Conceptualization.

Acknowledgements

The authors would like to acknowledge the facilities and technical support of the Manufacturing Technology Centre. The authors would also like to thank Prototal UK Ltd. for providing test specimens and powder samples, and to ASTM for funding the laser sintering build cycles which were completed by Prototal UK Ltd.

5.1 Abstract

Powder bed fusion (PBF) is an additive manufacturing technique capable of fabricating highly complex, individualised, and lightweight polymer components. However, to maximise the potential of PBF, in terms of both economic efficiency and environmental sustainability, a successful powder re-use strategy is essential. During a build, aging and degradation processes affect the re-usability of un-sintered powder, so used powder is usually refreshed with virgin material before re-use. This study considers the effectiveness of using a 70:30 (used: virgin) refresh ratio in a specific PBF technique: laser sintering (LS). Across a total of seven printing cycles, polyamide-12 (PA-12) powder refreshed with 30% virgin material after each build, revealed a 4.5 °C increase in melting temperature. There was also a 20% reduction in particle flowability, which may be related to the presence of fine satellite particles and considerable particle cracking. This deterioration in powder quality resulted in a 5.8% increase in total part porosity, and an 11% reduction in the ultimate tensile strength of fabricated parts, over the seven build cycles. A Pearson correlation test indicated that the reduction in powder flowability was the most significant (p-value of 0.005) cause for the loss of part strength; emphasising that the revolution powder analyser could be a useful complimentary technique for determining the quality of used powder within laser sintering. Nonetheless, compared to previous studies which re-used 100% aged PA-12 powder, without refreshing with any virgin material, the observed reduction in part strength is relatively modest. This suggests that a 70:30 refresh ratio offers a good compromise between maintaining part performance, particularly for non-critical applications, without having to add an unnecessary amount of virgin powder. Therefore, this study reveals the relationship between the

deterioration of powder properties and reductions in part strength; yet highlights the benefits of operating with a 70:30 refresh ratio when re-using PA-12 powder across multiple build cycles.

5.2 Graphical Abstract

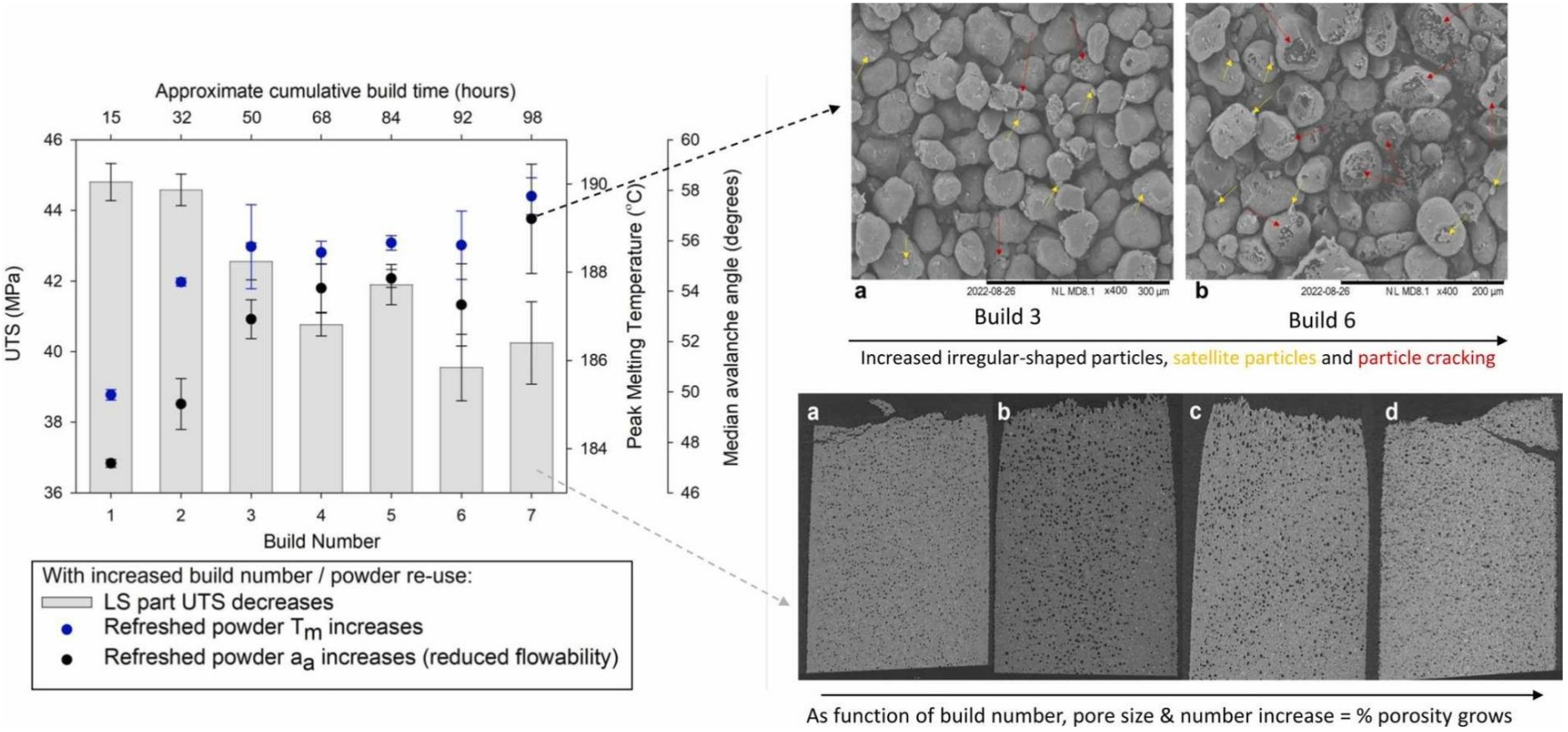

5.3 Introduction

Laser sintering (LS) is a powder bed fusion process which has gained prominence in the additive manufacturing industry and is increasingly used for the fabrication of commercial polymer products. LS offers many benefits over more conventional techniques such as injection moulding, and other AM methods e.g., stereolithography. LS provides great design freedom, which allows the production of highly complex, individualised products [13, 18]. Other advantages of LS include dimensional precision, light-weighting, and the manufacture of components with strong mechanical properties [13, 14, 16-18, 207]. As a result, LS has become increasingly popular in medical (e.g., individualised prosthesis), aerospace, and architectural application areas.

In LS, thermoplastic powder, most commonly polyamide-12 (PA-12) [15, 21, 22, 38, 51], is stored within a build chamber at elevated temperatures. Typical LS build temperatures are between 168 °C to 172 °C [14, 38], which is above the crystallisation temperature (T_c), yet just below the melting temperature (T_m), of PA-12. A CO_2 laser then provides the extra energy required to melt selected regions of the powder layer, based on the 3D-CAD data provided for the designed part. The build platform is lowered, and a fresh layer of powder is deposited before another scan causes polymer particles to fuse together, in the desired shape for that 2D cross-section [16, 17]. This is repeated until all the necessary powder coalesces, layer-by-layer, to form a 3D part [13, 14, 39, 40]. During the LS process, the build chamber utilises an inert gas environment to restrict oxidative degradation [28], however many state of the art LS machines still contain 2-5% residual oxygen [38, 168]. Within LS, PA-12 dominates the market for polymeric feedstock materials due

to its wide processing window, whereby there is a large temperature range between the start of melting and the start of crystallisation. This helps maximise powder consolidation and limit part warpage [169, 207, 208]. PA-12 powder also displays good flowability, relatively low moisture absorption, and a high sintering rate [38, 169, 193, 207].

Another significant advantage of LS is that the sintered and consolidated particles are contained within an unfused powder bed, so the removal of support structures is not required [13, 17, 19, 20]. Unconnected islands and overhangs are supported by the surrounding, un-sintered powder within the build chamber [13, 19]. As a result, the most complex features can be manufactured and multiple parts, of different sizes and geometries, can be arranged together, without restrictions, within the powder bed. This enhances part nesting and increases productivity [13, 16-18, 20]. On the other hand, as the majority of powder within a build chamber is used as support material, LS has an inefficient powder utilisation rate and, for each build, only ~10-20% of the powder deposited is consolidated into final parts [16, 23, 25, 26, 49].Therefore, the remaining 80-90% of un-sintered powder must be re-used to ensure the process is financially feasible and environmentally sustainable [16, 17, 21].

LS-grade PA-12 powder is estimated to be 5000% more expensive, per kg, than equivalent polyamide feedstock for injection moulding [64]. Therefore, maximising powder re-use is economically vital [17, 21, 26, 64]. However, during a build cycle, PA-12 powder is exposed to high temperatures for extended periods of time. This inevitably results in aging and degradation processes which limit the re-usability of the material [16-18, 21, 23, 38, 51, 53]. LS also involves a cooling stage, which is

often double the duration of the build, prolonging aging of the un-sintered powder [16, 17, 33]. Aging and degradation processes possess the capability to alter the intrinsic and extrinsic properties of PA-12 powder; following multiple refreshing cycles the feedstock material may display heterogeneous behaviour, with a wide variation in properties [208]. This is problematic because, to ensure the fabrication of high-quality parts, LS must follow stringent processing conditions and requires extremely close control of material properties [62, 64]. Key intrinsic parameters include thermal properties such as the processing window, T_m, and development of crystallinity. Whilst particle morphology (e.g., sphericity, shape, and size), and particle flowability are crucial extrinsic characteristics that are imperative to the successful production of LS parts [62, 64]. As such, aging processes may limit the re-usability and processability of PA-12 powder, which could ultimately result in the manufacture of underperforming LS components. Therefore, it is common practice for virgin PA-12 powder to be added to the un-sintered, “used” powder, in an attempt to restore the material properties. This refreshed blend is then used in subsequent builds. The refresh ratio defines the ratio of used to virgin material, and commonly 50-70% of used powder is recycled for future use, although the exact refresh rate differs from supplier to supplier [16-18, 21, 23]. Nevertheless, many operators continue to exclusively use a 50:50 refresh ratio, in an attempt to maximise part quality. However, refreshing with 50% virgin powder often results in relatively un-aged powder being discarded unnecessarily, so this recycling strategy can be inefficient and wasteful. In order to improve powder recycling, a compromise between maximising powder re-use, without causing a significant reduction in powder and final part quality is required.

Aging and degradation of PA-12 powder within LS is a complex problem. At the typical powder bed temperature of ~170 °C, there is an interplay between various chemical aging processes as they often occur simultaneously [24, 28]. Solid-state polycondensation (post-condensation) of un-sintered PA-12 powder involves lengthening of polymer chains through reactions of end groups; this linear chain growth leads to an increase in molecular weight (M_w) [15, 21, 26, 53, 65]. On the other hand, chain scission and cross-linking, which usually have opposing effects, can occur as a result of thermo-oxidation [18, 26, 38]. Most LS machines utilise an inert (or low oxygen) environment in an attempt to limit the effects of thermo-oxidation. Nonetheless, laser radiation can locally form hydrogen molecule radicals [54, 168]. With extended time, these free radicals can combine with the unavoidable, residual oxygen remaining in the build chamber and initiate oxidation [168]. Furthermore, when semi-crystalline polymers are heated to higher temperatures, there is increased chain mobility in the amorphous regions which may allow developments in crystallinity via a secondary crystallisation process, such as lamella thickening [105, 117, 199, 209]. Previous studies have suggested that polycondensation is the dominant aging phenomenon within LS [15, 25, 26, 38, 41, 61, 67, 160], however, the possibility of other processes occurring with repeated powder re-use cannot be ignored.

The effect of aging on the re-usability of PA-12 powder within LS has previously been explored from a range of perspectives. Multiple papers have attempted to simulate the conditions found within a LS build chamber by storing PA-12 powder at various temperatures, for a range of time periods, within a nitrogen flushed or vacuum oven [16, 25, 28, 39, 210]. These authors used a range of techniques such as differential

scanning calorimetry (DSC), scanning electron microscopy (SEM), and size exclusion chromatography (SEC) to investigate the change in powder properties as a result of aging. Although useful for improving the understanding of aging and degradation, oven conditions cannot be directly compared to a LS build process, nor reveal the effect aging has on the mechanical properties of LS parts. Other studies have focussed specifically on the effect of oven conditioning, or powder re-use within LS, on the change in melt viscosity of PA-12 powder, often using melt flow rate (MFR) as the primary measurement [17, 18, 21, 66, 210]. Generally, they reported that, with increased aging of PA-12 powder, MFR significantly reduced, indicating an increase in melt viscosity. This correlates to an increase in molecular weight (M_w), which was attributed to polycondensation. However, exclusively using MFR to characterise a change in powder properties has limitations, as it is an energy-intensive technique and only concentrates on one material property. Consequently, MFR is unable to detect other types of aging, such as secondary crystallisation; it also fails to account for more process-relevant parameters, such as particle morphology and flowability, which likely have a significant effect on the property profile of laser sintered parts.

Furthermore, some papers compared virgin, aged, and once-recycled powder samples by characterising the change in T_m, coalescence behaviour, particle flowability, and M_w as a result of aging [15, 38, 51, 167]. Zarringhalam et al., re-used PA-12 powder with a 67:33 refresh rate and observed a 143% increase in M_w after just one build cycle [51]. Conversely, using a 50:50 refresh ratio, Sillani et al., saw a 170% increase in M_w [15]. Comparing these two papers suggests that the extent of polycondensation, and subsequent increases in M_w, is greater within the study that refreshed with more virgin powder. Although there may have been slight differences

in the specific build processing parameters between these two investigations, which could have altered the rate of polycondensation, these results indicate that using higher refresh rates may not always be beneficial for controlling the properties of feedstock powder. This one example provides some insight into the inefficiency of current powder re-use strategies, such as exclusively using a 50:50 refresh ratio. Nevertheless, despite providing valuable insight into the change in powder behaviour across one build cycle, further investigation is required to determine the effect on powder and part properties across multiple build cycles. This is necessary because, within industry, it is essential that powder is re-used for multiple cycles, particularly when aiming to minimise environmental impact and cost.

Multiple papers have begun to explore the effect of aging when re-using PA-12 powder across multiple build cycles, without refreshing with virgin material [26, 53, 160, 169, 193, 194, 208]. They reported that with increased PA-12 powder re-use, there is an increase in melt viscosity [26, 53, 160, 194] which ultimately contributes to reductions in part density and part strength [53, 160, 194]. However, these studies either don’t reveal build times, so the total cumulative build time is unknown [160, 194, 211], or use build times much shorter than what is common within industry [26, 53]. As such, the cumulative build times, even across five process cycles, remain relatively modest (e.g., < 27 hours [26]) and the extent of material aging is limited. More recently Alo et al., exposed PA-12 powder to eight build cycles and, with increased cumulative build time, observed a significant decrease in the degree of crystallinity, as well as a change in the size and shape distribution of feedstock powder. This change in powder properties resulted in significant reductions in the strength of sintered parts [169, 208]. However, it is important to highlight that, in

between build cycles the feedstock material was not refreshed with virgin powder, which contradicts common industrial practice. As such, there is limited understanding regarding the effect of refreshing used powder with virgin material, when re-using PA-12 powder across an extended number of LS cycles, with a large cumulative build time. Determining whether virgin refresh rates are able to counteract the changes in used powder properties, as a result of aging, is crucial to help predict the property profile of LS parts. Current industry practices generally use either 50:50 or 70:30 refresh ratios. In this work a 30% refresh rate was implemented in order to investigate the possibility of re-using more powder, without compromising final part performance.

Therefore, this study intends to quantify the effect of aging on the relationship between process-relevant properties of PA-12 powder, and the behaviour of LS parts, when operating with a 70:30 refresh ratio. PA-12 feedstock, refreshed with 30% virgin powder before each build, was exposed to seven LS cycles, with an extended cumulative build time of over 200 hours, including the cool-down. This work provides quantitative data about the capability of a 30% refresh ratio for restoring the properties of used powder, and ultimately determines whether a 70:30 refresh ratio offers a good compromise between increasing powder re-use, without a detriment to final part quality. In addition, the most suitable characterisation techniques for determining PA-12 powder quality were identified, providing more information about the suitability of un-sintered powder for re-use within LS. This will help inform more efficient classification of used powder recovered from different build cycles, thereby helping the industry realise improved recycling strategies.

5.4 Experimental Methodology

5.4.1 Materials and sample preparation

An outline of the sample preparation procedure is shown in *Figure 5.1.* The work was carried out using industrial grade PA-12 powder (PA2200, EOS GmbH), whilst laser sintered parts were fabricated using standard EOS build parameters [212], so print conditions were 'locked-in'. For each build, the chamber temperature was 170±1 °C, and the unloading temperature was 130±1 °C. PA-12 powder was re-used for a total of seven build cycles, using a refresh ratio of 70:30 (used: virgin). Therefore, as the supplied powder is refreshed before each build, only ~12% of 'used' powder recovered from build 7 would have been through every build cycle. To quantify the time that refreshed powder was exposed to the processing temperature, and to better indicate the extent of powder aging, the cumulative build time (t_c) was also recorded. After seven builds, the t_c was 98 hours, whilst the total cumulative time (including the cool down) was 208 hours. The approximate cooldown time, of build to breakout temperature, ranged from 14 to 18 hours across the seven build cycles.

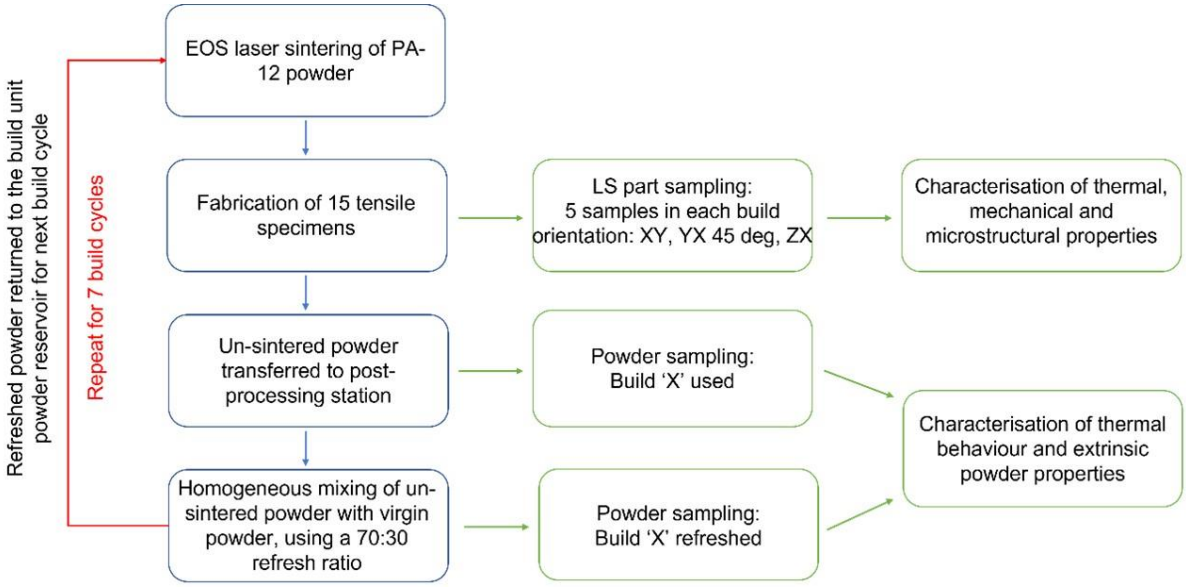

Figure 5.1 – Summary of the work package, sampling procedure and sample characterisation.

During each build the refreshed powder was used to produce tensile samples in 3 different build orientations (XY, ZX and YX 45 degree), as shown in *Figure 5.2.* The LS dog-bone tensile specimens had a gauge length of 70 mm, width 12.89 mm and thickness of ~3 mm, whereby a micrometre screw gauge was used to measure the sample thickness.

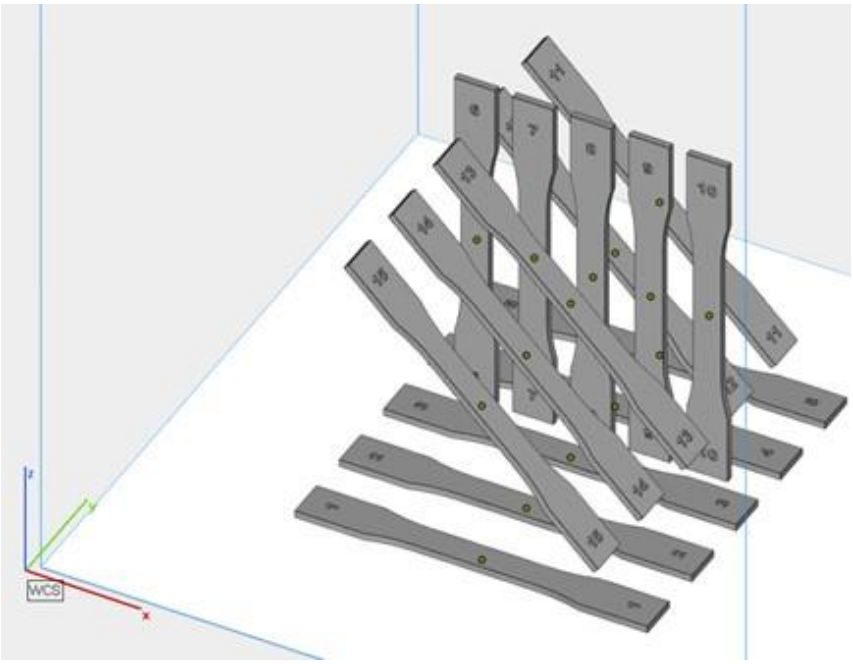

Figure 5.2 – Build orientations of tensile samples. 1-5 are horizontal orientation (XY), 6-10 are vertical orientation (ZX) and 11-15 have an angular orientation (YX 45 degree).

5.4.2 Powder characterisation

Differential scanning calorimetry (DSC) analysis of virgin, used, and refreshed powder was performed using a Mettler Toledo DSC-1. Before conducting material characterisation experiments, the DSC was calibrated using zinc (T_m 419.5 °C, ΔH_f 107.5 Jg^{-1}) and indium (T_m 156.6 °C, ΔH_f 28.45 Jg^{-1}); nitrogen gas (flow rate 100 $mLmin^{-1}$) was used to limit oxidative degradation occurring during experiments. Samples, with a mass of 6±0.5 mg, were heated from 25 °C to 220 °C, using a heating rate of 10 $°Cmin^{-1}$ and then cooled at the same rate. Analysis was primarily carried out on the first heating and cooling cycle, to understand the effect of the LS build conditions on the thermal properties of PA-12 powder. Integration of the endothermic melting peak provides a value for heat of fusion (ΔH_f). This can be used

to estimate percentage crystallinity (X_c) using *Equation 5.1* whereby ΔH_f^0 = 209.3 Jg^{-1} (100% crystalline PA-12) [15]. For every sample, 3 DSC repeats were conducted, and an average calculated.

$$\boldsymbol{X_c}\ (\%) = \frac{\Delta \boldsymbol{H_f}}{\Delta \boldsymbol{H_f^0}}\ \boldsymbol{X\ 100} \qquad \textit{(Equation 5.1)}$$

Various process relevant, extrinsic powder properties were also analysed for virgin, used, and refreshed powder samples. A Mercury Scientific revolution powder analyser (RPA) quantified particle flowability. A low RPM was used so that the flowability of powder particles could be measured by analysing a sequence of avalanches. Full experimental parameters are outlined in *Table 5.1.* For each batch of PA-12 powder, 3 repeats were recorded, and an average taken. The change in particle size distribution (PSD), with build number, was evaluated using a Malvern Mastersizer 2000 which uses laser diffraction to determine the particle size of PA-12 powder suspended in water. Tests were conducted according to the ASTM B822-10 standard test method for PSD of powders and compounds. Powder particle shape and microstructure was characterised using scanning electron microscopy (SEM). To prepare the sample a single layer of PA-12 powder was applied onto carbon adhesive, on an aluminium stub. Samples were sputter coated in gold using an Enscope Engineering LTD. SC500 gold sputter coater to reduce surface charging in the samples. To ensure the polymer sample was conductive, copper tape was applied from the aluminium stub to the powder surface. The sample was viewed using a tabletop Hitachi 3030+ SEM, under vacuum, with a voltage of 15kW and using a mix of back-scattered electrons (BSE) and secondary electrons (SE) signals. Magnifications ranged from 40x to 500x, depending on the feature of interest, and the

auto-focus/auto-contrast functions were utilised. This was repeated with each batch of refreshed PA-12 powder.

Table 5.1 - RPA flowability test set up parameters. Experiments were conducted under a room temperature of 25°C, and room humidity of 40%.

Parameter	Value
Sample Volume	25 cc (tap density)
Rotating speed	0.3 RPM
Preparation time	60 seconds
Avalanche threshold	0-65%
Angle calculation	Half
No. of avalanches recorded	150
Image capturing rate	25 frames per second

5.4.3 LS part characterisation

The thermal behaviour of LS parts was characterised using the same DSC method described in *section 5.4.2.* DSC samples, with a mass of 10±0.5 mg, were prepared by punching discs from the grip sections of tensile specimens.

To establish the influence of powder re-use on the mechanical properties of LS parts, all tensile samples were examined on an Instron 7877 material tester. Each experiment was run according to ASTM D638 tensile tension testing for plastics, with a 20 kN load cell and strain rate of 10 mm/min. Bluehill universal materials analysis software (Instron) provided measurements of ultimate tensile strength (UTS), yield

strength (YS), and elongation at break (EAB). The Young's modulus was estimated from the linear elastic region of the stress-strain curves. For each build number, in every build orientation, an average was taken from 5 samples. The statistical significance of the data was measured using ANOVA analysis and post-hoc T-tests, with the Bonferroni correction, to indicate which build number showed significant changes in mechanical properties.

Following mechanical testing, samples were further characterised using SEM. The fracture surface of randomly selected tensile specimens, from each build number, were prepared and viewed using the same method described in *section 5.4.2.* To quantify the change in porosity of LS tensile specimens with increased build number, multiple samples were analysed using x-ray computed topography (XCT). The scans were performed using a Diondo D2 micro-CT machine using a voltage of 30 kV, a current of 200 μA, and 2500 projections. The magnification was x17.3, which yields a sufficient voxel size to accurately measure porosity. Pore size, number, and overall percentage porosity were estimated using ImageJ software.

5.5 Results and discussion

5.5.1 Powder characterisation

5.5.1.1 Thermal behaviour

The change in the melting behaviour of used and refreshed powder, across a total of seven build cycles, was measured using DSC (*Figure 5.3)*. With increased powder re-use, used powder displayed a gradual increase in peak melting temperature (T_m) and endpoint of melting ($T_m e$), which is particularly important for subsequent LS builds. Conversely, the refreshed powder shows an initial increase in T_m, but then any further change is less significant.

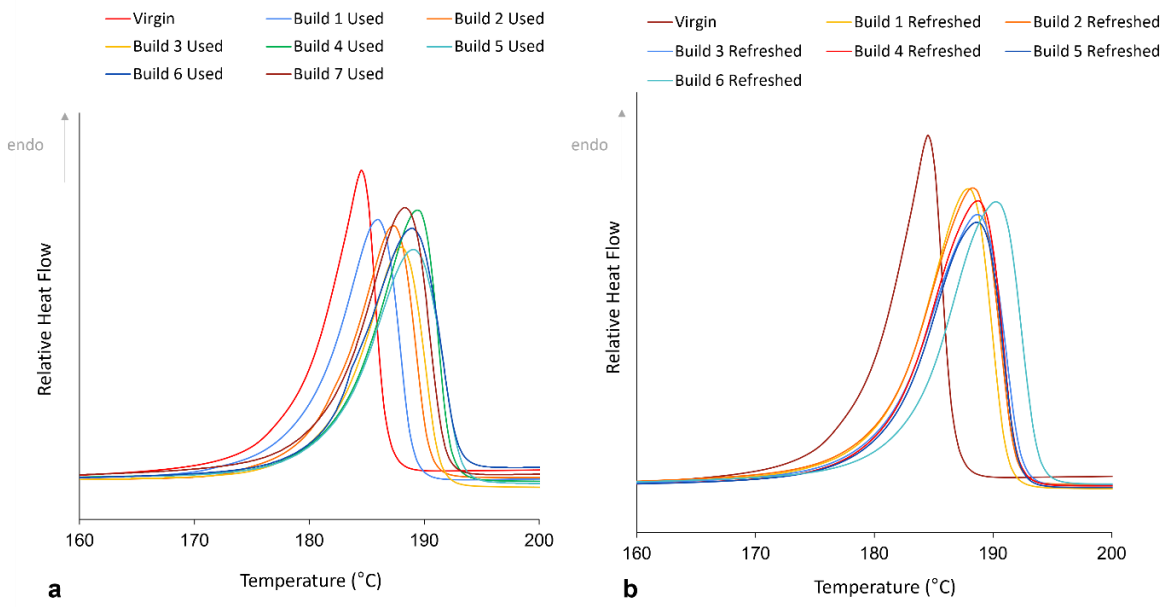

Figure 5.3 – The change in melting behaviour of a) used powder and b) refreshed powder, with increased build number.

The difference in the melting behaviour of used and refreshed powder, across multiple build cycles, is shown more clearly in *Figure 5.4.* The average peak T_m of used PA-12 powder increases almost linearly until build 5, at which point T_m is 4.2 °C greater than virgin material. This is followed by a 0.5 °C reduction in T_m; within the sensitivity of the DSC, this change is considered insignificant, nevertheless it represents a change in the observed trend. On the other hand, refreshed powder also shows an initial rise in T_m and by build 2, refreshed powder has a peak T_m 3.4 °C higher than virgin material. However, the increase then plateaus and there is no further change until build 6, where a 1 °C rise is observed *(Figure 5.4a).*

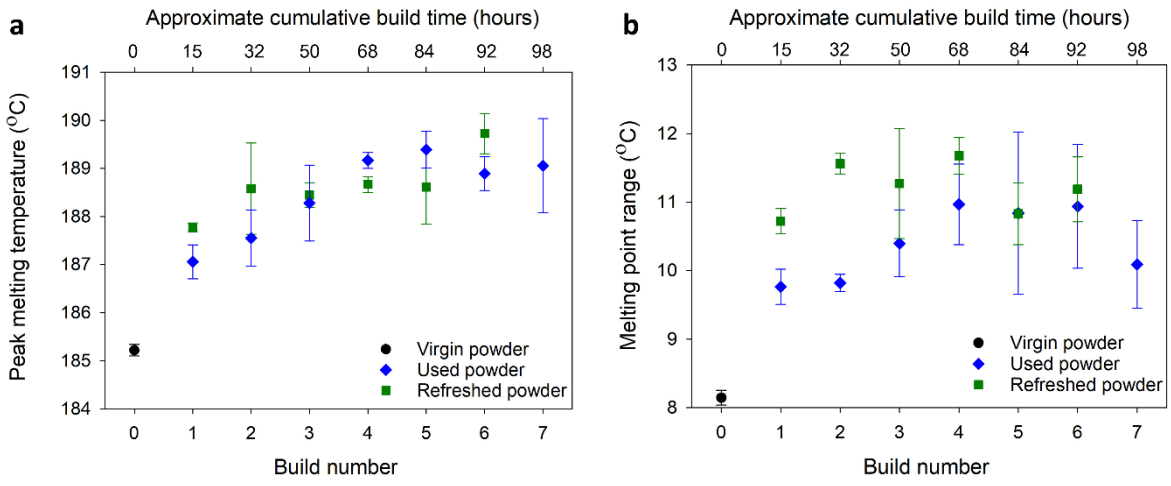

Figure 5.4 – Comparing the average change in a) Peak T_m and b) T_m range for used and refreshed PA-12 powder across 7 LS build cycles and as a function of t_c. All datapoints are taken as an average from 3 repeats.

In both used and refreshed powder, the increase in T_m may be explained by solid-state polycondensation, as reported previously [24, 25, 41, 160, 167]. Prior research revealed reservations about how a process which occurs primarily in the amorphous

phase can significantly affect the melting of crystalline structures [209]. Nonetheless, it is widely reported that the inert (or low oxygen) conditions found within a LS build chamber favours the polycondensation reaction, which increases the rate of macromolecular chain growth [15, 25, 26, 38, 41, 61, 67, 160]. This can lead to an increased molecular weight, resulting in a higher melting point [23, 24, 26]. Increases in T_m could also be attributed to cross-linking [24, 160], but cross-links usually form as a product of the thermo-oxidation cycle [82, 83, 159], so is unlikely to occur in a LS build chamber with limited oxygen. However, secondary crystallisation, an aging process often overlooked in previous LS studies, can also contribute to changes in the melting behaviour [23, 24, 26, 158, 159]. At the elevated temperatures found within an LS build chamber, amorphous chains have greater mobility, which can allow further crystallinity to develop via a continuous lamellar thickening process, resulting in an increased T_m [209]. The DSC was unable to identify a significant increase in sample crystallinity *(Table 5.2)* but this characterisation technique may not be sensitive enough to detect the gradual lamellar thickening process. Therefore, secondary crystallisation occurring within unfused PA-12 powder cannot be ruled out, and lamellar thickening may contribute to an increased T_m, in addition to the polycondensation process.

Table 5.2 - The change in thermal properties of used and refreshed powder, as a function of build number, measured via DSC.

	Used powder				***Refreshed powder***			
Build number	Peak T_m (°C)	Endpoint T_m (°C)	Peak T_c (°C)	Crystallinity (%)	Peak T_m (°C)	Endpoint T_m (°C)	Peak T_c (°C)	Crystallinity (%)
Virgin	185.2 (±0.12)	187.7 (±1.90)	145.8 (±0.77)	47 (±3.8)	185.2 (±0.12)	187.7 (±1.90)	145.8 (±0.77)	47 (±3.8)
1	187.1 (±0.35)	190.1 (±1.22)	144.0 (±0.88)	47 (±0.8)	187.8 (±0.09)	191.1 (±0.24))	146.0 (±0.00)	51 (±0.7)
2	187.6 (±0.59)	190.5 (±1.09)	143.9 (±0.70)	49 (±4.2)	188.6 (±0.95)	192.1 (±1.15)	145.7 (±0.96)	50 (±1.9)
3	188.3 (±0.79)	191.8 (±1.31)	143.2 (±1.02)	48 (±2.0)	188.4 (±0.25)	191.7 (±0.69)	145.7 (±0.00)	48 (±1.8)
4	189.2 (±0.17)	192.8 (±0.41)	144.4 (±0.20)	49 (±1.0)	188.7 (±0.17)	192.3 (±0.19)	145.8 (±0.19)	48 (±0.8)
5	189.4 (±0.38)	193.0 (±0.23)	144.8 (±0.19)	50 (±0.5)	188.6 (±0.77)	191.9 (±0.84)	146.0 (±0.88)	49 (±1.0)
6	188.9 (±0.35)	192.2 (±0.71)	144.7 (±0.00)	48 (±1.7)	189.7 (±0.42)	193.1 (±0.35)	144.7 (±0.33)	50 (±1.1)
7	189.1 (±0.98)	192.1 (±0.74)	144.8 (±0.69)	49 (±1.0)	-	-	-	-

In refreshed powder, virgin material is added in an attempt to try and restore powder properties; the aim is to prevent further increases in T_m and return the thermal properties back towards that of the virgin powder. However, in this work over the first two build cycles, the increase in T_m of refreshed powder is slightly greater than the change in used samples. Measuring the peak melting temperature of polymers within the DSC is only accurate to ±0.5 °C, so the initial variability between used and refreshed samples is not considered significant. Nonetheless, it does indicate that a 30% refresh ratio may not be high enough to completely overcome the effects of polycondensation and secondary crystallisation. As a result, over the first two build cycles, refreshed powder still shows a significant increase in melting temperature. This could be explained by previous suggestions that polycondensation occurs primarily on thermally unstressed (virgin) powder, whilst the rate of chain growth within used, aged powder is lowered due to the reduced availability of end-groups [18, 21, 24]. *Figure 5.4a* shows that the major increase in T_m occurs during build 1, where 100% of material is thermally “unstressed”. Following build 2, 50% of the powder has been used within two full build cycles, so the rate of polycondensation may reduce and refreshing with virgin powder now prevents further changes in the melting temperature. This is supported by the behaviour of used powder samples. Between virgin material to used powder recovered from build 1, the increase in T_m has a gradient of 1.8, whilst the gradient for the increase over builds 2 to 5 is 0.6, emphasising that the major change occurs on thermally unstressed material. In the used samples, no virgin material is added so T_m continues to increase, albeit at a reduced rate. On the other hand, the plateau observed in the refreshed samples after

build 2 emphasises that the refresh rate is now successful in inhibiting further changes in T_m.

Used and refreshed powder samples also show increases in melting point range, as a function of powder re-use, and at each build number the T_m range for the refreshed mixture is slightly greater than used powder (*Figure 5.4b)*. The difference between used and refreshed powder makes sense because, when 30% virgin powder is added to the used material, the refreshed blend now contains two separate populations; virgin powder particles which should melt at lower temperatures, and used powder particles that are expected to have a higher T_m. As a result, there is a change in shape and broadening of the endothermic melting peak. A rise in the endpoint of melting, as shown in *Table 5.2*, will also contribute to the increase in T_m range; this explains why there is a broadening of the melting interval within both used and refreshed samples, as a function of build number. Analogous to the changes in peak T_m, the most significant increase in T_m range occurs over the first two build cycles. Furthermore, in both types of powder, the thermal properties appear to become more heterogeneous with increased build number, demonstrated by rising standard deviation values. In the context of LS, increases in the endpoint of melting are important because it means that more energy is required for complete melting of powder particles. So, assuming that build processing parameters remain constant, this could lead to incomplete particle melting and an increased number of nascent particles, which hinders particle coalescence during sintering, resulting in greater pore density [23, 38, 53, 168]. The industrial significance of the observed variations in melting temperature, as a function of build number, can be further understood upon characterisation of the behaviour of final LS parts *(section 5.5.2.1).*

Increased powder re-use across multiple LS build cycles also influences the crystallisation behaviour of PA-12 on cooling from the melt *(Table 5.2).* Although the change in crystallisation temperature (T_c), with build number, does not follow the same trend as the melting behaviour, there is a similar difference between used and refreshed powder. In the used material there is an immediate reduction in T_c and used powder recovered from build 3 has a T_c 2.6 °C lower than virgin material. Reductions in T_c provide further evidence of solid-state polycondensation occurring within un-sintered powder during LS builds. Lengthening of polymer chains via polycondensation leads to a greater number of entanglements, which hinders chain ordering and postpones the crystallisation process [16, 17, 26, 28, 38, 51]. Following build 3, there is no further change in T_c of used powder, which further supports the suggestion that the rate of the chain growth decreases within aged powder, due to a reduced availability of active end groups [18, 21, 24].

In refreshed powder, the only significant change in crystallisation behaviour occurs after 5 build cycles, at which point there is a 1.5 °C reduction in T_c, mirroring the 1.1 °C increase in T_m observed at the same build number. At this point, a higher volume of powder has been re-used in multiple build cycles, so one might expect the recovered material to be more degraded. The change in trend following build 5 indicates the point at which a refresh ratio of 70:30 may be insufficient to restore the thermal properties of PA-12 powder. Providing that there is close monitoring of powder quality after each build, there is potential for industry to extend powder re-usability. Small modifications of the processing parameters (e.g., laser power and scanning speed) at the stage where it appears the thermal properties can no longer be restored, could help ensure that the powder is still suitable for re-use in

subsequent builds. However, it should be recognised that altering processing parameters may then alter the rate of degradation processes. Alternatively, for industrial applications where the control of thermal properties is especially crucial, the use of flexible refresh ratios could be explored. For example, over the first two build cycles, where the rate of polycondensation is heightened, a greater proportion of virgin powder could be added to try and prevent the observed increases in melting temperature. A similar approach could also be taken following further changes in thermal properties after build 5. However, the use of different refresh ratios was beyond the scope of this project; further work would be required to investigate the effectiveness of higher virgin refresh rates.

5.5.1.2 Extrinsic powder properties

The re-usability of PA-12 powder across multiple LS builds is heavily dependent on various material properties [62, 64]. In this section, analysis has been focused on ‘refreshed’ samples because this was the powder reintroduced into the bed chamber before each build, and the material that final LS components were fabricated from. Within industry, the importance of utilising a more modern powder characterisation methodology, which provides understanding of the material properties required to fabricate high quality parts consistently, has been recognised in recent years [64, 213]. As such, there is currently a growing demand for a more equivalent analysis method to determine flowability in LS systems [213]. Powder flowability is closely related with spreadability, which is required within LS to ensure a uniform layer thickness, smooth even surfaces, and equal particle size distribution across a powder bed. This ensures homogeneous powder layers and subsequently consistent properties of LS parts. The revolution powder analyser (RPA) is a particularly useful

characterisation technique because it can measure the flowability of powder particles under a similar stress state to when powder is spread over the build platform during LS. Although the RPA is not a direct representation of what occurs during LS with regards to the re-coater blade, it provides more process relevant data than other, more commonly used characterisation techniques, such as melt flow rate. The RPA exports high volumes of data, however the key characterisation indexes regarding particle flowability are avalanche angle (a_a), avalanche time (a_t), and avalanche energy (a_e) [15, 213, 214], so these parameters are the focus of this study. With increased build number there is an increase in the median a_a and a_a distribution, both of which indicate a reduction in flowability of refreshed powder *(Figure 5.5a).* This was supported by an ANOVA analysis, which emphasised that there was a statistically significant difference in a_a as a function of build number *(Figure 5.5b).* The change in a_a follows an almost identical trend to the melting behaviour of refreshed powder, which increases confidence in the significance of these results. Across the first two builds there was a 12.2% increase in a_a, this was followed by a plateau, before another 7% increase following build 6. Post-hoc t-tests, with the Bonferroni correction, emphasised that, the powder recovered from build 2 showed a statistically significant difference to virgin powder, as denoted by * in *Figure 5.5b*.

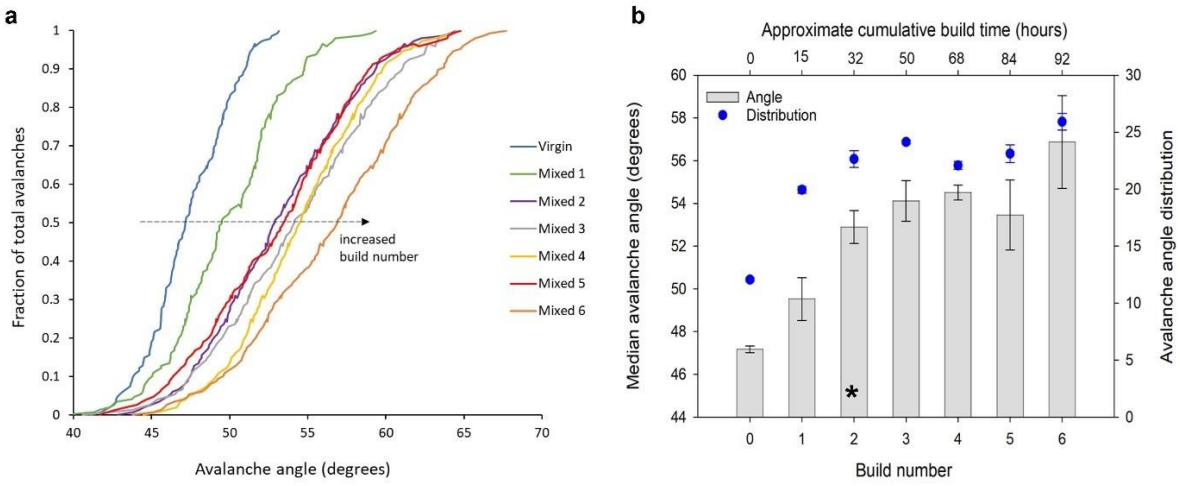

Figure 5.5 – Displays the change in a) cumulative avalanche angle and b) average avalanche angle / average avalanche angle distribution, as a function of build number and t_c. All datapoints in a) and b) are taken as an average of 3 repeats.

Avalanche energy and avalanche time showed similar behaviour to the observed increase in avalanche angle (*Table 5.3).* These changes emphasise that, with increased powder re-use, there was a reduction in powder flowability. This may have consequences for subsequent LS builds because when using powder with reduced particle flow, it may hinder how easily powder can be spread across the build platform. Therefore, powder may not be uniformly distributed, and during sintering this could result in the fabrication of parts with decreased density, increased porosity, and significant layer delamination [38, 53, 154]. These factors have the potential to decrease the mechanical properties and aesthetics (e.g., orange peel) of parts, which may render the component un-suitable for use in its industrial application.

Table 5.3 – Average change in the key markers of refreshed powder particle flowability, with build number, measured using the revolution particle analyser.

Build Number	Avalanche angle (degrees)	Avalanche energy (mJ)	Avalanche time (seconds)
0	47.2 ±0.16	11.5 ±0.73	4.1 ±0.42
1	49.5 ±0.97	12.6 ±1.20	4.7 ±0.62
2	52.9 ±0.85	12.9 ±1.30	4.9 ±0.45
3	54.1 ±0.91	12.7±1.12	5.0 ±0.46
4	54.5 ±0.92	13.1 ±1.18	5.1 ±0.05
5	53.5 ±0.61	13.5 ±0.73	5.1 ±0.49
6	56.87±0.88	14.7 ±0.94	5.4±0.25

Reductions in particle flowability have previously been associated with changes in particle size [38, 53, 62, 154]. LS polymer powders require a particle size distribution between 20 μm and 80 μm; fine particles that are too small induce stickiness whilst larger particles hinder the flowability of the powder across the powder bed [62]. Some authors have reported a broadening of the polydispersity index (PDI) in used powder, which indicates the presence of large molecules [24, 25, 158]. These large particles may form in aged powder due to severe agglomeration as a result of greater cohesive forces between particles [168, 208]. Particle size analysis was carried out to try and understand whether the reductions in powder flowability were caused by a significant change in particle size. However, with increasing build number the Malvern mastersizer was unable to detect any change in particle size distribution

(Table 5.4). Therefore, although there is evidence of polycondensation occurring *(section 5.5.1.1),* it does not appear to cause agglomeration of particles, or an increase in particle size, so may not explain the reduction in powder flow observed in this study.

Table 5.4 – Particle size distribution analysis of refreshed powder at each build number.

Build number	Dx10	Dx50	Dx90
0	37.0±0.90	56.8±0.50	85.0±0.70
1	37.2±0.78	56.9±0.45	84.8±0.46
2	36.8±0.72	56.4±0.64	84.5±0.38
3	37.0±1.42	56.2±0.87	83.5±0.72
4	37.1±0.20	56.5±0.31	84.9±0.40
5	33.9±1.67	54.8±0.60	84.4±0.66
6	36.0±0.72	55.0±0.35	84.5±0.35

Changes in particle sphericity and surface smoothness can also affect the flowability of PA-12 powder. Perfectly spherical particles, with a smooth surface, allow adjacent particles to move freely past each other, which reduces friction and mechanical interlocking during re-coater spreading [208]. Smooth and spherical powder also assists powder flow, minimises agglomeration, and enables greater packing densities [38, 215]. Nonetheless, despite particle sphericity being highly beneficial for LS processing, most commercial PA-12 powders are produced via precipitation from

solvents, such as ethanol, and forming fully spherical particles using this method can be difficult [216-218]. Samples of virgin and refreshed PA-12 powder were analysed using SEM to monitor whether there was a change in particle morphology with build number. Virgin powder contained particles with a relatively spherical shape and fairly smooth surface, whilst there was limited particle cracking *(Figure 5.6a).* In contrast, the powder recovered from build 3, showed a greater number of non-spherical particles, with many displaying a more elongated, oval shape *(Figure 5.6b),* as observed in previous studies [193, 208, 218].

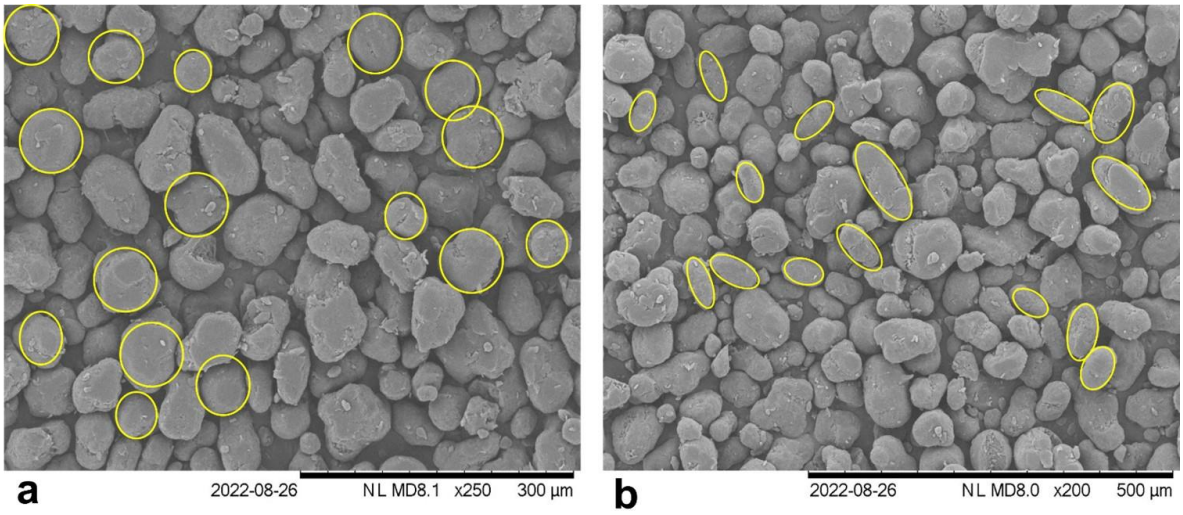

Figure 5.6 – SEM images of showing particle morphology of a) virgin powder and b) refreshed powder recovered from build 3.

Nevertheless, the more significant change in particle morphology is the considerable increase in particle cracking and the appearance of “satellite” particles which attach themselves to larger particles; it is likely these fine fragments cannot be detected by the Malvern Mastersizer as they are not considered as independent particles. Powder recovered from build 3 showed some evidence of particle cracking *(*Figure 5.7*a),* but, the extent of cracking is accentuated in powder recovered from build 6

(Figure 5.7b). Similarly, within virgin powder some fine satellite particles are present *(Figure 5.6),* however they significantly increase in number within samples which have been recovered after use in multiple LS builds (*Figure 5.7)*. In powder recovered from build 6, fragmented, satellite particles are widespread and appear to cluster around crack regions within bigger particles. Satellite particles are thought to form as a result of the high temperatures present within a LS build chamber which makes finer particles stick to the surface of larger particles [208].

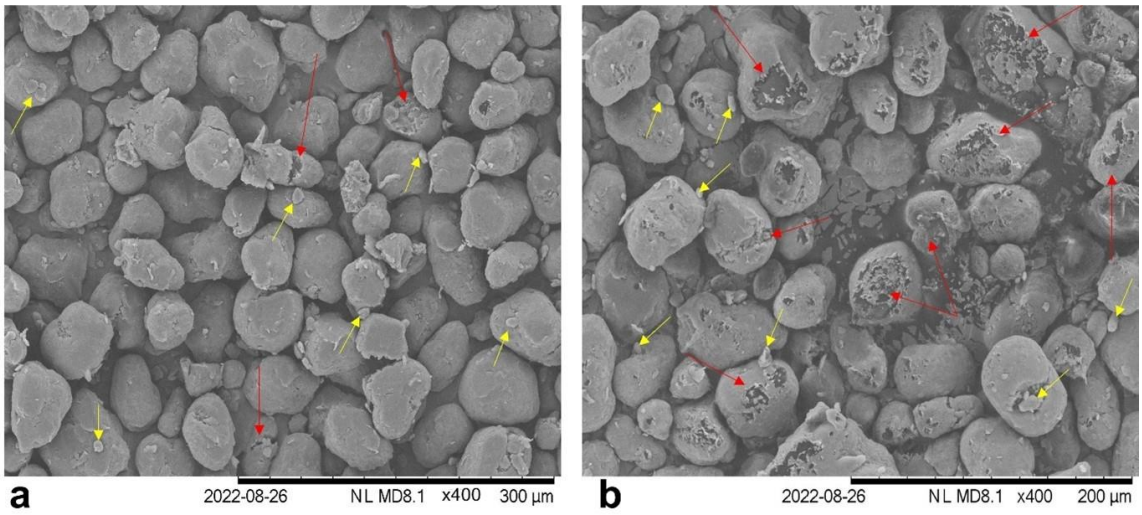

Figure 5.7 – SEM images displaying evidence of significant particle cracking (red arrows) and presence of "satellite particles" (yellow arrows) in a) refreshed powder recovered from build 3, and more significantly in b) refreshed powder revered from build 6.

It should be noted that the presence of irregular particle shapes and particle cracking can still exist in virgin powder, but to a much lesser extent. As such, these results indicate that with increased powder re-use there is a deterioration of particle structure and a reduction in surface smoothness, which can be explained by a variety of

factors. Evaporation of the ethanol solvent used in powder processing, or moisture remaining in the material, may explain the formation of particle cracks [38]. With increased time spent at the elevated temperatures found within a LS build chamber, evaporation will likely occur to a greater extent, so could contribute to the deterioration of powder structure. Equally, if powder handling between build cycles is not conducted in a controlled environment, this may allow more moisture to diffuse into the powder, resulting in further evaporation in subsequent builds. Additionally, successive re-use in multiple builds exposes powder to repeated expansion and shrinkage cycles, which may also cause increased cracking and particle fragmentation [208, 219]. Similarly, deterioration of the particle surface could be related to a mechanical interaction with the re-coater blade.

The observed changes in powder morphology likely explains the reduction in particle flowability, and this could weaken the mechanical properties of sintered parts [53, 154]. Furthermore, particle cracking may impair the surface finish of parts, resulting in an ‘orange peel’ appearance, which has been commonly reported when parts are fabricated using severely degraded powder [16, 17, 23, 26, 38, 160].

5.5.2 LS part characterisation

Analysis of the physical and mechanical properties of LS parts provides more information about the relationship between the deterioration of powder properties and the reduced quality of final parts. This delivers increased understanding of the extent of quality compromise over multiple build cycles, when operating with a 70:30 refresh

ratio; demonstrating how much performance is lost with increased, extended powder re-use.

5.5.2.1 Part microstructure

5.5.2.1.1 Differential Scanning Calorimetry (DSC)

The thermal behaviour of sintered parts was characterised using DSC (*Figure 5.8).* Parts fabricated from fresh, virgin powder (build 1) show a single, symmetrical melting endotherm with a peak T_m of 182 °C. However, in parts produced from aged powder a secondary melting peak forms, as an upper-temperature shoulder peak, on the main melting endotherm. The development of this shoulder peak is likely related to the presence of un-molten regions at particle cores within LS parts [41]. Such particles have a higher T_m, and the additional heat provided by the laser is insufficient to fully melt the spherulitic structures present within the particle. The shoulder peak appearing between 190 °C to 193 °C supports this theory because this is a similar temperature to the endpoint of melting observed for powder samples recovered from builds 3, 5 and 7 *(Table 5.2).*

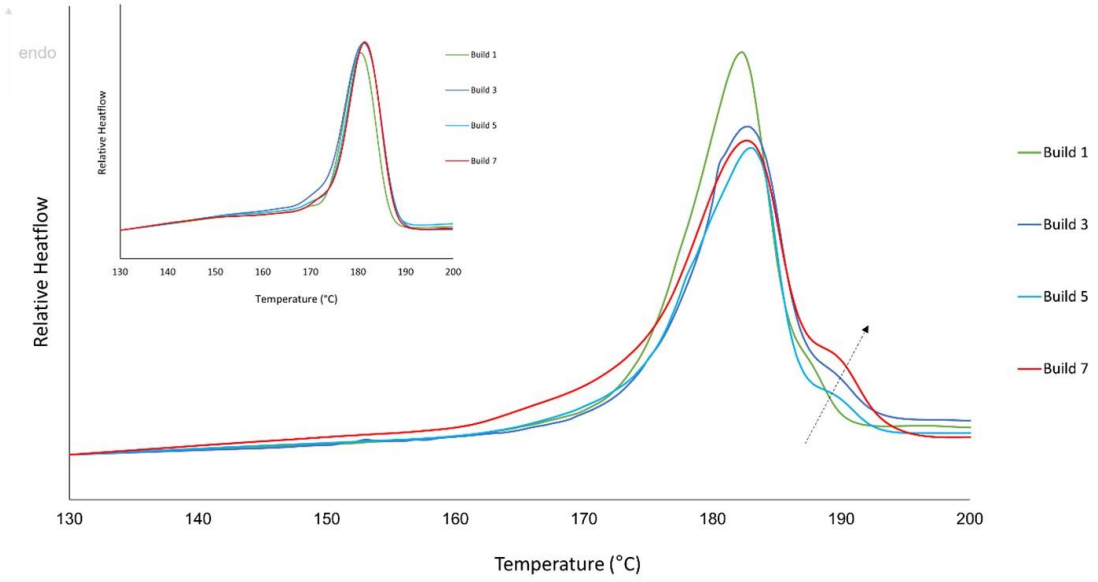

Figure 5.8 – First heating run recorded on the DSC shows the change in melting behaviour of LS parts as a function of build number. The arrow illustrates the growth of an upper temperature shoulder melting peak which appears in parts fabricated from re-used, aged powder. Insert displays the second heating run, where a single melting endotherm is observed.

In *section 5.5.1.1.,* it was suggested that polycondensation, and potentially secondary crystallisation, via lamellar thickening, caused T_m to shift to higher temperatures. Un-molten particle cores remaining in the structure of LS parts, indicates the presence of residual crystal fragments. As these fragments only appear in parts produced from aged powder, it would suggest that aged powder contains some particles with thicker crystalline lamellae that are unable to fully melt during the sintering process. On the second heating run *(Figure 5.8, insert)*, the shoulder peaks disappeared, and all samples displayed a symmetrical melting peak; the previously un-molten particle cores remaining after the build process were fully melted when exposed to higher temperatures within the DSC. This provides further evidence of lamellar thickening because secondary crystallisation is a reversible process.

Conversely, although polycondensation is fully reversible under the right conditions, the high temperatures present within a LS build chamber removes the water required for the reverse reaction to occur. Therefore, during LS, increased M_w due to polycondensation is effectively an irreversible change, and the higher T_m structures present in the first heating run would be expected to persist if caused by polycondensation. As such, the thermal behaviour of LS parts emphasises that lamellar thickening is likely occurring (alongside polycondensation), within un-sintered powder during the LS build process.

The presence of unmolten particle cores may lead to hindered particle coalescence, reduced material consolidation, and increased porosity in parts fabricated using re-used powder. Similarly, crystalline fragments remaining due to incomplete melting, could act as nucleation sites during solidification, which would affect the crystallisation kinetics and subsequent crystalline microstructure of LS parts. All of these factors may contribute to the observed reductions in mechanical properties *(section 5.5.2.2.2),* emphasising how deterioration of powder quality can alter the properties and functionality of LS parts. Thermal characterisation of LS parts also provides context to the changes in the melting behaviour of refreshed PA-12 powder *(section 5.5.1.1).* Evidence of incomplete particle melting highlights that 1 °C to 4 °C increases in the T_m of PA-12 powder are significant in terms of its suitability for re-use within LS. Within industry, the formation of unmolten regions is a product of aging which could be overcome by altering certain build parameters. For example, increasing laser power, and decreasing scan speed when printing with a higher proportion of re-used powder, would allow complete melting of all sintered powder particles.

5.5.2.1.2 Scanning Electron Microscopy (SEM)

The fracture surfaces of tensile samples were analysed to determine whether the deterioration of powder quality causes a change in the microstructure of LS parts. *Figure 5.9* compares the fracture surfaces of a LS part fabricated using virgin powder (build 1) with LS samples formed using powder recycled through 3 build cycles (build 4). Build 1 displays some evidence of pores forming but these are randomly situated and low in number. However, build 4 shows a significant increase in pore size and pore number, with an equal distribution of pores across the surface of the sample.

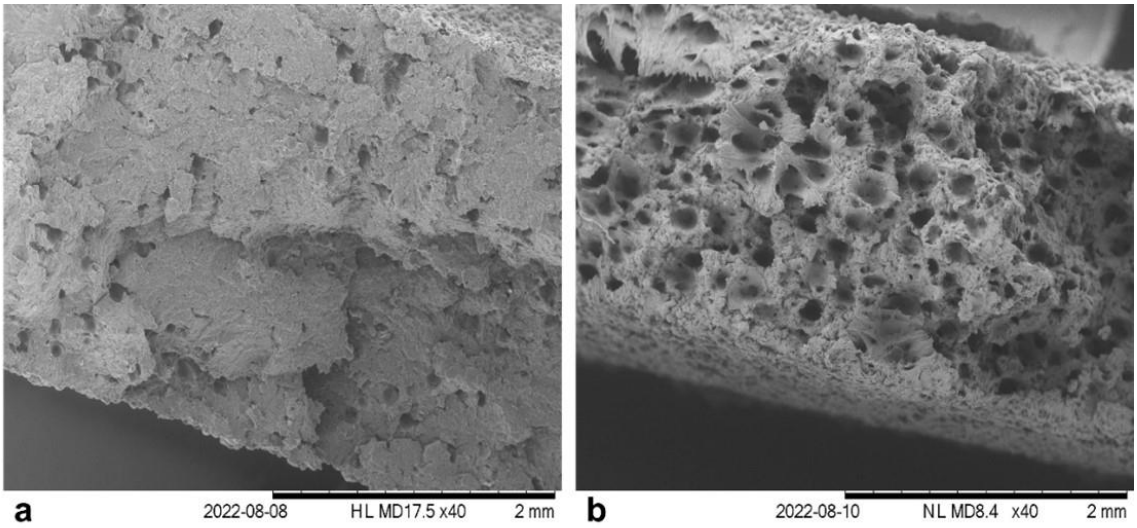

Figure 5.9 – SEM images, taken using a mix of BSE and SE, displaying the fracture surface of tensile samples, fabricated from a) virgin powder and b) refreshed powder re-used in 3 build cycles.

5.5.2.1.3 X-ray Computed Topography (XCT)

SEM images only reveal a small cross-section of the fracture surface, so tensile samples were further characterised using X-Ray computed topography (XCT) to quantify the change in porosity with increased build number. *Figure 5.10* shows that porosity is homogenous throughout all LS parts, and a significant number of pores

are present even in parts fabricated from virgin powder. This is due to limitations of the LS process which cause periodic and interlayer porosity, as well as incomplete melting of larger spherulites [38, 61, 169]. With increasing build number, porosity increases and, more importantly, there is a greater number of larger pores.

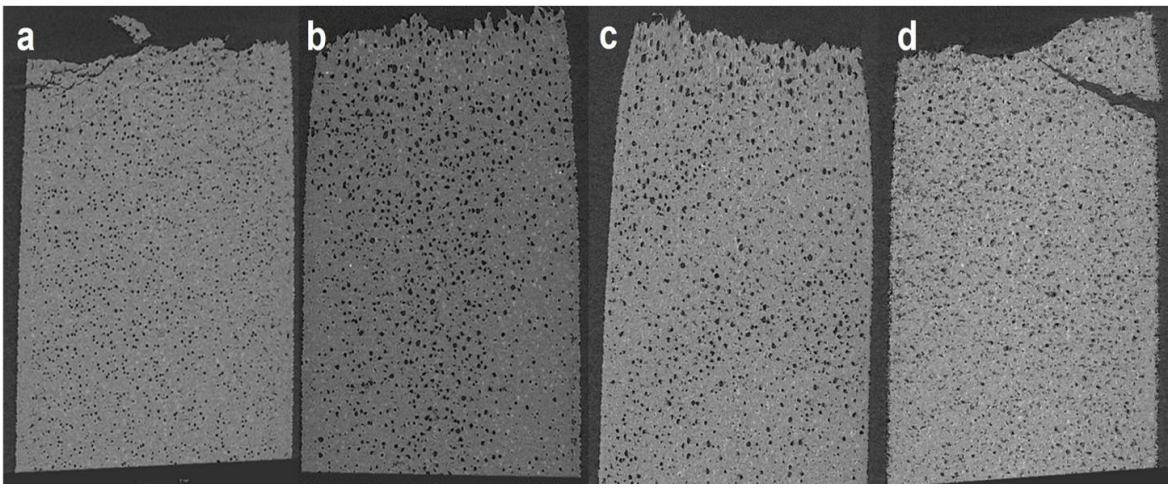

Figure 5.10 – XCT images taken as transversal cuts throughout the centre of LS tensile specimens recovered from different build cycles: a) 1; b) 4; c) 5 and d) 7.

The increase in porosity with build number is also displayed in *Figure 5.11a.* With repeated powder re-use, the average % porosity of parts increases from 4.4% in build 1 samples to 10.2% in samples recovered from build 7. With increased build number, % porosity also displays larger variability, further indicating that used/refreshed powder has a less homogeneous property profile than virgin powder. Across the first five build cycles, the increase in porosity is primarily caused by a 123% increase in pore size. After build 5 there is then a reduction in pore size which likely explains the subsequent plateau in % porosity. Furthermore, when analysing XCT images it became evident that, independent of build number, porosity is significantly limited when scans are captured near the edge of samples; upon

scanning through the thickness of the part, towards the centre, porosity reaches a maximum *(Figure 5.11b).* In this case, it appears that the increased porosity in the centre of parts is caused by a substantial increase in pore number, whilst pore size was generally unaffected. For example, in parts recovered from build 5, XCT scans taken at the edge of samples had an average pore count of 196, whereas the average number of pores in the centre of the part was 1590. This increase in pore number caused the overall porosity to increase from 1.04% at the part edge to 9.5% in the centre, as shown in *Figure 5.11b.*

The increase in porosity as a function of build number is likely multi-factorial. Aging processes, such as polycondensation and secondary crystallisation, can cause a rise in T_m and spherulite size, as explained in *section 5.5.1.1.* This could result in the presence of higher melting point particles and an increased number of un-molten spherulite cores *(Figure 5.8).* Furthermore, reduced powder flowability, as discussed in *section 5.5.1.2,* can cause a decrease in coalescence and consolidation of powder particles. Additionally, increased part porosity could be related to the significant particle cracking observed in refreshed powder samples [207], as displayed in *Figure 5.7.*

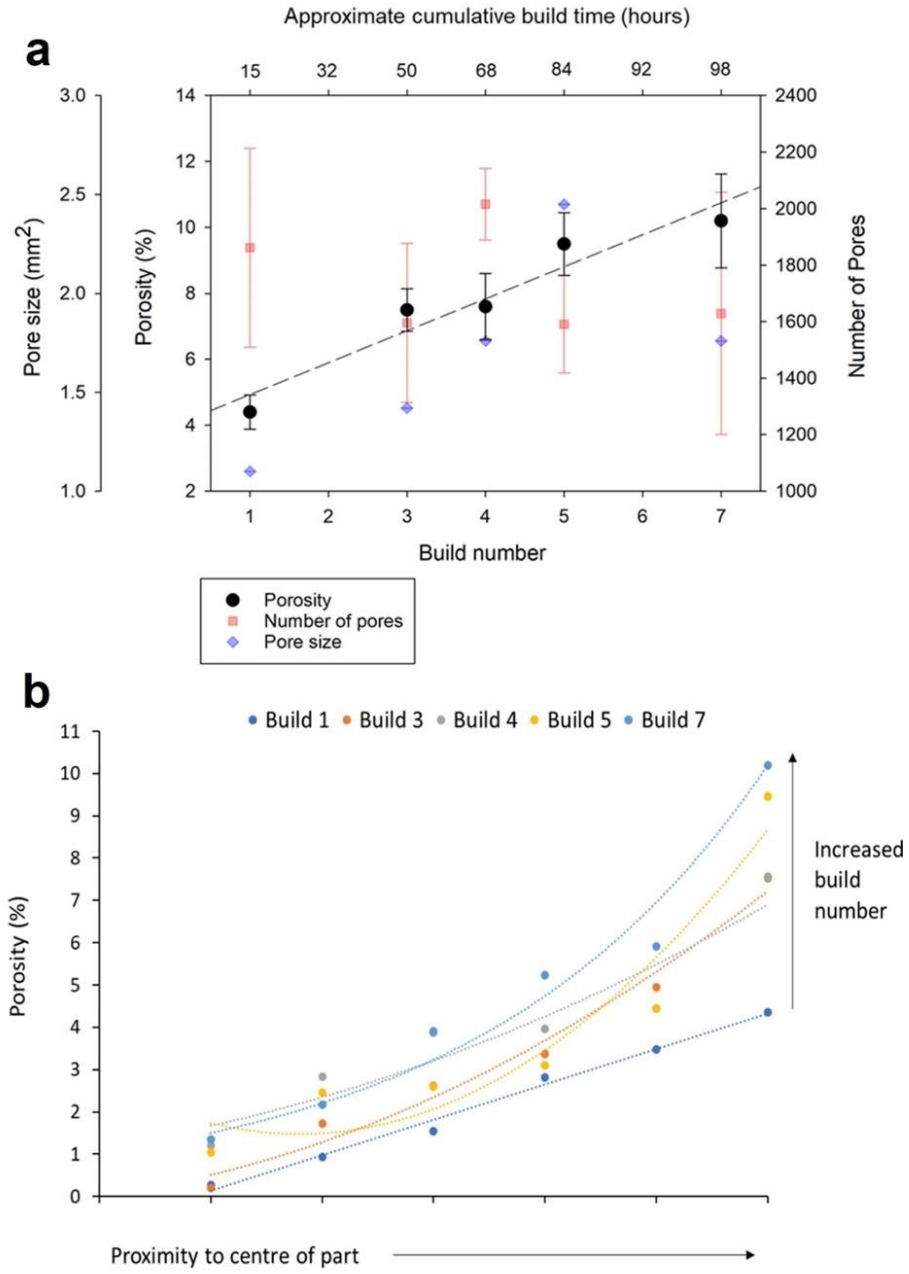

Figure 5.11 – a) displays the change in average porosity, pore size and pore number as a function of build number and t_c, b) demonstrates how porosity alters throughout the thickness of the 3D tensile specimen. In all cases datapoints are calculated as an average of 5 repeats.

5.5.2.2 Mechanical testing of LS parts

5.5.2.2.1 Effect of build orientation on mechanical properties

Independent of powder re-use, multiple processing parameters such as bed temperature, layer thickness, laser power and laser speed can all effect the mechanical properties of LS parts [149, 150]. However, for this study the standard EOS build parameters were locked, so could not be changed for each build. Nonetheless, the orientation of components within the build chamber is also important because parts display anisotropic behaviour, which can significantly affect part density and mechanical properties. *Figure 5.12* shows the overall change in various mechanical properties as a function of build number and build orientation. The most significant difference, in terms of build orientation, is that samples developed in the ZX (vertical) direction are significantly weaker and are the most brittle *(Figure 5.12a and Figure 5.12c).* Vertically positioned samples display weaker interlayer bonding, and during a tensile test, the force is applied perpendicular to the print and pore layer direction, which act as crack propagation and failure initiation sites [41, 153, 169]. Conversely, samples orientated in the horizontal (XY) direction display superior mechanical properties due to a larger and stronger particle bonding area [156, 220]. As a result, ZX tensile samples produced during build 2 had a UTS 3.7 MPa lower, and an EAB 14% less than samples aligned in the XY (horizontal) direction.

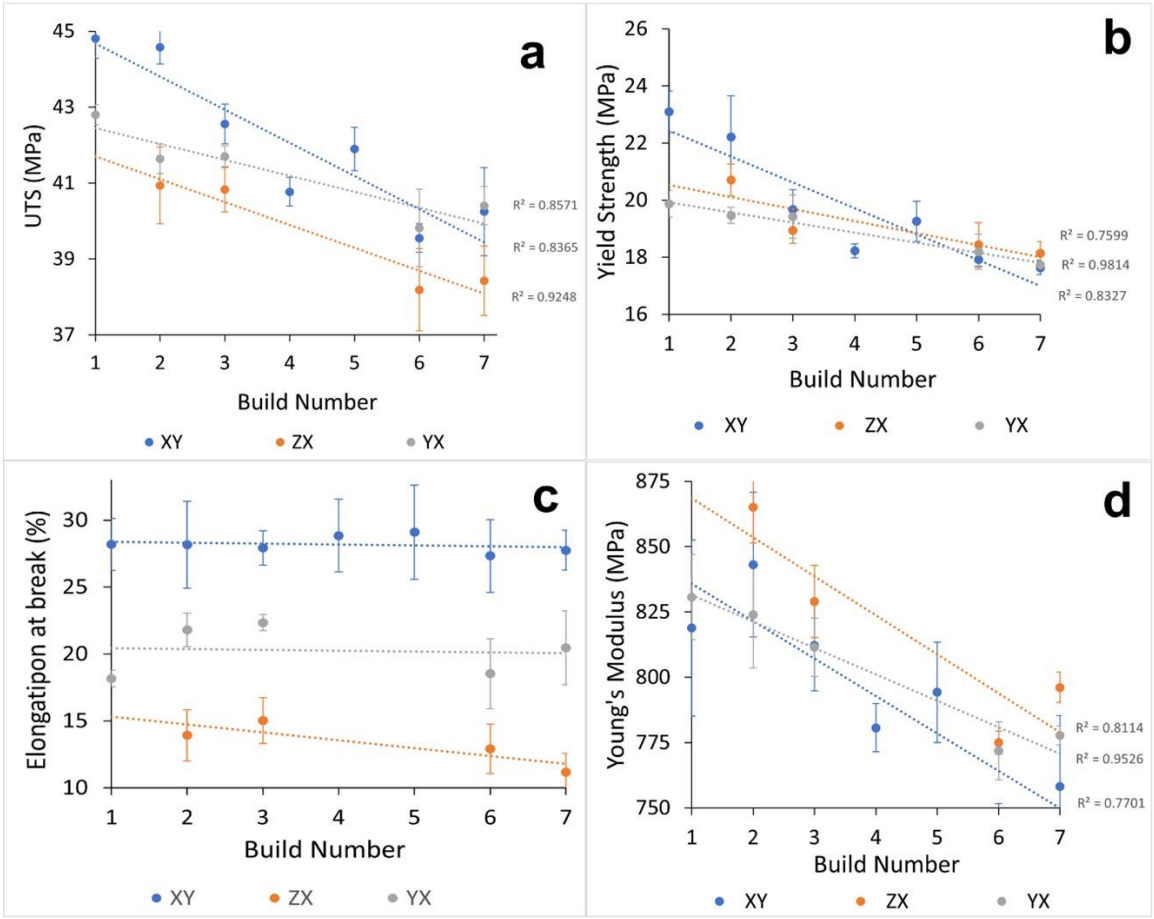

Figure 5.12 – The change in a) UTS, b) yield strength, c) elongation at break, and d) Young's modulus as a function of build orientation and build number. All datapoints were taken as an average of 5 repeats. Note that some datapoints are missing due to failed builds.

5.5.2.2.2 Effect of build number on mechanical properties

As shown in *Figure 5.12* there is a reduction in the strength and modulus of all samples, independent of orientation, as a function of build number. This implies that increased material re-use and subsequent aging of PA-12 powder, has a significant effect on the mechanical properties of fabricated parts in every build orientation. As tensile specimens orientated in the horizontal (XY) direction generally display superior mechanical properties, industrial operators are recommended to print

components in the XY orientation. Therefore, in this study, XY tensile specimens were analysed in more detail to show the change in properties as a function of build number.

Figure 5.13 shows that, across a total of 7 builds, yield strength and UTS reduce by 24% and 11%, respectively, whilst Young's modulus decreased by a relatively modest 7.41%. The reductions in strength can be explained by the changes in the behaviour of PA-12 powder with increased powder re-use. Increases in T_m, as a result of polycondensation and lamellar thickening, can cause incomplete melting and increase the number of nascent particles during sintering. Similarly, polycondensation leads to a higher molecular weight and increased melt viscosity, which may hinder particle coalescence within and between layers [23, 66, 168]. Reduced particle flowability, as discussed in *section 5.5.1.2,* will likely hinder the spread of powder across the build platform, resulting in voids or agglomeration of powder. As evidenced in *section 5.5.2.1.3*, all of these factors can contribute to increased pore density and an increased number of failure initiation sites, resulting in reductions in UTS and Young's modulus.

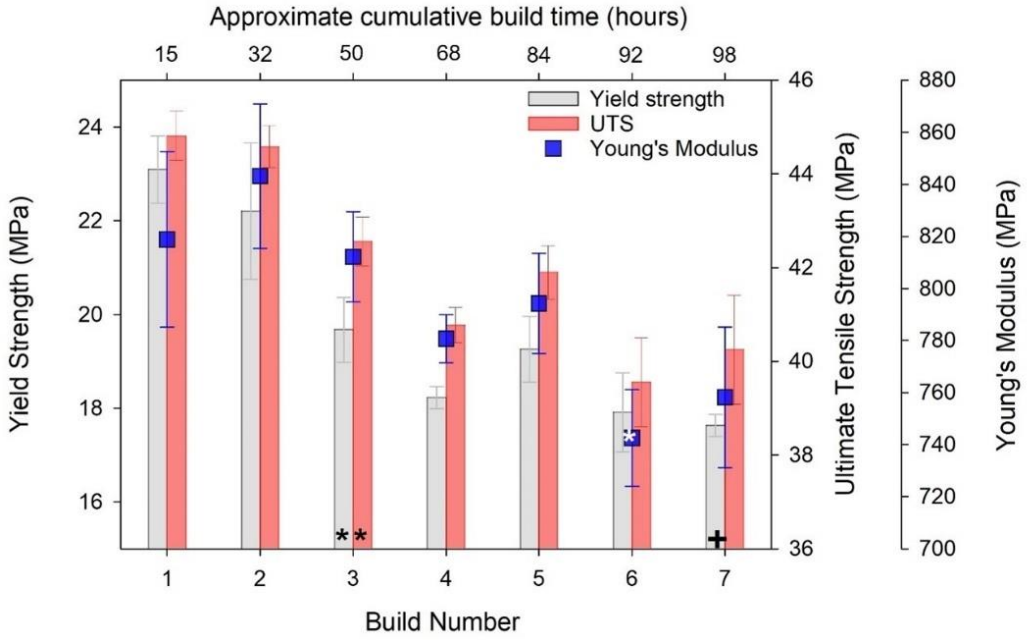

Figure 5.13 - ANOVA analysis showed that, in the XY build direction, there was a significant change in the averages of Ultimate Tensile Strength, Yield Strength, and Young's Modulus, as a function of build number / t_c. All datapoints are taken as an average of 5 repeats. Post-Hoc T-tests, with the Bonferroni correction, emphasise which build number shows a statistically significant (P<0.05) reduction compared to:
** Build 1*

+ Build 3

However, mechanical testing indicated that, as a function of build number, there was only a minimal change in the elongation at break (EAB) of LS parts. Considering the increase in part porosity, a more significant embrittlement of parts would have been expected. There does appear to be some part embrittlement, however the sample variation within each build is high so the statistical significance of the reductions in EAB is limited. Scattering of elongation at break data has been reported previously by Bourell et al.; they suggested that uneven heating and cooling of the powder bed chamber causes variability in pore distribution and, subsequently, inconsistencies in the ductility of LS samples [61]. Furthermore, due to limitations of the laser sintering technology, it is widely considered that the ductility of LS parts is generally an order

of magnitude lower than more traditional manufacturing methods, such as injection moulding [61, 221]. As shown in *Figure 5.10,* even virgin parts are relatively porous, consequently, they have a moderately low EAB of 28%. In parts made from re-used powder, pores remain well distributed throughout the sample, rather than clustering together; this may help prevent weak stress concentrations from forming. Therefore, the 5.8% increase in porosity across 7 build cycles, although appearing substantial, may not be high enough to induce further embrittlement of an already porous material.

The re-usability of PA-12 powder within LS is a complex problem because, with increased powder re-use, alterations in the property profile of un-sintered powder are multi-factorial and the properties of LS parts are difficult to predict. Statistical analysis of the mechanical performance of LS parts is useful because it emphasises the close relationship between the changes in feedstock powder quality, and subsequent part properties, when re-using PA-12 across multiple build cycles, with a 70:30 refresh ratio. From an industrial standpoint this is useful because it quantifies the stage at which powder re-use has a detrimental effect on part properties. In *section 5.5.1, Figure 5.4 and Figure* 5.5 showed that the most significant increases in T_m and avalanche angle occurred over the first 2 build cycles. Similarly, the largest rise in part porosity occurred between builds 1 to 3 *(Figure 5.11)*; consequently, there was a statistically significant reduction in average yield strength and UTS during the 3rd build cycle *(Figure 5.13).* Both powder and part behaviour then display a period of minimal change between build 3 and build 6. Finally, there is a further reduction in the strength of parts fabricated in build 7; directly corresponding to the point at which it was hypothesised that a 70:30 refresh rate was no longer sufficient for maintaining

powder quality. As a result, continued powder re-use beyond 7 build cycles would be expected to result in further, more substantial reductions in part strength. Due to the almost parallel changes in the behaviour of powder and sintered parts, the alterations in thermal properties and particle flowability of feedstock powder must explain the observed reduction in part strength. Nonetheless, interpreting the absolute significance of these changes is difficult because the impact is heavily dependent on the industrial application of the component. For example, non-safety critical applications, such as tooling, could withstand some loss of strength and stiffness, whereas in aerospace applications, any reduction in mechanical properties could be critical.

5.5.3 The relationship between the behaviour of refreshed powder and the properties of final LS parts

The close relationship between the deterioration of powder quality and the mechanical performance of LS parts is further shown in *Figure 5.14.* This emphasises how increases in T_m and avalanche angle, as a result of aging, are mirrored by a reduction in the UTS of LS parts. Understanding this connection is crucial to improving the recyclability of PA-12 powder. To clarify the sensitivity and effectiveness of the DSC and the RPA for accurately defining whether un-sintered powder is suitable for re-use, it is necessary to quantify the specific relationship between powder and part properties.

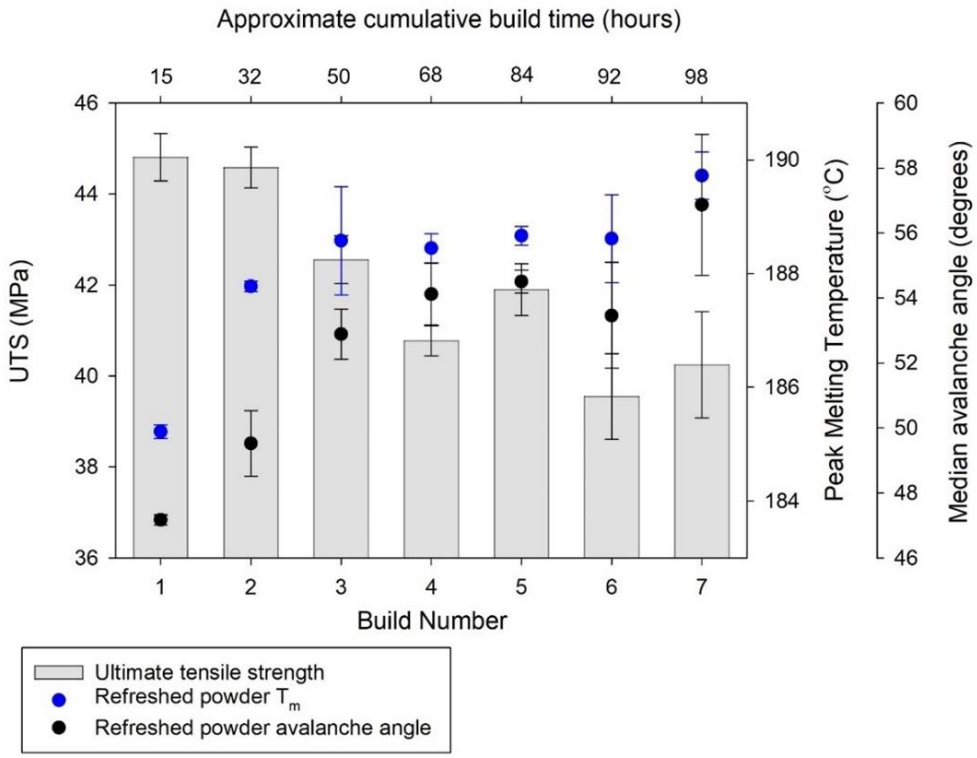

Figure 5.14 - The relationship between the thermal behaviour and flowability of PA-12 powder, with the mechanical properties of LS parts, as a function of build number and t_c.

A Pearson correlation test can quantify the strength of the relationship between two linearly related variables [222]. *Figure 5.15* shows that increases in melting temperature, and reductions in flowability, of the supplied powder tend to cause a decrease in the strength of final LS parts. A Pearson correlation test quantified that changes in both T_m and a_a have a statistically significant effect on UTS, as shown by the table in *Figure 5.15.* The relationship between a_a and UTS is stronger, emphasised by the higher Pearson co-efficient and lower p-value, then the same outputs for T_m. The UTS vs a_a correlation is significant to the 0.01 level, whilst UTS vs T_m is still statistically significant, but only to the 0.05 level. Therefore, with increased powder re-use, reduced powder flowability (increased a_a) appears to be the most prominent cause for the decline in mechanical properties of sintered parts.

Decreased particle flow can hinder the spread of powder across the build platform, resulting in an uneven, non-homogeneous powder layer; this may prevent full part coalescence and consolidation, leading to regions with significant porosity. Other powder changes, such as increased T_m and a higher number of unmolten particles, will also contribute to reductions in part strength, but the results outlined in this study suggest that decreased powder flow is the most significant factor.

This data suggests that thermal analysis of powder, which is a common characterisation technique within current LS studies, is not necessarily the best indicator of powder reusability. On the other hand, the RPA is a non-destructive, quick, and energy efficient testing method, which has rarely been used in previous literature, but could be a useful complementary tool for quantifying the quality of PA-12 powder within the LS industry. Therefore, there may be benefits of utilising the RPA alongside other characterisation techniques to optimise and manage the lifecycle of recycled PA-12 powders. As a result, data from this work has contributed to the development of an ASTM work item. This ASTM work item aims to facilitate the development of a standardised set of guidelines that will help define the effectiveness of different characterisation techniques for determining the quality of feedstock powder, and ultimately, its potential for re-use within LS.

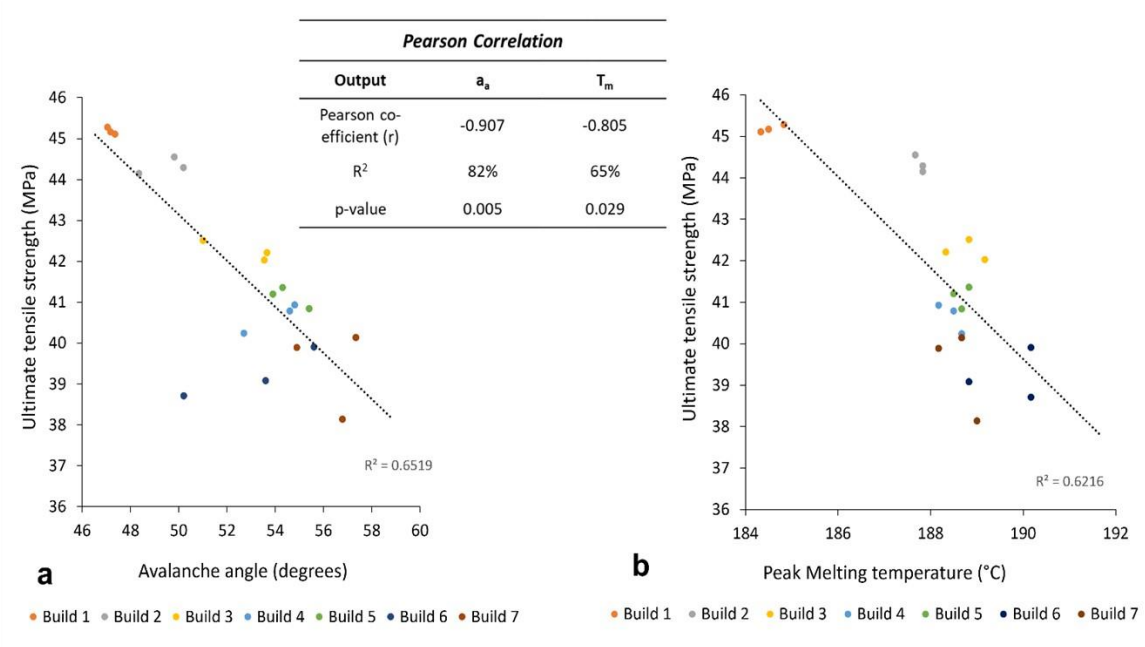

Figure 5.15 – Displays the negative correlation between UTS and a) increased T_m, and b) increased avalanche angle. A Pearson correlation table quantifies the statistical significance of these relationships.

Within the LS industry using a 30 or 50% refresh rate is common practice, but the effectiveness of these refresh ratios for maintaining powder and part quality, over multiple build cycles, has not been explored previously. In a refresh ratio, virgin material is added to dilute the effects of material aging on the thermal, chemical, and physical properties of feedstock powder; the aim is to ensure that the “refreshed” powder is capable of fabricating high-quality components. However, due to the environmental and economic cost of discarding un-sintered powder, and replacing it with high amounts of virgin material, a compromise is required. Therefore, in this study, a 30% refresh rate was used to investigate whether powder re-use can be maximised (relative to 50:50), without compromising the quality and functionality of LS parts.

Results showed that powder quality deteriorated as a function of build number, indicating that a 30% refresh rate may not be sufficient to prevent all the effects of aging that occur when re-using powder across multiple build cycles; as such, there was a corresponding reduction in the mechanical properties and density of LS parts. Nonetheless, across a total of 7 build cycles, there was only an 11% reduction in the ultimate tensile strength of sintered parts. This loss of part strength is relatively modest when compared to previous work which employed a similar experimental procedure, but without refreshing the feedstock with any virgin powder [23, 169]. Alo et al., stated that parts sintered using virgin powder had a UTS of 40.6 MPa, which is equivalent to the tensile strength measured for build 1 in this study. However, parts printed in build 6 (cumulative build time of ~62 hours) displayed a UTS of only 12.8 MPa, which represents a 69% reduction in UTS [169]. Similarly, Kuehnlein et al., saw a 30% reduction in UTS after re-using 100% used powder for 5 build cycles, which correlated to a cumulative build time of only 25 hours [23]. Therefore, the results of the current study suggest that, despite alterations in the quality of un-sintered powder, a 70:30 refresh ratio is successful at limiting severe reductions in part strength. This emphasises that a 30% refresh rate can fabricate LS parts with adequate mechanical properties for most industrial applications, for up to at least 7 build cycles. However, in some application areas, e.g., critical end-use products, an 11% reduction in strength would be deemed unacceptable. In this scenario, the supply chain could be better organised to re-distribute more severly aged powder to less critical applications, e.g., printing of prototypes. Alternatively, more virgin powder could then be added to the feedstock if necessary. As such, these results appear to show that a 50:50 refresh ratio is only required when manufacturing critical parts

where maintaining mechanical performance is vital. Overall, increasing the implementation of a 70:30 refresh rate within industry would reduce the production of LS parts with inadequate mechanical properties, that ultimately have to be discarded; whilst allowing 20% more un-sintered powder to be re-used every build cycle. This will help decrease the issue of waste, with significant economic and environmental benefits for the LS industry.

5.6 Conclusion

In this study, using a 70:30 refresh ratio, PA-12 powder was re-used for a total of 7 build cycles, with a cumulative build and cooling time of over 200 hours. The relationship between PA-12 powder properties, and the mechanical behaviour of the resulting LS parts, was quantified.

Differential scanning calorimetry (DSC) showed that, with increased build number, there was a rise in the peak melting temperature (T_m) and endpoint of melting ($T_m e$) of used PA-12 powder. These changes in thermal behaviour were attributed to polycondensation and secondary crystallisation. Refreshed powder, with 30% virgin powder added after each build, displayed an initial shift in T_m to higher temperatures over the first two build cycles, before a plateau. This plateau emphasises how an efficient refresh ratio can help control the thermal properties of feedstock powder. It could be argued that, in order to fully combat polycondensation and prevent increases in T_m, a higher refresh ratio should be applied for the first powder recycle, before reducing the amount of virgin powder added in subsequent builds. However, further work would be required to test this concept of flexible refresh ratios before

implementing this strategy within industry. Particle flowability of refreshed PA-12 powder was analysed using a revolution particle analyser (RPA). With increased re-use there was an increase in avalanche angle, energy, and time, which are all markers of decreased powder flow. The reduction in particle flowability may be explained by a larger number of irregularly shaped particles, the increased presence of fine, satellite particles, and a significant increase in particle cracking within used powder samples.

These observed changes in powder properties affected the property profile of LS parts. Thermal characterisation indicated the presence of un-molten particle cores in parts fabricated from re-used powder, providing evidence of secondary crystallisation occurring within un-sintered powder as a function of powder re-use. Similarly, with increased build number, X-Ray computed topography (XCT) images showed increases in part porosity; this could be related to higher T_m, incomplete particle melting, and reduced flowability of supplied PA-12 powder. Finally, as a function of powder re-use, there was a reduction in ultimate tensile strength (UTS), yield strength, and Young's modulus of LS parts; but part embrittlement was not as significant as expected. A Pearson correlation test quantified that the reduction in powder flow was the most significant cause for the decreased UTS of final parts. However, within certain industrial applications part aesthetics and surface finish may be particularly important, so future work should include an investigation into the effect of extended powder re-use on the aesthetics of the part.

This study provides understanding of the interplay between the quality of feedstock powder and the properties of sintered parts, indicating the benefits of using a 70:30 refresh ratio for the re-use of PA-12 powder in the LS industry. Results imply that the

RPA is a useful tool that could be utilised alongside other characterisation techniques to determine powder quality. Overall, data from this study could be utilised to inform improved classification of recycled powder, in order to determine the suitability of powder for re-use in future builds.

5.7 Additional un-published material

Although not included in the publication, further work has since been conducted that is complimentary to the findings of this paper. Therefore, a short summary of the additional results has been included here as they are directly relevant to the work discussed in this chapter.

5.7.1 Laser sintering surface roughness measurements

To the best of the authors knowledge, no previous papers have quantified the effect of extended powder re-use, across multiple build cycles, on the surface quality of PBF parts. Therefore, the surface roughness of laser sintered parts, as a function of build number, was analysed using an Alicona G4.

In the XY build orientation, LS parts fabricated from virgin powder showed an average surface roughness (S_a) of 12.29 µm, which is comparable to values reported by Petzold et al. [191]. With increased build number there is an increase in both parameters of surface roughness, S_a and S_q *(Figure 5.16)*; across a total of 7 build cycles S_a rises by 5.49 µm. However, Petzold et al., observed an 8.8 µm increase in S_a, when comparing parts made from “virgin” powder and components fabricated from “recycled” powder; in this case, the aging state of the recycled powder is relatively unknown because the number of re-use cycles has not been specified

[191]. Nevertheless, within the current study, although a change in surface roughness was observed as a function of build number, it would appear that the increase is relatively modest compared to previous work, which supports the change in mechanical properties of parts presented in *section 5.5.2.2.*

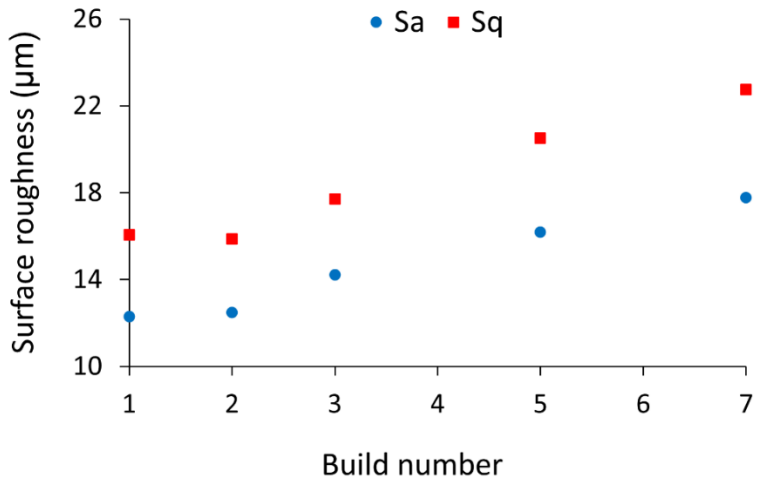

Figure 5.16 – Effect of build number on the surface roughness of LS parts built in the XY orientation. S_a is the arithmetic mean height, referring to the mean average height away from the surface. S_q is known as the root mean square height so corresponds to the standard deviation of the distance away from the surface plane [223].

Figure 5.17 emphasises that, for all build orientations, the surface roughness of LS parts deteriorates with increased build number. However, S_a is also heavily dependent on build orientation. Similarly to the change in mechanical properties displayed in *Figure 5.12,* the XY build orientation demonstrates more desirable surface roughness values, further highlighting that parts fabricated horizontally within the build chamber have the most robust property profile. However, LS parts oriented in the ZX (vertical) and, more significantly, the YX (45° angular) have a substantially rougher surface finish. It is generally reported that parts printed in the vertical direction have the worst physical and mechanical properties [41, 152-157].

Nonetheless, the results of this study indicate that the roughness of LS parts is considerably worse within components oriented at a 45° angle to the build platform. As such, this is another factor that LS operators need to consider when formulating a balanced build design.

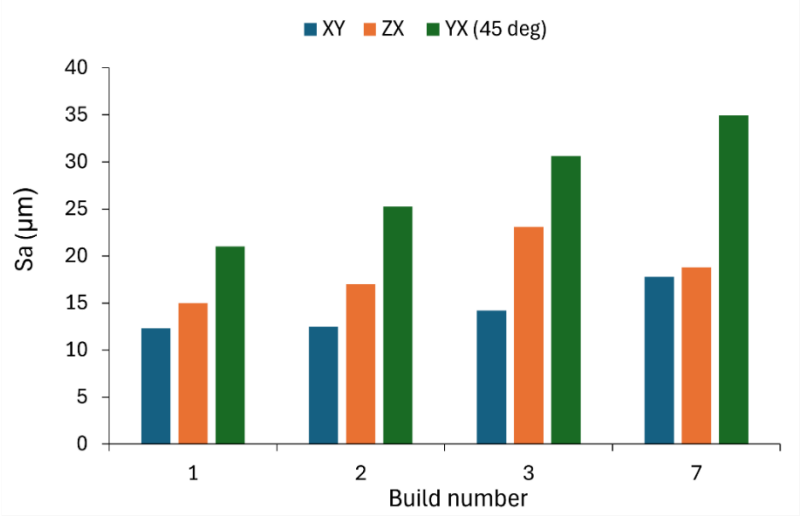

Figure 5.17 – Effect of build number and build orientation on the surface roughness of LS parts.

5.7.2 Re-use of PA-12 within multi-jet fusion (MJF)

To compare powder aging across different types of PBF machine, HP 3D High Reusability PA-12 powder was recycled across four multi-jet fusion (MJF) cycles, using the manufacturer recommended 80:20 refresh ratio. Due to time and funding constraints, the extent of the MJF study was substantially more limited than the LS scheme of work. As a result, within the MJF system, it was only possible to determine the effect of powder re-use on the thermal properties of PA-12 powder.

Table 5.5 indicates that re-using PA-12 powder across four MJF build cycles, with a cumulative build time of nearly 45 hours, has no significant effect on the thermal

properties of the material. Similarly, no discolouration of the powder samples was observed, despite MJF builds occurring within an oxygenated environment. These results suggest that an 80:20 refresh ratio is appropriate for restoring the thermal properties of PA-12 within MJF. Similarly, *Table 5.5* demonstrates that the thermal properties of PA-12 powder were not dependent on their location within the build chamber *(Figure 5.18),* suggesting that thermal gradients across the powder bed may not have a significant effect on powder aging. Nonetheless, in-situ measurements of the variation in temperature across the build chamber would be required to validate these results.

Furthermore, *Figure 5.19* compares the change in thermal properties when re-using PA-12 powder across 4 cycles within a LS and a MJF machine. However, it is worth noting that the cumulative build time within MJF is considerably shorter than the amassed time that un-sintered PA-12 powder was held in the LS build chamber. Across 4 build cycles, the T_m of PA-12 re-used within LS increases by 3.5 °C, whilst a modest 1.4 °C rise is observed following re-use in the MJF system (*Figure 5.19a).* Similarly, the crystallisation temperature of MJF grade PA-12 is lower than LS grade PA-12 *(Figure 5.19b);* this is advantageous because it expands the processing window of the material. One of the main differences between these two PBF technologies is that the MJF printing process involves the use of a fusing agent and a detailing agent; these printing inks may explain the improved recyclability of the feedstock powder. The detailing agent, which is added around the edge of the consolidated part, absorbs energy, preventing transmission of heat into the surrounding un-sintered powder. Moreover, the fusing agent contains carbon black which increases energy absorption and fusion of particles within the consolidated

part; as a result, the bed temperature and infrared thermal energy intensity can be minimised. Therefore, the un-sintered feedstock powder is exposed to less harsh thermal conditions during MJF, relative to LS. Nevertheless, it would be beneficial to investigate the aging behaviour of PA-12, across an extended number of MJF build cycles, using a wider range of characterisation techniques.

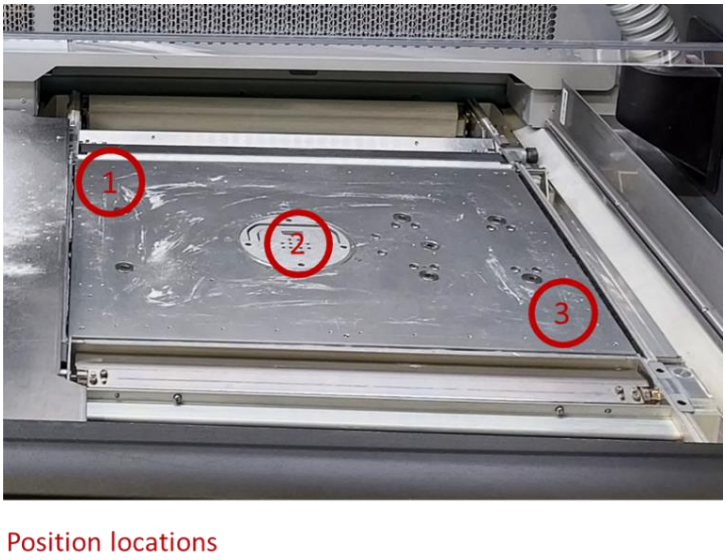

Figure 5.18 - Locations 1, 2, and 3 illustrate the regions of the bed chamber that powder was sampled from at the end of each build. However, these fixed locations are somewhat arbitrary because variations in temperature within the build chamber will likely depend on the position of the printed parts, among other processing parameters. As such, further work is required to determine whether thermal gradients exist within MJF.

Table 5.5 - The effect of cumulative build time, and location within the MJF build chamber, on the thermal properties of PA-12 powder when re-using HP 3D high reusability PA-12 across multiple build cycles with an 80:20 refresh ratio. Whereby build location is described in Figure 5.18.

Build Number	Cumulative Build time (hours)	Cumulative build time including cool-down (hours)	Build location	Peak melting temperature (°C)	Crystallinity (%)	Peak crystallisation temperature (°C)
Virgin powder	0	0	-	185.7 (±0.09)	51 (±1.5)	142.0 (±0.19)
1	13.01	26.02	Pre-build	186.8 (±0.10)	50 (±0.8)	142.0 (±0.33)
			1	186.6 (±0.54)	49 (±2.6)	142.0 (±0.33)
			2	186.4 (±0.10)	51 (±1.9)	142.2 (±0.19)
			3	186.8 (±0.17)	50 (±1.4)	142.0 (±0.00)
2	21.46	42.92	Pre-build	186.8 (±0.00)	50 (±0.8)	142.0 (±0.33)
			1	186.9 (±0.42)	48 (±1.3)	142.0 (±0.00)
			2	186.6 (±0.10)	52 (±0.4)	142.3 (±0.00)
			3	186.8 (±0.17)	50 (±1.1)	142.0 (±0.00)
3	37.11	74.22	Pre-build	187.1 (±0.40)	49 (±2.4)	142.4 (±0.20)
			1	186.8 (±0.34)	49 (±2.1)	142.1 (±0.20)
			2	187.2 (±0.17)	48 (±1.9)	142.2 (±0.19)
			3	186.8 (±0.20)	49 (±1.6)	142.4 (±0.20)
4	43.41	86.82	Pre-build	187.1 (±0.10)	50 (±1.1)	142.1 (±0.10)
			1	187.0 (±0.17)	49 (±1.3)	141.9 (±0.19)
			2	187.3 (±0.77)	50 (±2.6)	141.6 (±1.1)
			3	186.5 (±0.00)	51 (±0.3)	142.1 (±0.20)

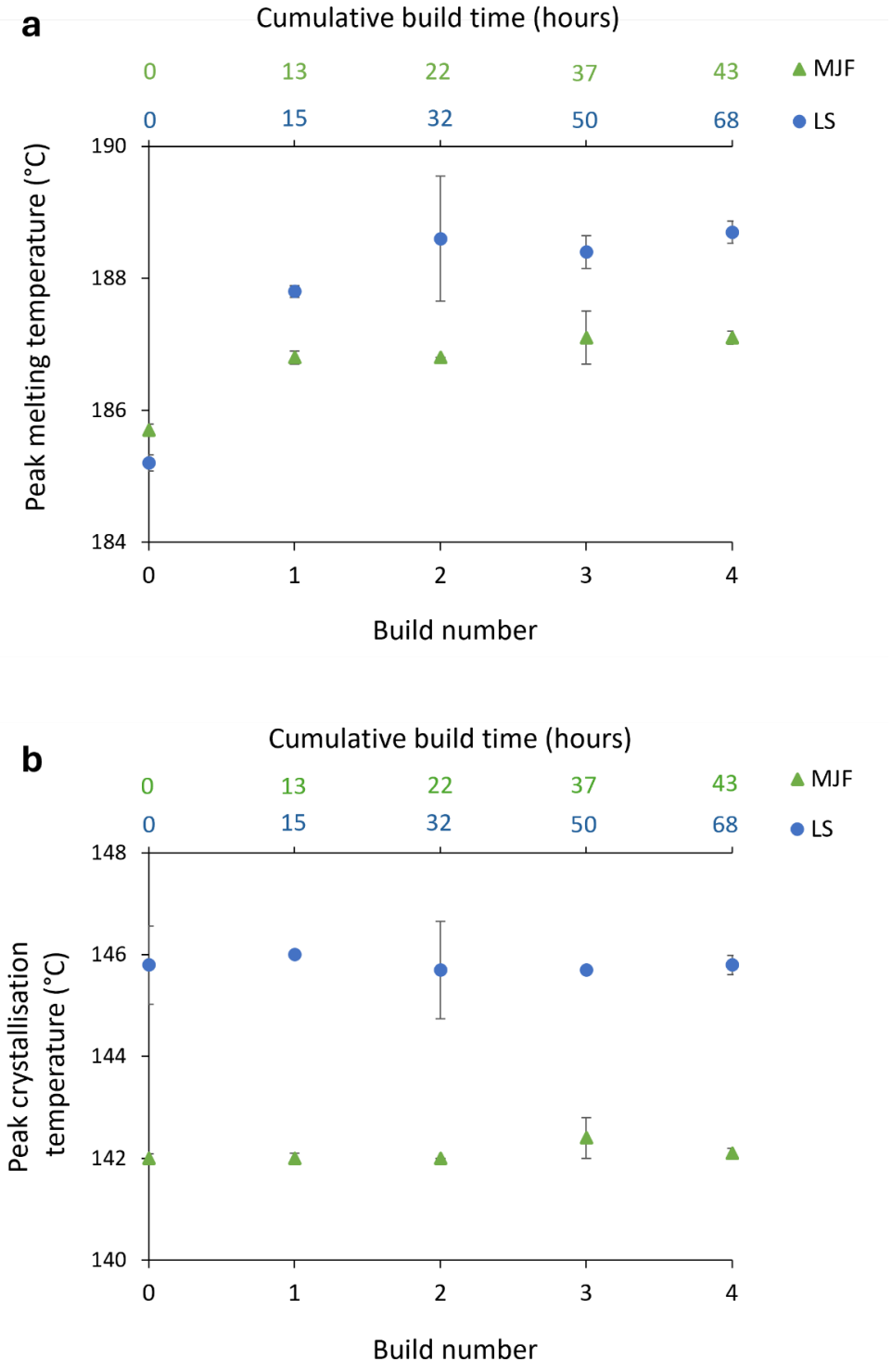

Figure 5.19 - Comparing the a) melting behaviour and b) crystallisation behaviour of HP 3D High Reusability PA-12 powder, and EOS PA2200 PA-12 powder, re-used across multiple MJF and LS build cycles, respectively.

5.7.3 Porosity Pearson correlation test

Figure 5.20 further demonstrates the relationship between powder and part properties, as a function of powder re-use; increases in both avalanche angle and T_m tend to cause an increase in part porosity. The Pearson correlation table indicates that, with repeated powder re-use, the increase in a_a has a more significant effect on part porosity (significant to the 0.01 level), whereas the increase in T_m does not have a statistically significant effect on part porosity. This relationship between powder and part properties supports the results shown in *Figure 5.15* in *section 5.5.3.*

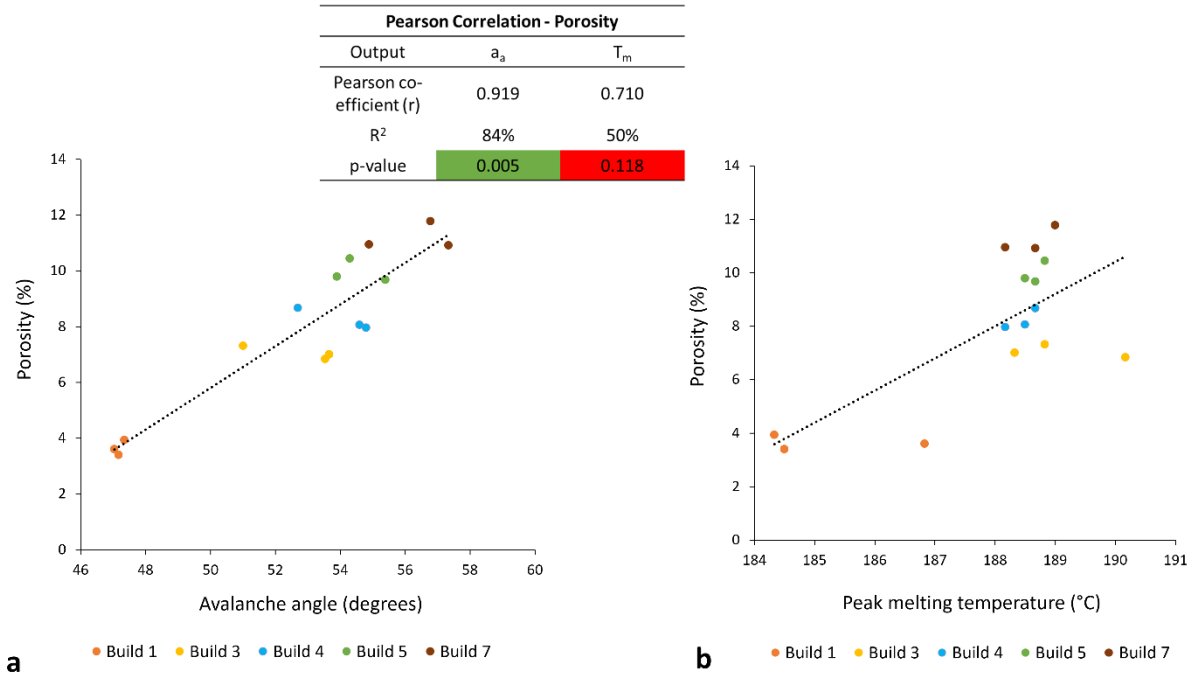

Figure 5.20 - Displays the positive correlation between porosity and a) increased avalanche angle (a_a), and b) increased melting temperature (T_m) as a function of build number.

CHAPTER 6 – EFFECT OF POWDER RE-USE ON THE COALESCENCE BEHAVIOUR AND ISOTHERMAL CRYSTALLISATION KINETICS OF POLYAMIDE-12 WITHIN POWDER BED FUSION

Published article.

Alterations to published article made within this thesis:

1. *Page 199 – Table 6.1 – Colour coded the table with conditional formatting to highlight the lowest s values. Caption of Table 6.1 was also adjusted accordingly.*
2. *Page 210 – Figure S5 - Edited figure so that both y-axes are aligned to the same values.*

Polymers *2024,* 16*(5), 612; 23 February 2024;*

https://doi.org/10.3390/polym16050612

Benjamin Sanders[1], Edward Cant[2], Catherine A. Kelly[3], and Mike Jenkins[1*]

1. School of Metallurgy and Materials, University of Birmingham, Elms Road, Birmingham B15 2SE, UK
2. The Manufacturing Technology Centre, Ansty Park, Coventry CV7 9JU, UK
3. Independent Researcher, Worcester, UK

Author contributions:

Sanders, Benjamin: Writing – original draft preparation, Writing – review & editing, Investigation, Visualisation, Methodology, Investigation, Formal analysis, Data curation, Conceptualisation, Project administration. Cant, Edward: Writing – review & editing, Supervision, Conceptualisation, Resources, Funding acquisition. Kelly, Catherine A.: Methodology, Validation, Data curation, Writing – review and editing. Jenkins, Michael: Writing – review & editing, Validation, Supervision, Methodology, Conceptualisation, Resources.

6.1 Abstract

Polymer powder bed fusion (PBF) is becoming increasingly popular for the fabrication of lightweight, high-performance parts, particularly for medical and aerospace applications. This study investigates the effect of powder re-use and material aging on the coalescence behaviour, melt flowability, and isothermal crystallisation kinetics of polyamide-12 (PA-12) powder. With increased powder re-use, a progressive reduction in melt flowability and material coalescence is observed; at 200 °C, the particle consolidation time increases from 15 s in virgin powder to 180 s in powder recovered from build 6. The observed changes in the behaviour of PA-12 were attributed to polycondensation and cross-linking; these aging phenomena also create structural defects, which hinder the rate and extent of primary crystallisation. At an isothermal crystallisation temperature of 165 °C, the crystallisation half-time increased from 12.78 min in virgin powder to 23.95 min in powder re-used across six build cycles. As a result, the commonly used Avrami model was found to be unsuitable for modelling the crystallisation behaviour of aged PA-12 powder, with the co-efficient of determination (R^2) reducing from >0.995 for virgin powder to as low as 0.795 for re-used powder. On the other hand, an alternative method, the Hay model, is able to successfully track full phase transformation within re-used powder (R^2 > 0.99). These results highlight the importance of selecting the most appropriate model for analysing the crystallisation kinetics of PA-12 powder re-used across multiple build cycles. This understanding is crucial for obtaining the strong mechanical properties and dimensional precision required for the fabrication of functional, end-use parts within PBF.

6.2 Graphical Abstract

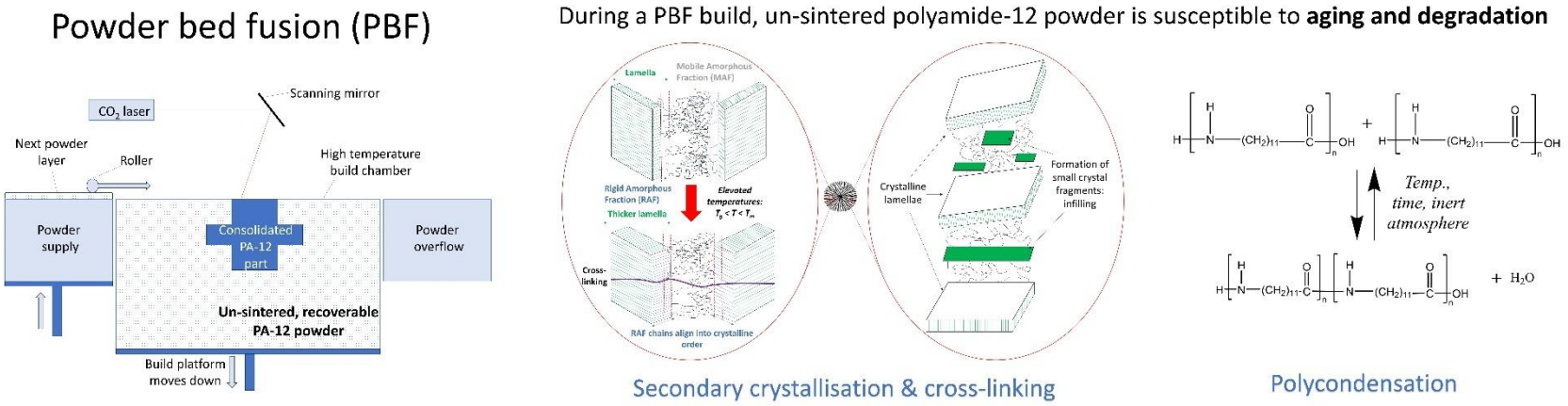

Aging processes reduce the quality of un-sintered PA-12 powder, restricting its **suitability for re-use**

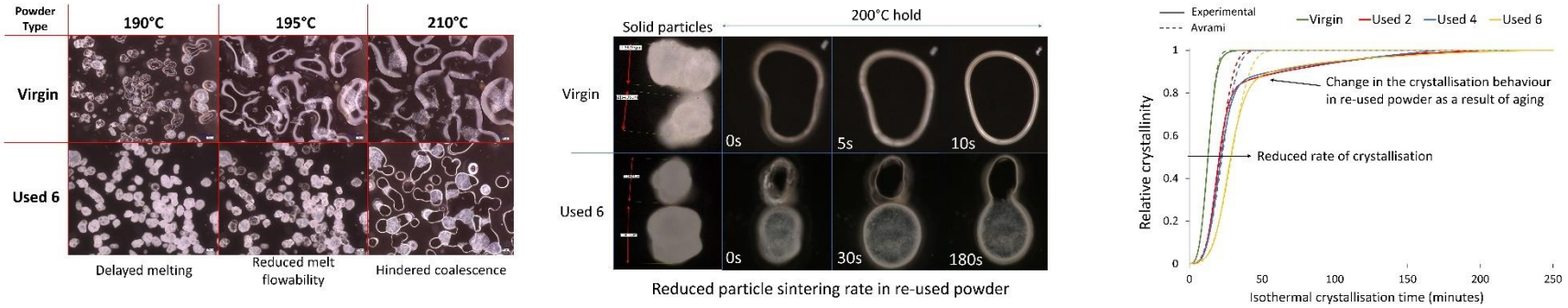

6.3 Introduction

Laser sintering (LS) is a subset of additive manufacturing (AM), whereby parts are fabricated layer by layer, from a powdered polymeric material, using a three-dimensional computer-aided design (3D-CAD) geometry file [13-15]. LS of semi-crystalline, thermoplastic materials, most commonly polyamide-12 (PA-12) [15, 21, 23, 28, 38, 53], has become increasingly popular for low-volume production of end-use parts. Application areas include medical (e.g., customised prothesis), aerospace (e.g., complex impellers), and retail (e.g., innovative insoles for trainers).

LS can offer complex, customised parts with high dimensional precision. Another key advantage is lightweighting and the fabrication of parts with a high strength-to-weight ratio [13, 14, 16-18]. Given the climate crisis, it is becoming increasingly necessary for the manufacturing industry to transition toward more sustainable processing methods. The ability to produce lightweight parts, with sufficient mechanical properties, could be crucial in reducing fuel consumption and CO_2 emissions, especially within aerospace applications. However, the mechanical and physical properties of thermoplastic polymers are heavily influenced by the crystallisation process and crystalline morphology [224]. This is of particular importance for critical end-use parts, such as aerospace components, where dimensional precision and mechanical performance are vital. During LS, crystallisation is associated with a volume reduction, which can affect the geometrical accuracy of the final part; non-uniform crystallisation within parts can result in warpage, rendering the component unserviceable [127].

Polyamide-12 (PA-12) is the most common commercial polymer within laser sintering, and a key characteristic of this material is a large processing window [15, 21, 38, 51]. This ensures that there is a substantial difference between the crystallisation temperature (T_c) and the melting temperature (T_m), preventing crystallisation occurring during the build and reducing the shrinkage process. However, the crystallisation kinetics of PA-12 are also heavily dependent on multiple processing parameters, such as temperature, time, cooling rate, pressure, and melt orientation [28, 112]. Furthermore, PA-12 is metastable and polymorphic, which can result in a multi-phase crystallisation process whereby, depending on temperature, PA-12 may transform into various different crystal phases [28]. From an industrial standpoint, understanding this behaviour is crucial because changes in the extent of crystallinity development, and type of crystalline morphology, can significantly affect the thermal and mechanical properties of a fabricated part [112].

Polymer crystallisation involves primary and secondary processes, which are often treated in isolation. Primary crystallisation is initiated when the polymer melt is cooled below T_m, via a process known as nucleation. Homogenous nucleation is where disordered molecules, within entangled amorphous polymer chains, are able to rotate, allowing small nuclei to form spontaneously throughout the polymer melt [87]. However, nucleation can also occur heterogeneously, whereby impurities present in the polymer system act as artificial primary nuclei [87]. Following the formation of stable nuclei, free rotation of flexible polymer chains allows chain folding and alignment into a lamellar structure, whereby adjacent crystalline blocks are separated by a mobile, inter-lamellar amorphous phase [89]. This results in the formation of spherulites, which grow radially from the nuclei until spherulite impingement,

indicating completion of the primary process. The rate of primary crystallisation is related to the degree of supercooling from the melt. At temperatures near the T_m, crystal growth is thermodynamically favoured so nucleation is limited, resulting in a relatively smaller number of nuclei that grow into large spherulites. The presence of large spherulites increases the strength of the polymer but also renders the material brittle, emphasising how an understanding of crystallisation kinetics can allow close control of material morphology and, subsequently, the mechanical properties of LS parts.

Traditionally, it was considered that secondary crystallisation describes any further developments of crystallinity, which occur following impingement of spherulites, permitting previously “non-crystallisable units”, which were unable to contribute to primary crystallisation, to integrate into the growing lamellae structure [97]. This can refer to lateral thickening of the crystalline lamella formed during primary crystallisation [96, 105, 146] and the growth of new, smaller crystal structures within the amorphous fraction through “infilling” [96, 105, 112] *(Figure S1).* During primary crystallisation, radial growth of lamellae generally occurs linearly with time until spherulite impingement [95]; however, an alternative kinetic mechanism is required to define the secondary process. Conventionally, a logarithmic increase in secondary crystallisation with time was reported [225-227], but more recently, it has been suggested that secondary crystallisation adheres to a root time dependence, which relates to a diffusion-controlled process [95-97, 146]. This theory was proposed by Hay, who also presented evidence for primary and secondary crystallisation occurring simultaneously, contradicting previous suggestions that the secondary process can only initiate following termination of primary crystallisation through

spherulite impingement [91]. Lamellae produced in the early stages of crystallisation, at the centre of the spherulite, were observed to be thicker than at the outer boundary, indicating that secondary crystallisation must occur within the spherulite as soon as lamellae are formed [95, 98].

Another important consideration of LS is the requirement for significant amounts of support material, resulting in 80–90% of feedstock powder remaining un-sintered during each build. Therefore, to ensure the economic and environmental sustainability of the process, un-sintered powder remaining in the build chamber must be re-used in future builds [16, 26]. However, during each build, PA-12 is exposed to temperatures close to the material melting point for prolonged time periods, leading to aging and degradation, which affect the quality and re-usability of the material. At the powder bed temperature of ~170 °C, multiple aging processes, namely, polycondensation, secondary crystallisation, cross-linking, and chain scission, often occur concurrently [24, 162, 209]. To counteract the effect of these aging phenomena, it is common for the un-sintered (“used”) powder to be “refreshed” with virgin material before re-use in subsequent builds. As such, a refresh ratio is commonly used, which refers to the proportion of recycled to virgin powder, and typically ranges from 30–50% virgin powder [66, 209]. Nonetheless, within the LS industry, there is currently a limited understanding regarding the effect of re-using PA-12 powder across multiple build cycles on the crystallisation kinetics of PA-12 powder.

Previous studies have shown that aging and degradation have the potential to alter the crystallisation behaviour, melt flowability, and particle coalescence of PA-12 powder. When polyamides are exposed to elevated temperatures, increased mobility

of amorphous regions can result in increased crystallinity via secondary crystallisation [24, 26, 168]. Multiple papers have reported that successive powder re-use, or simulated oven conditioning, causes a reduction in melt flow rate; this can be attributed to an increased cross-link density [23, 24, 168], or a rise in molecular weight (M_w), as a result of polycondensation [16, 23, 28, 38, 51]. In the context of LS, reductions in melt flowability can limit full coalescence of PA-12 particles. As LS occurs under atmospheric pressure, coalescence is particularly important because particle viscosity and surface tension become the driving force for complete consolidation and compaction of the powder layer [228]. Therefore, reductions in material coalescence can hinder the surface finish of LS parts [228] and cause increased part porosity, which often results in embrittlement of fabricated components [66, 150, 169]. However, there have been no previous investigations into the effect of powder re-use, aging, and virgin refresh rates on the isothermal crystallisation kinetics of PA-12 powder. As crystallisation is so crucial to fabricating LS parts with sufficient mechanical and structural properties, this research is necessary to help reveal more information about the behaviour of un-sintered powder and its suitability for re-use in future builds.

There are multiple models that aim to best illustrate the isothermal crystallisation kinetics of polymers. The Avrami model undoubtedly remains the most popular iso-thermal crystallisation model and has been used frequently to explain the crystallisation kinetics of various polyamides [229-231], including LS grade PA-12 powder [28, 127, 129, 162]. However, despite widespread use, the Avrami model has been criticised due to a number of limitations [131]. In practice, the Avrami model is only suitable for modelling primary crystallisation and is unable to accurately describe

the latter stages of crystallisation that follow spherulite impingement. As such, Avrami often returns non-integer values for the Avrami exponent, which provides limited information regarding the mechanism for nucleation and growth [91, 95, 232]. The Avrami model also fails to account for an induction time, and differential scanning calorimetry (DSC) often returns incomplete exotherms, leading to integration errors and inaccurate data [131]. These limitations have led various authors to propose alternative models that aim to resolve these problems by modifying the existing Avrami equation. These include, but are not limited to, the simplified Hillier [136], Tobin [138], Malkin [143], and Hay models [93, 96, 128, 146].

Previous work has begun to explore the isothermal crystallisation kinetics of PA-12 powder in the context of laser sintering [127, 129, 233]. A study from Neugebauer et al. explored both the isothermal and non-isothermal crystallisation kinetics of polyamide-12 used within LS [127]. This study intended to emulate the laser exposure found within the LS procedure. However, they used a cooling rate of only 40 °C/min to reach the target isothermal temperature, which is likely slower than the rate of cool-down that the powder experiences after laser scanning. Similarly, this rate may not be quick enough to prevent crystallisation initiating during cooling prior to the isothermal step. Zhao, Wudy, and Drummer explored the isothermal crystallisation kinetics of PA-12 between 160 °C to 168 °C, using a faster cooling rate of 60 °C/min. They observed that the Avrami model can only accurately fit 70% of the full crystallisation process; beyond this point, the experimental data deviate away from the modelled curve. However, their work was limited to the Avrami model alone, and the various alternative models were not considered [129]. Furthermore, these

papers do not explore the effect of powder re-use, and subsequent material aging, on the isothermal crystallisation kinetics of PA-12.

Paolucci et al. investigated the influence of aging on the crystallisation kinetics of PA-12 powder [28]. Virgin PA-12 powder was stored at a range of temperatures for extended time periods, in a nitrogen flushed oven, to replicate the conditions of a LS build chamber. Thermal treatment resulted in polycondensation, indicated by increases in M_w and melt viscosity. Fast scanning calorimetry experiments on the "annealed" PA-12 samples suggested that powder aging does not affect crystal nucleation but causes a reduction in the crystal growth rate of PA-12. Nevertheless, it was reported that this reduction in crystallisation kinetics only occurred in a specific temperature range between 100 °C to 150 °C, which is below the expected powder bed temperature during LS. Also, oven storage cannot directly replicate complex powder re-use procedures, such as the use of refresh ratios, which restricts the industrial relevance of their work.

This paper investigates the coalescence behaviour, melt flowability, and sintering kinetics of PA-12 powder in order to identify the key aging processes occurring when feedstock material is re-used across multiple LS build cycles with a 70:30 refresh ratio. Via differential scanning calorimetry experiments, the effect of powder re-use, and subsequent aging processes, on the isothermal crystallisation kinetics of PA-12 is quantified and modelled using the traditional Avrami model. Furthermore, to the best of the authors knowledge, the applicability of alternative models, namely, simplified Hillier, Tobin, Malkin, and Hay, to describe the crystallisation behaviour of LS grade PA-12 powder is yet to be determined. As such, this work also uses non-linear regression analysis to determine the suitability of each of these models for

describing the isothermal crystallisation behaviour of virgin and re-used (aged) PA-12 powder. Finally, the most appropriate model for analysing the crystallisation kinetics of virgin PA-12 powders, and PA-12 feedstock re-used in up to six LS build cycles, is proposed.

6.4 Experimental Method

Prototal UK Ltd. (Newbury, UK) provided industrial grade virgin PA-12 (PA2200) powder (EOS GmbH, Krailling, Germany) and refreshed PA-12 powder samples that had been re-used in up to 7 laser sintering builds, using a refresh ratio of 70:30 (used: virgin) for each build cycle. In this study, virgin powder and powder re-used in 2, 4, and 6 build cycles were analysed. These are referred to as used 2, used 4, and used 6, respectively.

6.4.1 Powder Characterisation

6.4.1.1 Hot-Stage Microscopy (HSM)

The effect of powder re-use on the melting and coalescence behaviour of PA-12 powder was visualised using a Keyence 4K digital microscope (Keyence UK Ltd., Milton Keynes, UK), equipped with a Linkam THMS600 heating stage and a Linkam TMS 94 temperature controller (Linkam Scientific Instruments Ltd., Redhill, UK). To investigate the coalescence behaviour, virgin and re-used powders were heated from 25 °C to 220 °C at 10 °C/min, and samples were viewed using a microscope magnification of 300X. Alternatively, for the isothermal particle “sintering” experiment, samples were heated from 25 °C to the sintering temperature (195 °C, 200 °C, 205

°C) at 150 °C/min and held at that temperature for 5 min. In this case, to focus on two individual powder particles, the magnification was 1000x.

6.4.1.2 Differential Scanning Calorimetry (DSC) – Isothermal Crystallisation

A Mettler Toledo differential scanning calorimeter, DSC 1 (Mettler Toledo, Schwerzenbach, Switzerland) calibrated with zinc (Tm 419.5 °C, ΔHf 107.5 Jg^{-1}) and indium (Tm 156.6 °C, ΔHf 28.45 Jg^{-1}), was used to determine the isothermal crystallisation kinetics of the PA-12 powder. Powder samples (6 ± 0.5 mg), were placed into Mettler Toledo 40 µL aluminium DSC pans, capped with aluminium lids, and sealed with a press. All experiments were conducted under a nitrogen flow rate of 100 cm^3/min, and a pinhole was placed in the top of each DSC pan. A Huber TC100 immersion cooler (Huber Kaltemaschinenbau AG, Offenburg, Germany) provided temperature control for extended isothermal segments.

The DSC protocol involved isothermal experiments from the molten state, also known as melt-crystallisation. In each DSC experiment, samples were heated at 30 °C/min to 220 °C and held for 3 min to eliminate any residual crystals. They were then cooled at 70 °C/min to the designated isothermal T_c (162 °C to 169 °C) and held for up to 420 min. The cooling rate of 70 °C/min is the maximum capability of the DSC-1 system and was selected to try and prevent any crystallisation initiating on the cool-down. Following the isothermal hold, samples were immediately re-heated to 220 °C at 10 °C/min to analyse the effect of isothermal temperature on the polymers melt behaviour. The heat of fusion (ΔH_f) was determined from the melting peak and used

to calculate percentage crystallinity (X_c) using Equation 6.1, whereby ΔH_f^0 = 209.3 Jg^{-1} (100% crystalline PA-12) [15].

$$X_c\ (\%) = \frac{\Delta H_f}{\Delta H_f^0} \times 100 \qquad \textit{(Equation 6.1)}$$

To investigate the isothermal crystallisation kinetics of virgin powder and material re-used in 2, 4, and 6 LS build cycles, raw data from the isothermal DSC segment was extracted and the change in heat flow, as a function of time, measured. This raw data, after being subjected to baseline and induction time corrections, was used to analyse and compare the Avrami [133], simplified Hillier [136, 137] , Tobin [138], and Malkin [143] models (*section 2.4.1 - Table 2.1*). To enable visual comparison with the Hay model [95, 144], cumulative crystallinity data were converted to true fractional crystallinity using *Equation 6.2.*

$$\boldsymbol{Fractional\ crystallinity} = \frac{\boldsymbol{Cumulative\ area\ under\ the\ exotherm\ (Wsg^{-1})}}{\boldsymbol{Heat\ of\ fusion\ (Jg^{-1})}}$$

(Equation 6.2)

Following the isothermal crystallisation experiments, the crystallisation kinetic parameters were estimated from traditional double log plots for the Avrami, simplified Hillier, Tobin, and Hay models, whilst the Malkin parameters were established from the Avrami results. Using SPSS software (IBM, Portsmouth, UK), the calculated parameters were then employed with each model to produce fractional crystallinity versus time plots. The fit of these plots was compared with experimental data and analysed using visual evaluation, as well as values for the coefficient of determination (R^2) and standard error of regression, s *(Equation 6.3).*

$$s = \sqrt{\frac{\sum(X_t - X'_t)^2}{n-2}} \qquad \textit{(Equation 6.3)}$$

Where s is the standard error of regression, X_t is experimental fractional crystallinity, X'_t is the modelled fractional crystallinity, and n is the number of data points. Additionally, SPSS was utilised to generate curve fittings for each model using non-linear regression. This produced multivariable kinetic parameters, which were also used to produce fractional crystallinity curves and analysed via the same methods. These various statistical analysis techniques were applied to understand the applicability of each model as a function of aging state; as such, the most suitable model for both virgin and re-used PA-12 powder was determined.

6.5 Results and Discussion

6.5.1 The Effect of Powder Re-Use on Sintering and Coalescence Behaviour of PA-12

The melt flowability and coalescence behaviour of PA-12 powder is a useful indicator of powder quality because it can have a significant effect on the structural and mechanical properties of final LS parts. Nonetheless, the use of hot-stage microscopy for characterising recycled polymeric powder is less common than other techniques such as DSC or melt-flow index. In this study, HSM showed a reduction in melt flowability and material coalescence as a function of powder re-use *(Figure 6.1).* Upon heating, virgin powder particles remain solid until at least 180 °C; however, by 190 °C, melting has already begun, and at 195 °C, the material is in an entirely molten state. Therefore, melting of virgin material occurs sharply with a moderate

melting point range. The molten polymer can flow easily without restriction; by 210 °C, there is minimal free volume remaining within the sample, which represents an increased coalescence rate and good melt flowability. However, with increased powder re-use, melting initiates at progressively higher temperatures (indicated by the theoretical yellow arrow in *Figure 6.1*) and over a notably broader temperature range. This is further shown by DSC experiments, where an increased peak T_m and T_m range is observed as a function of build number *(Figure S2).* In used powder samples, consolidation of the molten material is limited, even at temperatures as high as 210 °C, suggesting a significant decrease in powder coalescence and melt flowability. Similarly, in used 4 and 6 powder samples, un-molten particle cores are present at 200 °C and 210 °C, respectively, indicating that increased powder re-use could lead to incomplete melting during the sintering process.

Successive re-use of PA-12 powder in LS builds could result in polycondensation, an aging process that causes macromolecular chain growth via reactions of free-chain end groups *(Figure S3).* Ultimately, this often results in a significant increase in M_w [15, 21, 26, 53, 65] and melt viscosity, which hinders the flowability of the molten phase [17, 24, 28, 38, 41]. For example, Sillani et al. calculated that the molecular weight of recycled PA-12 powder (50:50 refresh ratio) was 163% greater than virgin powder after only one build cycle [15]. Similarly, Wudy and Drummer used gel-permeation chromatography to show that the M_w of PA-12 powder almost doubles after re-use for five build cycles [26]. In both cases, the increase in M_w was attributed to the polycondensation process. Furthermore, storage of PA-12 powder at elevated temperatures during LS can cause intermolecular cross-linking, leading to the formation of “tie-chains” within the polymer structure *(Figure S1).* A tie chain

represents a portion of a disordered molecule, which is able to traverse the free space between adjacent crystalline lamellae unobstructed [74]. This forms a connection between lamellae structures, restricting the mobility of the inter-lamellae amorphous chains, leading to increases in melt viscosity [23, 66, 168]. As a result, cross-linking may also contribute to the observed reduction in melt flow and particle coalescence.

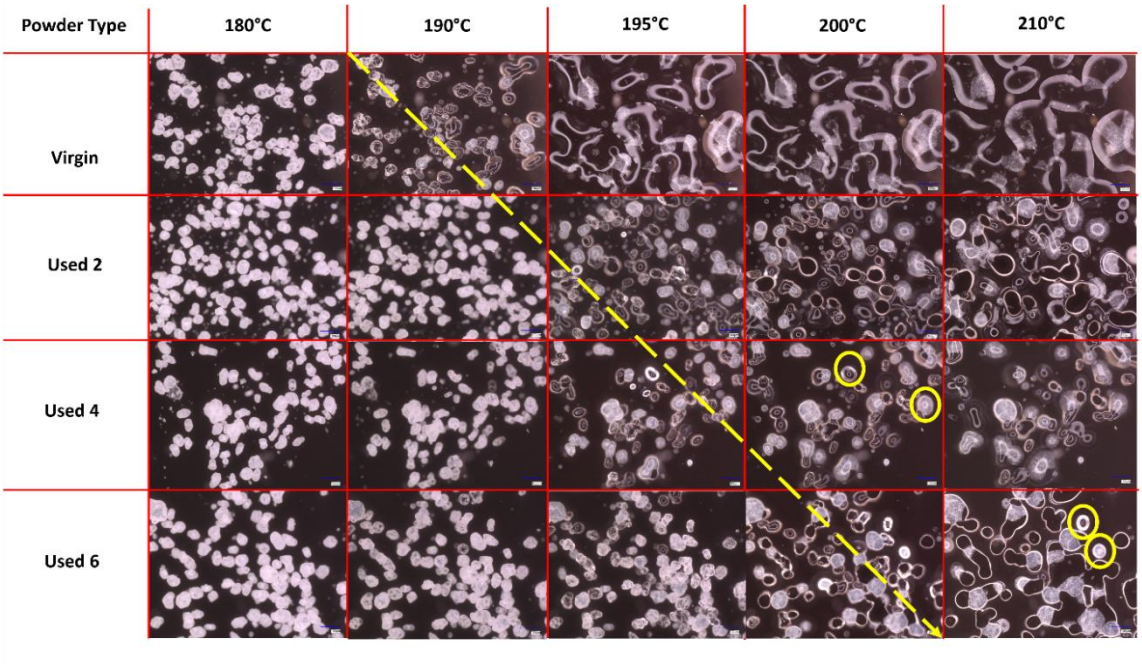

Figure 6.1 - Powder melting and coalescence behaviour of virgin and used powder, observed using hot stage microscopy by heating samples at a constant heating rate of 10 °C/min. The theoretical yellow arrow indicates the change from particle softening to melting and coalescence during heating; yellow circles provide examples of incomplete melting and the presence of un-molten particle cores.

The change in coalescence behaviour of PA-12 powder is also evident in *Figure 6.2.* In virgin material, at a constant 'sintering' temperature of 200 °C, two separate particles can combine to form one 'fused' particle within 10 s, exhibiting fast coalescence. However, in used powder, at the same temperature of 200 °C, particle coalescence is much slower. With increased powder re-use, a progressively higher thermal exposure time is required to ensure consolidation of the two particles, emphasising a reduction in the flowability and coalescence of the molten material. This experiment was also repeated at temperatures of 195 °C and 205 °C *(Figure S4).* The coalescence rate of PA-12 powders, as a function of powder re-use and isothermal temperature, was quantified using relative roundness, which describes the time it takes for two separate particles to merge into one "combined" particle *(Figure 6.3)*. Relative roundness *(Equation 6.4)* is measured using ImageJ and provides a qualitative, dimensionless value, whereby 0.0 relates to two separate particles and 1.0 correlates to a fully consolidated, single, 'round' particle.

$$4 \times \frac{[\text{Area}]}{\pi \times [\text{Major axis}]^2} \qquad \textit{(Equation 6.4)}$$

The data presented in *Figure 6.3* demonstrate that the coalescence behaviour is heavily dependent on temperature. Independent of powder type, with increased hold temperature, the rate of particle coalescence increases. For example, at 205 °C, powder recovered from build 6 reaches a relative roundness of 1.0 after only 120 s, significantly faster than the 250 s required at a temperature of 195 °C for the same powder type. However, relative roundness is also affected by powder re-use. At all temperatures, the coalescence time for virgin powder is less than 15 s, but with

increased build number, the time required for full particle coalescence progressively rises.

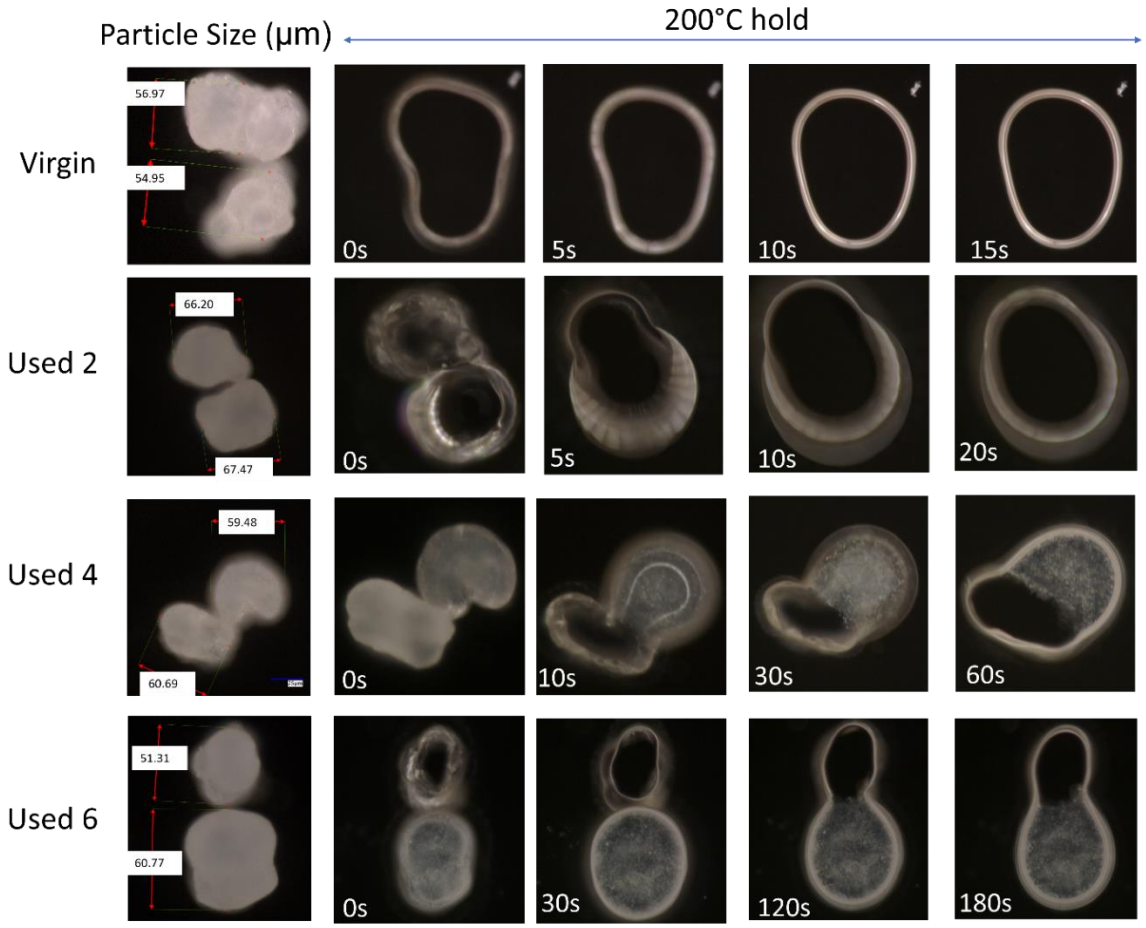

Figure 6.2 - The coalescence behaviour, at 200 °C, of two virgin powder particles, and powder recovered from different LS build cycles.

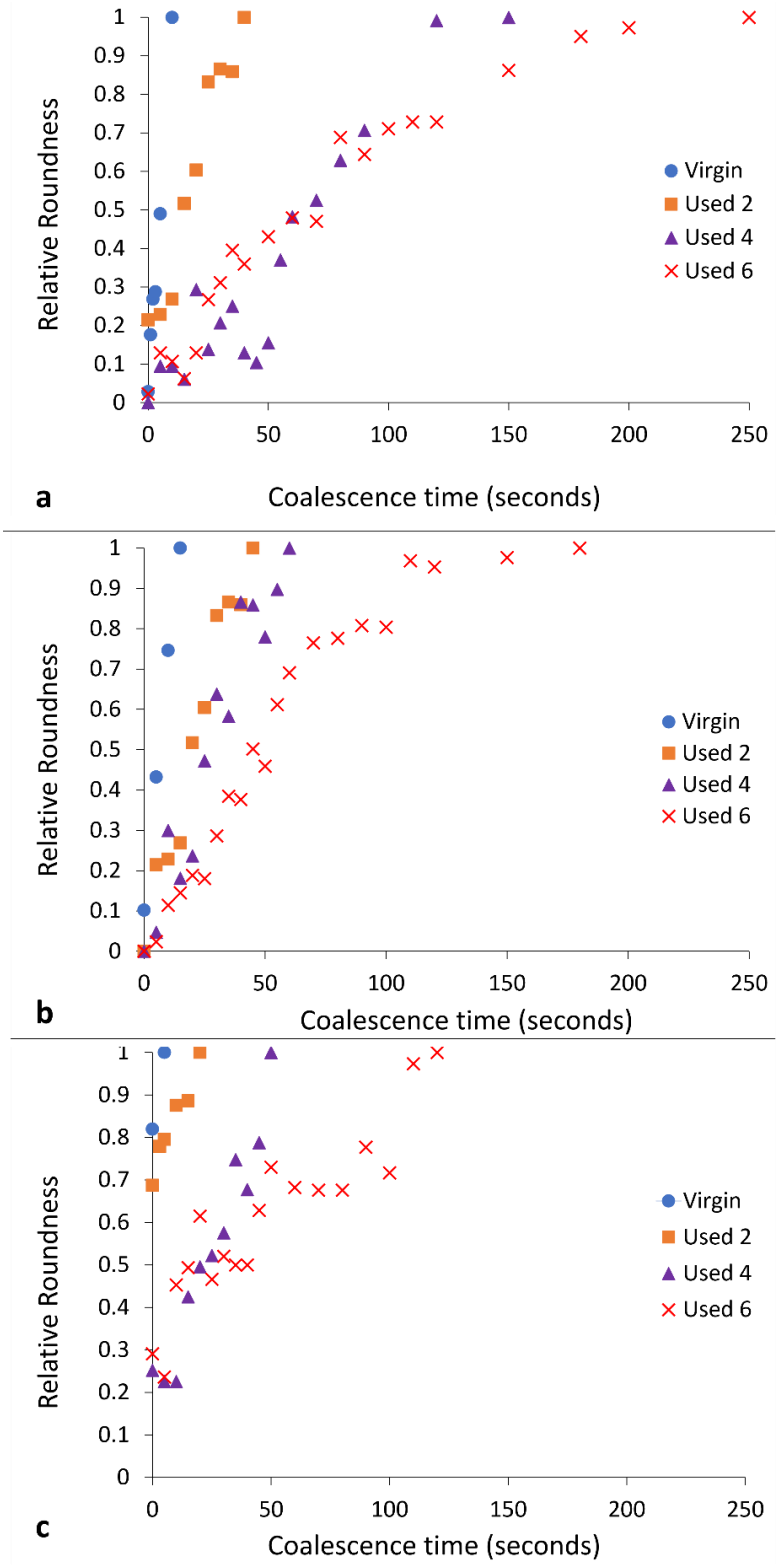

Figure 6.3 - The relative roundness of two powder particles coalescing into one consolidated, melted 'particle' as a function of time when holding at coalescence temperatures of (a) 195 °C, (b) 200 °C, and (c) 205 °C.

If the results shown in *Figure 6.1, Figure 6.2,* and *Figure 6.3* are contextualised to the scale of a laser sintering build chamber, then the impact of reduced melt flowability and restricted coalescence become increasingly relevant. Assuming that build processing parameters remain constant, the higher melting points of used powder (*Figure 6.1*) may cause incomplete melting during the sintering process, resulting in the presence of un-molten particle cores [38, 168]. In addition, the influence of temperature on the coalescence behaviour of virgin and re-used powder is significant when considering the layer-by-layer nature of the LS process. To ensure sufficient coalescence of particles within each layer, and vertically between layers, a high melt flowability is required. However, as the number of layers for a particular component progressively increases, the bottom layers of that part become further away from the heat-source, causing a decrease in the localised temperature. Similarly, it is possible for large temperature gradients to form within a LS build chamber [61, 168]. *Figure 6.3* demonstrated that reductions in temperature, and increased powder re-use, hinder the rate of particle coalescence. As such, there may be limited thermal energy, or insufficient time, for complete coalescence in the lower layers of the build chamber, which prevents full interlayer bonding and increases pore density within vertically orientated parts. This could contribute to the anisotropic behaviour often observed in LS parts, whereby vertically orientated samples have the weakest tensile strength and are the most brittle [53,57]. Overall, un-molten particles and reduced melt flow rate cause reduced material coalescence, resulting in surface defects (orange peel) [228] and increased porosity [66, 169, 234] within parts fabricated from re-used powder. Increased porosity reduces part strength and induces embrittlement

[66, 150], which could render LS parts un-fit for purpose, particularly in critical end-use applications.

6.5.2 The Effect of Powder Re-Use on Crystallisation Behaviour of PA-12

The mechanical and physical properties of LS parts are also heavily dependent on the crystallisation process and the crystalline morphology that develops. Therefore, isothermal crystallisation experiments were conducted using DSC to understand the effect of powder re-use and subsequent aging processes on the crystallisation behaviour of PA-12. During these experiments, values for absolute crystallinity, measured from the isothermal crystallisation exotherm, and peak melting temperature, recorded on the immediate re-heat after the isothermal hold, were obtained (*Figure 6.4*). Independent of powder aging state, with increased isothermal T_c, there is an increase in peak melting temperature because diffusion and growth dominate nucleation, so thicker and more perfect lamellae can develop [84, 129]. More importantly, at each isothermal crystallisation temperature, used powder samples display a higher T_m than the respective virgin sample, indicating that powder re-use increases melting temperature. Previous literature suggests that an increase in the T_m of polyamides can be caused by polycondensation [16, 24, 41], secondary crystallisation [23, 26, 159], and cross-linking [24, 160]. However, the increases in T_m observed in this experiment cannot be explained by secondary crystallisation because all traces of crystallinity are removed on the heating segment prior to the isothermal hold. On the other hand, although polycondensation is typically a

reversible reaction, an LS build chamber combines high temperatures with an inert atmosphere, which forces the reaction towards continuous water removal. As such, under the conditions present during LS, un-sintered PA-12 powder is effectively exposed to a non-reversible polycondensation reaction. Cross-linking is also irreversible, so both of these processes cause permanent structural changes to PA-12. As such, polycondensation and cross-linking appear to be the dominant cause for the observed increase in T_m with successive powder re-use, and this may have significant consequences for the quality of final LS parts, as explained in *section 6.5.1.*

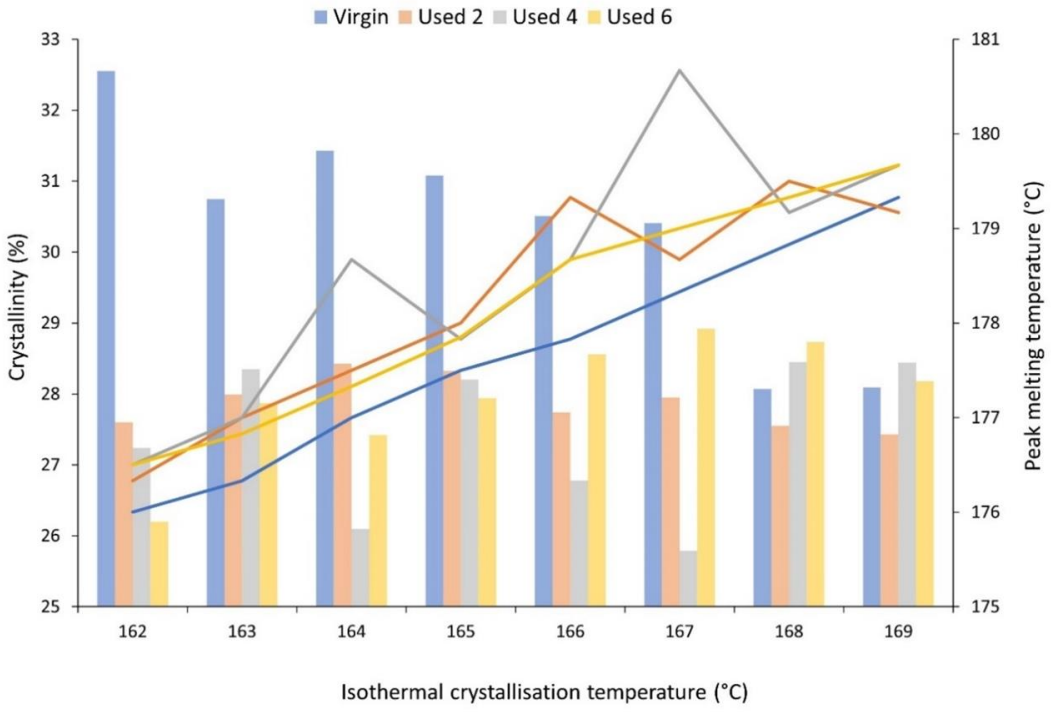

Figure 6.4 - The change in absolute crystallinity (columns), measured from the exothermal crystallisation peak, and peak melting temperature (lines), measured on the subsequent re-heat, as a function of isothermal crystallisation temperature for virgin and used powder samples.

Additionally, for isothermal T_c's between 162 °C to 167 °C, crystallinity development is higher within virgin powder samples than re-used material, which provides further evidence for the occurrence of polycondensation and cross-linking during LS (*Figure 6.4*). These aging processes result in structural defects, which reduce chain mobility and prevent amorphous fractions from re-ordering. This hinders the crystallisation process, resulting in reduced crystallinity development within used powder samples during isothermal crystallisation. The reported values for crystallinity were calculated using the enthalpy of crystallisation (ΔH_c) from the isothermal crystallisation exotherm. To ensure that no reorganisation processes were occurring during re-heating, enthalpy of fusion (ΔH_f) was also measured from the melting endotherm, and, within the limits of experimental variability, the change in ΔH_f is equal to the change in ΔH_c (*Figure* S5). This confirms that the observed changes in thermal properties and crystallisation behaviour, as a function of powder re-use, were a result of aging rather than crystal reorganisation during re-heating. Furthermore, the most significant increase in T_m, and the largest reduction in crystallinity, occurs over the first two build cycles (*Figure 6.4*). For example, at an isothermal T_c of 162 °C, there is a 3.45% reduction in absolute crystallinity between virgin powder and material recovered from build 2; similarly, T_m increases by 0.9 °C. However, these changes are followed by a plateau, whereby the difference across the next four build cycles is minimal. It has been suggested previously that polycondensation occurs more rapidly in thermally unstressed material, i.e., virgin PA-12 powder; in used, aged powder, further chain growth is hindered by a reduced availability of end groups [18, 21, 24, 234].

It is generally agreed that the glass transition temperature (T_g) of linear polymers is dependent upon the average M_w of the system; polymers with a greater M_w usually have a higher T_g [235-238]. This relationship is related to the free-volume present in the system, whereby a reduction in free volume limits the mobility of amorphous chains, therefore causing an increase in T_g [161, 235]. Polycondensation [15, 21, 26, 53, 65] and cross-linking [23, 24, 66] are both thought to increase the M_w of PA-12. These aging processes also cause an increase in cross-link density, which decreases the free-volume present in the inter-lamellae amorphous phase. With increased powder re-use, there is an increase in the onset and midpoint of T_g, thus suggesting an increase in M_w *(Figure 6.5).* This provides further evidence of polycondensation and cross-linking occurring with successive re-use of PA-12 within LS.

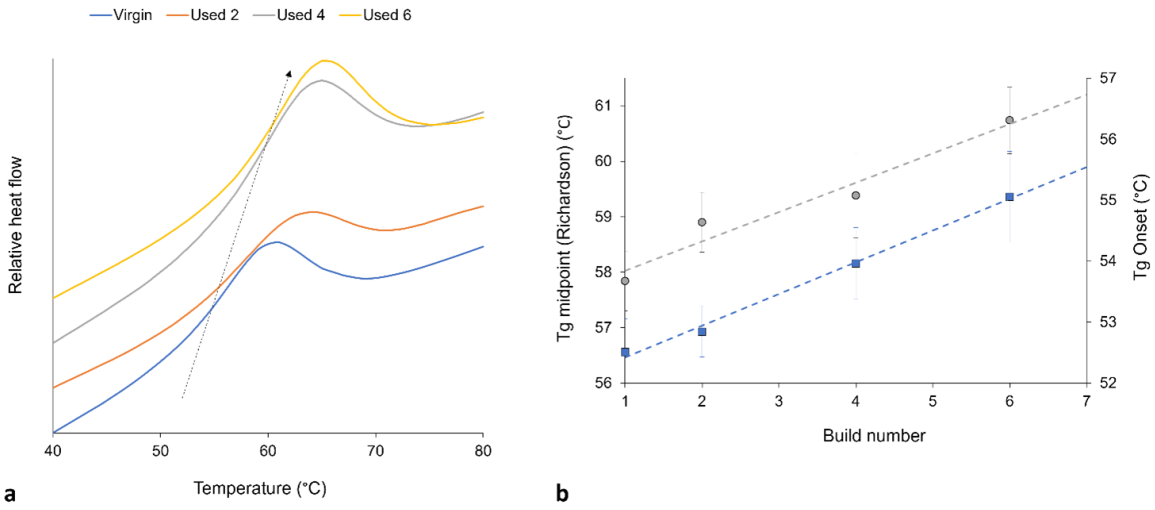

Figure 6.5 - a) With increased powder re-use, there is a shift in T_g to higher temperatures (represented by arrow), as recorded by DSC; b) shows the increase in T_g onset (blue datapoints) and T_g midpoint (gray datapoints), whereby T_g is measured using the Richardson approach, and the plotted values are taken as an average from 10 repeats.

6.5.3 Avrami Analysis of Isothermal Crystallisation

Section 6.5.1 and *section 6.5.2* have provided evidence that shows polycondensation and cross-linking are the key aging processes occurring when PA-12 is recycled across multiple LS builds. In addition to hindering material coalescence, reducing melt flowability, and decreasing the extent of crystallinity development, these processes also influence the rate of isothermal crystallisation of PA-12. Avrami is the most commonly used kinetic model for describing the crystallisation behaviour of polymeric materials. However, the effect of powder re-use, and related aging processes, on the applicability of the Avrami model is yet to be determined. Therefore, isothermal crystallisation experiments were conducted, for each powder type, in the temperature range of 162 °C to 169 °C, and the raw data are presented in *Figure S6.* In both virgin and used powder, as the T_c increases, there is a reduction in the rate of crystallisation, as reported previously [127, 129, 233]. Using the Avrami model*,* the raw DSC data were converted into double log plots, whereby the experimental data are limited to primary crystallisation alone *(Figure S7).* Data are restricted to the linear region so that the Avrami crystallisation kinetic parameters, n and k, can be accurately estimated from the gradient and y-intercept, respectively. The estimated kinetic parameters are displayed in *Table S1.* This data was used to create the plots presented in *Figure 6.6*, highlighting that with increased powder re-use, there is a reduction in the crystallisation kinetics of PA-12. Used powder was found to have a greater crystallisation half-life (t ½) than virgin material *(Figure 6.6a),* indicating a reduction in the rate of crystallisation due to morphological changes caused by polycondensation and cross-linking. Chain entanglements, knots, and permanent, non-reversible tie-chains create disorder and steric hindrance, reducing

the number of stable nuclei, which can form within the polymer system. These structural changes also restrict chain mobility and prevent chains from re-ordering into a crystalline structure. As such, the rate of both nucleation and growth decreases, reducing the crystallisation kinetics and overall extent of crystallinity development. The reduction in crystallisation rate is further shown in *Figure 6.6b,* which, particularly for lower isothermal T_c's, displays a reduction in the Avrami rate constant, k_a.

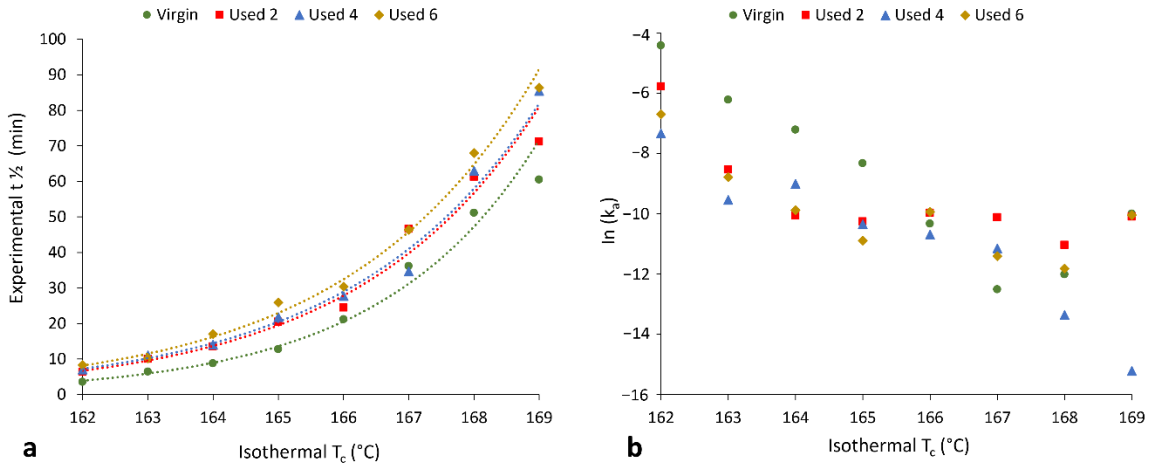

Figure 6.6 - The change in (a) crystallisation half-life and (b) Avrami rate constant (k_a) as a function of isothermal crystallisation temperature for each powder type.

To better understand the effect of powder re-use on the crystallisation behaviour of PA-12 powder at every isothermal crystallisation temperature, the kinetic parameters (n_a and k_a) presented in *Table S1* were applied to create multiple relative cumulative crystallinity curves using the Avrami equation *(Figure.6.7).* These plots track the progression of phase transformation as a function of time for each powder type, providing information about the crystallisation process and the fit of the Avrami model. In virgin powder, at every crystallisation temperature, the experimental data

form a typical sigmoidal curve. Initially, there is a crystallisation induction time, followed by accelerated primary crystallisation at a constant rate before retardation of the crystallisation process. In the latter stages of crystallisation, the rate of change in relative crystallinity with time is very small, and a pseudo-equilibrium level of crystallinity is obtained, which represents completion of the process [74]. In virgin material, the Avrami model almost parallels the experimental data *(Figure.6.7a),* and the constant, linear increase in crystallinity, as a function of time, continues until an almost complete phase transformation. This illustrates that the crystallisation behaviour of virgin PA-12 powder adheres to the Avrami model, and termination proceeds via spherulite impingement. This is further supported by co-efficient of determination (R^2) values of >0.995 for the virgin samples *(Table S2).*

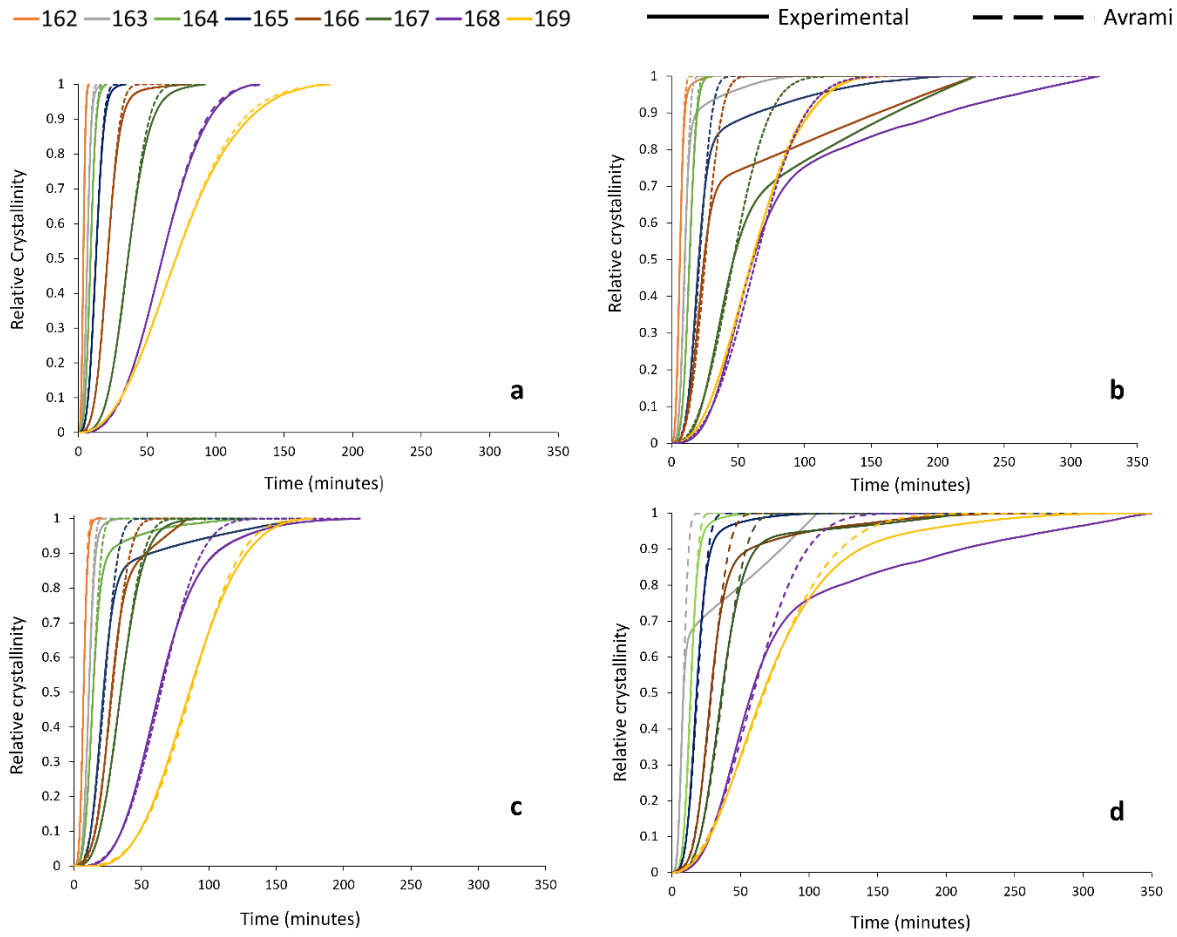

Figure.6.7 - Relative crystallinity vs. time curves, created from both experimental data and the Avrami model within SPSS for (a) virgin powder and used powder collected from build (b) 2, (c) 4, and (d) 6.

However, the used powder experimental data deviate away from the Avrami model at significantly lower levels of phase transformation. This is most clearly visualised in *Figure.6.7b*, whereby, at multiple isothermal T_c's, used powder recovered from build 2 only conforms to the Avrami theory for up to ~60–70% of transformation. Beyond this point, there are considerable deviations, and the crystallisation rate reduces significantly. A similar trend is observed in used powder recovered from builds 4 and 6; however, the difference between the experimental data and the Avrami model is

most significant with used 2 powder. This is also reflected by the R^2 values for used material *(Table S2),* which are substantially lower than virgin samples, indicating that the Avrami theory can only accurately model a portion of the crystallisation process within aged powder.

Previous work from Mandelkern et al. suggests that deviations from the Avrami expression occur as M_w increases [161, 239]. The influence of M_w may explain why, within re-used powder, the Avrami expression can accurately explain the early stages of crystallisation but fails as phase transformation progresses. The observation that Avrami is unable to fit the experimental data at higher levels of phase transformation indicates that the crystallisation process is no longer obliging to the Avrami theory of termination via spherulite impingement [161]. Instead, other factors, such as microstructural defects, must become involved as crystallisation progresses. This paper has provided significant evidence to suggest that polycondensation and cross-linking occur when PA-12 powder is re-used across multiple LS build cycles. Both processes cause an increase in M_w, which alters the morphology and microstructure of the polymer; therefore, they are the most likely cause for the observed deviation from the Avrami model in used powder samples. Polycondensation and the lengthening of non-crystalline amorphous polymer chains causes an increase in the concentration of permanent structural defects, such as chain entanglements and knots, which are unable to participate in the crystallisation process. Similarly, intermolecular cross-linking results in tie-chains, and these structures cannot be reversed or dissipated during melting or crystallisation. Therefore, there are fewer crystallisable units available within the polymer system, and the rate of nucleation and growth cannot continue at the assumed constant rate. Therefore, at this stage,

there is no longer a linear increase in relative crystallinity as a function of time, so the progression of primary crystallisation is impeded [161], causing the experimental data to deviate away from the Avrami model at earlier stages of phase transformation. Furthermore, the level of deviation is most significant in powder recovered from build 2, which can be explained by the suggestion that polycondensation occurs more readily within thermally unstressed material. This supports the crystallisation behaviour displayed in *Figure 6.4,* whereby the largest change in crystallinity development and T_m occurred over the first two build cycles, before a plateau was observed.

6.5.4 Modelling the Crystallisation Kinetics of Re-Used PA-12 Powder

Although the most commonly used model for analysing the isothermal crystallisation kinetics of polymers, the Avrami theory can only accurately model a portion of the crystallisation process within aged material. Consequently, Avrami is unsuitable for modelling the overall crystallisation behaviour of re-used PA-12 powder, and a more appropriate model is required for used, aged powder. As explained in *section 6.4.1.2*, the Avrami*,* simplified Hillier, Tobin, and Hay crystallisation kinetic parameters were obtained from traditional double log plots, whilst the Malkin parameters were calculated from Avrami data *(Table S3, Table S4, and Table S5).* To investigate the suitability of each kinetic model as a function of powder re-use, SPSS software determined the fit of these kinetic parameters to the experimental data for each powder type at a constant crystallisation temperature of 165 °C (*Figure 6.8*). In this case, all cumulative data were converted to actual fractional crystallinity using *Equation 6.2*. A temperature of 165 °C was selected because it is in the middle of the

crystallisation temperature range studied, so there is a compromise in terms of crystallisation rate. This ensures that crystallisation does not occur too rapidly, yet fast enough that the small changes in heat flow, with time, can still be consistently measured accurately. Nonetheless, similar behaviour was observed at every isothermal crystallisation temperature.

In virgin powder, the Avrami model sufficiently describes the full crystallisation process, emphasised by an R^2 value of 0.999, whilst the simplified Hillier and Malkin models also produce high R^2 values. Since virgin powder has not been exposed to aging processes, the experimental data do not deviate away from the constant primary crystallisation rate assumed within the Avrami model. Conversely, the Hay and Tobin models have lower R^2 values and are unable to accurately track the whole crystallisation process. Therefore, the traditional Avrami theory is the most suitable model for describing the crystallisation behaviour of virgin LS-grade PA-12 powder. On the other hand, *Figure 6.8* emphasises that Avrami is unable to precisely model the full phase transformation for re-used PA-12 powder, supporting the results shown in *Figure.6.7.* The Avrami equation sufficiently defines primary crystallisation; however, it cannot accurately track the region where the rate of change in fractional crystallinity significantly reduces. As such, relative to virgin PA-12 powder, the Avrami model has substantially lower R^2 values for re-used powder.

As mentioned in *section 6.5.3*, deviations away from the Avrami model, within used powder, occur when primary crystallisation becomes limited due to restricted mobility of long, entangled, and knotted polymer chains. As such, re-used powder contains more “non-crystallisable units” that are unable to contribute to the primary process, so the rate and extent of primary crystallisation reduces. Therefore, for full phase

transformation to occur, a greater contribution from secondary crystallisation is required. It is thought that secondary crystallisation is a thickening process that adheres to either a log [225-227] or a root time [97, 128] dependence, so it occurs relatively slowly compared to primary crystallisation. For the secondary process to occur, rearrangement of relatively immobile, highly entangled inter-lamellar amorphous regions is required. Additionally, polycondensdation and cross-linking also reduce the rate of secondary crystallisation as lamellar thickening becomes restricted by diffusion of structural defects away from the lamellar growth front [146]; this further increases the time required for full phase transformation within re-used powder samples. Hay suggested that the overlap of primary and secondary crystallisation explains the non-integer n values commonly observed when using the Avrami equation in polymer crystallisation [95, 144]. Hay also presented evidence to demonstrate that primary and secondary processes occur simultaneously [95, 98, 144], so the Hay model is designed to include contributions from both primary and secondary crystallisation throughout the entire curve. As a result, Hay's model is the most effective for describing the full crystallisation behaviour of used powder because it can accurately estimate the latter stages of crystallisation when the contribution from the secondary process is more significant. This is emphasised by the high R^2 values reported when modelling the isothermal crystallisation of used 2, used 4, and used 6 datasets with the Hay theory *(Figure 6.8).* Using SPSS software, the experimental data were also curve-fitted to each respective model via nonlinear, multivariable regression analysis *(Figure 6.9).* These curves revealed almost identical results and similar R^2 values for both virgin and re-used powder. This further demonstrates that although the Avrami model is suitable for modelling the behaviour

of virgin PA-12 powder, the Hay model is most appropriate for describing the full crystallisation process within re-used, aged material.

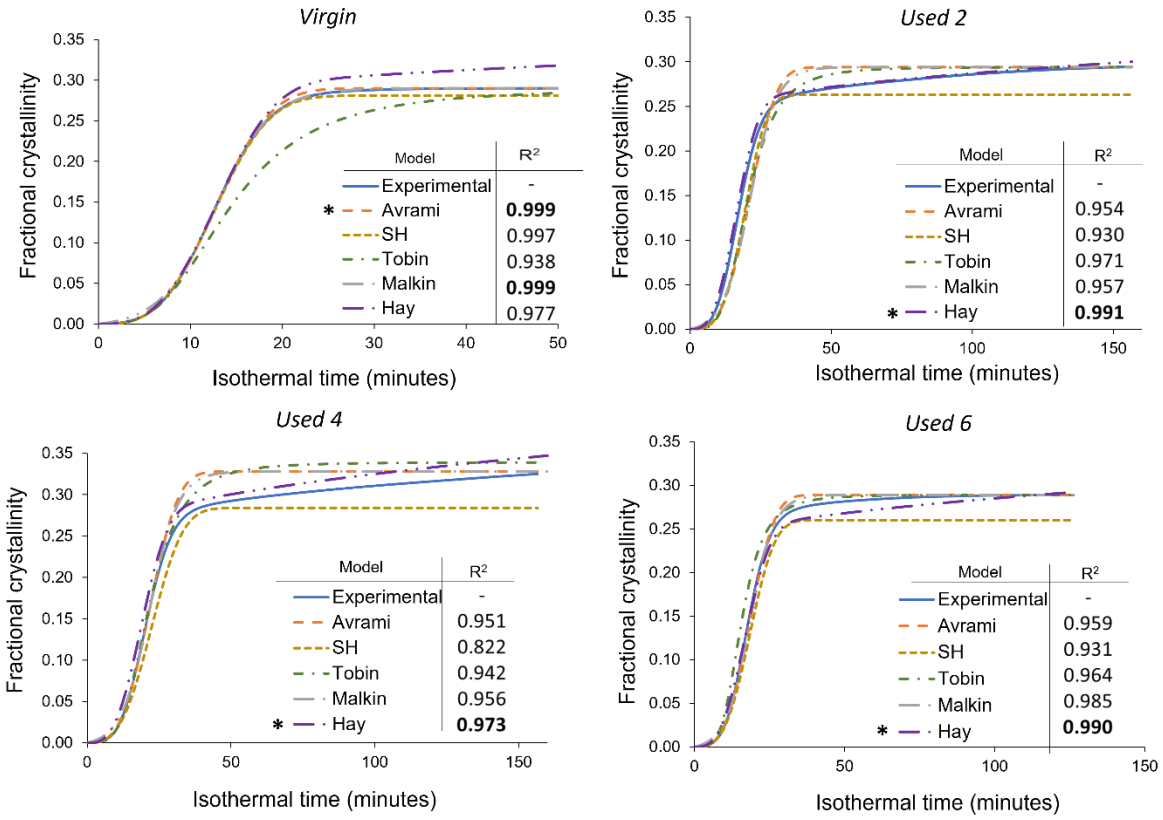

*Figure 6.8 - Comparison of the Avrami, simplified Hillier, Tobin, Malkin, and Hay models with experimental data obtained for PA-12 at 165 °C for each powder type. Fractional crystallinity curves were fabricated by inputting the crystallisation kinetic parameters (Table S3, Table S4, and Table S5) into the corresponding models. Superimposed on each plot is a key and the respective co-efficient of determination (R^2) value for each model, * represents the model with the highest R^2 in each plot.*

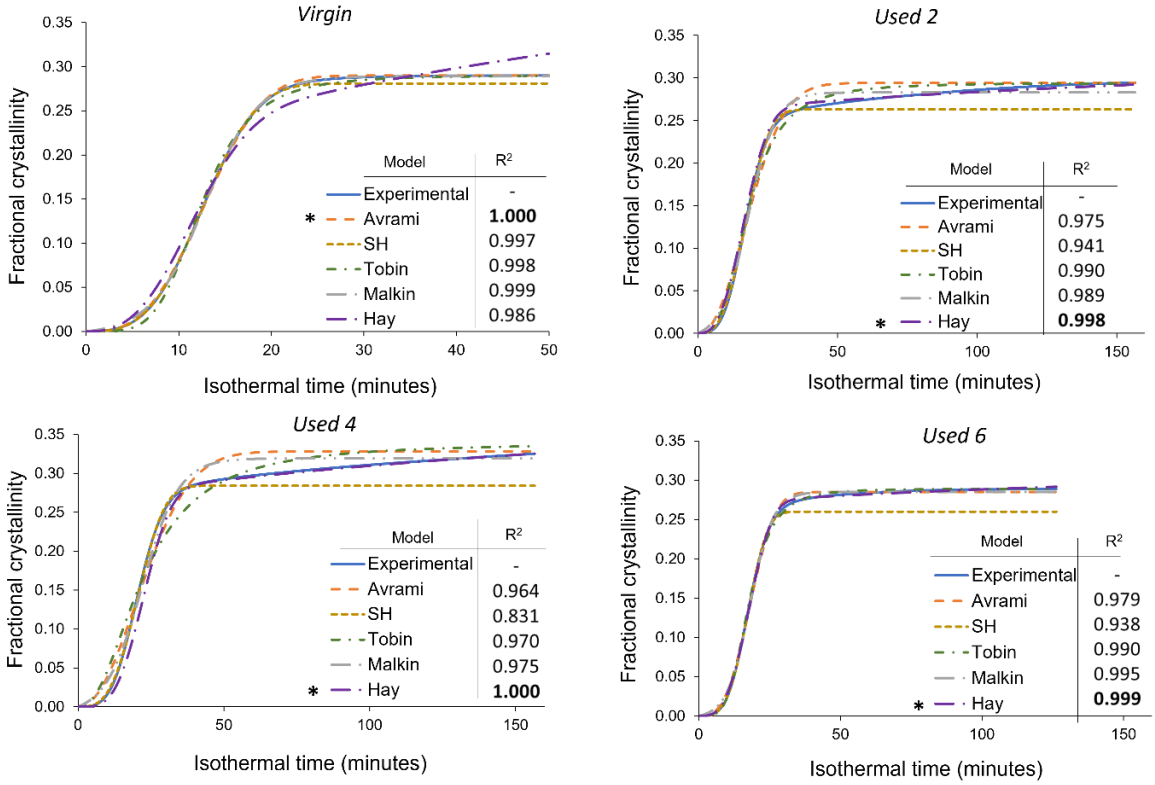

Figure 6.9 - Nonlinear multivariable curve fitting of the Avrami, simplified Hillier, Tobin, Malkin, and Hay kinetic models to the isothermal crystallisation of PA-12 at 165 °C for each powder type. Superimposed on each plot is a key and the respective co-efficient of determination (R^2) value for each model, represents the model with the highest R^2 in each plot.*

A more comprehensive approach for comparing different models is to consider the standard error of regression, s, *(Equation 6.3)* for four individual areas of the cumulative fractional crystallinity curve, whereby the lower the s value, the better the fit between the model and experimental data. These four regions resemble the initial stages of crystallisation, the region dominated by primary crystallisation, a transition segment, and the secondary crystallisation region. Other than the initial stage ($0 < X_t < 0.1$), the exact X_t values for each region varies depending on powder type. This method of analysis allows the suitability of each model to be compared at different

stages of the crystallisation process. The data presented in *Table 6.1* show that within virgin powder, all models have low s values for the initial and primary regions of crystallisation, suggesting that each model can accurately describe the crystallisation induction period and primary crystallisation process. However, only the Avrami and Malkin models could successfully model the transition and secondary crystallisation regions. This is because in virgin powder, primary crystallisation dominates, and there is limited involvement of the secondary crystallisation process. The Hay model, for example, expects a rise in fractional crystallinity due to secondary crystallisation; in reality, as the primary process is not limited by hindered chain mobility, almost full phase transformation occurs without much input from the secondary process. As such, the s values shown in *Table 6.1* emphasise that the Avrami (and Malkin) models provide the closest fit to the experimental data for each stage of the crystallisation process in virgin powder.

Table 6.1 - Standard error of regression for each isothermal crystallisation kinetic model over four selected regions of the cumulative fractional crystallinity curve. S values < 0.005 are highlighted green to emphasise the models that best fit the experimental data for each region and powder type – note that in used powder samples the Hay model displays the lowest S values, particularly for the secondary region.

Powder Type	Region	X_t Range	Avrami		Simplified Hillier		Tobin		Malkin		Hay	
			DLP	CF	DLP	CF	DLP	CF	DLP	CF	DLP	CF
Virgin	Initial	0.0–0.1	0.0003	0.0011	0.0003	0.0003	0.0004	0.0052	0.0044	0.0034	0.0009	0.0058
	Primary	0.1–0.8	0.001	0.002	0.0016	0.0004	0.0286	0.0064	0.0018	0.0017	0.002	0.0109
	Transition	0.8–0.95	0.0053	0.002	0.0013	0.0008	0.0527	0.0049	0.0007	0.0012	0.0101	0.0173
	Secondary	0.95–1.0	0.0024	0.0019	0.0077	0.0077	0.0232	0.0032	0.0006	0.0005	0.0212	0.0135
Used 2	Initial	0.0–0.1	0.002	0.01	0.003	0.002	0.003	0.005	0.002	0.008	0.002	0.006
	Primary	0.1–0.7	0.037	0.012	0.029	0.002	0.032	0.01	0.037	0.007	0.011	0.011
	Transition	0.7–0.9	0.026	0.013	0.009	0.002	0.02	0.01	0.023	0.009	0.009	0.007
	Secondary	0.9–1.0	0.013	0.013	0.022	0.022	0.01	0.008	0.013	0.008	0.002	0.003
Used 4	Initial	0.0–0.1	0.0012	0.0149	0.0008	0.0016	0.0004	0.0201	0.0058	0.0123	0.0076	0.0019
	Primary	0.1–0.7	0.0121	0.0186	0.0257	0.0018	0.0041	0.024	0.0045	0.0113	0.0225	0.0023
	Transition	0.7–0.9	0.0293	0.0226	0.014	0.0058	0.0254	0.0213	0.0317	0.0173	0.0108	0.0014
	Secondary	0.9–1.0	0.0172	0.0169	0.0309	0.0309	0.0253	0.0136	0.0172	0.0107	0.0163	0.0006
Used 6	Initial	0.0–0.1	0.0008	0.0035	0.0005	0.0004	0.0048	0.0054	0.0055	0.001	0.0018	0.0015
	Primary	0.1–0.8	0.0061	0.0051	0.0193	0.0012	0.0062	0.0038	0.0324	0.0035	0.0023	0.0012
	Transition	0.8–0.95	0.0125	0.0073	0.0157	0.0081	0.0075	0.0055	0.0083	0.0047	0.0012	0.0004
	Secondary	0.95–1.0	0.005	0.0036	0.0258	0.0258	0.0046	0.0033	0.0031	0.0021	0.0014	0.0005

On the other hand, in re-used PA-12 powder, the Hay model generally has the lowest s values, especially in the transition and secondary crystallisation regions of the fractional crystallinity curve. Compared to virgin material, all models are less successful at tracking primary crystallisation. In virgin powder, the standard error of regression for the primary region was commonly calculated to be less than 0.002, whilst in re-used powder samples, s values are usually greater than 0.01. The higher s values are particularly noticeable in powder recovered from builds 2 and 4. In used powder, polycondensation and cross-linking reduce the rate of primary crystallisation, resulting in an inconsistent growth rate. Therefore, predicting and describing the change in fractional crystallinity as a function of time becomes more difficult. These aging processes also limit the extent of the primary crystallisation process, causing the experimental data to deviate away from the Avrami model. As such, the s values in the transition and secondary regions are also generally greater within used powder than the respective values in virgin samples *(Table 6.1).*

The Avrami model is unable to accurately describe the latter stages of phase transformation in re-used powder because Avrami assumes that the rate of crystal growth is linear and constant. However, structural defects caused by polycondensation and cross-linking reduce the availability of crystallisable polymer units; therefore, the rate of nucleation and growth are no longer constant, with respect to the extent of phase transformation [161]. The simplified Hillier, Tobin, and Malkin models are derived from, and closely related to, Avrami and therefore display similar results. Hay is the only model that accounts for primary and secondary crystallisation simultaneously. Similarly, Hay does not presume a constant nucleation and growth rate, so it is better suited to describe the behaviour of aged PA-12 powder, whereby structural defects hinder the crystallisation rate in the latter stages

of phase transformation. As such, within re-used powder samples, Hay is considerably more successful at modelling the transition and secondary crystallisation portion of the curves, and s values are typically 0.005 or less.

These results, calculated for an isothermal crystallisation temperature of 165 °C, are highlighted by the data presented in *Table S6* and *Table S7*, which show that comparable results were obtained at every isothermal T_c. In this data, there is a focus on the Avrami and Hay models because they were the two most successful models for describing the crystallisation behaviour of virgin and used powder, respectively. *Table S6* illustrates that for virgin powder, the Avrami model has the highest R^2 values, whilst the Hay model has higher R^2 values for every batch of re-used powder. This is further shown by *Table S7,* which compares the s values of virgin and re-used powder at each isothermal T_c for the Avrami and Hay models. At 168 °C and 169 °C, datapoints are missing for the Hay model. This theory is unsuitable at higher temperatures because the crystallisation rate becomes so slow that extended isothermal times of > 8 hours are required to fully model the whole crystallisation process. It was observed that the DSC is unable to precisely maintain temperature over this extended time period or accurately monitor the small changes in heat-flow. Nonetheless, 162 °C to 167 °C is a sufficient temperature range to demonstrate the advantages of using the Hay model to investigate the isothermal crystallisation of aged PA-12 powder.

To fully understand the suitability of the Hay model for describing the crystallisation behaviour of used powder, it is necessary to explore the relationship between powder type and Hay's kinetic parameters. Crystallisation half-time ($t_{½}$) can also be estimated using the Hay model, whereby half-time is taken to be the time at which

$X_t = \frac{X_{p,inf}}{2}$ [144], whereby $X_{p,inf}$ describes the final fractional crystallinity upon completion of the Avrami primary process. *Figure 6.10* demonstrates that with an increased isothermal T_c, and increased powder re-use, there is generally a reduction in Hay's primary rate constant (k_p) and Hay's t ½. These same trends were observed when using the Avrami model to calculate k_a and $t_{½}$ *(Figure 6.6),* and the similarity between the Hay and Avrami estimations is shown in *Figure 6.11*. Therefore, independent of the kinetic model employed, it is clear that there is a reduction in the primary crystallisation rate as a function of powder re-use. The Hay model offers additional, unique parameters that can reveal more information about the full crystallisation process following the primary region. Although there does not appear to be a significant change in the secondary rate constant (k_s), as a function of powder re-use *(Table S8),* a reduction in $X_{p,inf}$ is observed *(Figure 6.10a).* This shows that primary crystallisation terminates at lower levels of phase transformation within re-used powder, further supporting the relative crystallinity curves presented in *Figure.6.7.* Values of $X_{p,inf}$ are also important when considering the estimations of crystallisation half-time using the Hay method. The extent of the increase in t ½, as a function of powder re-use, is modest when calculated using Hay compared to Avrami *(Figure 6.11b).* In virgin material, the values for t ½ are almost identical; however, in used powder, Hay calculates t ½ to be lower. This occurs because Hay's estimation of t ½ only includes the primary crystallisation process, and with increased powder re-use, the extent of the primary process is reduced, leading to lower values for t ½. Overall, the similarity between the values of the kinetic parameters for Avrami and Hay emphasises that both models can successfully model the primary region of crystallisation for all powder types. However, Hay has the unique advantage of being able to estimate the point at which the primary process terminates and can

successfully model the secondary crystallisation region. Further comparisons of the Hay and Avrami kinetic parameters, at every isothermal T_c, are provided in *Table S8.*

The results outlined in this section have emphasised that although the traditional Avrami model is the most suitable for describing the crystallisation behaviour of virgin LS grade PA-12 powder, it is unsuitable and inaccurate for powder that has been re-used in multiple LS builds. However, the Hay model can sufficiently describe the complete crystallisation process for re-used PA-12 powder. To the best of the author's knowledge, this is the first study to establish the most appropriate kinetic model for describing the crystallisation behaviour of re-used and aged PA-12.

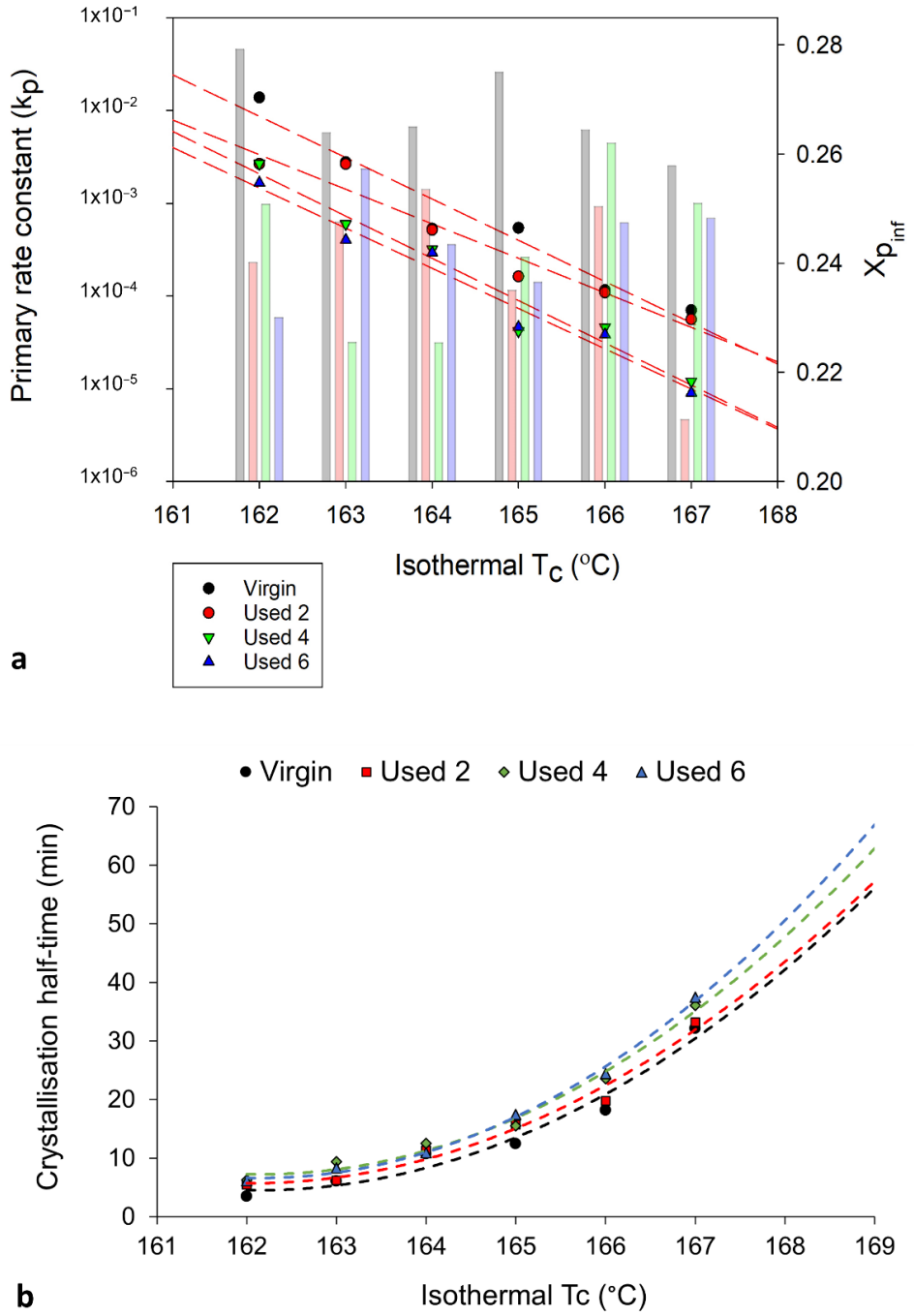

Figure 6.10 - The change in (a) the primary crystallisation rate constant, k_p (datapoints) and Xp_{inf} (columns) and (b) the crystallisation half-time, whereby the trendline is extrapolated to include isothermal T_c's: 168 °C and 169 °C, calculated using the Hay model, as a function of isothermal T_c and powder type.

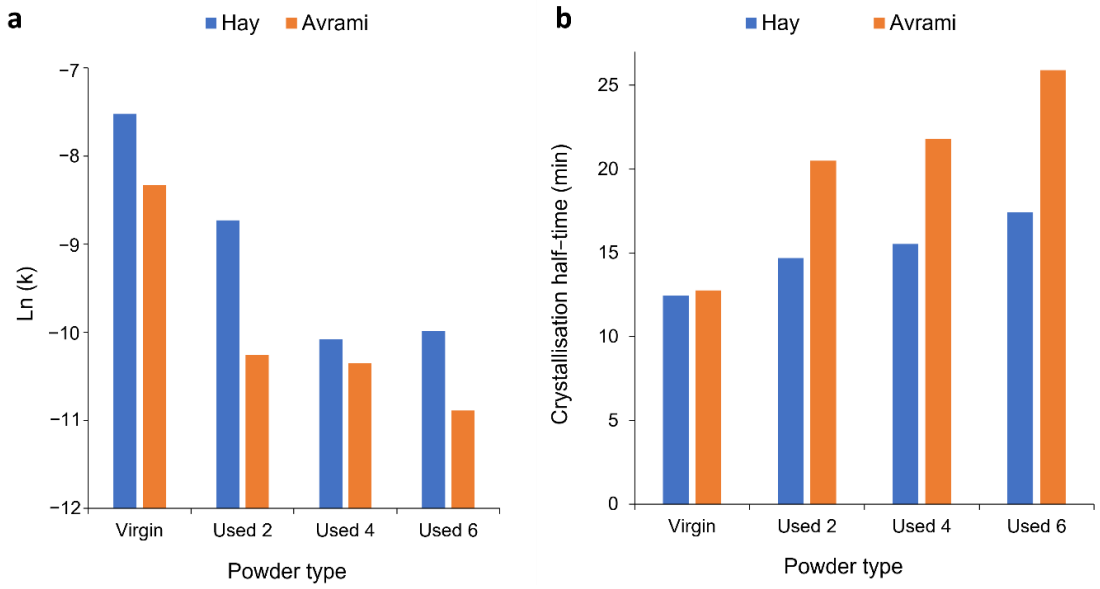

Figure 6.11 - Comparison of the values of (a) k_p and (b) $t_{½}$ using both the Hay and Avrami models, for each powder type, at an isothermal T_c of 165 °C.

6.6 Conclusions

In this study, PA-12 powder was re-used for a total of seven laser sintering (LS) build cycles, using a 70:30 refresh ratio. Hot-stage microscopy indicated that as a function of powder re-use, there is an increase in melting temperature, a reduction in melt flowability, and restricted particle coalescence. These changes in the thermal behaviour of PA-12, attributed to polycondensation and cross-linking, can cause increased porosity and reduced mechanical properties within LS parts fabricated from re-used powder. The mechanical and structural properties of final parts are also heavily dependent on the crystallisation behaviour of the polymer. In this work, the isothermal crystallisation of PA-12 was studied using a range of models, namely, Avrami, simplified Hillier, Tobin, Malkin, and Hay. For virgin material, the Avrami model was found to be the most successful at modelling the entire crystallisation process. However, in re-used powder, polycondensation and cross-linking cause

structural defects that reduce the rate and extent of primary crystallisation, limiting the applicability of the Avrami model. Nonetheless, as a result of accounting for both primary and secondary crystallisation, the Hay model accurately describes the whole crystallisation process and is therefore the optimum method for defining the crystallisation behaviour of aged polymeric material. From an industry perspective, applying the Hay model to better understand the crystallisation behaviour of re-used PA-12 powder could help ensure the fabrication of LS parts with sufficient mechanical properties and a high dimensional precision.

6.7 Supplementary Information

Figure S1 - Schematic diagram displaying different mechanisms of secondary crystallisation and cross-linking: a) lamellar thickening, b) lamellar infilling, and c) tie-chain formation as a result of cross-linking.

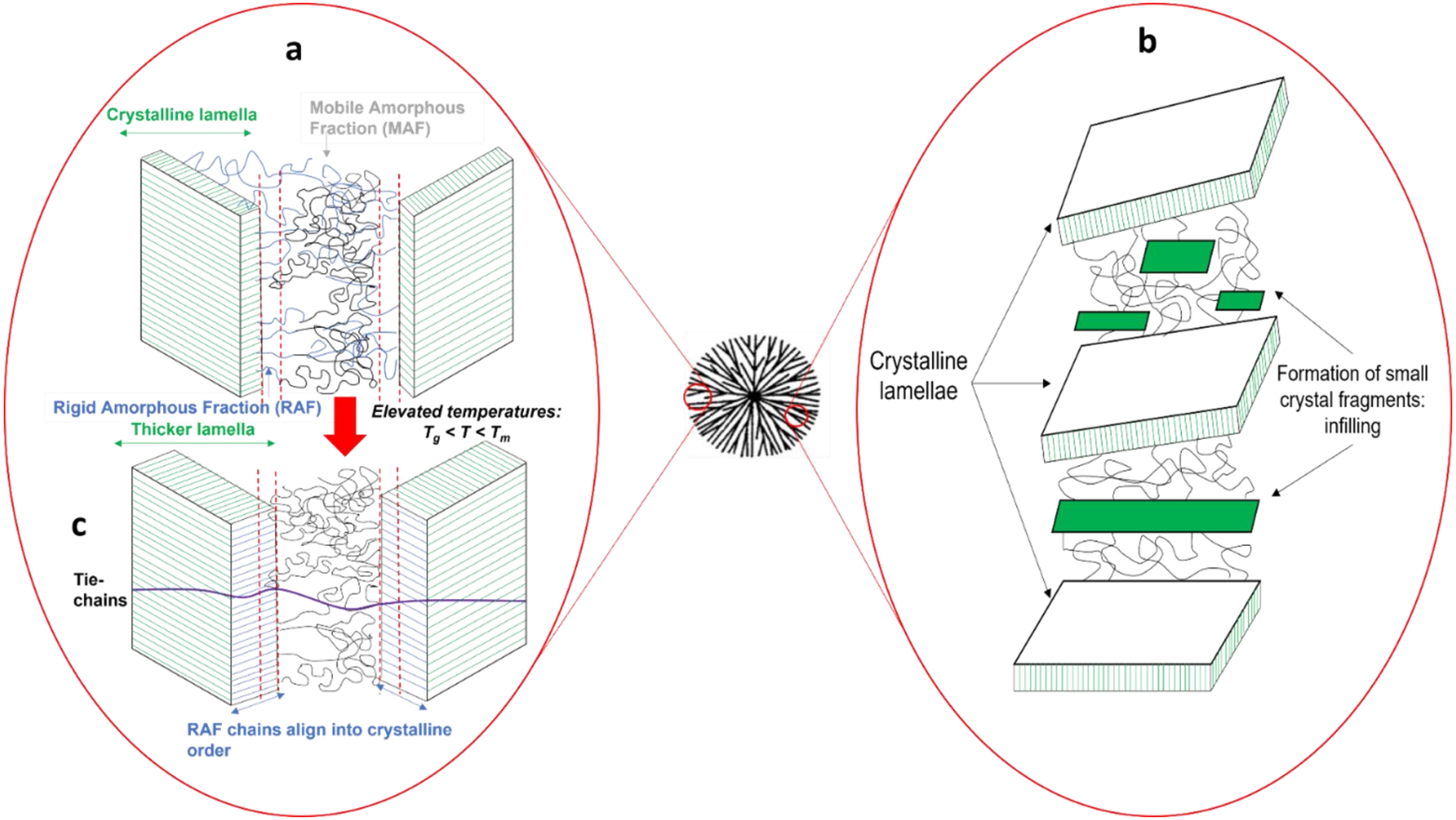

Figure S2 - The change in a) peak T_m and b) T_m range with increased build number, whereby each datapoint is taken as an average of 3 repeats.

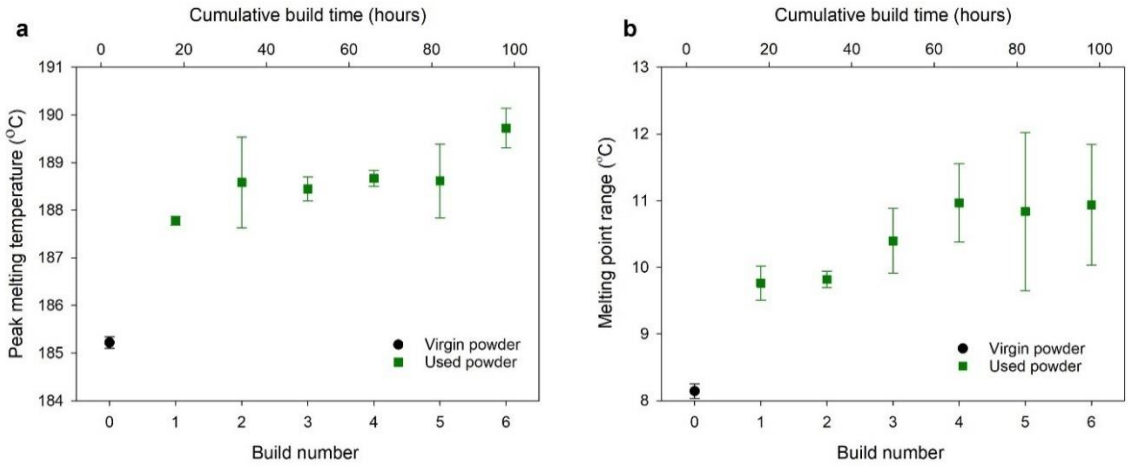

Figure S3 - Schematic diagram representing the polycondensation process, emphasising the entangled, knotted chain structures present in re-used powder.

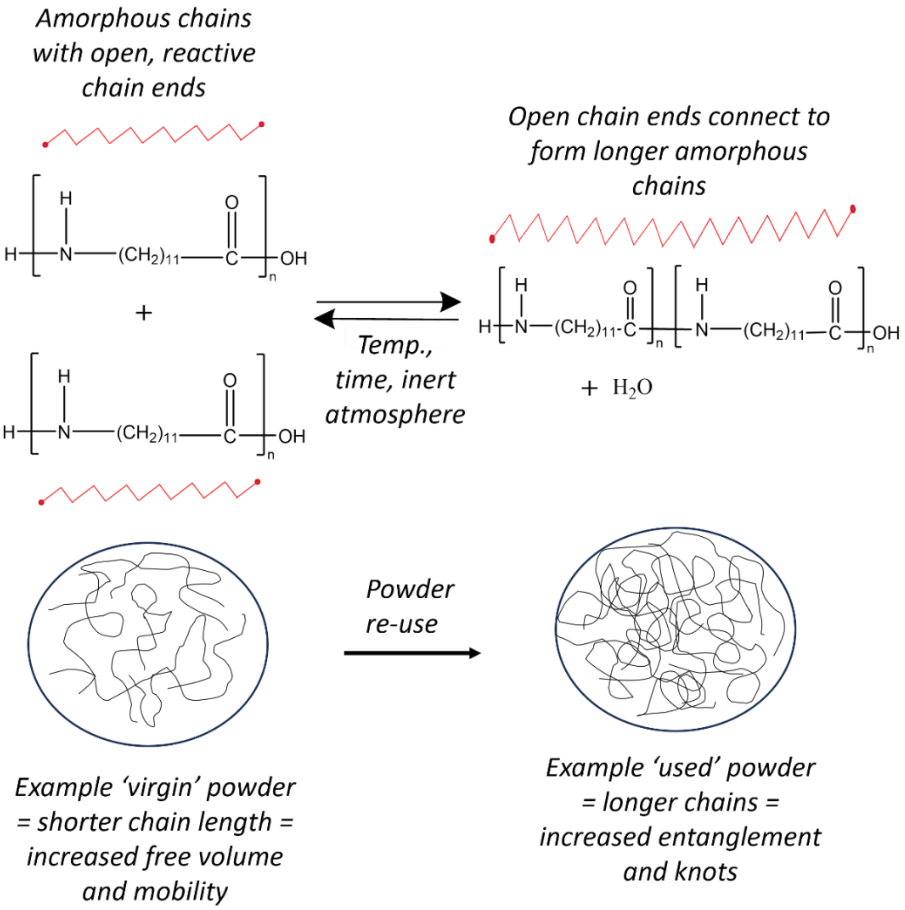

Figure S4 - The coalescence behaviour of two virgin powder particles, and powder recovered from different LS build cycles at a) 195 °C and b) 205 °C.

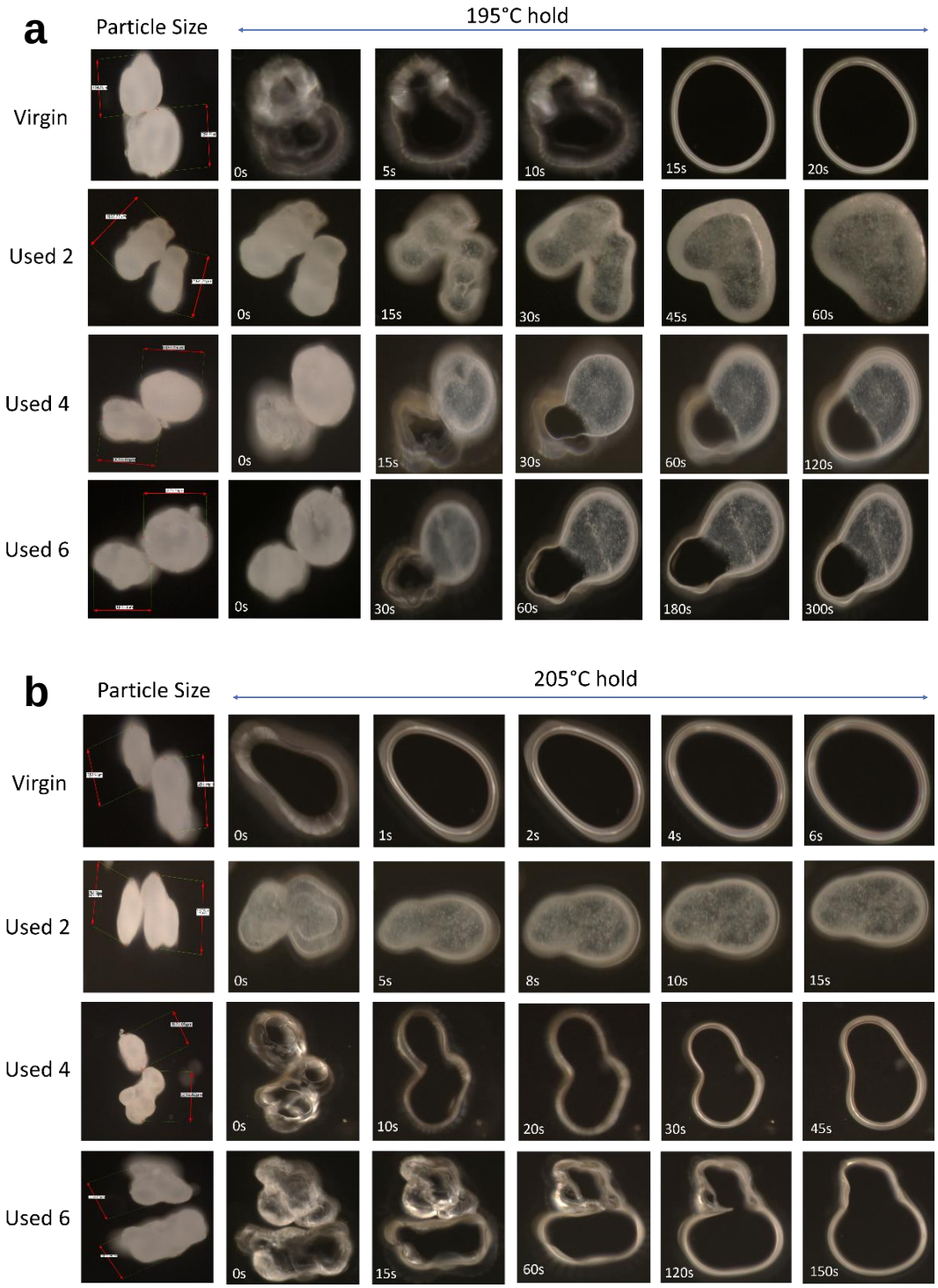

Figure S5 - The change in enthalpy of crystallisation, measured from the exothermic peak during the isothermal segment (column) and enthalpy of fusion, measured from the endothermic melting peak, when re-heating at 10 °C min^{-1} (dotted line), as a function of isothermal crystallisation temperature, and powder re-use.

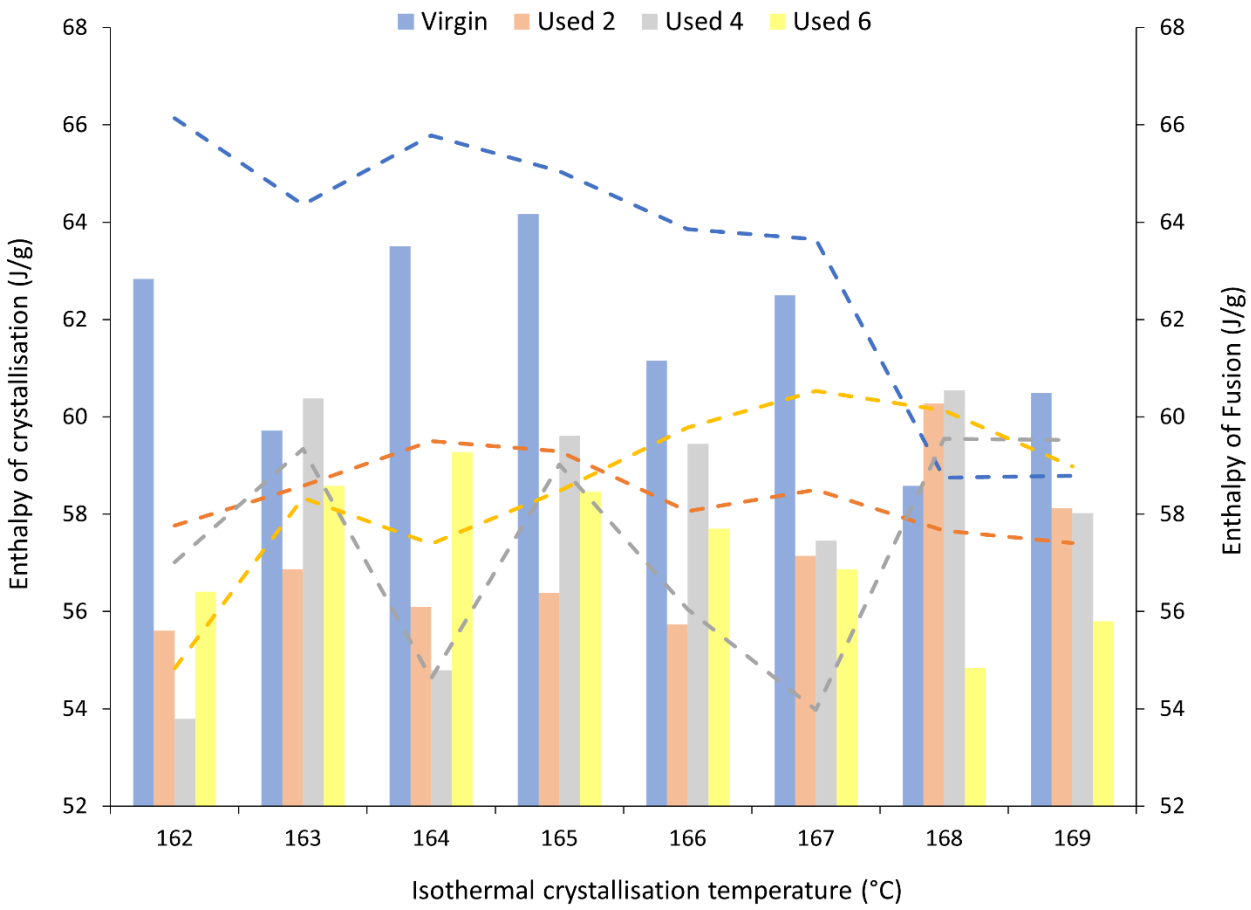

Figure S6 - Raw data from the DSC displaying the change in the shape and position of the exothermic crystallisation peak, as a function of isothermal crystallisation temperature for a) virgin, b) used 2, c) used 4, and d) used 6 powder types.

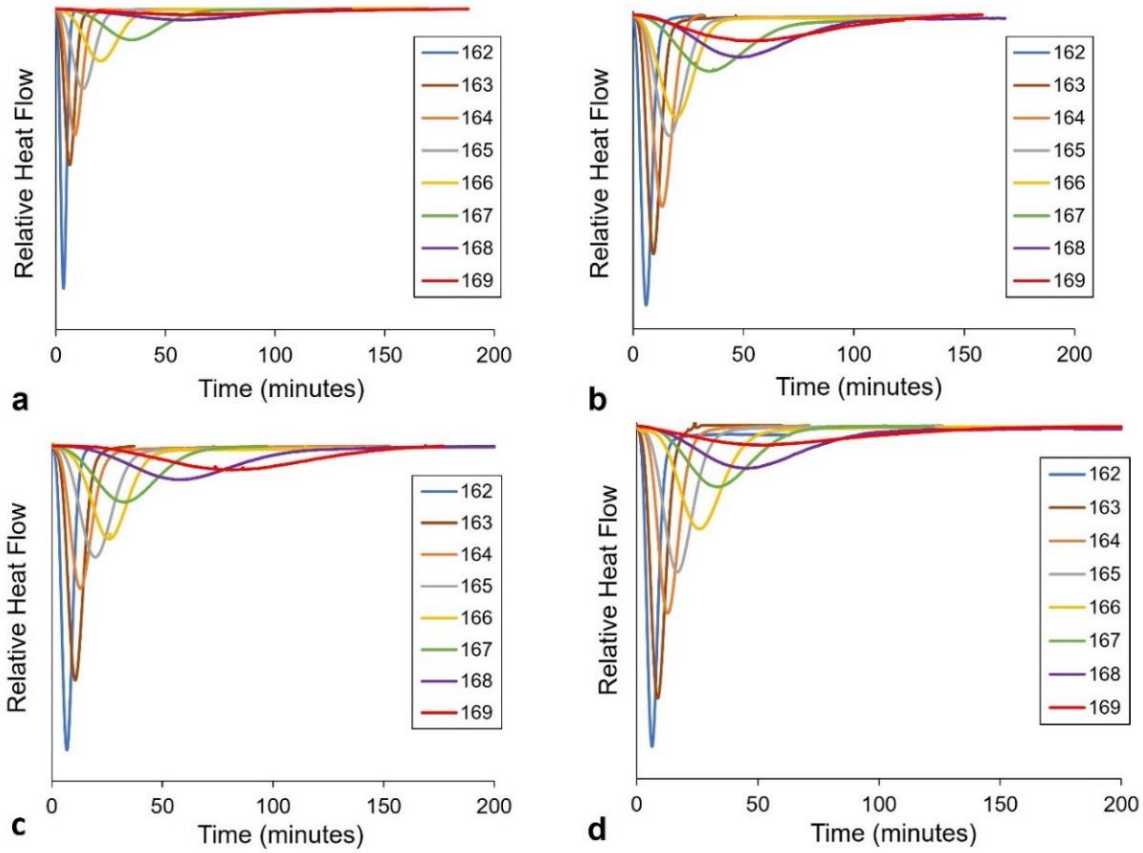

Figure S7 - Avrami double log plots for each powder type, in each case the X_t data range was restricted to the linear region to ensure an $R_2 > 0.99$.

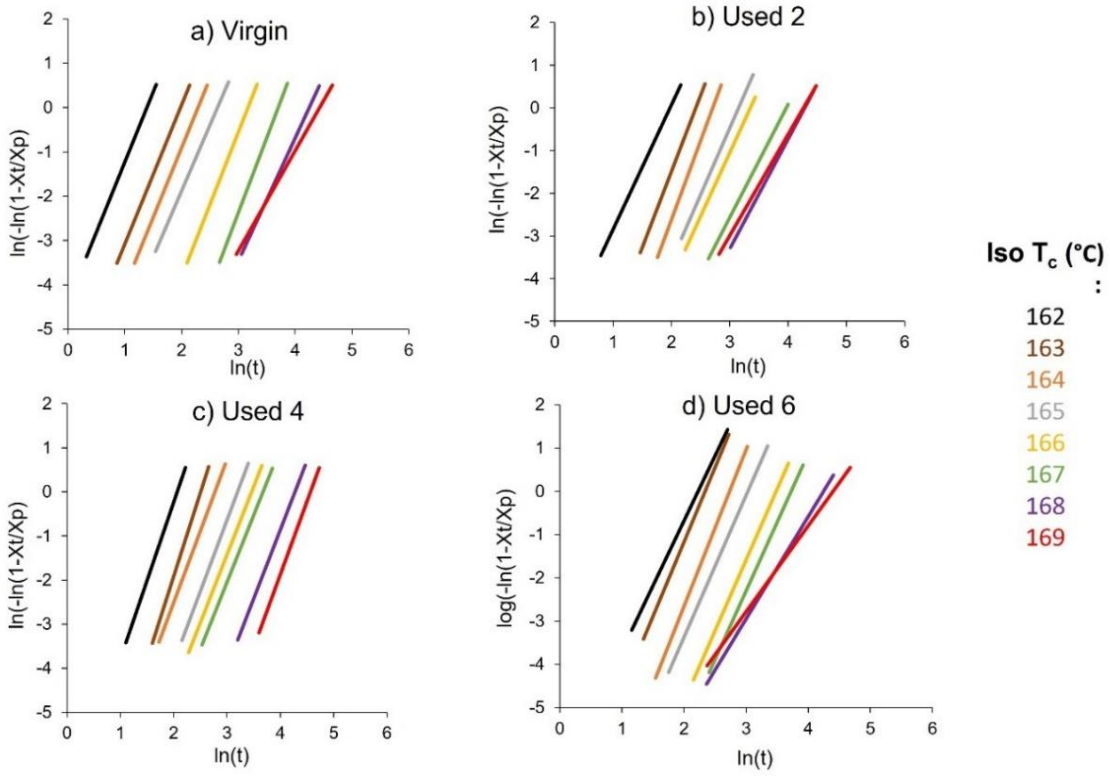

Table S1 - Avrami crystallisation kinetic parameters and coefficients of determination (R^2) derived from double log plots over iso crystallisation range of 162 – 169 °C. X_t range restricted to ensure a R^2 value of > 0.99.

Iso T_c	Virgin					Used 2				
	t ½ (min)	n_a	$k_a x10^{-3}$ (min^{-n})	R^2	X_t range	t ½ (min)	n_a	$k_a x10^{-3}$ (min^{-n})	R^2	X_t range
162	3.57	3.18	12.061	0.9997	0.03-0.95	6.35	2.93	3.085	0.9997	0.03-0.80
163	6.45	3.15	1.982	0.9999	0.03-0.95	10.18	3.52	0.196	0.9959	0.03-0.80
164	8.80	3.15	0.738	0.9999	0.03-0.95	13.60	3.71	0.043	0.9997	0.03-0.80
165	12.78	3.12	0.242	0.9999	0.03-0.95	21.18	3.24	0.035	0.9991	0.03-0.80
166	21.23	3.26	0.033	0.9998	0.03-0.95	25.43	2.97	0.046	0.9935	0.03-0.65
167	36.25	3.38	0.004	0.9995	0.03-0.95	46.56	2.54	0.040	0.9901	0.03-0.65
168	51.15	2.83	0.006	0.9992	0.03-0.95	63.57	2.57	0.016	0.9900	0.03-0.70
169	61.10	2.26	0.046	0.9997	0.03-0.95	71.25	2.37	0.041	0.9998	0.03-0.80
Iso T_c	Used 4					Used 6				
	t ½ (min)	n_a	$k_a x10^{-3}$ (min^{-n})	R^2	X_t range	t ½ (min)	n_a	$k_a x10^{-3}$ (min^{-n})	R^2	X_t range
162	7.10	3.55	0.652	0.9992	0.03-0.80	8.33	3.01	0.231	0.9912	0.07-0.55
163	11.10	3.81	0.072	0.9988	0.03-0.80	10.17	2.66	0.317	0.9992	0.03-0.90
164	14.10	3.25	0.123	0.9970	0.03-0.80	14.57	3.62	0.0511	0.9973	0.03-0.90
165	22.50	3.24	0.032	0.9965	0.03-0.80	23.95	3.28	0.0485	0.9951	0.03-0.90
166	28.25	3.09	0.023	0.9979	0.03-0.80	28.38	3.28	0.0112	0.9970	0.03-0.80
167	34.80	3.04	0.014	0.9996	0.03-0.80	36.38	3.17	0.0074	0.9977	0.03-0.80
168	64.40	3.12	0.002	0.9976	0.03-0.80	58.00	2.37	0.0432	0.9908	0.05-0.70
169	86.52	3.33	0.0002	0.9986	0.03-0.80	76.38	2.00	0.0153	0.9975	0.1-0.80

Table S2 - Co-efficient of determination (R^2) values, calculated using SPSS software, for each isothermal crystallisation temperature and powder type.

Isothermal T_c (°C)	SPSS Avrami R^2 values			
	Virgin	Used 2	Used 4	Used 6
162	0.999	0.997	0.999	0.234
163	0.997	0.976	0.894	0.953
164	0.998	0.999	0.979	0.997
165	0.999	0.954	0.951	0.959
166	0.999	0.912	0.795	0.875
167	0.995	0.817	0.899	0.897
168	1.000	0.818	0.988	0.887
169	0.999	0.985	0.903	0.993

Table S3 - Crystallisation kinetic parameters derived from double log plots (n and k) and from non-linear multi-variable regression analysis in SPSS (n and k*).*

Powder type	Model	n	n*	Difference in n	k ($x10^{-3}$)	k* ($x10^{-3}$)	R^2
Virgin	Avrami	3.12	2.99	0.13	0.24	0.33	1
	SH	3.11	3.16	-0.05	0.257	0.23	0.997
	Tobin	3.77	4.62	-0.85	0.073	0.0085	0.998
Used 2	Avrami	3.24	2.19	1.05	0.035	1.133	0.975
	SH	3.56	3.01	0.55	0.018	0.13	0.941
	Tobin	4.03	3.06	1.03	0.0051	0.14	0.990
Used 4	Avrami	3.24	2.10	1.14	0.032	0.98	0.964
	SH	3.08	3.26	-0.12	0.047	0.37	0.831
	Tobin	3.88	2.26	1.62	0.0064	0.87	0.970
Used 6	Avrami	3.28	3.03	0.25	0.0485	0.0108	0.969
	SH	3.42	3.56	0.14	0.0422	0.0273	0.938
	Tobin	4.19	4.10	0.09	0.00573	0.00584	0.990

Table S4 - A comparison of the kinetic parameters derived from double log plots (n and k) with the kinetic parameters derived from non-linear multi-variable regression analysis in SPSS (n and k*) for the Hay model.*

Powder type	n	n*	Difference in n	k_p ($x10^{-3}$) (min^{-n})	k_p* ($x10^{-3}$) (min^{-n})	k_s (min^{-n})	k_s* (min^{-n})	R^2
Virgin	3.00	2.62	0.38	0.33	1.28	0.0283	0.1393	0.986
Used 2	3.00	2.75	0.25	0.16	0.31	0.0221	0.1381	0.998
Used 4	3.00	3.19	-0.19	0.11	0.047	0.0348	0.0250	1.000
Used 6	3.00	3.23	-0.23	0.15	0.0654	0.0525	0.0110	0.999

Table S5 - A comparison of the Malkin kinetic parameters C_0 and C_1 with the Malkin kinetic parameters derived from non-linear multi-variable regression analysis in SPSS (C_0^* and C_1^*)

Powder Type	C_0	C_0*	Difference in C_0	C_1	C_1*	Difference in C_1	R^2
Virgin	71.80	83.23	-11.43	0.336	0.346	-0.01	1.000
Used 2	84.73	39.39	45.34	0.210	0.204	0.006	0.989
Used 4	84.93	32.84	52.09	0.204	0.159	0.045	0.975
Used 6	90.35	87.53	2.82	0.245	0.248	0.003	0.997

Table S6 - Co-efficient of determination (R^2) values for the Avrami and Hay models at every isothermal crystallisation temperature. DLP curve is produced from parameters calculated through double log plots, CF curve is produced via curve fitting in SPSS.

	Virgin				**Used 2**				**Used 4**				**Used 6**			
Iso Tc	Avrami		Hay		Avrami		Hay		Avrami		Hay		Avrami		Hay	
	DLP	CF	DLP	CF	DLP	CF	DLP	CF	DLP	CF	DLP	CF	DLP	CF	DLP	CF
162	0.999	1.000	1.000	1.000	0.997	0.998	0.986	0.999	0.999	0.999	1.000	0.999	0.953	0.996	1.000	0.999
163	0.997	0.998	1.000	1.000	0.976	0.980	0.996	1.000	0.894	0.949	0.989	1.000	0.234	0.894	0.974	0.996
164	0.998	0.999	0.812	0.997	0.999	1.000	0.961	0.996	0.979	0.984	1.000	1.000	0.997	0.999	0.993	1.000
165	0.999	1.000	0.977	0.986	0.954	0.975	0.991	0.998	0.951	0.964	0.973	1.000	0.959	0.969	0.999	0.999
166	0.999	0.999	0.992	1.000	0.912	0.947	0.979	0.997	0.795	0.856	0.901	0.922	0.875	0.931	0.999	0.999
167	0.995	0.999	1.000	0.999	0.817	0.971	0.882	0.999	0.899	0.954	0.990	0.997	0.897	0.917	0.970	0.975
168	1.000	1.000	-	-	0.818	0.963	-	-	0.988	0.998	-	-	0.887	0.979	-	-
169	0.999	1.000	-	-	0.985	0.992	-	-	0.903	0.993	-	-	0.993	0.988	-	-

Table S7 - Standard error of regression, s, values for the Avrami and Hay models, at every isothermal crystallisation temperature. DLP curve is produced from parameters calculated through double log plots, CF curve is produced via curve fitting in SPSS.

Iso Tc	*Region*	**Virgin**				**Used 2**				**Used 4**				**Used 6**			
		Avrami		Hay		Avrami		Hay		Avrami		Hay		Avrami		Hay	
		DLP	CF	DLP	CF	DLP	CF	DLP	CF	DLP	CF	DLP	CF	DLP	CF	DLP	CF
162	*Initial*	0.0004	0.0014	0.0010	0.0010	0.0003	0.0022	0.0003	0.0009	0.0002	0.0056	0.0006	0.0007	0.0190	0.0022	0.0016	0.0068
	Primary	0.0022	0.0015	0.0015	0.0010	0.0019	0.0034	0.0061	0.0013	0.0026	0.0952	0.0011	0.0014	0.0469	0.0032	0.0025	0.0104
	Transition	0.0034	0.0009	0.0018	0.0009	0.0093	0.0038	0.0093	0.0008	0.0083	0.1567	0.0044	0.0017	0.0198	0.0036	0.0034	0.0029
	Secondary	0.0027	0.0015	0.0002	0.0004	0.0043	0.0038	0.0080	0.0004	0.0031	0.1027	0.0010	0.0007	0.0031	0.0020	0.0007	0.0060
163	*Initial*	0.0006	0.0020	0.0009	0.0020	0.0007	0.0082	0.0046	0.0104	0.0003	0.0029	0.0023	0.0023	0.0016	0.0436	0.0131	0.0044
	Primary	0.0047	0.0035	0.0017	0.0043	0.0063	0.0113	0.0139	0.1445	0.0061	0.0572	0.0064	0.0018	0.0946	0.0291	0.0347	0.0045
	Transition	0.0116	0.0041	0.0011	0.0010	0.0216	0.0180	0.0054	0.2592	0.0125	0.1609	0.0009	0.0009	0.0528	0.0152	0.0092	0.0010
	Secondary	0.0046	0.0043	0.0000	0.0012	0.0760	0.0760	0.0004	0.2750	0.0043	0.0875	0.0006	0.0004	0.0115	0.0362	0.0007	0.0010
164	*Initial*	0.0005	0.0014	0.0088	0.0047	0.0006	0.0015	0.0001	0.0001	0.0007	0.0168	0.0008	0.0013	0.0006	0.0031	0.0085	0.0016
	Primary	0.0039	0.0026	0.0890	0.0088	0.0020	0.0025	0.0026	0.0006	0.0061	0.0572	0.0011	0.0014	0.0051	0.0044	0.0212	0.0022
	Transition	0.0091	0.0027	0.0545	0.0066	0.0076	0.0026	0.0049	0.0031	0.0206	0.0579	0.0002	0.0006	0.0113	0.0058	0.0034	0.0015
	Secondary	0.0037	0.0032	0.0002	0.0029	0.0033	0.0022	0.0192	0.0038	0.0061	0.1111	0.0002	0.0001	0.0040	0.0029	0.0001	0.0006
165	*Initial*	0.0003	0.0011	0.0009	0.0058	0.0020	0.0100	0.0035	0.0057	0.0012	0.0149	0.0076	0.0019	0.0008	0.0035	0.0018	0.0015
	Primary	0.0010	0.0020	0.0020	0.0109	0.0370	0.0120	0.0114	0.0106	0.0121	0.0186	0.0213	0.0021	0.0061	0.0051	0.0023	0.0012
	Transition	0.0053	0.0020	0.0100	0.0173	0.0260	0.0130	0.0090	0.0070	0.0293	0.0226	0.0093	0.0015	0.0125	0.0073	0.0012	0.0004
	Secondary	0.0024	0.0019	0.0212	0.0135	0.0130	0.0130	0.0024	0.0026	0.0172	0.0169	0.0163	0.0006	0.0050	0.0036	0.0014	0.0005
166	*Initial*	0.0006	0.0022	0.0038	0.0011	0.0037	0.0256	0.0005	0.0005	0.0041	0.0421	0.0025	0.0003	0.0015	0.0062	0.0031	0.0048
	Primary	0.0033	0.0038	0.0228	0.0011	0.0318	0.0281	0.0085	0.0005	0.0699	0.0282	0.0145	0.0233	0.0068	0.0097	0.0044	0.0076
	Transition	0.0115	0.0044	0.0047	0.0008	0.0313	0.0207	0.0220	0.0006	0.0189	0.0094	0.0850	0.0987	0.0263	0.0130	0.0016	0.0018

	Secondary	0.0044	0.0040	0.0002	0.0002	0.0910	0.0910	0.0314	0.0002	0.0040	0.0026	0.0112	0.0022	0.0080	0.0069	0.0021	0.0023
167	*Initial*	0.0013	0.0026	0.0020	0.0059	0.0020	0.0359	0.0083	0.0040	0.0001	0.0017	0.0004	0.0011	0.0004	0.0035	0.0146	0.0022
	Primary	0.0094	0.0040	0.0028	0.0094	0.0649	0.0241	0.0421	0.0008	0.0021	0.0023	0.0011	0.0020	0.0049	0.0042	0.0098	0.0010
	Transition	0.0161	0.0043	0.0005	0.0010	0.0534	0.0139	0.0524	0.0002	0.0063	0.0022	0.0015	0.0007	0.0086	0.0047	0.0657	0.0761
	Secondary	0.0049	0.0039	0.0006	0.0010	0.0116	0.0040	0.0565	0.0003	0.0300	0.0300	0.0025	0.0007	0.0170	0.0063	0.0023	0.0004
168	*Initial*	0.0005	0.0002	-	-	0.0023	0.0433	-	-	0.0031	0.0047	-	-	0.0025	0.0216	-	-
	Primary	0.0010	0.0004	-	-	0.0638	0.0291	-	-	0.0180	0.0057	-	-	0.0383	0.0181	-	-
	Transition	0.0014	0.0005	-	-	0.0529	0.0144	-	-	0.0227	0.0067	-	-	0.0477	0.0136	-	-
	Secondary	0.0006	0.0007	-	-	0.0121	0.0055	-	-	0.0041	0.0033	-	-	0.0113	0.0170	-	-
169	*Initial*	0.0002	0.0003	-	-	0.0030	0.0022	-	-	0.0017	0.0007	-	-	0.0014	0.0033	-	-
	Primary	0.0014	0.0006	-	-	0.0210	0.0312	-	-	0.0176	0.0032	-	-	0.0026	0.0031	-	-
	Transition	0.0027	0.0007	-	-	0.0370	0.0298	-	-	0.0088	0.0051	-	-	0.0100	0.0031	-	-
	Secondary	0.0009	0.0003	-	-	0.100	0.0981	-	-	0.0020	0.0019	-	-	0.0052	0.0029	-	-

Table S8 - The change in kinetic parameters, as a function of powder re-use, calculated using the Hay and Avrami models.

Powder Type	Isothermal T_c (°C)	Hay				Avrami	
		Xp_{inf}	k_s	k_p	t ½ (min)	k_p	t ½ (min)
Virgin	162	0.279	0.0784	0.013801	3.50	0.012061	3.57
	163	0.264	0.0489	0.002760	6.05	0.001983	6.43
	164	0.265	0.0298	0.000530	10.75	0.000738	8.80
	165	0.275	0.0283	0.0005420	12.44	0.000242	12.76
	166	0.264	0.0242	0.0001150	18.20	0.000033	21.17
	167	0.258	0.0433	0.000070	32.15	0.000004	36.13
	168	-	-	-	-	0.000006	51.13
	169	-	-	-	-	0.000046	60.52
Used 2	162	0.240	0.0254	0.002661	5.48	0.003085	6.32
	163	0.248	0.0178	0.002650	6.22	0.000197	9.98
	164	0.254	0.0036	0.000516	11.31	0.000043	13.55
	165	0.235	0.0221	0.000162	13.68	0.000035	20.50
	166	0.250	0.0084	0.000109	19.76	0.000047	24.47
	167	0.211	0.0608	0.000056	33.2	0.000040	46.63
	168	-	-	-	-	0.000016	61.23
	169	-	-	-	-	0.000041	71.18
Used 4	162	0.251	0.0120	0.002670	6.25	0.000652	7.05
	163	0.226	0.0874	0.000597	9.40	0.000072	11.00
	164	0.225	0.0895	0.000320	12.52	0.000123	14.10
	165	0.241	0.0348	0.000042	15.53	0.000032	21.80
	166	0.262	0.0191	0.000046	23.58	0.000023	27.75
	167	0.251	0.0245	0.000012	36.10	0.000014	34.70
	168	-	-	-	-	0.000002	63.00
	169	-	-	-	-	0.0000003	85.48
Used 6	162	0.230	0.0326	0.001657	6.14	0.001231	8.33
	163	0.257	0.0393	0.000402	8.33	0.003166	10.17
	164	0.243	0.0456	0.000292	10.93	0.000051	17.00
	165	0.237	0.0525	0.000046	17.42	0.000049	25.90
	166	0.247	0.0400	0.000038	24.42	0.000011	30.38
	167	0.248	0.0411	0.000009	37.50	0.000007	46.38
	168	-	-	-	-	0.000043	68.00
	169	-	-	-	-	0.000153	86.38

CHAPTER 7 – INVESTIGATING SECONDARY CRYSTALLISATION OF PA-12 USING FAST SCANNING CALORIMETRY

7.1 Introduction

Polyamide-12 (PA-12) is a semi-crystalline thermoplastic with a repeat unit containing an aliphatic chain of 11 methylene sequences, separated by an amide group [54, 56, 57, 240, 241]. Within PA-12, polymeric chains are organised to try and maximise hydrogen bonding between N-H and C=O groups across adjacent chain segments [54, 59]. This allows highly crystalline structures to develop, providing PA-12 with excellent physical properties such as high strength, stiffness, and toughness [162, 242]. In addition, due to its relatively long methylene sequence, PA-12 is more resistant to water absorption than other polyamides [55, 56, 209]. Owing to these superior material properties, PA-12 is commonly used within advanced processing methods, such as powder bed fusion (PBF) [15, 24, 38, 234], for the fabrication of functional, end-use components [61, 119]. Nonetheless, the strong property profile of PA-12 is related to its inherent semi-crystalline microstructure, including degree of crystallinity, as well as the morphology, size, shape, and stability of crystals [117, 243]. Therefore, the final properties of manufactured parts will depend on crystallisation conditions during processing, particularly the level of supercooling of the melt and developments in crystallinity via secondary crystallisation [56, 117, 162,

243]. As such, investigating the isothermal crystallisation behaviour of PA-12 is vital to understanding the effect of temperature and time on crystalline morphology and, subsequently, how this influences the processability of the material.

Traditionally the crystallisation behaviour of polymers was investigated using various characterisation techniques such as wide-angle X-ray diffraction (WAXD) [117, 242], small-angle X-ray scattering (SAXS) [100, 117], and differential scanning calorimetry (DSC) [119, 129, 131, 231]. However, DSC is only able to analyse the isothermal crystallisation kinetics of PA-12 at very low supercooling and is unable to model the processing conditions of modern manufacturing methods, where heating and cooling rates can be as high as 5,000 °C/s to 10,000 °C/s [56, 163, 244]. Therefore, more recent studies have started to utilise a modern, state-of-the-art thermal characterisation technique known as fast scanning calorimetry (FSC) [56, 123, 162, 243, 245, 246]. This method operates with extremely fast heating and cooling rates of up to 30,000 °C/s and 4,000 °C/s, respectively [244, 247]. Operating with such high scanning rates can prevent reorganisation on heating, which ensures the original material behaviour, prior to processing, can be determined. Similarly, melt crystallisation during cooling can be supressed, resulting in what is often assumed to be a fully amorphous sample, so that the isolated effects of isothermal crystallisation can be established [244].

Nonetheless, the most beneficial aspect of FSC for the purpose of this study, is that it permits analysis of the isothermal crystallisation kinetics of PA-12 across the full temperature range between the glass transition temperature (T_g) and the melting temperature (T_m) [56, 243-245]. This is a significant advantage over conventional DSC, where any investigations into isothermal crystallisation kinetics are limited to

high crystallisation temperatures (T_c), close to T_m. Traditional crystallisation theories, such as the Turbull-Fischer equation [87, 248], suggest that crystallisation rate shows a parabolic curve, whereby the maximum crystallisation rate occurs in-between T_g and T_m. According to nucleation theory, the free energy barrier for crystal nucleation is dominant at low supercooling of the melt, whilst the activation barrier for short range diffusion controls the nucleation rate at lower crystallisation temperatures, tending to T_g [91, 124, 229]. However, within PA-12, a bimodal temperature dependence to isothermal crystallisation kinetics is expected, whereby there is a change in nucleation mechanism from homogeneous nucleation at high supercooling to heterogeneous nucleation at low supercooling [56, 115, 162, 229, 245, 249]. Similar behaviour has also been reported within various other polyamides [121, 123, 124, 229, 243, 250].

The complex crystallisation behaviour of PA-12 is heightened by its metastability and polymorphic nature, whereby different crystal types can form at various levels of supercooling and, during heating, these crystalline regions can go through transformations into different crystal structures [244]. Polymorphism occurs due to the varying temperature dependence of Van der Waals forces and hydrogen bonding, which alters the extent of thermal expansion, causing a change in the crystal structure [117, 162]. Utilising a combination of WAXD, SAXS, and FSC, previous studies have reported that, within PA-12, the gamma (γ) phase is the dominant crystalline state [58, 115, 162, 242, 245, 251, 252]. However, depending on the crystallisation or processing conditions, PA-12 can also crystallise into the γ', α, or α' phase [115, 117, 162, 242]. In the γ phase, chains are aligned parallel into an orthorhombic lattice, whereby hydrogen bonds can swing out of the plane, resulting

in a relatively mobile hexagonal structure *(Figure 7.1)* [115, 117, 242]. The γ’ phase, commonly referred to as the mesophase or mesomorphic phase, is a defected version of the γ phase, thus displays a similar, albeit less stable, pseudohexagonal crystal structure [117, 121, 162, 242, 243]. On the other hand, alpha-prime (α’) crystals have a monoclinic formation, whereby the molecular chains are arranged anti-parallel to each other, so hydrogen bonding between extended chains can be attained more easily *(Figure 7.1)* [117, 162, 242]. Previous studies have shown that, within polyamides, the mesomorphic phase commonly forms at high levels of supercooling [117, 122, 162, 242, 245]. As crystallisation temperature increases beyond 100 °C, it is expected that γ crystals begin to grow and become the dominant crystal population [115, 124, 162, 245, 250]. At even higher crystallisation temperatures (low levels of supercooling) a transition from the γ to α’ phase has been reported [56, 162]. Therefore, the bimodal rate dependence of PA-12 could also be related to polymorphism; at low temperatures, a high nucleation rate causes crystallisation to be dominated by the mesophase whilst the high temperature maxima is dominated by γ or α’ formation [124, 245, 250].

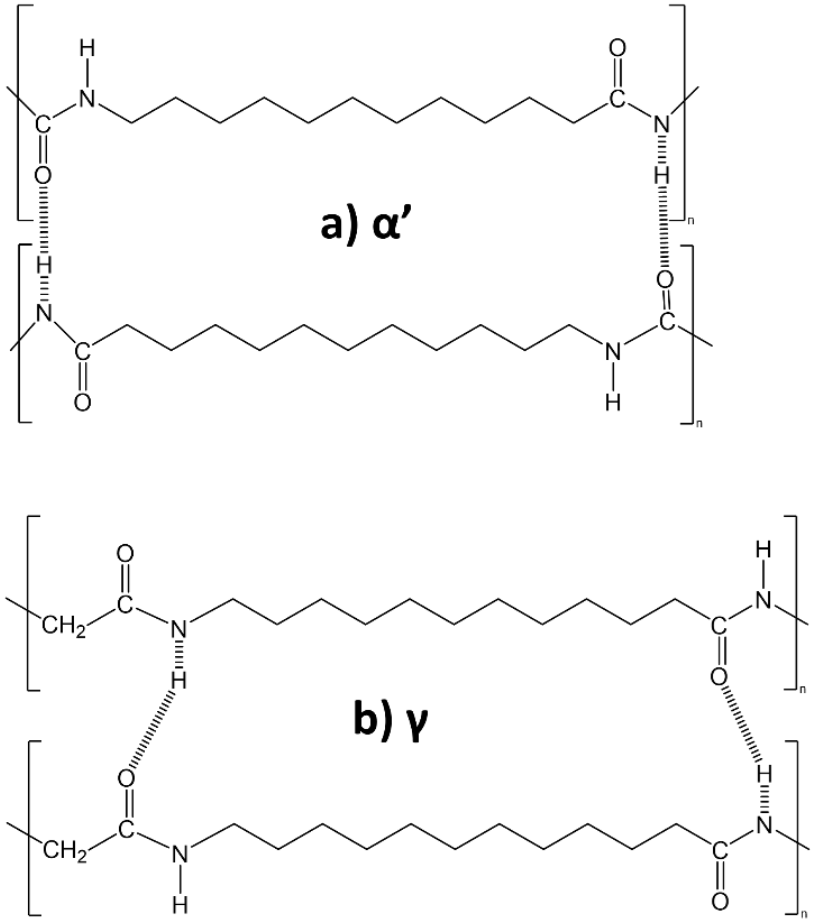

Figure 7.1 - Schematic diagram depicting the difference in the a) alpha-prime (α') and b) gamma (γ) crystal structures, whereby hydrogen bonds are illustrated by the dashed line.

In the context of polymer processing, polymorphism is crucial because different crystal structures affect molecular chain packing, the extent of hydrogen bonding, chain mobility, and lamellar thickness of the polymer [117, 243]. As a result, previous studies have thoroughly investigated the formation of the mesophase, within polyamides, using a wide range of characterisation techniques. Under quiescent conditions, crystallisation of polyamides results in the formation of a three-dimensional spherulitic superstructure and, given sufficient time, lamellar growth will continue until spherulite impingement [253]. However, at low crystallisation

temperatures, there is an absence of lamellae. The mesophase instead displays a fine, non-spherulitic, nodular structure [121, 124, 162, 245, 250, 254], where hydrogen bonds are randomly oriented, which results in a highly metastable material [123, 124, 245]. The absence of spherulites is due to a combination of the distinctly higher nucleation density at high supercooling, and reduced chain mobility, which both hinder extended lateral growth of stable nuclei into lamella structures [115, 123, 124, 245, 250]. Previous studies have used atomic force microscopy and optical microscopy to prove the existence of a nodular mesophase, whereby numerous domains as small as 10 nm exist [121, 124]. The presence of non-spherulitic nodular structures alters material properties, particularly its mechanical behaviour. For example, the tensile strength, Young's modulus, and elongation at break of the mesophase is significantly lower than the γ phase, due to the presence of defects which prevents close packing of molecular chains, resulting in a weaker, less stable crystalline structure [115, 242].

Evidently, previous studies have begun to analyse the isothermal crystallisation behaviour of PA-12 across the full temperature range between T_g and T_m, with a particular focus on the formation of the mesomorphic phase. These works have provided an improved understanding of the effects of nucleation mechanisms and polymorphism on primary crystallisation rate and the resulting crystal structure. Nonetheless, a further complexity of semi-crystalline polymers, such as PA-12, is that following spherulite impingement, developments in crystallinity can continue via secondary crystallisation [100, 114]. It is generally considered that secondary crystallisation can occur via lamellar thickening [99-103], lamellar insertion (infill) [113, 114] or, indeed, a combination of both mechanisms. Improved understanding of

the secondary process is of immense industrial importance because, under the correct conditions, developments in crystallinity due to secondary crystallisation could have a drastic effect on the physical properties of polymeric materials [100, 164, 255]. Previous studies have indicated that the mechanical behaviour, thermal conductivity, and insulating ability of semi-crystalline polymers can be enhanced by thickened lamellae [99]. For example, doubling the lamellar thickness from 20 nm to 40 nm, caused the yield stress of polyethylene to increase from 15 MPa to 30 MPa [164]. Similarly, increases in crystallinity heightens intermolecular hydrogen bonding, which increases the strength and stiffness of the material [35, 51, 160, 193, 196], but also leads to embrittlement [35, 43, 50]. On the other hand, lamellar insertion results in the development of new, thin lamellae structures that are thought to reduce the thermal stability and physical behaviour of polymeric materials [113].

Overall, there is current uncertainty regarding the exact mechanism of secondary crystallisation within PA-12. As such, to the best of the authors knowledge, this paper presents the first study to investigate the secondary crystallisation of PBF-grade PA-12 powder (Hewlett-Packard 3D High Reusability PA-12) using FSC. The complex crystallisation behaviour of PA-12 is analysed over a wide temperature range, whilst the change in the rate and mechanism of secondary crystallisation, at different degrees of supercooling, is quantified.

7.2 Experimental methodology

7.2.1 Material

The material studied in this work is a commercial, industry grade PA-12 powder (HP 3D High Reusability PA-12), which was provided as virgin powder from Hewlett-Packard (Reading, UK). This material has an average particle size of 60 µm, bulk density of 0.425 g/cm^3, a melting point of 187 °C, and a glass-transition temperature of ~45 °C [256].

7.2.2 Fast scanning chip calorimetry

The isothermal crystallisation kinetics at low and high supercooling was studied by means of the differential fast scanning chip (FSC) calorimeter FLASH DSC 1 from Mettler Toledo (Schwerzenbach, Switzerland), combined with a Huber TC100 immersion cooler (Huber Kaltemaschinenbau AG, Offenburg, Germany). To limit the extent of thermo-oxidation, nitrogen was used as a purge gas, with a flow rate of 30 mL/min. Nanogram samples of PA-12 powder, with an estimated mass of between 25 ng and 50 ng, were transferred to the centre of a MultiSTAR UFS 1 sensor (Mettler Toledo, Schwerzenbach, Switzerland). The chip sensors were received pre-calibrated using an electrical method described by Iervolino et al. [257], and, for quality control purposes, each chip is conditioned and corrected prior to loading a sample [244]. More details of the FSC technique can be found in previous works [122, 244, 247, 258].

7.2.3 Isothermal crystallisation kinetics

The applied thermal protocol for investigating the isothermal crystallisation kinetics of PA-12 powder is outlined in *Figure 7.2.* Samples were heated to and held briefly at

250 °C, substantially beyond the T_m of PA-12, to ensure that no residual crystals remained in the melt that could act as seeds for self-nucleation. Samples were then cooled at 4,000 °C/s, the maximum attainable cooling rate within the Mettler Toledo FDSC-1 system [259], to the selected isothermal T_c. The sample was held isothermally at this temperature for a range of timescales between 0.01 seconds and 10,000 seconds, before being cooled again at 4,000 °C/s to 0 °C. Finally, samples were re-heated to 250 °C at 1,000 °C/s. This thermal profile was repeated for every isothermal T_c and t_c. Before each separate isothermal T_c experiment, a simple heat-cool cycle. If the "baseline" thermal transitions moved, then a new sample was made for the next experiment. This ensured that the sample was not degrading between experiments. Due to the very small sample size, and rapid crystallisation rates in the temperature region between T_g and T_m, it is not possible to measure crystallinity development during the isothermal segment. Therefore, the subsequent re-heat (bold red in *Figure 7.2)* was used to evaluate the isothermal crystallisation behaviour of PA-12. As cooling rates are sufficient to prevent crystal growth on cooling, measuring the melting enthalpy of the endothermic peaks on heating represents the crystals that formed during isothermal crystallisation; therefore, the development of crystallinity with increased isothermal time can be calculated. Nonetheless, due to unavoidable crystal nucleation on cooling and melt-recrystallisation on heating, it is necessary to isolate the endotherms formed by the melting of isothermally grown crystals from endotherms that develop as a result of reorganisation on heating. This is explained in more detail in *section 7.3.1.*

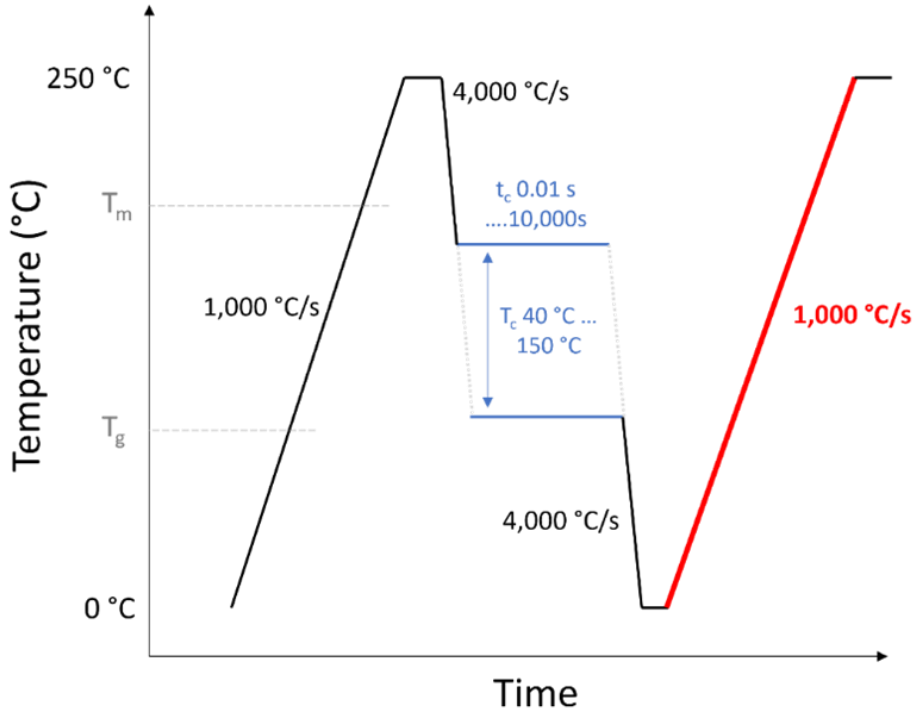

Figure 7.2 - Temperature-time protocol for analysing the isothermal crystallisation kinetics of PA-12. Isothermal crystallisation was studied at 10 °C intervals between 40 °C and 150 °C, whilst isothermal crystallisation time (t_c) varied from 0.01 seconds to 10,000 seconds.

7.3 Results and discussion

7.3.1 Rationale for FSC scanning rates

A heating rate of 1,000 °C/s and a cooling rate of 4,000 °C/s were used for each experiment within this study, following a similar protocol to previous works on polyamides [115, 162, 243, 245]. The rationale for selecting these exact scanning rates is outlined below.

Figure 7.3 displays the thermal behaviour of PA-12 when it is re-heated at 1000 °C/s after cooling at various rates. The absence of a cold crystallisation (CC) peak for cooling rates less than 100 °C/s suggests that full crystallisation is occurring during

cooling, because there is no further crystal growth on heating. After cooling at > 100 °C/s, the re-heat displays a notable CC peak at approximately 75 °C which progressively grows in size with increased cooling rate; this indicates that, due to restricted time, the extent of crystal growth on cooling is reducing. For cooling rates > 2000 °C/s, the CC enthalpy becomes constant, because no crystal growth has occurred on cooling, resulting in the formation of the stable γ phase during heating. This supports previous studies that reported a cooling rate > 2000 °C/s is adequate to prevent crystallisation during cooling [56, 162, 229, 243]. Therefore, at sufficiently high cooling rates, the sample should be fully amorphous and, in theory, developments in crystallinity via isothermal crystallisation alone, can be investigated [244]. Nevertheless, fast cooling cannot supress crystal nucleation, unless cooling at rates greater than 50,000 °C/s, which is significantly beyond the capabilities of the Flash DSC [56, 229, 243]. Consequently, in the current study, the maximum possible cooling rate of 4,000 °C/s was selected to try and minimise the extent of crystal nucleation on cooling. Although the sample appears amorphous at a cooling rate of 4,000 °C, it can be assumed that there will be some unavoidable nuclei formation during cooling; however, it has been suggested that these nuclei will not influence crystallisation halftime during the isothermal process [56, 229]. Therefore, providing the cooling rate is kept constant, the change in crystallisation behaviour of PA-12, as a function of isothermal crystallisation temperature and time, can be analysed accurately.

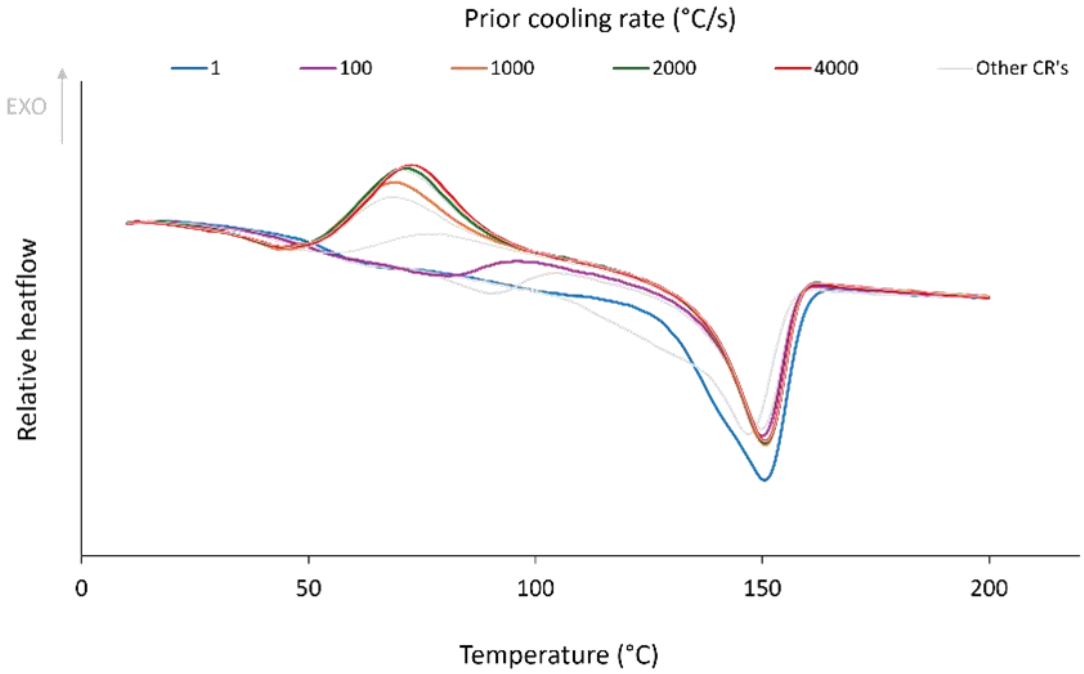

Figure 7.3 - Thermal behaviour of PA-12 upon heating at 1,000 °C/s following non-isothermal cooling at a range of cooling rates between 1 °C/s and 4000 °C/s, emphasising that a cooling rate of 2,000 °C is sufficient to prevent crystal growth on cooling.

The presence of CC exotherms in *Figure 7.3* also demonstrates that a heating rate of 1000 °C/s cannot prevent material reorganisation on heating. Unavoidable crystal nuclei that form at a cooling rate of 4,000 °C/s can then undergo crystal growth during the subsequent re-heat at 1000 °C/s, resulting in the appearance of CC peaks. Furthermore, variations in cooling rate alter the size, stability, and subsequent melting behaviour of the crystals that form during non-isothermal cooling. For example, cooling at < 100 °C/s provides more time for crystal growth, which allows the formation of larger, more stable crystals that require no further reorganisation on heating. However, for cooling rates > 100 °C/s, the endothermic melting peak is constant at ~152 °C, establishing that, on heating the crystalline structure is able to

reorganise and increase in stability via melt-recrystallisation because the crystal structure that formed during faster cooling remains metastable. Previous studies have shown that reorganisation can only be supressed when heating at greater than 30,000 °C/s, because the driving force for melt-recrystallisation is very high, particularly at high supercooling [56, 229, 243, 245]. Unfortunately, at such high heating rates there is severe distortion in the recorded heat flow, which limits accurate analysis [229]. Therefore, preventing reorganisation of PA-12 was not possible using the Mettler Toledo Flash DSC 1 system.

As such, a heating rate of 1,000 °C/s has been selected for this study because it provides the most accurate heat flow curves with minimal thermal lag. This is demonstrated within *Figure 7.4* whereby the thermal behaviour of PA-12, following isothermal crystallisation at 100 °C, is compared at a range of heating rates. The melting behaviour at a heating rate of 15,000 °C/s is indicative of reorganisation because it is predicted that the very broad, asymmetric melting endotherm is actually composed of multiple melt-recrystallisation events [56]. However, at such high heating rates, the Flash DSC is only able to detect the overall, net change in heat flow, so it appears as a singular melting peak. Therefore, within this melting peak it is difficult to isolate the crystals which developed during isothermal crystallisation, from the crystal population that formed as a result of CC or melt-recrystallisation on heating. As heating rate is reduced, melting peaks become less broad and more symmetrical; at a lower heating rate of 1000 °C/s dual melting is observed for an isothermal time of 10 seconds. In this case, only the first endothermic peak represents the melting of the thin, unstable crystals formed during isothermal crystallisation, which then immediately recrystallise before melting again at a higher

temperature (second endothermic peak), i.e., melt – recrystallisation – remelting. In comparison, an isothermal hold time of only 0.1 seconds is insufficient to allow crystallisation, so a CC exotherm is observed on the subsequent re-heat, followed by an endothermic melting peak. On this occasion it is easy to decipher that the endothermic peak represents the melting of crystals which formed via reorganisation on heating, because the CC and melting enthalpies are almost identical, suggesting that no crystals formed via isothermal crystallisation. As a result, a heating rate of 1000 °C/s has been selected for this study because the change in crystalline structure, as a result of isothermal crystallisation alone, can be identified; this provides more accurate understanding of the crystallisation behaviour of PA-12.

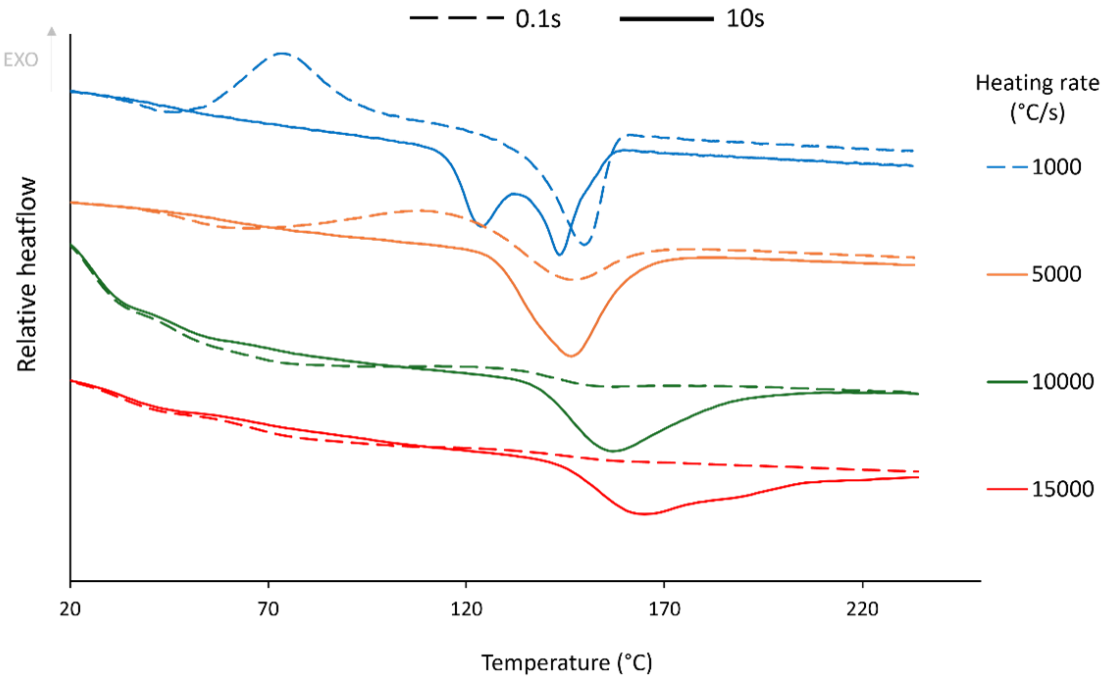

Figure 7.4 - Compares the effect of heating rate on the melting behaviour of PA-12, following isothermal crystallisation at 100 °C, for either 0.1 seconds (dashed line) or 10 seconds (solid line). Only a heating rate of 1,000 °C/s is capable of separating the crystal population formed during isothermal crystallisation, from the crystals formed during cold-crystallisation or melt-recrystallisation on heating, indicated by the dual melting peaks at 1000 °C/s.

7.3.2 Isothermal crystallisation kinetics

Previous studies have demonstrated that the isothermal crystallisation kinetics of PA-12 follows a bimodal dependence on crystallisation temperature, which is caused by alterations in the crystal nucleation mechanism [56, 115, 162, 229, 245, 249], and the polymorphic nature of polyamides [124, 245, 250]. Similar behaviour was observed in this study; therefore, the analysis of the isothermal crystallisation kinetics of PA-12 has been divided into two sections.

7.3.2.1 High supercooling region – 40 °C to 90 °C

On the heating run after isothermal crystallisation at 70 °C, two distinct endotherms are observed *(Figure 7.5).* It is generally agreed that at high levels of supercooling, i.e., crystallisation temperatures < 100 °C, PA-12 crystallises into the mesomorphic phase [117, 122, 162, 242, 245]. Therefore, the first, low temperature endothermic peak most likely represents the melting of mesophase crystals that formed during the isothermal step. Due to reorganisation on heating, PA-12 immediately recrystallises into the more stable γ phase before melting at a higher temperature, signified by the second endotherm. Independent of crystallisation time (t_c), the second endotherm is observed at a constant temperature of ~150 °C and the melting enthalpy remains unchanged, verifying that it represents the melting of reorganised γ phase material. In contrast, with increased crystallisation time, the first endothermic peak shifts to higher temperatures, which suggests an increase in the size and stability of the isothermally grown mesomorphic phase.

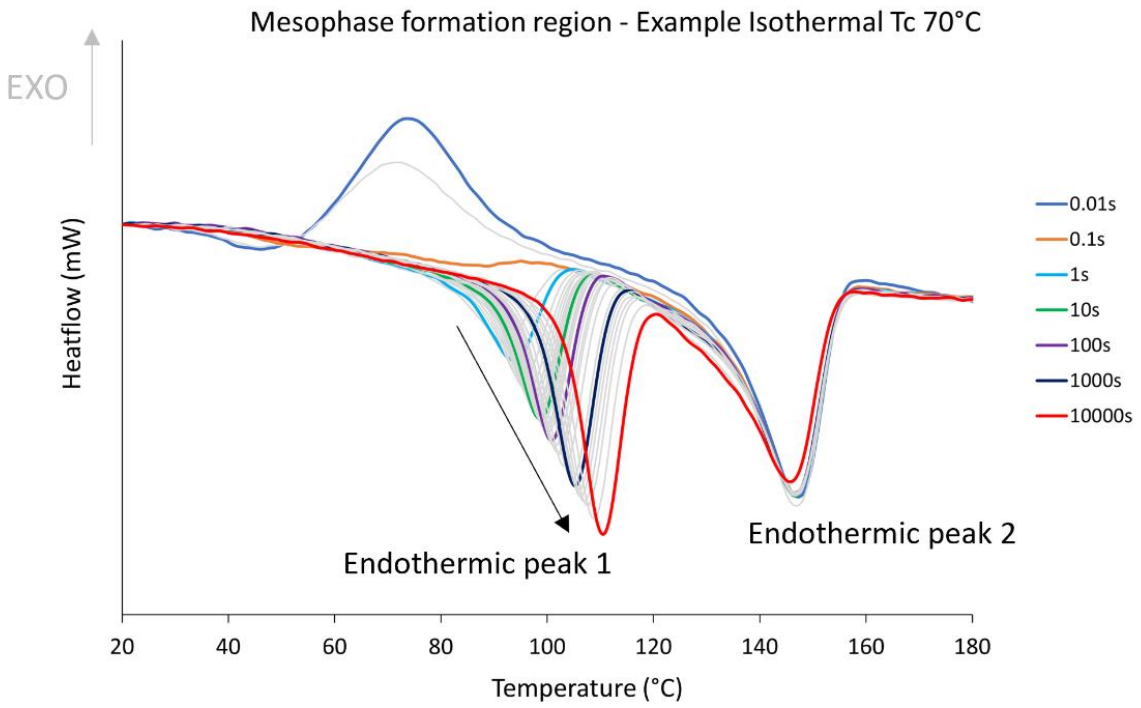

Figure 7.5 - FSC heating scans, at 1,000 °C/s, after isothermal crystallisation at 70 °C for up to 10,000 seconds; the arrow indicates the growth of the mesophase with increased t_c, whilst endothermic peak 2 remains constant for all crystallisation times as it represents the melting of the γ crystals that formed via recrystallisation on heating. This provides an example of the crystallisation behaviour of PA-12 in the isothermal temperature range of 40 °C to 90 °C, where the mesophase is expected to form.

Figure 7.6 demonstrates that similar crystallisation behaviour is observed at all isothermal temperatures in the high supercooling region of 40 °C to 90 °C. With increased isothermal T_c there is an upward shift in the melting temperature of the first endothermic peak *(Figure 7.6a).* This implies that the stability of mesomorphic material is also dependent on temperature; at crystallisation temperatures further away from the T_g, the size and stability of the mesophase increases.

Under quiescent conditions, crystallisation of PA-12 is expected to result in the formation of three-dimensional spherulitic superstructures whereby polymer fibrils

expand radially from the nucleation site, resulting in a multi-layered structure containing crystalline lamellae separated by inter-lamellae amorphous regions [88-90]. The growth of spherulites, as a function of crystallisation time, usually shows a sigmoidal relationship [74, 119]; however, *Figure 7.6b* displays a relatively linear increase in melting enthalpy. This implies that at high supercooling the formation of spherulites does not occur, in agreement with numerous studies that suggest the mesophase forms non-spherulitic, nodular structures [121, 124, 162, 245, 250, 254]. Furthermore, with increased T_c there is a reduction in the extent of mesophase formation *(Figure 7.6b)*, emphasising that the growth of mesomorphic material is most significant at temperatures just above T_g, where the rate of homogenous nucleation is at a maximum. Similarly, as the crystallisation temperature increases, and nucleation rate reduces, the isothermal growth of spherulitic structures will start to dominate [162, 245]. This may explain the decrease in mesophase melting enthalpy for crystallisation times > 1000 seconds following isothermal crystallisation at 80 °C and 90 °C. The initiation of isothermal γ crystal growth can be observed more clearly within *Figure 7.6a.* At 80 °C and 90 °C, three melting peaks appear, which are related to the melting of mesomorphic material, relatively weak and unstable γ crystals that begin to grow during the isothermal hold, and more stable γ crystals which formed through reorganisation of both the γ’ and the weaker γ phase on heating. Therefore, isothermal crystallisation at these temperatures represents a transition region whereby the mesophase and γ crystal growth can occur simultaneously, as observed previously [56, 162, 245].

Overall, the results presented in this section are complimentary to previous studies that suggested PA-12 crystallises into the mesomorphic phase at low crystallisation

temperatures. Details surrounding the formation of an unstable mesophase, and the effect it has on the properties of PA-12, has been analysed in more detail elsewhere [115, 117, 162, 245]. In contrast, the complete crystallisation behaviour of PA-12 at moderate and low degrees of supercooling, particularly the development of secondary crystallisation, is less well understood. Therefore, the remainder of this study will focus on isothermal crystallisation temperatures between 100 °C and 150 °C.

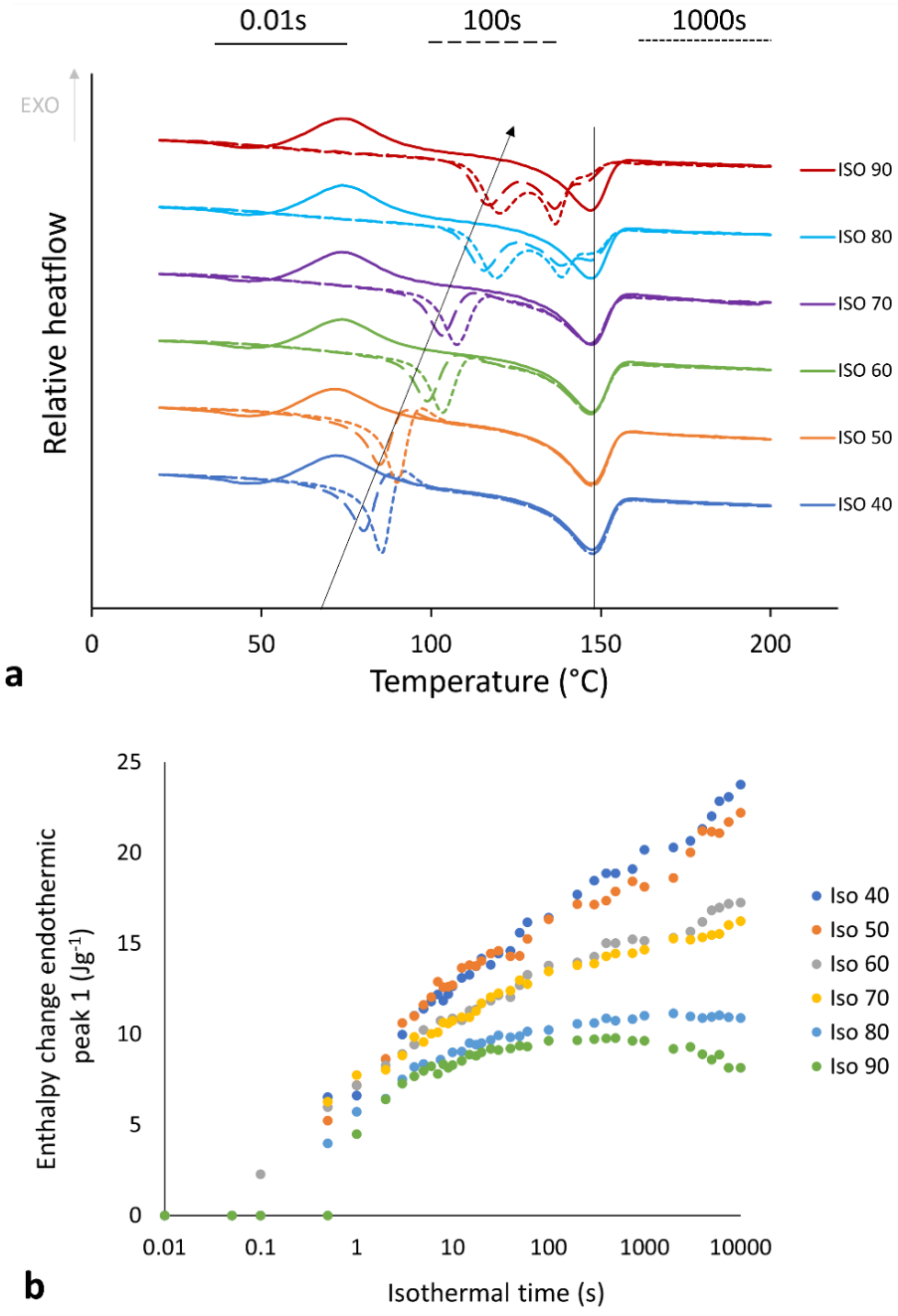

Figure 7.6 - a) FSC heating scans, at 1,000 °C/s, after isothermal crystallisation at temperatures between 40 °C and 90 °C, for three selected crystallisation times of 0.01 seconds, 100 seconds, and 1000 seconds. The arrow indicates the progressive increase in the size and stability of the mesophase with increased T_c, whilst the solid line at 150 °C emphasises that this melting peak represents the melting of crystals that formed via reorganisation, or melt-recrystallisation, on heating. b) The variation in melting enthalpy of the mesophase (i.e., "endothermic peak 1"), as a function of isothermal time, for isothermal crystallisation temperatures between 40 °C and 90 °C.

7.3.2.2 Moderate and low supercooling region – 100 °C to 150 °C

At crystallisation temperatures greater than ~100 °C, crystallisation is dominated by γ or α' formation [115, 117, 124, 162, 245, 250]. However, in the literature, there is some disagreement regarding the transition between the different crystal phases. *Figure 7.6* demonstrated that for isothermal temperatures of 80 °C and 90 °C, there is a transition region, whereby both the γ' and γ phase can develop simultaneously. Some studies have suggested that, beyond 100 °C, growth of the mesophase ceases and that in the temperature region of 100 °C to 130 °C, only γ crystals form [56, 117, 162]. However, the current work provides evidence to suggest that the mesophase can continue to grow up until isothermal crystallisation temperatures of 130 °C. As shown in *Figure 7.7,* at a T_c of 100 °C, dual melting peaks can be observed, signifying the presence of γ' and γ crystal populations. As T_c increases, the first endotherm begins to combine with the main melting peak, now existing as a low temperature shoulder peak, which likely represents the melting of progressively more stable mesomorphic material. This supports the findings of Verkinderen et al., who suggested that at crystallisation temperatures > 100 °C, the mesomorphic material becomes connected to the γ crystals that begin to form, which they defined as "mesomorphic patching" [245]. Furthermore, with increased crystallisation temperature, there is a shift in the main melting peak to higher temperatures *(Figure 7.7),* indicating that larger and more stable γ crystals are able to develop with increased T_c. This relates to traditional crystallisation theory, whereby as T_c increases, the crystallisation process becomes nucleation limited and crystal growth is thermodynamically favoured [120, 121], so larger crystalline structures are expected to form. This crystallisation behaviour, whereby mesomorphic patches form

alongside the growth of the dominant γ crystal population, continues until an isothermal crystallisation temperature of 130 °C.

However, for crystallisation temperatures of 140 °C and 150 °C, there is a change in the crystallisation behaviour whereby, for sufficiently long isothermal times, there is a sudden increase in the melting temperature of the main endotherm, which is distinctly different to the gradual increase observed at lower isothermal temperatures *(Figure 7.7).* The new, high temperature melting peak can be explained by the growth of α' crystals. This supports previous work from Paolucci et al., who used WAXD to identify that, at crystallisation temperatures > 135 °C, two diffraction peaks are observed, characteristic of the α' phase [162]. Therefore, *Figure 7.7* demonstrates that, in the temperature region of 100 °C to 130 °C, γ crystals are the dominant crystal population; whilst, for isothermal crystallisation temperatures > 130 °C α' crystals are able to grow. Nonetheless, it is also evident that crystallisation behaviour is highly dependent on crystallisation time, so it is necessary to analyse the respective time-temperature dependencies of the γ and α' phase in more detail.

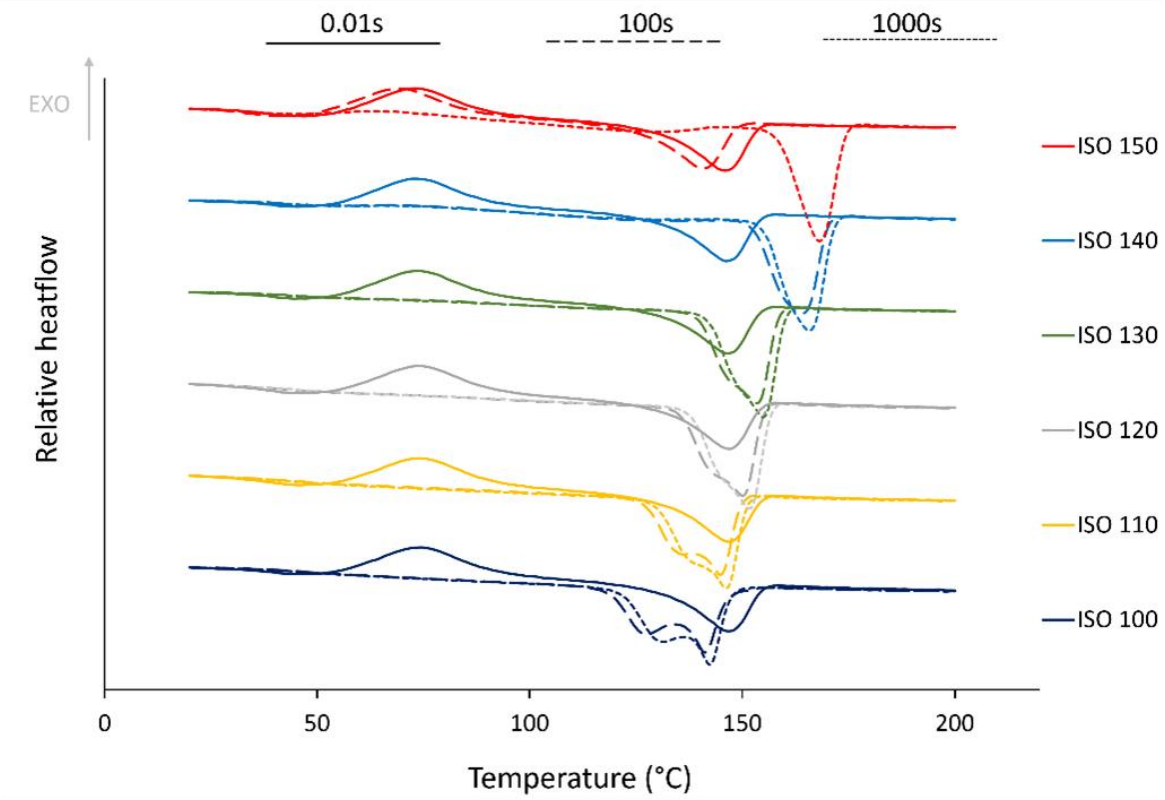

Figure 7.7 - FSC heating scans, at 1,000 °C/s, after isothermal crystallisation at temperatures between 100 °C and 150 °C, for three selected crystallisation times of 0.01 seconds, 100 seconds, and 1000 seconds, indicating the influence of isothermal T_c and t_c on the crystallisation behaviour of PA-12. For crystallisation temperatures > 130 °C there is a transition from the γ to the α' phase.

7.3.2.2.1 Formation of γ crystals – 100 °C to 130 °C

Isothermal crystallisation in the temperature range of 100 °C to 130 °C leads to the formation of γ crystals, as reported previously [115, 117, 162, 245]. *Figure 7.8a* displays the change in heat flow of FSC curves, as a function of crystallisation time, at an example T_c of 120 °C*; Figure 7.8b* shows a sigmoidal relationship between crystal growth and isothermal time, indicating that γ crystals form spherulitic superstructures [74, 119]. For crystallisation times < 2 seconds, the CC enthalpy on heating is equal to the melting enthalpy; low crystallisation times are insufficient to allow any crystal growth to occur via isothermal crystallisation. As crystal nucleation

cannot be prevented on cooling *(section 7.3.1)*, these nuclei grow into crystal structures on heating, resulting in a CC peak, followed by an identical endothermic peak that represents the melting of the crystals formed during CC. Isothermal crystallisation for > 2 seconds results in an exponential increase in the total change in enthalpy, caused by a combination of reduced CC enthalpy and increased melting enthalpy, signifying rapid crystal growth via primary crystallisation. For crystallisation times beyond 10 seconds, CC ceases and there is a notable reduction in the rate of total enthalpy change, representing spherulite impingement and completion of the primary crystallisation process *(Figure 7.8b).* However, the total enthalpy change continues to slowly increase, indicating that the crystallinity of PA-12 can continue to develop for extended periods of time, albeit at a reduced rate.

Further developments in crystallinity following spherulite impingement occur via secondary crystallisation, in the form of lamellar thickening [99-103] or lamellar insertion [113, 114]. However, to the best of the authors knowledge, the exact mechanism of the secondary process within PA-12 has not been investigated previously. *Figure 7.8a* demonstrates that at extended isothermal crystallisation times, there is a gradual upward shift in the temperature and enthalpy of the melting endotherm, which is indicative of a thickening of the pre-existing γ crystals. According to the Gibbs-Thomson equation, a rise in the T_m of polymer crystals is due to an increased lamella thickness, which increases crystal size and stability [99, 253, 260]. Although *Figure 7.8* only provides an example T_c of 120 °C, similar crystallisation behaviour was observed at all temperatures between 100 °C and 130 °C and further analysis of secondary crystallisation is provided in *section 7.3.3.*

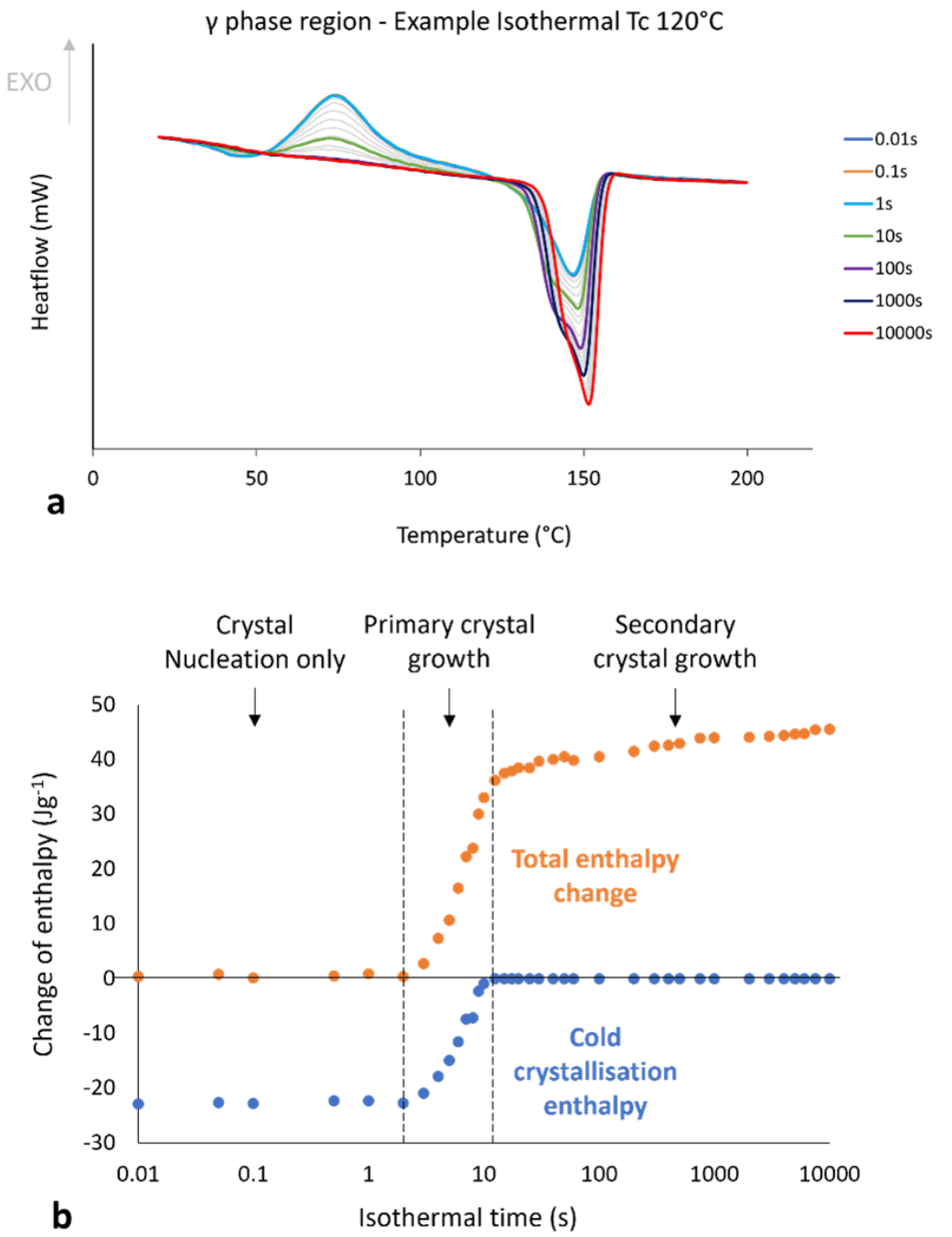

Figure 7.8 - a) FSC heating scans, at 1,000 °C/s, after isothermal crystallisation at 120 °C for crystallisation up to 10,000 seconds; this provides an example of the crystallisation behaviour of PA-12 in the isothermal temperature range of 100 °C to 130 °C, where the γ phase is expected to form. b) The change in cold crystallisation enthalpy and total enthalpy change, whereby total enthalpy = melting enthalpy – cold crystallisation enthalpy, as a function of isothermal crystallisation time at 120 °C. For extended crystallisation times, the gradual, progressive increase in total enthalpy is indicative of secondary crystallisation, via lamellar thickening.

7.3.2.2.2 α' crystal region – 140 °C to 150 °C

The FSC scans displayed in *Figure 7.7* suggest that, at crystallisation temperatures ≥ 140 °C, PA-12 crystallises into the α' crystal phase, which confirms the findings of previous studies on the polymorphism of PA-12 [117, 162]. *Figure 7.9a* provides more evidence to support this. Following isothermal crystallisation for < 10 seconds, the subsequent re-heat displays a CC exotherm at ~75°C, followed by an identical melting endotherm at ~150 °C which represents the melting of γ crystals that formed during CC. Aforementioned, this suggests that no isothermal crystallisation has occurred. Therefore, the induction time for α' crystal growth is significantly longer than γ crystal formation between 100 °C and 130 °C, whereby primary crystallisation initiated within 2 seconds. With increased isothermal time, a secondary endothermic peak appears, which represents the growth of the α' phase; simultaneously, there is a decrease in the CC peak, coinciding with an equal reduction in the melting enthalpy of the first endotherm. As shown by the total enthalpy change in *Figure 7.9b*, initial α' crystal growth is slow, but for isothermal crystallisation times between 30 and 100 seconds there is a rapid reduction in CC enthalpy and an exponential increase in the total melting enthalpy, which is indicative of primary crystallisation. Beyond 200 seconds, the cold crystallisation exotherm and the reorganisation endotherm (1st melting peak) disappear so a single high temperature melting enthalpy is observed *(Figure 7.9a).* Furthermore, analogous to the behaviour of the γ crystal population in *Figure 7.8,* for extended isothermal crystallisation times, there is a continued increase in the enthalpy and melting temperature of the α' crystals, indicative of the slow lamellar thickening process [94, 105, 116].

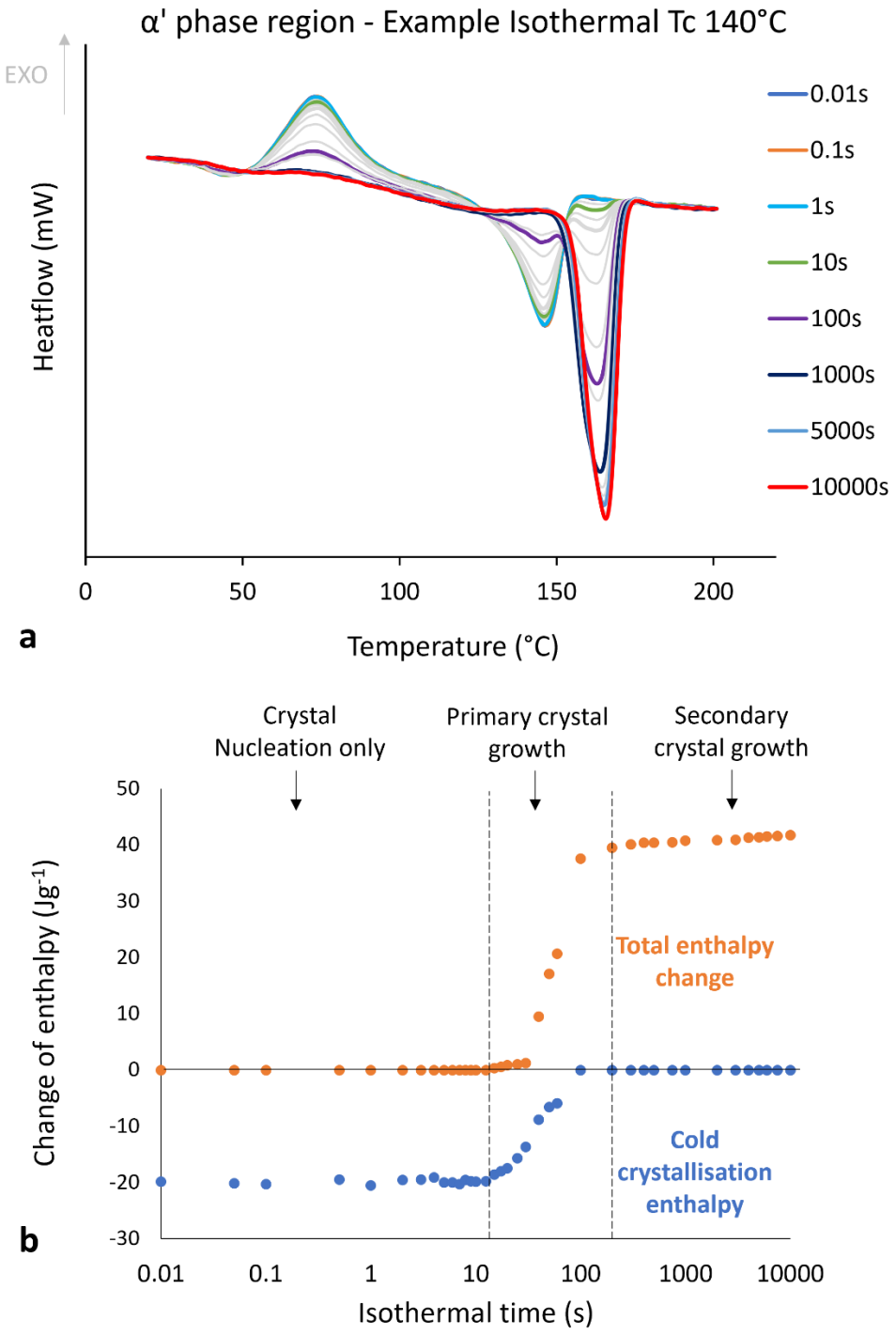

Figure 7.9 - a) FSC heating scans, at 1,000 °C/s, after isothermal crystallisation at 140 °C for up to 10,000 seconds; this provides an example of the crystallisation behaviour of PA-12 at isothermal temperatures > 140 °C, where the high temperature endotherm represents the formation of the α' phase. b) The change in cold crystallisation enthalpy and total enthalpy change, whereby total enthalpy change = total melting enthalpy – cold crystallisation enthalpy, as a function of isothermal crystallisation time at 140 °C.

7.3.3 Secondary crystallisation

The results presented in *section 7.3.2* provide significant evidence to suggest that, over a wide temperature range between 100 °C and 150 °C, PA-12 tends to undergo secondary crystallisation via lamellar thickening. During primary crystallisation, relatively thin crystalline lamellae form, whereby sufficiently mobile polymer chains are able to pass through the thin dimensions of the crystal by repeatedly folding back on itself at each lamella surface [99]. The resulting primary lamellae have a high surface to volume ratio and are thermodynamically metastable, so there is a tendency for lamellae to thicken in the chain axis direction in order to minimise the crystal to liquid interfacial free energy and achieve greater thermodynamic stability. Thus, lamellar thickening does not affect the total number of crystalline stems but causes existing crystals to thicken and become closer to thermodynamic equilibrium [99-103, 105]. This secondary process causes further developments in crystallinity that could significantly alter the materials properties and the subsequent performance of polymer products [99, 100, 255]; therefore, a greater understanding of the mechanisms causing lamellar thickening, and the rate at which thickening occurs, is required.

Figure 7.10 indicates that at all isothermal temperatures > 100 °C, developments in crystallinity, as a function of time, follow a sigmoidal relationship. An induction period, where no isothermal crystallisation occurs, proceeds an exponential increase in the melting enthalpy, representing the melting of the crystals that formed during primary crystallisation. The end of the exponential component signifies spherulite impingement and termination of primary crystallisation. However, rather than an abrupt plateau, spherulite growth is followed by a transition to the secondary

crystallisation region, whereby total enthalpy continues to gradually increase, albeit at a reduced rate. In addition, with increased crystallisation temperature, there is a reduction in the rate of primary crystallisation, evidenced by the sigmoidal curve shifting to extended crystallisation times as T_c increases. This reduction in primary crystallisation rate is to be expected because, as T_c tends towards T_m, an increase in thermal energy restricts the formation of stable nuclei, so nucleation rate reduces. Primary crystallisation rate also appears to be affected by polymorphism because more significant rate reductions occur at temperatures > 130 °C, which represents the transition from γ crystal growth to the formation of an α' phase. Nonetheless, independent of whether the γ or α' phase forms during primary crystallisation, there is clear evidence of secondary crystallisation occurring. With extended crystallisation times, total enthalpy continues to gradually increase, which signifies the slow, yet continuous thickening of the pre-existing lamella.

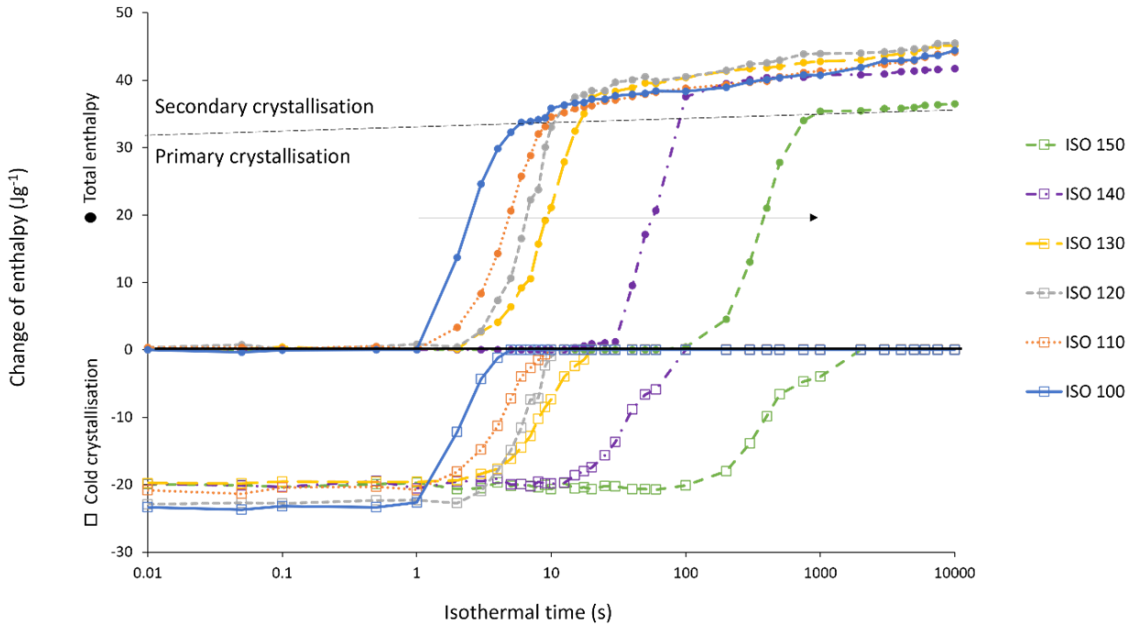

Figure 7.10 -- The change in cold crystallisation enthalpy and total enthalpy change, whereby total enthalpy change = total melting enthalpy – cold crystallisation enthalpy, as a function of isothermal crystallisation time for all crystallisation temperatures between 100 °C and 150 °C. The dotted line indicates the approximate transition from primary to secondary crystallisation, whilst the arrow represents a reduction in the primary crystallisation rate with increased isothermal T_c.

Furthermore, the rate of lamellar thickening also appears to be slower within α' crystals than γ crystals, signified by a reduction in the gradient of the 140 °C and 150 °C curves in the "secondary crystallisation" region of *Figure 7.10*. This is displayed more clearly in *Figure 7.11,* whereby the total enthalpy change, as a function of crystallisation time, is limited to the secondary crystallisation region. It has previously been reported that the rate of lamellar thickening within polymeric materials is greater at higher crystallisation temperatures [99, 100, 102]. These studies suggested that lamellar thickening is controlled by segmental mobility; therefore, increases in T_c provides additional thermal energy that enhances chain mobility, causing the rate of

thickening to increase [102]. That theory does not appear to be accurate within PA-12, as shown by the gradients presented in *Figure 7.11,* which allow comparisons between the rate of lamellar thickening at each crystallisation temperature. Between 100 °C to 130 °C, where γ crystals are dominant, the thickening rate remains relatively constant; at higher crystallisation temperatures of 140 °C and 150 °C, the gradient significantly reduces, indicating that the rate of lamellar thickening within α' crystals is lower.

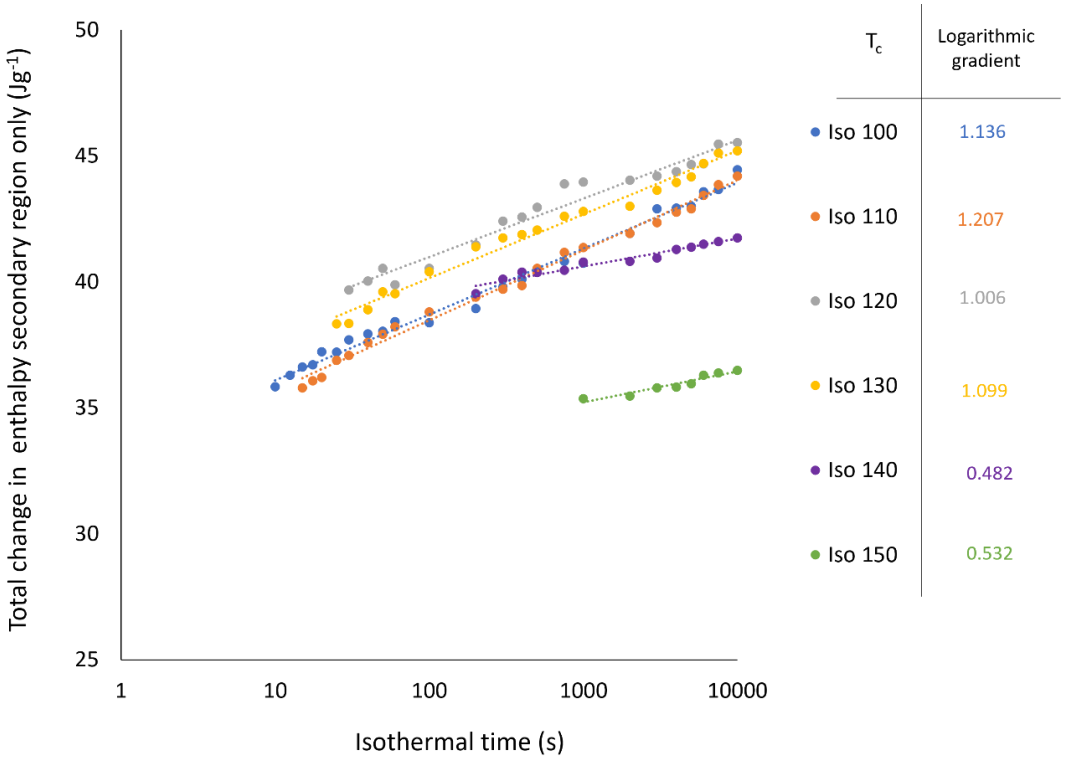

Figure 7.11 - The total change in enthalpy, as a function of isothermal crystallisation time for all crystallisation temperatures between 100 °C and 150 °C, whereby the curves are limited to the secondary crystallisation region alone. Superimposed is a table which compares the gradient of the secondary region at each isothermal T_c; the gradient is representative of the relative rate of lamellar thickening.

The change in the secondary crystallisation behaviour of PA-12 at higher crystallisation temperatures implies that polymorphism affects the rate of lamellar thickening; therefore, the exact mechanism of thickening may be different within the γ and α' phase. Previous studies have proposed several theories that may explain the lamellar thickening process within PA-12. Firstly, the results displayed in *section 7.3.2.1* suggested that the mesophase is able to continuously melt and recrystallise as it is heated to higher temperatures, resulting in a progressively larger nodular mesophase [245]. It is envisaged that, upon heating, the γ phase could undergo a similar melt-recrystallisation mechanism. Premature melting of thin, weak lamellae within lamella stacks, or surface melting of larger crystals, followed by an instantaneous re-crystallisation, could result in thicker, more stable structures [103, 105, 117]. This theory differs from other lamellar thickening mechanisms because it can occur during heating. Therefore, it is a reversible process because, by definition, the lamellae that form are capable of constantly melting and reforming as temperature continues to increase [105]. Melt-recrystallisation of PA-12 is supported by *Figure 7.7* and *Figure 7.8a,* where there is evidence of shoulder melting peaks. It was suggested in *section 7.3.2.1* that this represents mesomorphic patching, however shoulder peaks could also represent the premature melting of thin, isothermally formed γ crystals that immediately recrystalise into thicker lamellae before melting at a higher temperature. In this case, FSC may be incapable of resolving separate melting and recrystallisation events because they occur rapidly, and at similar temperatures to the main melting peak. Likewise, changes in heat flow during melt-recrystallisation would be small, and possibly below the detection threshold of the FSC system. Consequently, the melt-recrystallisation process cannot

be ruled out; however, continuously occurring melting and recrystallisation would be expected to result in more significant fluctuations in melting behaviour with increased crystallisation time [105]. A gradual, progressive increase in quantifiable rate parameters (e.g., melting enthalpy in *Figure 7.11*), as a function of t_c, implies that melt-recrystallisation is not the dominant cause of lamellar thickening, and an alternative thickening mechanism must be active during the isothermal crystallisation of PA-12.

For all crystallisation temperatures between 100 °C and 150 °C the enthalpy change of the secondary region increases linearly as a function of the logarithm of isothermal crystallisation time *(Figure 7.12a).* It has previously been reported that a logarithmic (log) time dependence provides evidence of a solid-state diffusion mechanism for lamellar thickening [99, 100, 102, 103, 113]. Following primary crystallisation, polymer chains are organised in a layered, chain-folded superstructure. Some have hypothesised that the folded chains present within primary lamella are able to rearrange into a more thermodynamically stable configuration. This can occur via solid-state diffusion, whereby folded chains reconfigure their arrangements via sliding or refolding such that the lamellae increase in thickness; these processes have subsequently been referred to as chain-sliding diffusion [99, 101-106] and chain refolding [79, 105, 107, 108], respectively. In these models, “diffusion” refers to a translational movement, whereby sufficiently mobile chains exhibit cooperative motion, allowing them to merge along the longitudinal chain axis of the primary lamella structure. Thus, the relative mobility of the monomer units present within the existing lamella is crucial to both chain sliding and chain refolding [99, 101, 102].

Although *Figure 7.12a* displays a linear increase in melting enthalpy, as a function of log time at all crystallisation temperatures between 100 °C and 150 °C, a notable decrease in the co-efficient of determination (R^2) is observed at 140 °C and 150 °C. This is further supported within *Figure 7.12b,* which plots peak melting temperature against log time, and displays an identical trend. Between 100 °C to 130 °C, R^2 is > 0.96; emphasising that, because the change in T_m displays a log time dependence, the dominant lamellar thickening mechanism within the γ phase is likely solid-state diffusion. Nonetheless, reduced gradients in *Figure 7.11* and decreased R^2 values in *Figure 7.12,* demonstrates that the thickening behaviour of PA-12 is different within the α' phase. At low levels of supercooling, there is a reduction in the nucleation rate, so crystallisation is growth dominated [91, 120, 121]. Therefore, relative to the γ phase, α' crystals are expected to form larger spherulites, with a greater degree of hydrogen bonding and an increased thermodynamic stability [117, 162, 242]. The increased stability of primary α' crystals will reduce the driving force for melt-recrystallisation. Furthermore, the α' phase has a higher T_m than the γ phase, which is verified in *Figure 7.9a* and *Figure 7.12b*. Thus, it can be assumed that α' crystals formed during isothermal crystallisation will not undergo melt-recrystallisation on heating because the primary lamellae are expected to be thick enough to prevent premature melting. This is demonstrated in *Figure 7.9a,* whereby the high temperature melting peak related to the α' phase displays a smooth, sharp, singular endotherm; the absence of shoulder melting peaks implies that melt-recrystallisation of the isothermally grown α' crystals does not occur.

Furthermore, the hexagonal γ phase has a loosely packed formation which permits considerable longitudinal movement of the chains [99]; therefore folded chains in the

lamellae of γ crystals have the necessary mobility to thicken via chain sliding or further refolding. In contrast, the greater hydrogen bond density within the α' phase results in a more rigid crystal structure, which limits the capacity for chains to rearrange via chain sliding and refolding. As a result, within α' crystals, the rate of solid-state diffusion likely decreases, or stops entirely, and further developments in crystallinity can be explained by a different lamellar thickening mechanism.

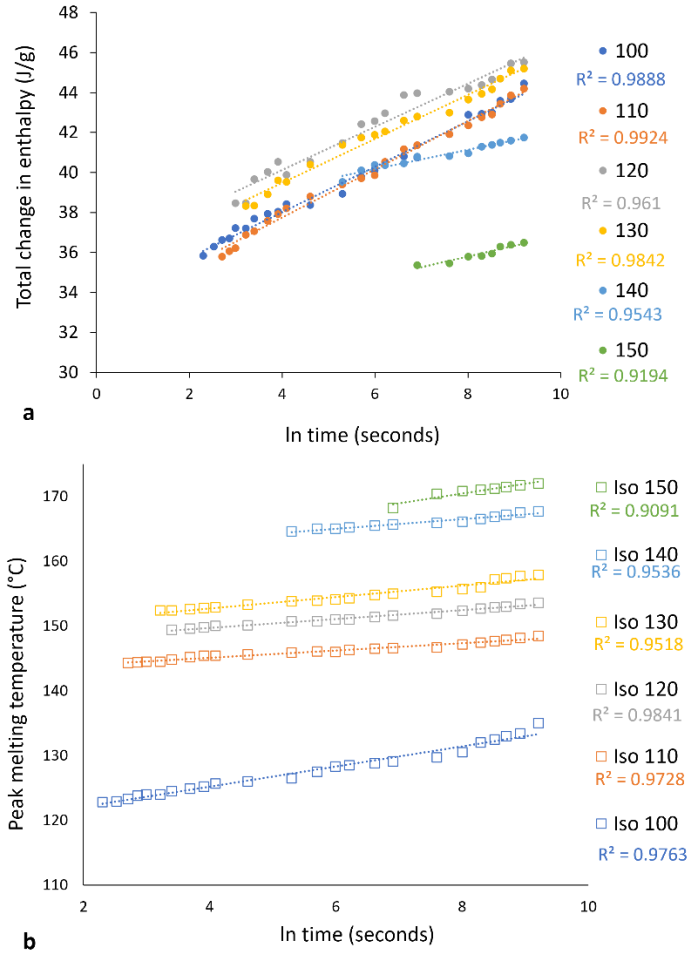

*Figure 7.12 - The change in a) total enthalpy and b) peak melting temperature, against the natural logarithm of isothermal crystallisation time, whereby data is limited to the secondary crystallisation region. The co-efficient of determination (R^2) values indicate how well the data fits a logarithmic time dependence at each isothermal T_c. * Signifies the reduction in R^2 at 140 °C and 150 °C, so at these crystallisation temperatures, lamellar thickening likely occurs via an alternative mechanism.*

The Hay model proposes an additional mechanism of lamellar thickening, whereby the process is strictly diffusion based [91, 144, 145]. The key differential of this theory is that diffusion refers to the movement of chains across the crystal boundary, so fractions of amorphous chains, within the polymer melt, merge into the pre-existing crystalline lamellae. It is envisaged that within the amorphous polymer melt, individual chains exist within virtual entangled tubes, where their size and shape is determined by other chains in the surrounding region of the polymer [91, 261-263]. The length of the chain segments that define the thickness of the lamellae are also constrained by chain entanglements, so for thickening to occur, some disentanglement is necessary. This occurs via reptation, whereby segments of individual chains rotate about the sequences of bonds, allowing chains to move backwards and forwards within the virtual tube [145]. Therefore, with increased crystallisation time, regions of chains such as loops, cilia, and loose sections present within the rigid amorphous fraction (RAF) *(Figure 7.13a)* are able to "diffuse" across the crystal-melt interface and become incorporated into the crystalline lamella. As regions of amorphous chains untangle and reorganise, the movement of the lamellae fold surface is less than the diameter of the virtual tube, which allows lamella to thicken via chain diffusion [91]. It has previously been observed that the diffusion of amorphous chains over a distance smaller than the diameter of the virtual tube follows a square root time dependence [91, 95, 109, 146]. Total melting enthalpy *(Figure 7.13b*) and peak melting temperature (*Figure 7.13c)* are displayed as a function of the square root of isothermal crystallisation time for crystallisation temperatures ≥ 140 °C. In this case, the R^2 values for 140 °C and 150 °C are significantly greater than in *Figure 7.12* indicating that, at these crystallisation

temperatures, lamellar thickening becomes dependent on the square root of time, rather than the logarithmic time dependence observed within γ crystals. Therefore, within the α' phase, it is likely that diffusion plays a role in the lamellar thickening process, and this may occur via the Hay reptation-diffusion theory. Overall, the mechanism of lamellar thickening, and the rate at which thickening occurs, is not only dependent on isothermal crystallisation temperature and time, but also the polymorphic nature of PA-12.

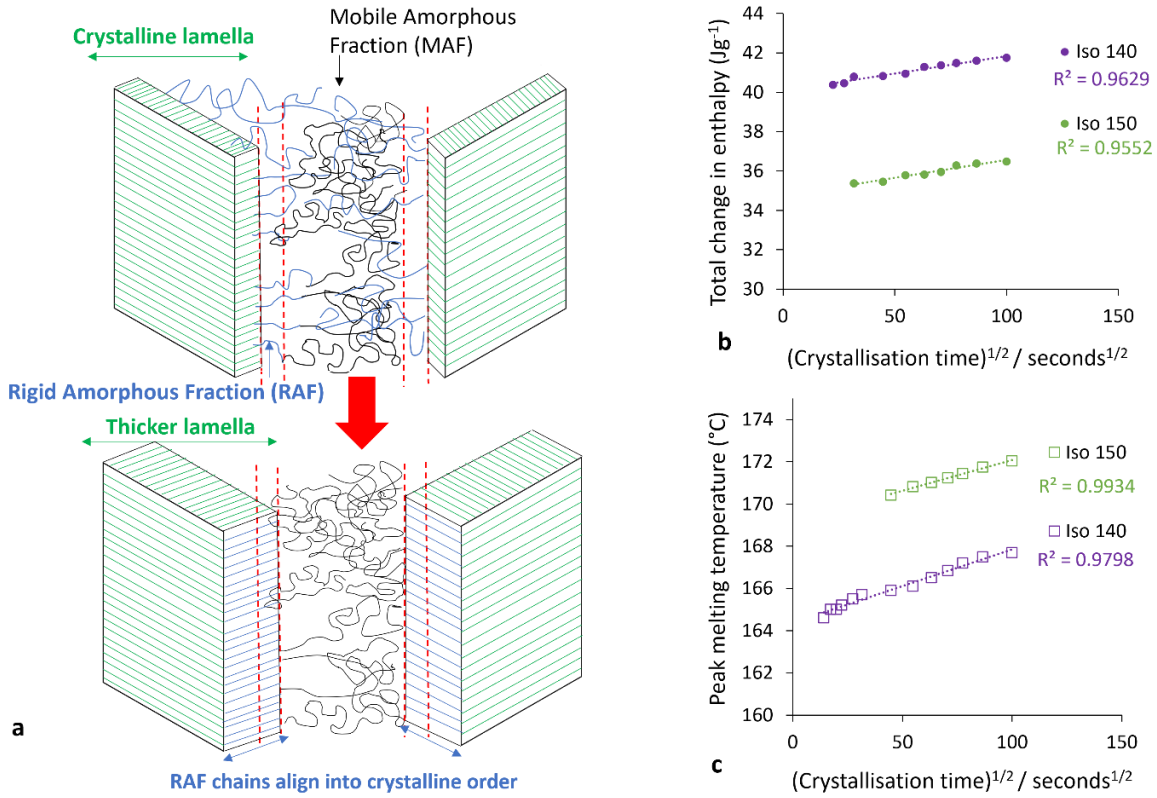

Figure 7.13 - Schematic illustration of lamellar thickening within semi-crystalline polymers via Hay's reptation-diffusion theory; the change in b) total enthalpy and c) peak melting temperature, against the square root of isothermal crystallisation time, whereby data is limited to the secondary crystallisation region. The co-efficient of determination (R^2) values displayed in b) and c) demonstrate that lamellar thickening follows a square root time dependence at isothermal crystallisation temperatures of 140 °C and 150 °C.

7.4 Conclusions

The property profile of polyamide 12 (PA-12) is dependent upon its ability to form highly crystalline structures, as well as the morphology, size, shape, and stability of the resulting crystals. Similarly, the crystallisation process, which causes concurrent volume shrinkage effects, is crucial to the performance and dimensional precision of powder bed fusion (PBF) parts. Secondary crystallisation, a process rarely studied in previous PA-12 literature, causes further developments in crystallinity that can alter the property profile of the material. As such, this study investigated the mechanism and rate of secondary crystallisation, across a wide isothermal crystallisation temperature (T_c) range, using fast scanning calorimetry (FSC). At crystallisation temperatures between 100 °C and 130 °C, PA-12 crystallises into the hexagonal γ phase and displays significant secondary crystallisation. For extended crystallisation times (t_c), the melting endotherm related to the crystal population formed during isothermal crystallisation, progressively shifts to higher temperatures; this is indicative of a slow, yet continuous lamella thickening process. The melting enthalpy, and melting temperature, increase linearly as a function of the logarithm of t_c, suggesting that solid-state diffusion processes such as chain-sliding and chain refolding are the dominant cause of lamellar thickening. However, when T_c > 130 °C, PA-12 crystallises into the α’ phase, whereby hydrogen bonding can be more easily attained and larger, more thermodynamically stable crystal structures develop. The rigid α’ phase reduces chain mobility, which limits the possibility of lamellar thickening via chain sliding or refolding. Consequently, thickening can only continue via a diffusion-based mechanism whereby chains are instead incorporated from the inter-lamellae rigid amorphous fraction. Diffusion-controlled thickening is a slower process,

so the rate of thickening within the α' phase reduces, and lamella thickening is now dependent on the square root of time, which is indicative of Hay's reptation-diffusion model. Evidently, the crystalline structure of PA-12, the rate and extent of secondary crystallisation, and the mechanism of lamellar thickening are all closely related to t_c and T_c. This insight into the secondary crystallisation behaviour of PA-12 could be useful to help predict the properties and performance of final PBF parts.

CHAPTER 8 – INTEGRATED DISCUSSION

8.1 Background

Given the climate crisis, government regulations have forced the manufacturing industry to explore more sustainable processing methods. Additive manufacturing (AM) is widely considered an essential aspect of advanced material processing because it can assist the transition from a linear economy manufacturing model, towards a more sustainable circular economy, whereby waste is minimised [1]. Powder bed fusion (PBF) of thermoplastic materials, such as polyamide-12 (PA-12), is an AM technique capable of providing complex, individualised components with a high strength-to-weight ratio [5, 7, 13, 17, 18, 20]. PBF poses significant advantages within many applications across a wide range of industries, including aerospace, automotive, medical, and sporting goods [45]. However, as consolidated parts are contained within an un-fused powder bed, 80-90% of powder remains un-sintered during each build [16, 18, 21]. The remaining powder is recoverable, and can be re-used, but it has been exposed to elevated temperatures, for extended periods of time. This results in physical aging and degradation processes, which hinder the recyclability of the material [21, 27, 28]. Therefore, in an attempt to counteract the effects of aging, un-sintered (“used”) powder remaining in the build chamber is typically blended with virgin powder before re-use.

However, within industry, there is a general lack of understanding regarding the complex aging behaviour of PA-12 during PBF. Similarly, the effect of aging on the

property profile of feedstock powder, and subsequent part properties, is relatively unknown. Accordingly, there is currently no standard procedure for evaluating the quality of recycled PA-12 powder, leading to uncertainty as to whether or not used feedstock material can be re-used in future builds. As a result, current powder recycling methods involve rigid, arbitrary refresh rates of 50% or 70% used powder, which are inefficient because they do not account for any variation in the properties of the recovered powder. PBF operators are constantly working with refreshed powder mixtures of an unknown, inconsistent quality, so the property profile of final parts is difficult to predict. Consequently, material waste, such as that generated by throwing away relatively un-aged powder unnecessarily, or having to discard unserviceable final parts made from severely aged powder, remains a significant industry challenge.

This research aims to improve the cost effectiveness and environmental sustainability of the PBF process by unravelling the complex aging mechanisms occurring during a build cycle, identifying the influence that each individual aging phenomena has on both powder and part properties. Furthermore, the most appropriate characterisation techniques for managing the lifecycle of recycled powder are established, offering guidance to PBF operators on best practices for incorporating used PA-12 powder into future build cycles.

8.2 Material characterisation studies

In order to improve the current PBF powder re-use strategy, it is first necessary to gain an understanding of the interplay between the aging and degradation phenomena that can occur within PA-12, and how these processes influence the property profile of the material. Commercial grade virgin, 3D high reusability PA-12 powder (Hewlett-Packard) was conditioned for up to 336 hours, within an oxygenated oven, at the understood powder bed temperature of 170 °C. This exposes PA-12 powder to a harsh combination of elevated temperatures, long storage times, and an oxygenated atmosphere, which represents a “worst case scenario” with respect to material degradation. Such conditions were selected to enable a holistic examination of the capabilities of PA-12 in the context of PBF, because exposing the material to this environment presents the opportunity for a wide range of aging and degradation processes to occur.

Characterisation of the conditioned powder samples revealed that the aging behaviour of PA-12 is very complex, whereby multiple processes can occur simultaneously and interact with each other. As a function of storage time, variations in the thermal, chemical, and physical properties of PA-12 powder demonstrated two separate, time-dependent trends. Over the first 100 hours, differential scanning calorimetry (DSC) displayed an increase in melting temperature (T_m) and developments in crystallinity (X_c). The majority of previous PBF studies attribute increases in T_m to a rise in molecular weight due to polycondensation [15, 25, 28, 38, 41, 160]. Nonetheless, polycondensation causes increased chain entanglements which restricts the mobility of amorphous chains, preventing them from contributing to further developments in crystallinity. As a result, an upward shift in both T_m and X_c

indicates that an alternative aging process, namely secondary crystallisation, occurs when PA-12 is stored at elevated temperatures. Polycondensation may still be active, but this aging process cannot explain the observed increase in crystallinity, providing substantial evidence that secondary crystallisation is also affecting the structure and properties of PA-12.

Investigating the isothermal crystallisation kinetics of PA-12 using fast scanning calorimetry (FSC), provided further evidence that secondary crystallisation occurs when PA-12 is stored at temperatures ≥ 100 °C. For extended crystallisation times, there is progressive shift in T_m and X_c, which is indicative of a slow, yet continuous lamellar thickening process. PA-12 is polymorphic so can crystallise into a range of different structures. It has been reported that the γ phase is the most common crystalline structure within PA-12 [58, 115, 162, 245]. However, the relatively high T_m of PBF modified PA-12 powder [34, 58] may indicate that the α' phase is the dominant crystal structure within un-sintered PA-12 powder located in a PBF build chamber. The results presented in *Chapter 7* suggest that the rate of lamellar thickening is slower within the α' phase of PA-12, and that thickening becomes dependent on the square root of time, which is indicative of Hay's reptation-diffusion model. The change in T_m observed during the first 100 hours of oven conditioning was plotted against the square root of oven conditioning time; a linear increase in T_m was observed, with a co-efficient of determination of 0.999. This indicates that, when stored at 170 °C, primary crystalline lamellae within PA-12 powder can undergo further developments in crystallinity via a diffusion controlled lamellar thickening process.

Nonetheless, for extended storage times beyond 100 hours, alterations in T_m and X_c initially plateau, followed by a rapid and substantial reduction. Additionally, Fourier transform infrared spectroscopy (FTIR) showed a higher concentration of imide bonds, a common by-product of oxidative degradation of PA-12. Reductions in tensile strength, severe embrittlement, and significant sample discolouration provided further evidence that thermo-oxidative chain scission becomes the dominant aging process following prolonged storage at 170 °C. Pre-drying PA-12 powder, prior to oven conditioning, causes a reduction in all markers of degradation, including imide growth and sample discolouration. This indicates that, due to the hygroscopic nature of PA-12, moisture within the material or the surrounding atmosphere causes hydrolysis, which accelerates thermo-oxidation. Therefore, in the context of PBF, it is essential that powder handling between build cycles occurs within a closely controlled atmosphere to restrict any further degradation; additionally, feedstock powder could be preconditioned, prior to printing, in order to remove any residual moisture.

This oven conditioning experiment simulates the thermal conditions that un-sintered powder is exposed to within a multi-jet fusion (MJF) build chamber, providing an understanding of the aging processes that may occur when PA-12 is repeatedly re-used across multiple MJF processing cycles. However, the results displayed in *section 5.7.2* suggest that oven conditioning cannot offer a direct replication of the MJF build process. The same material, HP 3D High Reusability PA-12 powder, was also recycled across four MJF build cycles, using the manufacturer recommended 80:20 refresh ratio. After 4 build cycles, the cumulative build time is only 43 hours, or 86 hours if the cool-down is included, so the conditioning time is significantly lower

than the prior oven conditioning study. Nevertheless, this is a sufficient period of time for aging to influence material behaviour. With increased build number, there was no significant change in the thermal properties of the material, contrary to the substantial increase in T_m and X_c that was witnessed after 48 hours of oven conditioning.

Therefore, upon reflection, some of the conclusions made in *Chapter 4* may not be as industrially relevant as it was initially perceived. It appears that the changes in the properties of aged PA-12 powder, following oven conditioning, are not an entirely accurate representation of how the polymer behaves during successive re-use within MJF. During the MJF process, multiple other factors, such as build parameters, the use of fusing and detailing agents, part packing density, and refresh ratios *(section 3.1.2)* can also affect the quality of PA-12 feedstock. Similarly, the mass of powder used in oven conditioning studies is often considerably less than the volume of powder present within a MJF build chamber; due to the low thermal conductivity of PA-12, this may also influence the extent of the various different aging phenomena. As a result, it is important that industry operators are aware that isolated oven conditioning studies may not be comprehensive enough to accurately quantify the re-usability and processability of PA-12 within PBF, which is undoubtedly a complex problem. When formulating a suitable powder recycling strategy, it is crucial that various processing parameters are considered as well. Nonetheless, the oven conditioning experiments conducted in this project provide valuable insight into the aging and degradation behaviour of PA-12, which was a necessary pre-cursor for the conceptualisation of subsequent schemes of work.

8.3 Laser sintering studies

Following the material characterisation studies, improved understanding of aging and degradation was utilised to investigate how aging affects the processability and reusability of PA-12 within laser PBF. This work outlines optimal strategies for quantifying the effect of aging on PA-12 powder recycled across multiple build cycles, using a 70:30 refresh ratio. Commercial grade PA-12 (EOS PA2200) powder, refreshed with 30% virgin powder, was re-used across seven laser sintering (LS) build cycles. With increased build number there was a close relationship between the deterioration of powder quality, and subsequent changes in the properties of laser sintered parts.

DSC demonstrated that, as a function of powder re-use, there is an increase in the melting temperature of PA-12 powder. An increase in avalanche angle is also observed, which represents a reduction in particle flowability and cohesion. Avalanche angle was measured using the revolution powder analyser, proving it to be a useful characterisation technique, despite being rarely used within previous PBF studies. It was expected that reductions in particle flowability would have been caused by changes in the particle size distribution of PA-12 [38, 62, 154]; particles < 20 μm induce stickiness, whilst particles > 80 μm restrict powder flow across the build platform. Nonetheless, measurements taken on a Malvern mastersizer imply there is no change in particle size distribution. Upon further characterisation of the re-used powder using scanning electron microscopy (SEM), it became clear that with increased powder re-use, there was an increase in the number of irregularly shaped particles, increased appearance of fragmented, ‘satellite’ particles, and significant

particle cracking. Hence, these changes in particle morphology likely explain the observed reduction in particle flowability.

Evidently, the satellite particles present within re-used powder samples were not detected using particle size analysis, which has previously been regarded as a key powder characterisation technique within PBF [35, 38, 168, 264, 265]. Furthermore, although a liquid dispersion unit is the most common method of sample dispersion for particle size measurements, it may result in the removal of particle agglomerates [266]. Therefore, the Malvern mastersizer experiments conducted in this study may have been unable to adequately quantify the size and extent of particle agglomeration as a result of powder re-use. This reveals a limitation of using particle size distribution for determining the suitability of recycled powder for re-use in future builds. For example, if PBF operators were given the particle size analysis as an isolated dataset, it would appear that PA-12 powder morphology is highly resistant to laser sintering processing cycles. SEM images indicated that this is not the case, as the shape, stability, and surface quality of particles were susceptible to deterioration. This could have significant consequences for the processability of the material because satellite particles can affect the flowability of the polymer. Satellite fragments attach themselves to larger particles and induce stickiness, preventing the re-coater blade from moving freely throughout the material deposited on the build platform. This could result in a non-homogeneous powder layer, whereby particles are not uniformly distributed, which ultimately leads to layer delamination and enhanced porosity within final parts, as well as surface defects that could render the component unserviceable.

Similarly, in the context of powder re-use, increases in melting temperature are significant. Assuming that build processing parameters remain constant, increased T_m may result in incomplete particle melting, whereby unmolten spherulite cores remain, which prevents full material coalescence. As such, the melt flowability and coalescence behaviour of virgin and re-used PA-12 powder samples was investigated using hot-stage microscopy (HSM). As a function of powder re-use, there was a progressive increase in the onset of melting, and with further upward shifts in temperature, re-used samples displayed restricted melt flowability and limited coalescence compared to virgin samples. This provides evidence of polycondensation and cross-linking, both of which cause increases in molecular weight and melt viscosity, resulting in restricted melt flow.

Furthermore, even at temperatures higher than the endpoint of melting recorded within the DSC, there is evidence of spherulite cores remaining in powder recovered from build 4 and build 6. Incomplete particle melting is also observed through thermal characterisation of LS parts. DSC of parts fabricated from re-used powder show the formation of an upper-temperature shoulder melting peak, representing the presence of higher melting point particles that did not fully melt during the build process. Confirmation of un-molten spherulite cores remaining within used powder samples suggests that some particles contain thicker crystalline lamellae. This behaviour is evident of secondary crystallisation, via lamellar thickening, occurring with repeated powder re-use. This is a crucial observation because, prior to this study, previous research into the aging of PA-12 within PBF has focused almost exclusively on polycondensation [15, 25, 28, 38, 41, 160], and secondary crystallisation has often been overlooked. As discussed in *Chapter 7,* FSC experiments provided substantial

evidence that primary crystalline lamellae tend to thicken when PA-12 is held at isothermal crystallisation temperatures between 100 °C and 150 °C. Nonetheless, identifying that lamellar thickening also occurs during the build process is pivotal because it could have significant industrial implications. Continuation of the crystallisation process during secondary crystallisation may cause further volume shrinkage effects, leading to poor dimensional precision. This may also help explain why LS parts often display inconsistent mechanical properties [61], which has prevented the widespread use of this technology for the fabrication of functional, end-use components. Similarly, as shown within this study, lamellar thickening also reduces the suitability of un-sintered powder for re-use in future build cycles. During the sintering process, the thermal energy provided by the laser cannot fully melt thicker, more stable crystalline lamellae present within re-used powder, resulting in residual crystal fragments. These un-molten particle cores hinder material coalescence, material fusion, and complete part consolidation.

Variations in powder properties emphasises the complexity of PA-12 powder aging during LS, because there is evidence to suggest that polycondensation, cross-linking, and secondary crystallisation all occur simultaneously. From an industry perspective, it is imperative to understand how the observed changes in powder properties influence the subsequent behaviour of LS components. A combination of SEM and X-ray computed topography (XCT) confirmed an increase in the porosity of parts fabricated from re-used powder. In addition, with increased build number, there was a reduction in the ultimate tensile strength, and a rise in the average surface roughness, of LS components. ANOVA statistical analysis summarised that the loss of mechanical performance was caused by increases in the melting temperature and

avalanche angle of PA-12 powder. Moreover, a Pearson correlation test indicated that reductions in particle flowability have a more significant effect on part strength then changes in the thermal properties of PA-12 powder. The strong relationship between particle flowability and the performance of final PBF components is further demonstrated by *Figure 5.20* in *section 5.7.3*. With repeated powder re-use, increased avalanche angle also has a statistically significant effect on the total porosity of manufactured parts. As a result, this suggests that the Revolution powder analyser, a cheap, quick, and non-destructive testing method, can successfully optimise and manage the lifecycle of PA-12 powders.

Although these results indicate how a reduction in powder quality can alter the performance and functionality of final components, an 11% decrease in strength across seven build cycles is relatively modest. Previous work that re-used 100% used powder, without refreshing with any virgin material, observed a more substantial loss of mechanical performance, emphasising the benefits of refreshing with virgin material. This suggests that a 70:30 refresh ratio offers a good compromise between maximising powder re-use without detriment to final part quality. Whilst many operators continue to exclusively use a 50:50 refresh ratio, these results indicate that refreshing with only 30% fresh powder is generally sufficient, particularly for non-critical applications. As for more critical end-use parts, the supply chain could be better organised to redistribute more severely aged powder to other application areas. This demonstrates that operating with more flexible refresh ratios, whereby the required volume of virgin material is adjusted based on experimentally defined powder quality data, would help reduce waste and increase the sustainability of the LS process.

The performance of LS parts is also dependent on the materials crystallisation behaviour. Therefore, the isothermal crystallisation kinetics of PA-12 was analysed over a crystallisation temperature (T_c) range of 162 °C to 169 °C. Although, this crystallisation temperature range is slightly below the common powder bed temperature of 170 °C, some PBF machines operate with a slightly lower temperature of 168 °C [26, 62]; similarly, there have been reports of non-uniform heating and temperature variations within the part chamber [61]. Therefore, it is conceivable that, following interaction with the laser, molten polymeric material could be exposed to temperatures lower than 170 °C. Isothermal crystallisation experiments indicated that, with decreased T_c, the rate of isothermal crystallisation significantly increases, which is caused by a reduction in the free energy barrier for crystal nucleation, as reported previously [127, 129, 233]. At an isothermal T_c of 168 °C the crystallisation half-time (t ½) is 51 minutes, but t ½ reduces to 13 minutes at a T_c of 165 °C; at 162 °C, t ½ is only 3.5 minutes. This suggests that within a LS build chamber, some components could easily crystallise during the building process prior to the cool-down step. Parts in the lower layers of the build chamber may be particularly susceptible because they are further away from the laser heat source, so reductions in temperature become increasingly likely. Previous studies have assumed that because PA-12 has a large processing window, crystallisation should be prevented until the cool-down phase [21, 22, 24, 62], at which point the crystallisation process can be controlled by the cooling rate. However, the results of this study suggest that crystallisation could be instigated during the build cycle; this is problematic because premature crystallisation results in volume shrinkage of PA-12 and significant distortion or warpage of final parts.

Isothermal crystallisation behaviour of PA-12 is also affected by powder re-use. Previous powder characterisation indicated that polycondensation and cross-linking occur within PA-12 with increased powder re-use. These aging processes cause increased molecular weight and reduced chain mobility, due to structural changes such as increased chain entanglements, tie-chains, and knots. This increases the concentration of less crystallisable units within the polymer, leading to a reduction in the rate of primary crystallisation. As a result, the commonly used Avrami model becomes unsuitable for modelling the crystallisation behaviour of re-used PA-12 powder. Nonetheless, the Hay model, not previously used for defining the crystallisation behaviour of PA-12, is able to successfully track full phase transformation within re-used powder.

The Hay model differentiates from previous crystallisation models, most of which are variations of the traditional Avrami method, because it accounts for both primary and secondary crystallisation. Within used material, the rate and extent of primary crystallisation is limited by aging; as such, the resulting primary lamellae are less thermodynamically stable, and a greater contribution from the secondary process is required for full phase transformation. Therefore, following spherulite impingement the fractional crystallinity of used powder continued to increase, and the developments in crystallinity followed a square root time dependence, representative of the Hay model. This work supports the conclusions presented in *Chapter 7,* whereby it was observed that the α' crystal phase, formed at crystallisation temperatures > 140 °C, tends to thicken via Hay's reptation-diffusion theory. As such, these results provide further evidence to suggest that lamellar thickening could occur within PA-12 during LS. Such elevated temperatures found within a build chamber

increase the mobility of amorphous chains, allowing them to transport into adjacent crystalline lamellae via diffusion. These findings could help predict the crystallisation behaviour of PA-12 during the build process, which is vital for obtaining the mechanical properties and dimensional precision required for the fabrication of functional, high-performance components.

The aim of this work was to provide industry operators with solutions for how to characterise used powder quality at the end of each build cycle, and how to maximise its re-use across future build cycles without detriment to the quality and performance of final parts. *Figure 8.1* highlights the most important steps that should be considered when formulating a powder re-use strategy. These factors are critical to maintaining powder quality between each build, and ensuring that the recovered powder is suitable for re-use in future build cycles. With an understanding of the degradation processes that effect powder quality, *Figure 8.2* suggests a potential strategy for determining the condition of a batch of un-sintered powder recovered from a PBF build cycle. Furthermore, the results of this project have helped develop an ASTM (ASTM WK75265), which provides additional information and further recommendations to industrialists. The ASTM work item proposes a standardised set of guidelines that PBF operators can use to determine the most suitable characterisation techniques for quantifying the properties of used powder, and its potential for re-use within PBF. If adopted appropriately, this ASTM could have substantial impact within AM in terms of minimising material waste and enhancing cost effectiveness in various industrial applications.

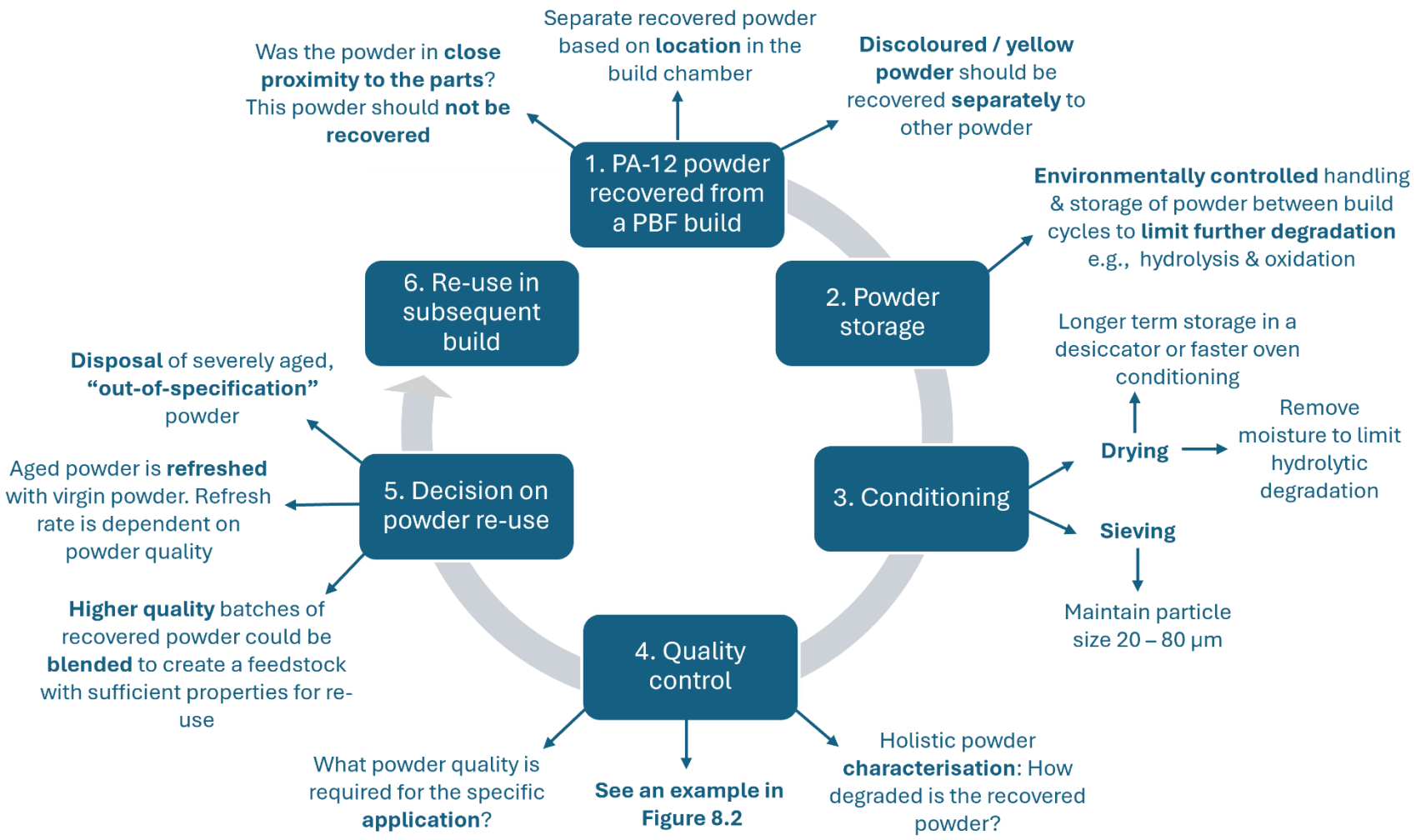

Figure 8.1 - Demonstrates the steps involved in a PBF processing cycle and recommendations that can be implemented in order to improve powder re-use. Further information can be found within Figure 8.2 and ASTM WK75265.

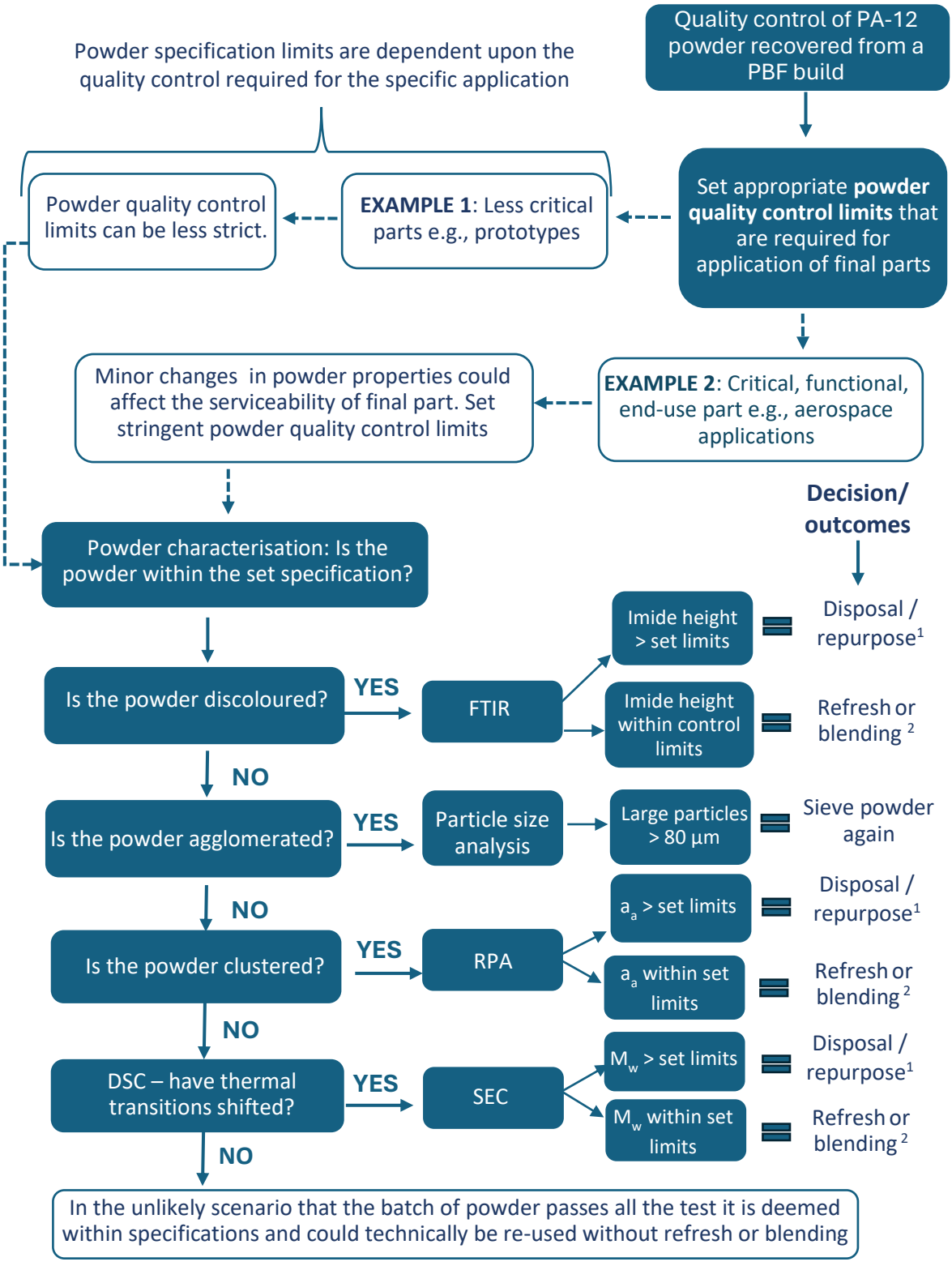

Figure 8.2 - An example flow chart that outlines strategies for characterising the quality of recovered powder. [1] Before disposal, check whether the powder could be re-purposed for use in a different manufacturing technique that has less stringent specifications. [2] Operate with flexible refresh/blending rates that are adjusted based on specific powder quality and intended part application.

8.4 Conclusions

Collectively, the key findings of this thesis have highlighted the importance of quantifying the quality of used, un-sintered powder before re-use in future build cycles. Upon reflection of the results presented in *Chapter 5,* in order to maximise powder re-use, and reduce material waste, operators of PBF technology are now encouraged to utilise flexible refresh ratios, whereby the virgin refresh rate is adjusted based on the properties of used powder. This thesis has also established the strengths and weakness of various testing methods for defining powder quality, and its suitability for re-use in subsequent builds. As a function of powder re-use, a decrease in particle flowability and an increased melting temperature, were directly correlated to a reduction in the density and ultimate tensile strength of final parts. Therefore, these are vital powder properties that must be monitored and regulated, throughout the lifecycle of the powder, in order to maintain part performance. Additionally, secondary crystallisation is a crucial aging process often overlooked in previous studies. Fast scanning calorimetry demonstrated that when PA-12 is stored at elevated temperatures, it is likely to undergo further developments in crystallinity via lamellar thickening. Not only does this affect the properties of un-sintered PA-12 powder, and its potential for re-use in future builds, but also the performance of fabricated parts. As such, lamellar thickening must be considered when formulating future powder recycling strategies. An investigation into the isothermal crystallisation kinetics of PA-12, identified that consolidated parts may begin to crystallise during an ongoing build cycle. The crystallisation process is associated with a volume shrinkage that causes part warpage. Consequently, uncontrolled crystallisation may contribute to the production of unserviceable final parts with inconsistent mechanical

properties and poor dimensional precision, which is currently a major challenge hindering the advancement of polymer additive manufacturing. Overall, the findings of this work can improve the environmental sustainability and economic proficiency of PBF, helping the manufacturing industry move toward a more circular economy.

8.5 Further research

The results discussed in *Chapter 5* and *Chapter 6* indicate that a 70:30 refresh rate is more efficient than the industry recommended 50:50 refresh ratio, without too big a detriment to final part quality. However, it would be useful to repeat this study at various other refresh ratios, such as 50:50, 60:40, 80:20, and 100:0. Understanding the specific effect of different virgin refresh rates, on powder and part properties, may allow the development of a standardised system, whereby PBF operators can select the refresh ratio required to fabricate a part with sufficient properties for its intended application, based on the quality of each specific batch of used powder.

Furthermore, expanding on the data presented in *section 5.7.2* would be beneficial in order to fully investigate the capabilities of the MJF system. The data collected so far suggests that MJF is a more material efficient process than LS, permitting enhanced powder re-use. However, to confirm these results, further work is required to extend the study across a larger number of build cycles, with an increased cumulative build time. In addition, more extensive characterisation is necessary because, at present, only the thermal properties of the powder have been analysed. Investigating the effect of powder re-use, across multiple (>10) MJF build cycles, on the behaviour of

powder and part properties, would allow a full comparison of the recyclability of PA-12 within LS and MJF.

In PBF, powder recovered from the same build chamber is often varying in quality and this could be related to temperature variations across the build chamber. It has been reported previously that thermal gradients and heat affected zones can exist in MJF and LS, respectively [44, 61, 168, 206]. Similarly, in this thesis, the work presented in *section 5.7.2* began to consider potential temperature variations within a MJF build chamber. However, to the best of the authors knowledge, no previous studies have revealed specific temperature profiles. Therefore, in-situ measurements of the exact temperature at different regions across the powder bed, via the use of thermocouples or thermal imaging cameras, would be valuable. This would reveal whether it is necessary to separate un-sintered powder based on the thermal conditions that it was exposed to during the build cycle, which may help create a more homogenous feedstock and more consistent final part properties.

Finally, as the additive manufacturing industry continues to evolve, new high-performance materials are constantly being developed that are capable of fabricating structural components to be used within more demanding environments. For example, HP high-reusability PA12 glass bead powder is reported to have significantly greater mechanical properties and load bearing capacity than neat PA-12 feedstock. However, the interaction between the polymer matrix and the glass beads will also affect the thermal, optical, and crystallisation behaviour of the material. A study characterising the processability and reusability of the various new materials would allow the continued development of the PBF process, allowing the adoption of this technology within a wider range of applications.

References

[1] Jayawardane H, Davies IJ, Gamage JR, John M, Biswas WK. Sustainability perspectives – a review of additive and subtractive manufacturing. Sustainable Manufacturing and Service Economics [Internet]. 2023 2023/04/01/; 2:[100015 p.]. Available from: https://www.sciencedirect.com/science/article/pii/S2667344423000075.

[2] Durakovic B. Design for Additive Manufacturing: Benefits, Trends and Challenges. Periodicals of Engineering and Natural Sciences. 2018;6:179-91

[3] Huang Y, Leu MC, Mazumder J, Donmez A. Additive Manufacturing: Current State, Future Potential, Gaps and Needs, and Recommendations. Journal of Manufacturing Science and Engineering [Internet]. 2015; 137(1). Available from: https://doi.org/10.1115/1.4028725.

[4] Gebhardt A, Hötter J-S. 1 - Basics, Definitions, and Application Levels. In: Gebhardt A, Hötter J-S, editors. Additive Manufacturing: Hanser; 2016. p. 1-19. https://doi-org.ezproxyd.bham.ac.uk/10.3139/9781569905838.001

[5] Diegel O. 10.02 - Additive Manufacturing: An Overview. In: Hashmi S, Batalha GF, Van Tyne CJ, Yilbas B, editors. Comprehensive Materials Processing. Oxford: Elsevier; 2014. p. 3-18. https://doi.org/10.1016/B978-0-08-096532-1.01000-1

[6] Ngo TD, Kashani A, Imbalzano G, Nguyen KTQ, Hui D. Additive manufacturing (3D printing): A review of materials, methods, applications and challenges. Composites Part B: Engineering [Internet]. 2018; 143:[172-96 pp.]. Available from: https://www.sciencedirect.com/science/article/pii/S1359836817342944.

[7] Zhang J, Jung Y-G. Additive Manufacturing: Materials, Processes, Quantifications and Applications. Cambridge, Massachusetts: Elsevier Science & Technology; 2018.

[8] Gibson I, Rosen D, Stucker B, Khorasani M. Additive manufacturing technologies: Springer; 2014.

[9] Yoon H-S, Lee J-Y, Kim H-S, Kim M-S, Kim E-S, Shin Y-J, et al. A comparison of energy consumption in bulk forming, subtractive, and additive processes: Review and case study. International Journal of Precision Engineering and Manufacturing-Green Technology [Internet]. 2014; 1(3):[261-79 pp.]. Available from: https://doi.org/10.1007/s40684-014-0033-0.

[10] Priarone PC, Ingarao G. Towards criteria for sustainable process selection: On the modelling of pure subtractive versus additive/subtractive integrated manufacturing approaches. Journal of Cleaner Production [Internet]. 2017 2017/02/15/; 144:[57-68 pp.]. Available from: https://www.sciencedirect.com/science/article/pii/S0959652616322284.

[11] Alfattni R. Comprehensive Study on Materials used in Different Types of Additive Manufacturing and their Applications. International Journal of Mathematical, Engineering and Management Sciences [Internet]. 2022; 7(1):[92-114 pp.]. Available from: https://doi.org/10.33889/IJMEMS.2022.7.1.007.

[12] ASTM. 52900:2021(E) Additive Manufacturing - General principles - Fundamentals and vocabulary 2021. p. 1-14.

[13] Goodridge RD, Ziegelmeier S. 7 - Powder bed fusion of polymers. 2017. In: Laser Additive Manufacturing [Internet]. Cambridge, UK: Woodhead Publishing Series in Electronic and Optical Materials; [181-204]. Available from: https://doi.org/10.1016/B978-0-08-100433-3.00007-5.

[14] Goodridge RD, Tuck CJ, Hague RJM. Laser sintering of polyamides and other polymers. Progress in Materials Science [Internet]. 2012; 57(2):[229-67 pp.]. Available from: https://www.sciencedirect.com/science/article/pii/S0079642511000648.

[15] Sillani F, Kleijnen RG, Vetterli M, Schmid M, Wegener K. Selective laser sintering and multi jet fusion: Process-induced modification of the raw materials and analyses of parts performance.

Additive Manufacturing [Internet]. 2019; 27:[32-41 pp.]. Available from: http://www.sciencedirect.com/science/article/pii/S2214860418308972.
[16] Pham DT, Dotchev KD, Yusoff WAY. Deterioration of polyamide powder properties in the laser sintering process. Proceedings of the Institution of Mechanical Engineers, Part C: Journal of Mechanical Engineering Science [Internet]. 2008; 222(11):[2163-76 pp.]. Available from: https://doi.org/10.1243/09544062JMES839.
[17] Dotchev K, Yusoff W. Recycling of polyamide 12 based powders in the laser sintering process. Rapid prototyping journal [Internet]. 2009; 15(3):[192-203 pp.]. Available from: https://doi.org/10.1108/13552540910960299.
[18] Weinmann S, Bonten C. Recycling of PA12 powder for selective laser sintering. AIP Conference Proceedings [Internet]. 2020; 2289(1):[020056 p.]. Available from: https://doi.org/10.1063/5.0029945.
[19] Rosso S, Meneghello R, Biasetto L, Grigolato L, Concheri G, Savio G. In-depth comparison of polyamide 12 parts manufactured by Multi Jet Fusion and Selective Laser Sintering. Additive Manufacturing [Internet]. 2020; 36:[101713 p.]. Available from: https://doi.org/10.1016/j.addma.2020.101713.
[20] Calignano F, Giuffrida F, Galati M. Effect of the build orientation on the mechanical performance of polymeric parts produced by multi jet fusion and selective laser sintering. Journal of Manufacturing Processes [Internet]. 2021; 65:[271-82 pp.]. Available from: https://doi.org/10.1016/j.jmapro.2021.03.018.
[21] Josupeit S, Schmid H-J. Experimental analysis and modeling of local ageing effects during laser sintering of polyamide 12 in regard to individual thermal histories. Journal of Applied Polymer Science [Internet]. 2017; 134(42):[45435 p.]. Available from: https://doi.org/10.1002/app.45435.
[22] O'Connor HJ, Dickson AN, Dowling DP. Evaluation of the mechanical performance of polymer parts fabricated using a production scale multi jet fusion printing process. Additive Manufacturing [Internet]. 2018; 22:[381-7 pp.]. Available from: https://doi.org/10.1016/j.addma.2018.05.035.
[23] Kuehnlein F, Drummer D, Rietzel D, Seefried A. Degradation behavior and material properties of PA12-plastic powders processed by powder bed fusion additive manufacturing technologies 2010; 21, No. 1(1726-9679). Available from: https://www.daaam.info/Downloads/Pdfs/proceedings/proceedings_2010/24969_Annals_1_head.pdf.
[24] Riedelbauch J, Rietzel D, Witt G. Analysis of material aging and the influence on the mechanical properties of polyamide 12 in the Multi Jet Fusion process. Additive Manufacturing [Internet]. 2019; 27:[259-66 pp.]. Available from: http://www.sciencedirect.com/science/article/pii/S2214860418307991.
[25] Duddleston L, Puck A, Harris A, Doll N, Osswald T, editors. Differential Scanning Calorimetry (DSC) Quantification of Polyamide 12 (Nylon 12) Degradation during the Selective Laser Sintering (SLS) Process. 2016.
[26] Wudy K, Drummer D. Aging effects of polyamide 12 in selective laser sintering: Molecular weight distribution and thermal properties. Additive Manufacturing [Internet]. 2019; 25:[1-9 pp.]. Available from: http://www.sciencedirect.com/science/article/pii/S2214860418307024.
[27] Kumar S, Czekanski A. Development of filaments using selective laser sintering waste powder. Journal of Cleaner Production [Internet]. 2017; 165:[1188-96 pp.]. Available from: https://doi.org/10.1016/j.jclepro.2017.07.202.
[28] Paolucci F, van Mook MJH, Govaert LE, Peters GWM. Influence of post-condensation on the crystallization kinetics of PA12: From virgin to reused powder. Polymer. 2019;175:161-70. https://doi.org/10.1016/j.polymer.2019.05.009
[29] Thiesse F, Wirth M, Kemper H-G, Moisa M, Morar D, Lasi H, et al. Economic implications of additive manufacturing and the contribution of MIS. Business & Information Systems Engineering

[Internet]. 2015; 57:[139-48 pp.]. Available from: https://link.springer.com/article/10.1007/s12599-015-0374-4.
[30] Prior M. What can we expect from the additive manufacturing market over the next 5 years? 3D Natives2023 [Available from: https://www.3dnatives.com/en/additive-manufacturing-market-next-5-years-120120234/#.
[31] O' Connor HJ, Dowling DP. Comparison between the properties of polyamide 12 and glass bead filled polyamide 12 using the multi jet fusion printing process. Additive Manufacturing [Internet]. 2020; 31:[100961 p.]. Available from: https://www.sciencedirect.com/science/article/pii/S2214860419300958.
[32] Wang Y, Xu Z, Wu D, Bai J. Current Status and Prospects of Polymer Powder 3D Printing Technologies2020; 13(Generic). Available from: https://doi.org/10.3390/ma13102406.
[33] Mokrane A, Boutaous Mh, Xin S. Process of selective laser sintering of polymer powders: Modeling, simulation, and validation. Comptes Rendus Mécanique [Internet]. 2018; 346(11):[1087-103 pp.]. Available from: https://www.sciencedirect.com/science/article/pii/S1631072118301712.
[34] Chen P, Tang M, Zhu W, Yang L, Wen S, Yan C, et al. Systematical mechanism of Polyamide-12 aging and its micro-structural evolution during laser sintering. Polymer Testing [Internet]. 2018; 67:[370-9 pp.]. Available from: http://www.sciencedirect.com/science/article/pii/S0142941817319049.
[35] Yang F, Zobeiry N, Mamidala R, Chen X. A review of aging, degradation, and reusability of PA12 powders in selective laser sintering additive manufacturing. Materials Today Communications. 2023;34:105279. https://doi.org/10.1016/j.mtcomm.2022.105279
[36] Wegner A, Mielicki C, Grimm T, Gronhoff B, Witt G, Wortberg J. Determination of robust material qualities and processing conditions for laser sintering of polyamide 12. Polymer Engineering and Science [Internet]. 2014; 54(7):[1540-54 pp.]. Available from: http://dx.doi.org/10.1002/pen.23696.
[37] Kummert C, Josupeit S, Schmid H-J. Thermoplastic elastomer part color as function of temperature histories and oxygen atmosphere during selective laser sintering. JOM [Internet]. 2018; 70:[425-30 pp.]. Available from: https://link.springer.com/article/10.1007/s11837-017-2658-2.
[38] Dadbakhsh S, Verbelen L, Verkinderen O, Strobbe D, Van Puyvelde P, Kruth J-P. Effect of PA12 powder reuse on coalescence behaviour and microstructure of SLS parts. European Polymer Journal [Internet]. 2017; 92:[250-62 pp.]. Available from: http://www.sciencedirect.com/science/article/pii/S0014305716316615.
[39] Goodridge RD, Hague RJM, Tuck CJ. Effect of long-term ageing on the tensile properties of a polyamide 12 laser sintering material. Polymer Testing [Internet]. 2010; 29(4):[483-93 pp.]. Available from: https://www.sciencedirect.com/science/article/pii/S0142941810000292.
[40] Yan C, Shi Y, Hao L. Investigation into the Differences in the Selective Laser Sintering between Amorphous and Semi-crystalline Polymers. International Polymer Processing [Internet]. 2011; 26(4):[416-23 pp.]. Available from: https://doi.org/10.3139/217.2452.
[41] Cai C, Tey WS, Chen J, Zhu W, Liu X, Liu T, et al. Comparative study on 3D printing of polyamide 12 by selective laser sintering and multi jet fusion. Journal of Materials Processing Technology [Internet]. 2021; 288:[116882 p.]. Available from: https://www.sciencedirect.com/science/article/pii/S092401362030296X.
[42] Galati M, Calignano F, Defanti S, Denti L. Disclosing the build-up mechanisms of multi jet fusion: Experimental insight into the characteristics of starting materials and finished parts. Journal of Manufacturing Processes [Internet]. 2020; 57:[244-53 pp.]. Available from: http://dx.doi.org/10.1016/j.jmapro.2020.06.029.
[43] Mele M, Campana G, Pisaneschi G, Monti GL. Investigation into effects of cooling rate on properties of polyamide 12 parts in the multi jet fusion process. Rapid Prototyping Journal [Internet]. 2020; 26(10):[1789-95 pp.]. Available from: https://doi.org/10.1108/RPJ-04-2020-0080.

[44] Sagbas B, Gümüş BE, Kahraman Y, Dowling DP. Impact of print bed build location on the dimensional accuracy and surface quality of parts printed by multi jet fusion. Journal of Manufacturing Processes [Internet]. 2021; 70:[290-9 pp.]. Available from: https://doi.org/10.1016/j.jmapro.2021.08.036.
[45] Wiese M, Thiede S, Herrmann C. Rapid manufacturing of automotive polymer series parts: A systematic review of processes, materials and challenges. Additive Manufacturing [Internet]. 2020 2020/12/01/; 36:[101582 p.]. Available from: https://www.sciencedirect.com/science/article/pii/S2214860420309544.
[46] Duan B, Wang M. Selective laser sintering and its application in biomedical engineering. MRS Bulletin [Internet]. 2011; 36(12):[998-1005 pp.]. Available from: https://doi.org/10.1557/mrs.2011.270.
[47] What is Selective Laser Sintering 3D Printing Used For? 2019 [Available from: https://www.spilasers.com/application-additive-manufacturing/what-is-selective-laser-sintering-used-for/.
[48] Alexandrea P. The Complete Guide to Selective Laser Sintering (SLS) in 3D Printing 2019 [Available from: https://www.3dnatives.com/en/selective-laser-sintering100420174/.
[49] Pandelidi C, Lee KPM, Kajtaz M. Effects of polyamide-11 powder refresh ratios in multi-jet fusion: A comparison of new and used powder. Additive Manufacturing [Internet]. 2021; 40:[101933 p.]. Available from: https://doi.org/10.1016/j.addma.2021.101933.
[50] Dupin S, Lame O, Barrès C, Charmeau J-Y. Microstructural origin of physical and mechanical properties of polyamide 12 processed by laser sintering. European Polymer Journal [Internet]. 2012; 48(9):[1611-21 pp.]. Available from: https://www.sciencedirect.com/science/article/pii/S0014305712001954.
[51] Zarringhalam H, Hopkinson N, Kamperman NF, de Vlieger JJ. Effects of processing on microstructure and properties of SLS Nylon 12. Materials Science and Engineering A [Internet]. 2006; 435-436:[172-80 pp.]. Available from: http://dx.doi.org/10.1016/j.msea.2006.07.084.
[52] Vasquez M, Haworth B, Hopkinson N. Optimum sintering region for laser sintered nylon-12. Proceedings of the Institution of Mechanical Engineers, Part B: Journal of Engineering Manufacture [Internet]. 2011; 225(12):[2240-8 pp.]. Available from: https://doi.org/10.1177/0954405411414994.
[53] Wudy K, Drummer D, editors. Aging behavior of polyamide 12: interrelation between bulk characteristics and part properties. Proceedings of the 26th Annual International Solid Freeform Fabrication Symposium, Austin, TX, USA; 2016.
[54] Kohan M. Nylon Plastics Handbook. Munich (Germany): Hanser 1995.
[55] Seltzer R, de la Escalera FM, Segurado J. Effect of water conditioning on the fracture behavior of PA12 composites processed by selective laser sintering. Materials Science and Engineering: A [Internet]. 2011; 528(22-23):[6927-33 pp.]. Available from: https://doi.org/10.1016/j.msea.2011.05.045.
[56] Zhang R, Jariyavidyanont K, Du M, Zhuravlev E, Schick C, Androsch R. Nucleation and crystallization kinetics of polyamide 12 investigated by fast scanning calorimetry. Journal of Polymer Science [Internet]. 2022; 60(5):[842-55 pp.]. Available from: https://doi.org/10.1002/pol.20210813.
[57] Griehl W, Ruestem D. Nylon-12-preparation, properties, and applications. Industrial & Engineering Chemistry [Internet]. 1970; 62(3):[16-22 pp.]. Available from: https://doi.org/10.1021/ie50723a005.
[58] Simha Martynková G, Slíva A, Kratošová G, Čech Barabaszová K, Študentová S, Klusák J, et al. Polyamide 12 Materials Study of Morpho-Structural Changes during Laser Sintering of 3D Printing2021; 13(Generic). Available from: https://doi.org/10.3390/polym13050810.
[59] Roberts MF, Jenekhe SA. Site-specific reversible scission of hydrogen bonds in polymers: an investigation of polyamides and their Lewis acid-base complexes by infrared spectroscopy. Macromolecules [Internet]. 1991; 24(11):[3142-6 pp.]. Available from: https://doi.org/10.1021/ma00011a017.

[60] Mandelkern L. Crystallization of Polymers. 2nd ed. Cambridge, United Kingdom: Cambridge University Press 2002.
[61] Bourell DL, Watt TJ, Leigh DK, Fulcher B. Performance Limitations in Polymer Laser Sintering. Physics Procedia [Internet]. 2014; 56:[147-56 pp.]. Available from: https://www.sciencedirect.com/science/article/pii/S1875389214003022.
[62] Schmid M, Amado A, Wegener K. Materials perspective of polymers for additive manufacturing with selective laser sintering. Journal of Materials Research [Internet]. 2014; 29(17):[1824-32 pp.]. Available from: https://link.springer.com/article/10.1557/jmr.2014.138.
[63] Simon F, Mélanie D. Additive manufacturing and sustainability: an exploratory study of the advantages and challenges. Journal of Cleaner Production [Internet]. 2016; 137:[1573-87 pp.]. Available from: https://www.sciencedirect.com/science/article/pii/S0959652616304395.
[64] Mwania FM, Maringa M, van der Walt JG. A review of the techniques used to characterize laser sintering of polymeric powders for use and re-use in additive manufacturing. Manufacturing Review [Internet]. 2021; 8:[14 p.]. Available from: https://doi.org/10.1051/mfreview/2021012.
[65] Drummer D, Wudy K, Drexler M. Influence of Energy Input on Degradation Behavior of Plastic Components Manufactured by Selective Laser Melting. Physics Procedia [Internet]. 2014; 56:[176-83 pp.]. Available from: http://www.sciencedirect.com/science/article/pii/S1875389214003058.
[66] Wudy K, Drummer D, Kühnlein F, Drexler M. Influence of degradation behavior of polyamide 12 powders in laser sintering process on produced parts. AIP Conference Proceedings [Internet]. 2014; 1593(1):[691-5 pp.]. Available from: https://aip.scitation.org/doi/abs/10.1063/1.4873873.
[67] Duddleston L. Polyamide (Nylon) 12 powder degradation during the selective laser sintering process 2015.
[68] Young RJ, Lovell PA. Introduction to Polymers. 3rd ed. Bosa Roca, USA: CRC Press, Taylor & Francis Group; 2011.
[69] Collins English Dictionary. Thermosetting.
[70] Collins English Dictionary. Thermoplastics.
[71] Laboratory S. Amorphous Polymers. Electron Microscopy of Polymers. Berlin, Heidelberg: Springer; 2008 p. 277-93.
[72] Cowie JMG. Polymers: Chemistry & physics of modern materials. 2nd ed. Cheltenham: Nelson Thornes; 1991.
[73] Balani KV, Vivek; Agarwal, Arvind; Narayan, Roger. Chapter A1 - Physical, Thermal, and Mechanical properties of polymers Biosurfaces: A Materials Science and Engineering Perspective 1st ed. New Jersey, USA: John Wiley & Sons 2015.
[74] The crystalline state. In: Samulski E, Wignall G, Koenig J, Mark J, Ngai K, Mandelkern L, et al., editors. Physical Properties of Polymers. 3 ed. Cambridge: Cambridge University Press; 2004. p. 209-315.
[75] Wunderlich B. Macromolecular Physics: Crystal Melting. London: Academic Press (London); 1980.
[76] Wunderlich B. Macromolecular Physics: Crystal Structure, Morphology, Defects. New York and London: Academic Press; 1973.
[77] Gueguen O, Ahzi S, Makradi A, Belouettar S. A new three-phase model to estimate the effective elastic properties of semi-crystalline polymers: Application to PET. Mechanics of Materials [Internet]. 2010 2010/01/01/; 42(1):[1-10 pp.]. Available from: https://www.sciencedirect.com/science/article/pii/S0167663609000994.
[78] Sedighiamiri A, Van Erp T, Peters G, Govaert L, Van Dommelen J. Micromechanical modeling of the elastic properties of semicrystalline polymers: A three-phase approach. Journal of Polymer Science Part B: Polymer Physics [Internet]. 2010; 48(20):[2173-84 pp.]. Available from: https://doi.org/10.1002/polb.22099.
[79] Hoffman JD. Theoretical aspects of polymer crystallization with chain folds: Bulk polymers. Polymer Engineering & Science. 1964;4(4):315-62. https://doi.org/10.1002/pen.760040413

[80] Yamamoto T. Molecular dynamics modeling of polymer crystallization from the melt. Polymer [Internet]. 2004 2004/02/01/; 45(4):[1357-64 pp.]. Available from: https://www.sciencedirect.com/science/article/pii/S0032386103010656.
[81] Bower DI. An Introduction to Polymer Physics Cambridge: Cambridge University Press; 2002.
[82] Seguela R. Critical review of the molecular topology of semicrystalline polymers: The origin and assessment of intercrystalline tie molecules and chain entanglements. Journal of Polymer Science Part B: Polymer Physics [Internet]. 2005; 43(14):[1729-48 pp.]. Available from: https://onlinelibrary.wiley.com/doi/abs/10.1002/polb.20414.
[83] Kiyotsukuri T, Hashiba T, Ozawa N, Tsutsumi N. Thermo-oxidative crosslinking of polyamides by torsional braid analysis. Journal of Polymer Science Part A: Polymer Chemistry [Internet]. 1988; 26(12):[3409-13 pp.]. Available from: https://doi.org/10.1002/pola.1988.080261224.
[84] Hoffman JD, Weeks JJ. Melting process and the equilibrium melting temperature of polychlorotrifluoroethylene. Journal of Research of the National Bureau of Standards Section A: Physics and Chemistry. 1962:13.
[85] Sangroniz L, Cavallo D, Müller AJ. Self-Nucleation Effects on Polymer Crystallization. Macromolecules [Internet]. 2020 2020/06/23; 53(12):[4581-604 pp.]. Available from: https://doi.org/10.1021/acs.macromol.0c00223.
[86] Hejmady P, van Breemen LCA, Hermida-Merino D, Anderson PD, Cardinaels R. Laser sintering of PA12 particles studied by in-situ optical, thermal and X-ray characterization. Additive Manufacturing [Internet]. 2022 2022/04/01/; 52:[102624 p.]. Available from: https://www.sciencedirect.com/science/article/pii/S221486042200032X.
[87] Wunderlich B. Macromolecular Physics: Crystal Nucleation, Growth, Annealing. New York: Academic Press; 1976.
[88] Hoffman JD, Guttman CM, DiMarzio EA. On the problem of crystallization of polymers from the melt with chain folding. Faraday Discussions of the Chemical Society [Internet]. 1979; 68(0):[177-97 pp.]. Available from: http://dx.doi.org/10.1039/DC9796800177.
[89] Hoffman JD. Role of reptation in the rate of crystallization of polyethylene fractions from the melt. Polymer [Internet]. 1982 1982/05/01/; 23(5):[656-70 pp.]. Available from: https://www.sciencedirect.com/science/article/pii/0032386182900489.
[90] Lauritzen JIJH, John D. Extension of theory of growth of chain-folded polymer crystals to large undercoolings. Journal of Applied Physics [Internet]. 1973; 44(10):[4340-52 pp.]. Available from: https://aip.scitation.org/doi/abs/10.1063/1.1661962.
[91] Hay JN. Secondary crystallization kinetics. Polymer crystallization [Internet]. 2018; 1(2):[e10007 p.]. Available from: https://doi.org/10.1002/pcr2.10007.
[92] Hay JN. Crystallisation kinetics and melting studies. British Polymer Journal [Internet]. 1979; 11(3):[137-45 pp.]. Available from: https://doi.org/10.1002/pi.4980110307.
[93] Hay JN. Application of the modified avrami equations to polymer crystallisation kinetics. British Polymer Journal. 1971;3(2):74-82.
[94] Kolb R, Wutz C, Stribeck N, von Krosigk G, Riekel C. Investigation of secondary crystallization of polymers by means of microbeam X-ray scattering. Polymer [Internet]. 2001 2001/06/01/; 42(12):[5257-66 pp.]. Available from: https://www.sciencedirect.com/science/article/pii/S0032386100009204.
[95] Phillipson K, Jenkins MJ, Hay JN. The effect of a secondary process on crystallization kinetics–Poly (ϵ-caprolactone) revisited. European Polymer Journal [Internet]. 2016; 84:[708-14 pp.]. Available from: https://doi.org/10.1016/j.eurpolymj.2016.09.037.
[96] Chen Z, Hay JN, Jenkins M. The kinetics of crystallization of poly (ethylene terephthalate) measured by FTIR spectroscopy. European polymer journal [Internet]. 2013; 49(6):[1722-30 pp.]. Available from: https://doi.org/10.1016/j.eurpolymj.2013.03.020.

[97] Chen Z, Jenkins M, Hay J. Annealing of poly (ethylene terephthalate). European polymer journal [Internet]. 2014; 50:[235-42 pp.]. Available from: https://doi.org/10.1016/j.eurpolymj.2013.11.004.
[98] Abo el Maaty MI, Bassett DC. Evidence for isothermal lamellar thickening at and behind the growth front as polyethylene crystallizes from the melt. Polymer [Internet]. 2005 2005/09/23/; 46(20):[8682-8 pp.]. Available from: https://www.sciencedirect.com/science/article/pii/S0032386105007536.
[99] Yang S-G, Lei J, Zhong G-J, Xu J-Z, Li Z-M. Role of lamellar thickening in thick lamellae formation in isotactic polypropylene when crystallizing under flow and pressure. Polymer [Internet]. 2019; 179:[121641 p.]. Available from: https://doi.org/10.1016/j.polymer.2019.121641.
[100] Liu Y-X, Li J-F, Zhu D-S, Chen E-Q, Zhang H-D. Direct observation and modeling of transient nucleation in isothermal thickening of polymer lamellar crystal monolayers. Macromolecules [Internet]. 2009; 42(8):[2886-90 pp.]. Available from: https://doi.org/10.1021/ma802806q.
[101] Sanchez I, Peterlin A, Eby R, McCrackin F. Theory of polymer crystal thickening during annealing. Journal of Applied Physics [Internet]. 1974; 45(10):[4216-9 pp.]. Available from: https://doi.org/10.1063/1.1663038.
[102] Marand H, Huang Z. Isothermal lamellar thickening in linear polyethylene: Correlation between the evolution of the degree of crystallinity and the melting temperature. Macromolecules [Internet]. 2004; 37(17):[6492-7 pp.]. Available from: https://doi.org/10.1021/ma0497198.
[103] Rastogi S, Spoelstra A, Goossens J, Lemstra P. Chain mobility in polymer systems: on the borderline between solid and melt. 1. Lamellar doubling during annealing of polyethylene. Macromolecules [Internet]. 1997; 30(25):[7880-9 pp.]. Available from: https://doi.org/10.1021/ma970519o.
[104] Schultz M. Qualitative theory for the picture frame morphology of annealed lamellar crystals. Journal of Macromolecular Science, Part B [Internet]. 1970; 4(4):[775-81 pp.]. Available from: https://doi.org/10.1080/00222347008217122.
[105] Fischer EW. Effect of annealing and temperature on the morphological structure of polymers. Pure and Applied Chemistry [Internet]. 1972; 31(1-2):[113-32 pp.]. Available from: https://doi.org/10.1351/pac197231010113.
[106] Hikosaka M, Amano K, Rastogi S, Keller A. Lamellar thickening growth of an extended chain single crystal of polyethylene (II) : ΔT dependence of lamellar thickening growth rate and comparison with lamellar thickening. Journal of Materials Science [Internet]. 2000 2000/10/01; 35(20):[5157-68 pp.]. Available from: https://doi.org/10.1023/A:1004804420369.
[107] Dreyfus P, Keller A. A simple chain refolding scheme for the annealing behavior of polymer crystals. Journal of Polymer Science Part B: Polymer Letters [Internet]. 1970; 8(4):[253-8 pp.]. Available from: https://doi.org/10.1002/pol.1970.110080407.
[108] Reneker DH. Point dislocations in crystals of high polymer molecules. Journal of Polymer Science [Internet]. 1962; 59(168):[S39-S42 pp.]. Available from: https://doi.org/10.1002/pol.1962.1205916822.
[109] Phillipson K, Jenkins MJ, Hay JN. The kinetics of crystallization of poly (ε-caprolactone) measured by FTIR spectroscopy. Journal of Thermal Analysis and Calorimetry [Internet]. 2016; 123:[1491-500 pp.]. Available from: https://link.springer.com/article/10.1007/s10973-015-5047-5.
[110] Faraj J, Boyard N, Pignon B, Bailleul J-L, Delaunay D, Orange G. Crystallization kinetics of new low viscosity polyamides 66 for thermoplastic composites processing. Thermochimica Acta [Internet]. 2016; 624:[27-34 pp.]. Available from: https://www.sciencedirect.com/science/article/pii/S0040603115004761.
[111] Wang G, Bu H. Crystallization and melting of nylon610. Chinese Journal of Polymer Science. 1998;16:241.

[112] Kelly CA, Jenkins MJ. Modeling the crystallization kinetics of polymers displaying high levels of secondary crystallization. Polymer Journal [Internet]. 2022; 54(3):[249-57 pp.]. Available from: https://www.nature.com/articles/s41428-021-00581-0.
[113] Androsch R, Toda A, Furushima Y, Schick C. Insertion-crystallization-induced low-temperature annealing peaks in melt-crystallized poly (L-lactic acid). Macromolecular Chemistry and Physics [Internet]. 2021; 222(18). Available from: https://doi.org/10.1002/macp.202100177.
[114] van Drongelen M, Roozemond P, Troisi E, Doufas A, Peters G. Characterization of the primary and secondary crystallization kinetics of a linear low-density polyethylene in quiescent-and flow-conditions. Polymer [Internet]. 2015; 76:[254-70 pp.]. Available from: https://doi.org/10.1016/j.polymer.2015.09.010.
[115] Fischer C, Seefried A, Drummer D. Crystallization and Component Properties of Polyamide 12 at Processing-Relevant Cooling Conditions. Polymer Engineering & Science [Internet]. 2017; 57(4):[450-7 pp.]. Available from: https://doi.org/10.1002/pen.24441.
[116] Bassett DC. Principles of Polymer Morphology Cambridge: Cambridge Univeristy Press; 1981.
[117] Li L, Koch MH, de Jeu WH. Crystalline structure and morphology in nylon-12: A small-and wide-angle X-ray scattering study. Macromolecules [Internet]. 2003; 36(5):[1626-32 pp.]. Available from: https://doi.org/10.1021/ma025732l.
[118] Bassett DC, Olley RH, Al Raheil IAM. On crystallization phenomena in PEEK. Polymer [Internet]. 1988 1988/10/01/; 29(10):[1745-54 pp.]. Available from: https://www.sciencedirect.com/science/article/pii/0032386188903862.
[119] Sanders B, Cant E, Kelly CA, Jenkins M. The Effect of Powder Re-Use on the Coalescence Behaviour and Isothermal Crystallisation Kinetics of Polyamide 12 within Powder Bed Fusion. Polymers [Internet]. 2024; 16(5):[612 p.]. Available from: https://doi.org/10.3390/polym16050612.
[120] Androsch R, Jariyavidyanont K, Schick C. Enthalpy Relaxation of Polyamide 11 of Different Morphology Far Below the Glass Transition Temperature. Entropy [Internet]. 2019; 21(10):[984 p.]. Available from: https://www.mdpi.com/1099-4300/21/10/984.
[121] Gohn AM, Rhoades AM, Wonderling N, Tighe T, Androsch R. The effect of supercooling of the melt on the semicrystalline morphology of PA 66. Thermochimica Acta [Internet]. 2017 2017/09/10/; 655:[313-8 pp.]. Available from: https://www.sciencedirect.com/science/article/pii/S0040603117301818.
[122] Kolesov I, Mileva D, Androsch R, Schick C. Structure formation of polyamide 6 from the glassy state by fast scanning chip calorimetry. Polymer [Internet]. 2011; 52(22):[5156-65 pp.]. Available from: https://www.sciencedirect.com/science/article/pii/S0032386111007488.
[123] Rhoades AM, Wonderling N, Schick C, Androsch R. Supercooling-controlled heterogeneous and homogenous crystal nucleation of polyamide 11 and its effect onto the crystal/mesophase polymorphism. Polymer [Internet]. 2016; 106:[29-34 pp.]. Available from: https://doi.org/10.1016/j.polymer.2016.10.050.
[124] Mollova A, Androsch R, Mileva D, Schick C, Benhamida A. Effect of supercooling on crystallization of polyamide 11. Macromolecules [Internet]. 2013; 46(3):[828-35 pp.]. Available from: https://doi.org/10.1021/ma302238r.
[125] Murmu UK, Adhikari J, Naskar A, Dey D, Roy A, Ghosh A, et al. Mechanical Properties of Crystalline and Semicrystalline Polymer Systems. 2022 2022/01/01/. In: Encyclopedia of Materials: Plastics and Polymers [Internet]. Oxford: Elsevier; [917-27]. Available from: https://www.sciencedirect.com/science/article/pii/B9780128203521002480.
[126] Way JL, Atkinson JR, Nutting J. The effect of spherulite size on the fracture morphology of polypropylene. Journal of Materials Science [Internet]. 1974 1974/02/01; 9(2):[293-9 pp.]. Available from: https://doi.org/10.1007/BF00550954.
[127] Neugebauer F, Ploshikhin V, Ambrosy J, Witt G. Isothermal and non-isothermal crystallization kinetics of polyamide 12 used in laser sintering. Journal of Thermal Analysis and Calorimetry

[Internet]. 2016 2016/05/01; 124(2):[925-33 pp.]. Available from: https://doi.org/10.1007/s10973-015-5214-8.
[128] Kelly CA, Hay JN, Turner RP, Jenkins MJ. The effect of a secondary process on the analysis of isothermal crystallisation kinetics by differential scanning calorimetry. Polymers [Internet]. 2019; 12(1):[19 p.]. Available from: https://pubmed.ncbi.nlm.nih.gov/31861861/.
[129] Zhao M, Wudy K, Drummer D. Crystallization Kinetics of Polyamide 12 during Selective Laser Sintering2018; 10(Generic). Available from: https://www.mdpi.com/2073-4360/10/2/168.
[130] Liu M, Zhao Q, Wang Y, Zhang C, Mo Z, Cao S. Melting behaviors, isothermal and non-isothermal crystallization kinetics of nylon 1212. Polymer [Internet]. 2003; 44(8):[2537-45 pp.]. Available from: https://doi.org/10.1016/S0032-3861(03)00101-0.
[131] Lorenzo AT, Arnal ML, Albuerne J, Müller AJ. DSC isothermal polymer crystallization kinetics measurements and the use of the Avrami equation to fit the data: Guidelines to avoid common problems. Polymer testing [Internet]. 2007; 26(2):[222-31 pp.]. Available from: https://doi.org/10.1016/j.polymertesting.2006.10.005.
[132] Supaphol P. Application of the Avrami, Tobin, Malkin, and Urbanovici–Segal macrokinetic models to isothermal crystallization of syndiotactic polypropylene. Thermochimica Acta [Internet]. 2001; 370(1-2):[37-48 pp.]. Available from: https://doi.org/10.1016/S0040-6031(00)00767-X.
[133] Avrami M. Kinetics of phase change. I General theory. The Journal of chemical physics [Internet]. 1939; 7(12):[1103-12 pp.]. Available from: https://doi.org/10.1063/1.1750380.
[134] Avrami M. Kinetics of phase change. II transformation-time relations for random distribution of nuclei. The Journal of chemical physics [Internet]. 1940; 8(2):[212-24 pp.]. Available from: https://doi.org/10.1063/1.1750631.
[135] Avrami M. Granulation, phase change, and microstructure kinetics of phase change. III. The Journal of chemical physics [Internet]. 1941; 9(2):[177-84 pp.]. Available from: https://doi.org/10.1063/1.1750872.
[136] Hillier I. Modified avrami equation for the bulk crystallization kinetics of spherulitic polymers. Journal of Polymer Science Part A: General Papers [Internet]. 1965; 3(9):[3067-78 pp.]. Available from: https://doi.org/10.1002/pol.1965.100030902.
[137] Ravindranath K, Jog JP. Polymer crystallization kinetics: Poly(ethylene terephthalate) and poly(phenylene sulfide). Journal of Applied Polymer Science [Internet]. 1993; 49(8):[1395-403 pp.]. Available from: https://onlinelibrary.wiley.com/doi/abs/10.1002/app.1993.070490807.
[138] Tobin MC. Theory of phase transition kinetics with growth site impingement. I. Homogeneous nucleation. Journal of Polymer Science: Polymer Physics Edition [Internet]. 1974; 12(2):[399-406 pp.]. Available from: https://doi.org/10.1002/pol.1974.180120212.
[139] Tobin MC. The theory of phase transition kinetics with growth site impingement. II. Heterogeneous nucleation. Journal of Polymer Science: Polymer Physics Edition. 1976;14(12):2253-7.
[140] Tobin MC. Theory of phase transition kinetics with growth site impingement. III. Mixed heterogeneous–homogeneous nucleation and nonintegral exponents of the time1977. Available from: https://doi.org/10.1002/pol.1977.180151217.
[141] Khoshkava V, Ghasemi H, Kamal MR. Effect of cellulose nanocrystals (CNC) on isothermal crystallization kinetics of polypropylene. Thermochimica Acta [Internet]. 2015; 608:[30-9 pp.]. Available from: https://doi.org/10.1016/j.tca.2015.04.007.
[142] Albano C, Papa J, Ichazo M, González J, Ustariz C. Application of different macrokinetic models to the isothermal crystallization of PP/talc blends. Composite structures [Internet]. 2003; 62(3-4):[291-302 pp.]. Available from: https://doi.org/10.1016/j.compstruct.2003.09.028.
[143] Malkin AY, Beghishev V, Keapin IA, Bolgov S. General treatment of polymer crystallization kinetics—part 1. A new macrokinetic equation and its experimental verification. Polymer Engineering & Science [Internet]. 1984; 24(18):[1396-401 pp.]. Available from: https://doi.org/10.1002/pen.760241805.

[144] Chen Z, Hay JN, Jenkins MJ. The effect of secondary crystallization on crystallization kinetics–Polyethylene terephthalate revisited. European Polymer Journal [Internet]. 2016; 81:[216-23 pp.]. Available from: https://doi.org/10.1016/j.eurpolymj.2016.05.028.
[145] Phillipson K, J Jenkins M, N Hay J. The ageing of poly (ϵ-caprolactone). Polymer International [Internet]. 2015; 64(12):[1695-705 pp.]. Available from: https://doi.org/10.1002/pi.4969.
[146] Chen Z, Hay J, Jenkins M. The effect of secondary crystallization on melting. European polymer journal [Internet]. 2013; 49(9):[2697-703 pp.]. Available from: https://doi.org/10.1016/j.eurpolymj.2013.05.028.
[147] Negi S, Mishra V, Ror CK, Sharma RK. Laser powder bed fusion of glass-filled polyamide-composite with enhanced physical properties. Journal of Reinforced Plastics and Composites [Internet]. 2023. Available from: https://doi.org/10.1177/07316844231152602.
[148] Negi S, Dhiman S, Sharma RK. Determining the effect of sintering conditions on mechanical properties of laser sintered glass filled polyamide parts using RSM. Measurement [Internet]. 2015 2015/05/01/; 68:[205-18 pp.]. Available from: https://www.sciencedirect.com/science/article/pii/S0263224115001219.
[149] Kozlovsky K, Schiltz J, Kreider T, Kumar M, Schmid S. Mechanical Properties of Reused Nylon Feedstock for Powder-bed Additive Manufacturing in Orthopedics. Procedia Manufacturing [Internet]. 2018; 26:[826-33 pp.]. Available from: https://www.sciencedirect.com/science/article/pii/S2351978918307741.
[150] Abbott CS, Sperry M, Crane NB. Relationships between porosity and mechanical properties of polyamide 12 parts produced using the laser sintering and multi-jet fusion powder bed fusion processes. Journal of Manufacturing Processes [Internet]. 2021; 70:[55-66 pp.]. Available from: https://doi.org/10.1016/j.jmapro.2021.08.012.
[151] Zhu Z, Majewski C. Understanding pore formation and the effect on mechanical properties of high speed sintered polyamide-12 parts: a focus on energy input. Materials & Design [Internet]. 2020; 194:[108937 p.]. Available from: https://doi.org/10.1016/j.matdes.2020.108937.
[152] Lopes A, Sampaio ÁM, Silva CS, Pontes A. Prediction of SLS parts properties using reprocessing powder. Rapid Prototyping Journal. 2021;27:496-506.
[153] Battu AK, Pope TR, Varga T, Christ JF, Fenn MD, Rosenthal WS, et al. Build orientation dependent microstructure in polymer laser sintering: Relationship to part performance and evolution with aging. Additive Manufacturing [Internet]. 2020; 36:[101464 p.]. Available from: https://www.sciencedirect.com/science/article/pii/S2214860420308368.
[154] Xu Z, Wang Y, Wu D, Ananth KP, Bai J. The process and performance comparison of polyamide 12 manufactured by multi jet fusion and selective laser sintering. Journal of Manufacturing Processes [Internet]. 2019; 47:[419-26 pp.]. Available from: http://www.sciencedirect.com/science/article/pii/S1526612518315123.
[155] Faes M, Wang Y, Lava P, Moens D, editors. Variability in the mechanical properties of laser sintered PA-12 components. 2015 International Solid Freeform Fabrication Symposium; 2015: University of Texas at Austin.
[156] Ajoku U, Saleh N, Hopkinson N, Hague R, Erasenthiran P. Investigating mechanical anisotropy and end-of-vector effect in laser-sintered nylon parts. Proceedings of the Institution of Mechanical Engineers, Part B: Journal of Engineering Manufacture [Internet]. 2006 2006/07/01; 220(7):[1077-86 pp.]. Available from: https://doi.org/10.1243/09544054JEM537.
[157] Gibson I, Shi D. Material properties and fabrication parameters in selective laser sintering process. Rapid prototyping journal [Internet]. 1997. Available from: https://doi.org/10.1108/13552549710191836.
[158] Gogolewski S, Gasiorek M, Czerniawska K, Pennings AJ. Annealing of melt-crystallized nylon 6. Colloid and Polymer Science [Internet]. 1982; 260(9):[859-63 pp.]. Available from: https://doi.org/10.1007/BF01419096.

[159] Gogolewski S, Czerntawska K, Gastorek M. Effect of annealing on thermal properties and crystalline structure of polyamides. Nylon 12 (polylaurolactam). Colloid and Polymer Science [Internet]. 1980; 258(10):[1130-6 pp.]. Available from: https://doi.org/10.1007/BF01382456.
[160] Gornet TJ, Davis KR, Starr TL, Mulloy KM, editors. Characterization of Selective Laser Sintering™ Materials to Determine Process Stability2002.
[161] The crystalline state. In: Samulski E, Wignall G, Koenig J, Mark J, Ngai K, Mandelkern L, et al., editors. Physical Properties of Polymers. 3 ed. Cambridge: Cambridge University Press; 2004. p. 245-66.
[162] Paolucci F, Baeten D, Roozemond PC, Goderis B, Peters GWM. Quantification of isothermal crystallization of polyamide 12: Modelling of crystallization kinetics and phase composition. Polymer [Internet]. 2018; 155:[187-98 pp.]. Available from: https://doi.org/10.1016/j.polymer.2018.09.037.
[163] Cholewa S, Drummer D. Crystallization behavior under process conditions in Powder Bed Fusion of polymers. Procedia CIRP [Internet]. 2022 2022/01/01/; 111:[23-7 pp.]. Available from: https://www.sciencedirect.com/science/article/pii/S2212827122009891.
[164] Kazmierczak T, Galeski A, Argon A. Plastic deformation of polyethylene crystals as a function of crystal thickness and compression rate. Polymer [Internet]. 2005; 46(21):[8926-36 pp.]. Available from: https://doi.org/10.1016/j.polymer.2005.06.073.
[165] Zhang Q, Mo Z, Liu S, Zhang H. Influence of Annealing on Structure of Nylon 11. Macromolecules [Internet]. 2000; 33(16):[5999-6005 pp.]. Available from: https://doi.org/10.1021/ma000298d.
[166] Maiza S, Lefebvre X, Brusselle-Dupend N, Klopffer MH, Cangemi L, Castagnet S, et al. Physicochemical and mechanical degradation of polyamide 11 induced by hydrolysis and thermal aging. Journal of Applied Polymer Science [Internet]. 2019; 136(23). Available from: http://dx.doi.org/10.1002/app.47628.
[167] Benz J, Bonten C. Temperature induced ageing of PA12 powder during selective laser sintering process. AIP Conference Proceedings [Internet]. 2019; 2055(1):[140001 p.]. Available from: https://aip.scitation.org/doi/abs/10.1063/1.5084904.
[168] Yang F, Jiang T, Lalier G, Bartolone J, Chen X. A process control and interlayer heating approach to reuse polyamide 12 powders and create parts with improved mechanical properties in selective laser sintering. Journal of Manufacturing Processes [Internet]. 2020; 57:[828-46 pp.]. Available from: http://www.sciencedirect.com/science/article/pii/S152661252030476X.
[169] Alo OA, Otunniyi IO, Mauchline D. Correlation of reuse extent with degradation degree of PA 12 powder during laser powder bed fusion and mechanical behavior of sintered parts. Polymer Engineering & Science [Internet]. 2023; 63(1):[126-38 pp.]. Available from: https://4spepublications.onlinelibrary.wiley.com/doi/abs/10.1002/pen.26191.
[170] Levantovskaya II, Kovarskaya BM, Dralyuk GV, Neiman MB. Mechanism of thermal oxidative degradation of polyamides. Polymer Science USSR [Internet]. 1964; 6(10):[2089-95 pp.]. Available from: https://www.sciencedirect.com/science/article/pii/0032395064906069.
[171] Alexey S. Kabalnov JTW, Vladek Kasperchik, inventorThree-dimensional (3d) printing patent WO2016175748A1. 2016.
[172] Dong W, Gijsman P. Influence of temperature on the thermo-oxidative degradation of polyamide 6 films. Polymer Degradation and Stability [Internet]. 2010; 95(6):[1054-62 pp.]. Available from: http://www.sciencedirect.com/science/article/pii/S0141391010001011.
[173] Richaud E, Okamba Diogo O, Fayolle B, Verdu J, Guilment J, Fernagut F. Review: Auto-oxidation of aliphatic polyamides. Polymer Degradation and Stability [Internet]. 2013; 98(9):[1929-39 pp.]. Available from: https://www.sciencedirect.com/science/article/pii/S0141391013001237.
[174] Pliquet M, Rapeaux M, Delange F, Bussiere PO, Therias S, Gardette JL. Multiscale analysis of the thermal degradation of polyamide 6,6: Correlating chemical structure to mechanical properties. Polymer Degradation and Stability [Internet]. 2021; 185:[109496 p.]. Available from: https://www.sciencedirect.com/science/article/pii/S0141391021000161.

[175] Goncalves ES, Poulsen L, Ogilby PR. Mechanism of the temperature-dependent degradation of polyamide 66 films exposed to water. Polymer Degradation and Stability [Internet]. 2007; 92(11):[1977-85 pp.]. Available from: http://dx.doi.org/10.1016/j.polymdegradstab.2007.08.007.
[176] Okamba-Diogo O, Richaud E, Verdu J, Fernagut F, Guilment J, Fayolle B. Investigation of polyamide 11 embrittlement during oxidative degradation. Polymer [Internet]. 2016; 82:[49-56 pp.]. Available from: http://dx.doi.org/10.1016/j.polymer.2015.11.025.
[177] Pandelidi C, Blakis R, Lee KPM, Bateman S, Brandt M, Kajtaz M. Thermal and Oxidative Aging Effects of Polyamide-11 Powder Used in Multi-Jet Fusion. Polymers [Internet]. 2023; 15(10):[2395 p.]. Available from: https://doi.org/10.3390/polym15102395.
[178] Valko EI, Chiklis CK. Effects of thermal exposure on the physicochemical properties of polyamides. Journal of Applied Polymer Science [Internet]. 1965; 9(8):[2855-77 pp.]. Available from: https://doi.org/10.1002/app.1965.070090820.
[179] Benzarti K, Colin X. Understanding the durability of advanced fibre-reinforced polymer (FRP) composites for structural applications. 2013. In: Advanced Fibre-Reinforced Polymer (FRP) Composites for Structural Applications [Internet]. Elsevier; [361-439]. Available from: https://doi.org/10.1533/9780857098641.3.361.
[180] Ksouri I, De Almeida O, Haddar N. Long term ageing of polyamide 6 and polyamide 6 reinforced with 30% of glass fibers: physicochemical, mechanical and morphological characterization. Journal of Polymer Research [Internet]. 2017; 24(8):[133 p.]. Available from: https://doi.org/10.1007/s10965-017-1292-6.
[181] Sang L, Wang C, Wang Y, Wei Z. Thermo-oxidative ageing effect on mechanical properties and morphology of short fibre reinforced polyamide composites – comparison of carbon and glass fibres. RSC Advances [Internet]. 2017; 7(69):[43334-44 pp.]. Available from: https://pubs.rsc.org/en/content/articlelanding/2017/ra/c7ra07884f.
[182] Shockley MF, Muliana AH. Modeling temporal and spatial changes during hydrolytic degradation and erosion in biodegradable polymers. Polymer Degradation and Stability [Internet]. 2020 2020/10/01/; 180:[109298 p.]. Available from: https://www.sciencedirect.com/science/article/pii/S0141391020302305.
[183] Weir N, Buchanan F, Orr J, Dickson G. Degradation of poly-L-lactide. Part 1: in vitro and in vivo physiological temperature degradation. Proceedings of the Institution of Mechanical Engineers, Part H: Journal of Engineering in Medicine [Internet]. 2004; 218(5):[307-19 pp.]. Available from: https://doi.org/10.1243/0954411041932782.
[184] Su K-H, Lin J-H, Lin C-C. Influence of reprocessing on the mechanical properties and structure of polyamide 6. Journal of Materials Processing Technology [Internet]. 2007; 192-193:[532-8 pp.]. Available from: https://www.sciencedirect.com/science/article/pii/S0924013607003986.
[185] Ferreira I, Melo C, Neto R, Machado M, Alves JL, Mould S. Study of the annealing influence on the mechanical performance of PA12 and PA12 fibre reinforced FFF printed specimens. Rapid Prototyping Journal [Internet]. 2020; 26(10):[1761-70 pp.]. Available from: https://doi.org/10.1108/RPJ-10-2019-0278.
[186] Ehrenstein GW, Pongratz S. Resistance and stability of polymers: Carl Hanser Verlag GmbH Co KG; 2013.
[187] Rabello MS, White JR. Crystallization and melting behaviour of photodegraded polypropylene — I. Chemi-crystallization. Polymer [Internet]. 1997; 38(26):[6379-87 pp.]. Available from: https://www.sciencedirect.com/science/article/pii/S0032386197002139.
[188] Deshoulles Q, Le Gall M, Dreanno C, Arhant M, Priour D, Le Gac PY. Modelling pure polyamide 6 hydrolysis: Influence of water content in the amorphous phase. Polymer Degradation and Stability [Internet]. 2021; 183:[109435 p.]. Available from: https://www.sciencedirect.com/science/article/pii/S0141391020303645.

[189] Crane NB, Ni Q, Ellis A, Hopkinson N. Impact of chemical finishing on laser-sintered nylon 12 materials. Additive Manufacturing [Internet]. 2017 2017/01/01/; 13:[149-55 pp.]. Available from: https://www.sciencedirect.com/science/article/pii/S2214860416302469.
[190] Johansson I. Post-processing for roughness reduction of additive manufactured polyamide 12 using a fully automated chemical vapor technique-The effect on micro and macrolevel. 2020.
[191] Petzold S, Klett J, Osswald T. A Statistical Study of Surface Roughness for Polyamide 12 Parts Produced Using Selective Laser Sintering. International Polymer Processing [Internet]. 2020; 35(2):[126-38 pp.]. Available from: https://doi.org/10.3139/217.3900.
[192] Gavcar B, Sumer EH, Sagbas B, Katiyar JK. Effect of build orientation on the green tribological properties of multi-jet fusion manufactured PA12 parts. Proceedings of the Institution of Mechanical Engineers, Part J: Journal of Engineering Tribology [Internet]. 2023; 237(12):[2213-23 pp.]. Available from: https://journals.sagepub.com/doi/abs/10.1177/13506501231209396.
[193] Yao B, Li Z, Zhu F. Effect of powder recycling on anisotropic tensile properties of selective laser sintered PA2200 polyamide. European Polymer Journal [Internet]. 2020; 141:[110093 p.]. Available from: https://www.sciencedirect.com/science/article/pii/S0014305720318073.
[194] Yang F, Schnuerch A, Chen X. Quantitative influences of successive reuse on thermal decomposition, molecular evolution, and elemental composition of polyamide 12 residues in selective laser sintering. The International Journal of Advanced Manufacturing Technology [Internet]. 2021; 115(9):[3121-38 pp.]. Available from: https://link.springer.com/article/10.1007/s00170-021-07368-w#Bib1.
[195] Bobaru F. Influence of van der Waals forces on increasing the strength and toughness in dynamic fracture of nanofibre networks: a peridynamic approach. Modelling and Simulation in Materials Science and Engineering [Internet]. 2007; 15(5):[397 p.]. Available from: https://iopscience.iop.org/article/10.1088/0965-0393/15/5/002/meta.
[196] Liu X, Tey WS, Choo JYC, Chen J, Tan P, Cai C, et al. Enhancing the mechanical strength of Multi Jet Fusion–printed polyamide 12 and its glass fiber-reinforced composite via high-temperature annealing. Additive Manufacturing [Internet]. 2021; 46:[102205 p.]. Available from: https://doi.org/10.1016/j.addma.2021.102205.
[197] Majewski CE, Zarringhalam H, Hopkinson N, editors. Effects of degree of particle melt and crystallinity in SLS Nylon-12 parts. 19th Annual International Solid Freeform Fabrication Symposium, SFF 2008, August 4, 2008 - August 6, 20; 2008; Austin, TX, United states: University of Texas at Austin (freeform).
[198] Berretta S, Evans K, Ghita O. Predicting processing parameters in high temperature laser sintering (HT-LS) from powder properties. Materials & Design [Internet]. 2016; 105:[301-14 pp.]. Available from: https://doi.org/10.1016/j.matdes.2016.04.097.
[199] Marchessault RH. Principles of polymer morphology, D. C. Bassett, Cambridge Solid State Series, Cambridge University Press, Cambridge, England, 1981, 250 pp. No price given. Journal of Polymer Science: Polymer Letters Edition [Internet]. 1982; 20(5):[279-80 pp.]. Available from: https://doi.org/10.1002/pol.1982.130200506.
[200] Snegirev AY, Talalov V, Stepanov V, Korobeinichev O, Gerasimov I, Shmakov A. Autocatalysis in thermal decomposition of polymers. Polymer Degradation and Stability [Internet]. 2017; 137:[151-61 pp.]. Available from: https://doi.org/10.1016/j.polymdegradstab.2017.01.008.
[201] Matisová-Rychlá L, Rychlý J, Tiemblo P, Gómez-Elvira J, Elvira M, editors. Thermal oxidation and its relation to chemiluminescence from polyolefins and polyamides. Macromolecular Symposia; 2004: Wiley Online Library.
[202] Flory PJ. Tensile strength in relation to molecular weight of high polymers. Journal of the american chemical society [Internet]. 1945; 67(11):[2048-50 pp.]. Available from: https://doi.org/10.1021/ja01227a506.

[203] Termonia Y, Meakin P, Smith P. Theoretical study of the influence of the molecular weight on the maximum tensile strength of polymer fibers. Macromolecules [Internet]. 1985; 18(11):[2246-52 pp.]. Available from: https://doi.org/10.1021/ma00153a032.
[204] Hallam M, Cansfield D, Ward I, Pollard G. A study of the effect of molecular weight on the tensile strength of ultra-high modulus polyethylenes. Journal of materials science [Internet]. 1986; 21(12):[4199-205 pp.]. Available from: https://link.springer.com/article/10.1007/BF01106531#.
[205] Fanconi BM. Chain scission and mechanical failure of polyethylene. Journal of Applied Physics [Internet]. 1983; 54(10):[5577-82 pp.]. Available from: https://doi.org/10.1063/1.331814.
[206] Schmid M. 4.2.1.1 Crystallization and Melting (Sintering Window). Laser Sintering with Plastics - Technology, Processes, and Materials: Hanser Publishers.
[207] Gomes PC, Piñeiro OG, Alves AC, Carneiro OS. On the reuse of SLS polyamide 12 powder. Materials [Internet]. 2022; 15(16):[5486 p.]. Available from: https://doi.org/10.3390/ma15165486.
[208] Alo OA, Otunniyi IO, Mauchline D. Effects of reuse on morphology, size and shape distributions of PA 12 powder in selective laser sintering and quality of printed parts. Journal of Polymer Research [Internet]. 2023; 30(2):[48 p.]. Available from: https://link.springer.com/article/10.1007/s10965-022-03423-6.
[209] Sanders B, Cant E, Amel H, Jenkins M. The Effect of Physical Aging and Degradation on the Re-Use of Polyamide 12 in Powder Bed Fusion. Polymers [Internet]. 2022; 14(13):[2682 p.]. Available from: https://doi.org/10.3390/polym14132682.
[210] Drummer D, Wudy K, Drexler M. Modelling of the aging behavior of polyamide 12 powder during laser melting process. AIP Conference Proceedings [Internet]. 2015; 1664(1):[160007 p.]. Available from: https://aip.scitation.org/doi/abs/10.1063/1.4918514.
[211] Eggers T, Rackl H, von Lacroix F. Investigation of the Influence of the Mixing Process on the Powder Characteristics for Cyclic Reuse in Selective Laser Sintering. Powders [Internet]. 2023; 2(1):[32-46 pp.]. Available from: https://www.mdpi.com/2674-0516/2/1/3.
[212] EOS. Technical Data EOS P396: EOS; [Available from: https://www.eos.info/en/industrial-3d-printer/plastic/eos-p-396.
[213] Amado A, Schmid M, Levy G, Wegener K, editors. Advances in SLS powder characterization. 22nd Annual International Solid Freeform Fabrication Symposium - An Additive Manufacturing Conference, SFF 2011; 2011 01/01; University of Texas, USA.
[214] Mercury Scientific. Flowability analysis with the Revolution [Available from: http://www.mercuryscientific.com/instruments/flowability-analysis-revolution.
[215] Ziegelmeier S, Wöllecke F, Tuck C, Goodridge R, editors. Characterizing the bulk & flow behaviour of LS polymer powders. 2013 International Solid Freeform Fabrication Symposium; 2013: University of Texas Austin.
[216] Ligon SC, Liska R, Stampfl J, Gurr M, Mülhaupt R. Polymers for 3D Printing and Customized Additive Manufacturing. Chemical Reviews [Internet]. 2017 2017/08/09; 117(15):[10212-90 pp.]. Available from: https://doi.org/10.1021/acs.chemrev.7b00074.
[217] Chatham CA, Long TE, Williams CB. A review of the process physics and material screening methods for polymer powder bed fusion additive manufacturing. Progress in Polymer Science [Internet]. 2019 2019/06/01/; 93:[68-95 pp.]. Available from: https://www.sciencedirect.com/science/article/pii/S0079670018303071.
[218] Schmid M, Wegener K. Additive Manufacturing: Polymers Applicable for Laser Sintering (LS). Procedia Engineering [Internet]. 2016 2016/01/01/; 149:[457-64 pp.]. Available from: https://www.sciencedirect.com/science/article/pii/S1877705816312073.
[219] Chen P, Wu H, Zhu W, Yang L, Li Z, Yan C, et al. Investigation into the processability, recyclability and crystalline structure of selective laser sintered Polyamide 6 in comparison with Polyamide 12. Polymer Testing [Internet]. 2018; 69:[366-74 pp.]. Available from: https://doi.org/10.1016/j.polymertesting.2018.05.045.

[220] Feng L, Wang Y, Wei Q. PA12 Powder Recycled from SLS for FDM. Polymers (Basel) [Internet]. 2019 Apr 22 PMC6523659]; 11(4). Available from: https://www.ncbi.nlm.nih.gov/pubmed/31013575.
[221] Van Hooreweder B, Moens D, Boonen R, Kruth J-P, Sas P. On the difference in material structure and fatigue properties of nylon specimens produced by injection molding and selective laser sintering. Polymer Testing [Internet]. 2013 2013/08/01/; 32(5):[972-81 pp.]. Available from: https://www.sciencedirect.com/science/article/pii/S0142941813001001.
[222] Nettleton D. Chapter 6 - Selection of Variables and Factor Derivation. 2014 2014/01/01/. In: Commercial Data Mining [Internet]. Boston: Morgan Kaufmann; [79-104]. Available from: https://www.sciencedirect.com/science/article/pii/B9780124166028000066.
[223] Bulaha N. Calculations of surface roughness 3D parameters for surfaces with irregular roughness. Engineering for rural development. 2018;23:1437-744.
[224] De Santis F, Pantani R, Titomanlio G. Nucleation and crystallization kinetics of poly(lactic acid). Thermochimica Acta [Internet]. 2011 2011/08/10/; 522(1):[128-34 pp.]. Available from: https://www.sciencedirect.com/science/article/pii/S0040603111003212.
[225] Biddlestone F, Harris A, Hay J, Hammond T. The physical ageing of amorphous poly (hydroxybutyrate). Polymer international [Internet]. 1996; 39(3):[221-9 pp.]. Available from: https://doi.org/10.1002/(SICI)1097-0126(199603)39:3%3C221::AID-PI511%3E3.0.CO;2-O.
[226] Wang ZG, Hsiao BS, Sauer BB, Kampert WG. The nature of secondary crystallization in poly(ethylene terephthalate). Polymer [Internet]. 1999 1999/07/01/; 40(16):[4615-27 pp.]. Available from: https://www.sciencedirect.com/science/article/pii/S0032386199000671.
[227] Verma R, Marand H, Hsiao B. Morphological changes during secondary crystallization and subsequent melting in poly (ether ether ketone) as studied by real time small angle X-ray scattering. Macromolecules [Internet]. 1996; 29(24):[7767-75 pp.]. Available from: https://doi.org/10.1021/ma951727o.
[228] Cholewa S, Jaksch A, Drummer D, editors. Coalescence Behavior of Polyamide 12 as Function of Zero-Shear Viscosity and Influence on Mechanical Performance. 2022 International Solid Freeform Fabrication Symposium; 2022; Austin, Texas.
[229] Li X, He Y, Dong X, Ren X, Gao H, Hu W. Effects of hydrogen-bonding density on polyamide crystallization kinetics. Polymer [Internet]. 2020 2020/02/17/; 189:[122165 p.]. Available from: https://www.sciencedirect.com/science/article/pii/S0032386120300100.
[230] Liu S, Yu Y, Cui Y, Zhang H, Mo Z. Isothermal and nonisothermal crystallization kinetics of nylon-11. Journal of Applied Polymer Science [Internet]. 1998; 70(12):[2371-80 pp.]. Available from: https://doi.org/10.1002/(SICI)1097-4628(19981219)70:12%3C2371::AID-APP9%3E3.0.CO;2-4.
[231] Zhang F, Zhou L, Xiong Y, Liu G, Xu W. Isothermal crystallization kinetics of high-flow nylon 6 by differential scanning calorimetry. Journal of Applied Polymer Science [Internet]. 2009; 111(6):[2930-7 pp.]. Available from: https://doi.org/10.1002/app.29352.
[232] Supaphol P, SPRUIELL JE. Application of the Avrami, Tobin, Malkin, and simultaneous Avrami macrokinetic models to isothermal crystallization of syndiotactic polypropylenes. Journal of Macromolecular Science, Part B [Internet]. 2000; 39(2):[257-77 pp.]. Available from: https://doi.org/10.1016/S0040-6031(00)00767-X.
[233] McFerran NL, Armstrong CG, McNally T. Nonisothermal and isothermal crystallization kinetics of nylon-12. Journal of applied polymer science [Internet]. 2008; 110(2):[1043-58 pp.]. Available from: https://doi.org/10.1002/app.28696.
[234] Sanders B, Cant E, Jenkins M. Re-use of polyamide-12 in powder bed fusion and its effect on process-relevant powder characteristics and final part properties. Additive Manufacturing [Internet]. 2024 2024/01/06/:[103961 p.]. Available from: https://www.sciencedirect.com/science/article/pii/S2214860424000071.
[235] Agapov AL, Sokolov AP. Does the Molecular Weight Dependence of Tg Correlate to Me? Macromolecules [Internet]. 2009 2009/04/14; 42(7):[2877-8 pp.]. Available from: https://doi.org/10.1021/ma9002825.

[236] Roland C, Casalini R. Temperature dependence of local segmental motion in polystyrene and its variation with molecular weight. The journal of chemical physics [Internet]. 2003; 119(3):[1838-42 pp.]. Available from: https://doi.org/10.1063/1.1581850.
[237] Izuka A, Winter HH, Hashimoto T. Molecular weight dependence of viscoelasticity of polycaprolactone critical gels. Macromolecules [Internet]. 1992; 25(9):[2422-8 pp.]. Available from: https://doi.org/10.1021/ma00035a020.
[238] Burfield DR, Doi Y. Differential scanning calorimetry characterization of polypropylene. Dependence of Tg on polymer tacticity and molecular weight. Macromolecules [Internet]. 1983; 16(4):[702-4 pp.]. Available from: https://doi.org/10.1021/ma00238a039.
[239] Ergoz E, Fatou J, Mandelkern L. Molecular weight dependence of the crystallization kinetics of linear polyethylene. I. Experimental results. Macromolecules [Internet]. 1972; 5(2):[147-57 pp.]. Available from: https://doi.org/10.1021/ma60026a011.
[240] Fornes T, Paul D. Structure and properties of nanocomposites based on nylon-11 and-12 compared with those based on nylon-6. Macromolecules [Internet]. 2004; 37(20):[7698-709 pp.]. Available from: https://doi.org/10.1021/ma048757o.
[241] Kinoshita Y. An investigation of the structures of polyamide series. Die Makromolekulare Chemie: Macromolecular Chemistry and Physics [Internet]. 1959; 33(1):[1-20 pp.]. Available from: https://doi.org/10.1002/macp.1959.020330101.
[242] Ma N, Liu W, Ma L, He S, Liu H, Zhang Z, et al. Crystal transition and thermal behavior of Nylon 12. e-Polymers [Internet]. 2020; 20(1):[346-52 pp.]. Available from: https://doi.org/10.1515/epoly-2020-0039.
[243] Jariyavidyanont K, Zhuravlev E, Schick C, Androsch R. Kinetics of homogeneous crystal nucleation of polyamide 11 near the glass transition temperature. Polymer Crystallization [Internet]. 2021; 4(1):[e10149 p.]. Available from: https://doi.org/10.1002/pcr2.10149.
[244] Schawe JEK, Pogatscher S. Material Characterization by Fast Scanning Calorimetry: Practice and Applications. In: Schick C, Mathot V, editors. Fast Scanning Calorimetry. Cham: Springer International Publishing; 2016. p. 3-80. 10.1007/978-3-319-31329-0_1
[245] Verkinderen O, Baeten D, Van Puyvelde P, Goderis B. The crystallization of PA11, PA12, and their random copolymers at increasing supercooling: From eutectic segregation to mesomorphic solid solutions. Polymer crystallization 2021;4(6):e10216. https://doi.org/10.1002/pcr2.10216
[246] Mileva D, Androsch R, Zhuravlev E, Schick C. Morphology of mesophase and crystals of polyamide 6 prepared in a fast scanning chip calorimeter. Polymer [Internet]. 2012; 53(18):[3994-4001 pp.]. Available from: https://doi.org/10.1016/j.polymer.2012.06.045.
[247] Mathot V, Pyda M, Pijpers T, Vanden Poel G, van de Kerkhof E, van Herwaarden S, et al. The Flash DSC 1, a power compensation twin-type, chip-based fast scanning calorimeter (FSC): First findings on polymers. Thermochimica Acta [Internet]. 2011; 522(1-2):[36-45 pp.]. Available from: https://doi.org/10.1016/j.tca.2011.02.031.
[248] Hoffman JD, Davis GT, Lauritzen Jr JI. The rate of crystallization of linear polymers with chain folding. Treatise on Solid State Chemistry: Volume 3 Crystalline and Noncrystalline Solids: Springer; 1976. p. 497-614.
[249] Androsch R, Schick C, Schmelzer JWP. Sequence of enthalpy relaxation, homogeneous crystal nucleation and crystal growth in glassy polyamide 6. European Polymer Journal [Internet]. 2014 2014/04/01/; 53:[100-8 pp.]. Available from: https://www.sciencedirect.com/science/article/pii/S0014305714000226.
[250] Rhoades AM, Williams JL, Androsch R. Crystallization kinetics of polyamide 66 at processing-relevant cooling conditions and high supercooling. Thermochimica Acta [Internet]. 2015 2015/03/10/; 603:[103-9 pp.]. Available from: https://www.sciencedirect.com/science/article/pii/S004060311400481X.
[251] Rahim TNAT, Abdullah AM, Md Akil H, Mohamad D, Rajion ZA. The improvement of mechanical and thermal properties of polyamide 12 3D printed parts by fused deposition modelling.

Express Polymer Letters [Internet]. 2017; 11(12):[963-82 pp.]. Available from: https://doi.org/10.3144/EXPRESSPOLYMLETT.2017.92.
[252] Murthy NS. Hydrogen bonding, mobility, and structural transitions in aliphatic polyamides. Journal of Polymer Science Part B: Polymer Physics [Internet]. 2006; 44(13):[1763-82 pp.]. Available from: https://onlinelibrary.wiley.com/doi/abs/10.1002/polb.20833.
[253] Marand H, Xu J, Srinivas S. Determination of the equilibrium melting temperature of polymer crystals: linear and nonlinear Hoffman− Weeks extrapolations. Macromolecules [Internet]. 1998; 31(23):[8219-29 pp.]. Available from: https://doi.org/10.1021/ma980747y.
[254] Jariyavidyanont K, Janke A, Androsch R. Crystal self-nucleation in polyamide 11. Thermochimica Acta [Internet]. 2019; 677:[139-43 pp.]. Available from: https://doi.org/10.1016/j.tca.2019.02.006.
[255] Kong Y, Hay J. The measurement of the crystallinity of polymers by DSC. Polymer [Internet]. 2002; 43(14):[3873-8 pp.]. Available from: https://doi.org/10.1016/S0032-3861(02)00235-5.
[256] Hewlett Packard: HP 3D Printing Materials. Available from: https://h20195.www2.hp.com/v2/getpdf.aspx/4AA7-1533ENA.pdf.
[257] Iervolino E, van Herwaarden AW, van Herwaarden FG, van de Kerkhof E, van Grinsven PPW, Leenaers ACHI, et al. Temperature calibration and electrical characterization of the differential scanning calorimeter chip UFS1 for the Mettler-Toledo Flash DSC 1. Thermochimica Acta. 2011;522(1):53-9. https://doi.org/10.1016/j.tca.2011.01.023
[258] van Herwaarden S, Iervolino E, van Herwaarden F, Wijffels T, Leenaers A, Mathot V. Design, performance and analysis of thermal lag of the UFS1 twin-calorimeter chip for fast scanning calorimetry using the Mettler-Toledo Flash DSC 1. Thermochimica Acta [Internet]. 2011 2011/08/10/; 522(1):[46-52 pp.]. Available from: https://www.sciencedirect.com/science/article/pii/S0040603111003121.
[259] Schawe JEK. Flash DSC 1: A novel fast differential scanning calorimeter2011.
[260] Yamada K, Hikosaka M, Toda A, Yamazaki S, Tagashira K. Equilibrium melting temperature of isotactic polypropylene with high tacticity: 1. Determination by differential scanning calorimetry. Macromolecules [Internet]. 2003; 36(13):[4790-801 pp.]. Available from: https://doi.org/10.1021/ma021206i.
[261] De Gennes P-G. Reptation of a polymer chain in the presence of fixed obstacles. The journal of chemical physics [Internet]. 1971; 55(2):[572-9 pp.]. Available from: https://doi.org/10.1063/1.1675789.
[262] Doi M, Edwards S. Dynamics of concentrated polymer systems. Part 1.—Brownian motion in the equilibrium state. Journal of the Chemical Society, Faraday Transactions 2: Molecular and Chemical Physics [Internet]. 1978; 74:[1789-801 pp.]. Available from: https://doi.org/10.1039/F29787401789.
[263] Doi M, Edwards S. Dynamics of concentrated polymer systems. Part 3.—The constitutive equation. Journal of the Chemical Society, Faraday Transactions 2: Molecular and Chemical Physics [Internet]. 1978; 74:[1818-32 pp.]. Available from: https://doi.org/10.1039/F29787401818.
[264] Mielicki C, Gronhoff B, Wortberg J, editors. Effects of laser sintering processing time and temperature on changes in polyamide 12 powder particle size, shape and distribution. AIP Conference Proceedings; 2014; Idaho, USA: American Institute of Physics.
[265] Parteli EJ, Pöschel T. Particle-based simulation of powder application in additive manufacturing. Powder Technology [Internet]. 2016; 288:[96-102 pp.]. Available from: https://doi.org/10.1016/j.powtec.2015.10.035.
[266] Instruments M. Application note: Wet or liquid dispersion method development for laser diffraction particle size measurements. 2013.